2021

Development of an Injectable Methylcellulose Hydrogel System for Nucleus Pulposus Repair and Regeneration

Nada A. Haq-Siddiqi
CUNY City College

Development of an Injectable Methylcellulose Hydrogel System for Nucleus Pulposus Repair and Regeneration

by Nada A. Haq-Siddiqi

A dissertation submitted to the Graduate Faculty in Engineering

In partial fulfillment of the requirements for the degree of

Doctor of Philosophy

The City College of New York

June 2021

This manuscript has been read and accepted for the Graduate Faculty in Engineering in satisfaction of the dissertation requirement for the degree of Doctor of Philosophy

Steven B. Nicoll, Ph.D. Chair of Examining Committee	Date
Ardie D. Walser, Ph.D. Associate Dean for Academic Affairs	Date

Examining Committee:

Steven B. Nicoll, Ph.D., Professor of Biomedical Engineering, The City College of New York

Mitchell B. Schaffler, Ph.D., Professor of Biomedical Engineering, The City College of New York

Sihong Wang, Ph.D., Associate Professor of Biomedical Engineering, The City College of New York

Raymond Tu, Ph.D., Associate Professor of Chemical Engineering, The City College of New York

and

James C. Iatridis, Ph.D., Professor of Orthopedics, Icahn School of Medicine at Mount Sinai

THE CITY COLLEGE OF NEW YORK

Dedicated to my Grandparents

Whose example of the utmost commitment to God,

family, and education have been a blessing and guide in my life

And my Children

My strength and my hope,

Always

Abstract

Development of an Injectable Methylcellulose Hydrogel System for Nucleus Pulposus Repair and Regeneration

By Nada A. Haq-Siddiqi

Advisor: Dr. Steven B. Nicoll

Low back pain is the most common cause of disability in the world and is often caused by degeneration or injury of the intervertebral disc (IVD). The IVD is a complex, fibrocartilaginous tissue that allows for the wide range of spinal mobility. Disc degeneration is a progressive condition believed to begin in the central, gelatinous nucleus pulposus (NP) region of the tissue, for which there are few preventative therapies. Current therapeutic strategies include pain management and exercise, or surgical intervention such as spinal fusion, none of which address the underlying cause of degeneration. With an increasingly aging population, the socioeconomic impact of disability associated with low back pain and disc degeneration cannot be understated. Tissue engineering strategies are increasingly being investigated as an alternative therapy by which early-stage degeneration may be halted and reversed, thus restoring disc mechanics and inducing biological repair to prevent more painful long-term degeneration and disability. In order to prevent further injury to the IVD, an ideal therapeutic should be injectable via small gauge needle, be retained within the high-pressure intradiscal space, restore biomechanical properties, and deliver therapeutic agents and/or cells to drive tissue regeneration. Therefore, the overall objective of this thesis was ***to develop and characterize an injectable, bioactive, cellulose-based hydrogel system for NP replacement and repair.***

Methylcellulose (MC) is cellulose derivative that forms physically crosslinked gels at increasing temperatures. Methacrylation of MC allows for the formation of more robust,

chemically crosslinked hydrogels with lower effective macromer concentration. The first aim of this thesis investigated the influence of methacrylation on the thermoresponsive behavior of MC with implications for injectability and *in situ* retention. Results showed that increasing methacrylation percentage increased hydrophobic interactions that drive thermogelation, lowering the thermogelation onset temperature to within physiologic range, and produced robust, rapidly gelling, dual-crosslinked hydrogels when formed at physiologic temperature versus room temperature with redox initiators. The addition of anionic groups to MC would allow the polymer to mimic the sulfated glycosaminoglycan-rich matrix of the NP, enhancing water retention and sequestration of cationic proteins such as TGF-β3 that are critical for regenerative repair. Thus, the second aim was to develop an injectable, sulfonated MC hydrogel capable of forming stable gels *in situ* and electrostatically sequestering TGF-β3 to improve bioavailability of the therapeutic molecule. Findings showed that using sulfonated methacrylate monomers, negatively charged moieties could be incorporated into the MC hydrogels without sacrificing thermoresponsiveness below 37°C. Sulfonation was easily tunable by increasing monomer concentration, and TGF-β3 sequestration was closely correlated with sulfonate concentration, resulting in a viable bioactive acellular biomaterial for NP replacement. Factorial design of macromer and sulfonate concentration allowed for selection of a sulfonated MC (sMC) formulation with optimal chemical and mechanical properties for injection into the NP. The third aim evaluated the bioactivity of the sMC hydrogels by encapsulating human bone-marrow derived mesenchymal stromal cells (hMSCs) with and without TGF-β3. Results demonstrated that sMC hydrogels with TGF-β3 were able to support NP-like matrix elaboration and maintained relevant mechanical properties. Overall, this work advanced the development of injectable cellulose-based hydrogels as potential bioactive NP replacements for IVD repair and regeneration.

Acknowledgements

First and foremost, the ultimate praise and thanks must go to Allah,
whose presence and mercy have been constant both in times of my weakness and strength.

اللَّهُمَّ انْفَعْنِي بِمَا عَلَّمْتَنِي وَ عَلِّمْنِي مَا يَنْفَعُنِي وَ زِدْنِي عِلْمًا

Allaahumman fa'nee bima 'allamtanee wa 'allimnee ma yanfa'unee wa zidnee 'ilma

O Allah, make what You teach me beneficial, teach me what is beneficial,
and increase me in knowledge

This thesis marks the culmination of years of collaborative efforts, and this only begins to scratch the surface of the numerous contributions that have made its completion possible. Firstly, I would like to thank my thesis advisor, Dr. Steven Nicoll for his support and mentorship. Not only has he provided invaluable academic and professional guidance and helped me grow as an independent researcher, but has been understanding and supportive through setbacks, for which I am truly grateful.

My thanks to my thesis committee, Dr. James Iatridis, Dr. Mitchell Schaffler, Dr. Sihong Wang, and Dr. Raymond Tu, who have all provided guidance, expertise, and a critical eye that has made this thesis and scientist better for it.

My number one advice to anyone embarking on a Ph.D. has been: find your people. The work will have its ups and downs but "your people" will get you through it. In my doctoral experience I have been blessed with *the best* people. From day one, Michelle, Devika, Gittel, Anna, Fabrice, Jesse, and Dave have been more friends than colleagues, and made our lab a fun and dynamic place to work. All the graduate students in CCNY's BME department, but in particular: Tanya, Shawn, Sean, Mykel, Kris, Karl, Anne Marie, Liz and Abbey, have made the graduate school experience infinitely easier and more fun by opening their lab doors, their homes, their knowledge

and their hearts to me. The fact that I still regularly turn to them for support and guidance after they have moved on in their respective careers is a testament to the bonds we've built. Though not technically a part of our department, Tyler from the Iatridis lab has been a friend and motivator in my last few years, and I am so happy to be crossing this finish line together.

Charles Darwin said, "It is the long history of humankind (and animal kind, too) those who learned to collaborate and improvise most effectively have prevailed." At the risk of leaving someone out, I would like to thank the Tarbell lab, Schaffler lab, Barabino lab, Vasquez lab, Wong lab, Williams lab, and especially Dr. Majeska and Dr. Qui in BME, as well as the Morris Lab, Tu lab, Gilchrist Lab and Biddinger Lab in Chem E, and Dr. Pradhan from the Chemistry and NMR Facility, and the Iatridis Lab at Mount Sinai, without who's generosity in materials, equipment, and expertise this research would not be possible. Thank you as well to my undergraduate mentees who have given me the opportunity to become a better scientist and a better mentor.

The aforementioned people have made this dissertation what it is, but I must also acknowledge those who have made *me* what I am: My parents, who have supported me throughout this long journey. They taught me that nothing other than God and family was more important than a good education, and look where it got me. My brother, who has taught me about bravery and being my own advocate. My whole life, my grandparents have been an example to me and the highest bar that I have hoped to achieve. I am heartbroken to have lost three of them during this arduous process, but I know their prayers are still with me. *Dadi, dekho maine thesis submit karli*. My in-laws, the Siddiqi family, there is nothing "in-law" about the love and support they have always given me, to say nothing of the greatest gift, Asad. It would not have been possible for me to complete this work without the help of Saba Iqbal, who has truly become a member of our family.

Long hours for me often meant long hours for her. As painful as it has been to be away from Shahbaz, it has always been a comfort to know that he is in the most loving hands.

"She is a friend of my mind. She gather me, man. The pieces I am, she gather them and give them back to me in all the right order. It's good, you know, when you got a woman who is a friend of your mind," wrote Toni Morrison in Beloved. To Hinna, Sofia, Yumnah, Naethra, Kiran, and so many more dear friends I cannot begin to list, I am so grateful to have you to put me back together when the pieces come apart and giving me the opportunity to do the same in turn.

I would need at least the full length of this thesis to begin to thank my husband Asad for everything he's been for me throughout this time. This is as much his effort as it is mine. We have gone through the lowest lows and the highest highs together, and during the times that I doubted myself and wanted to quit, his faith in me is what kept me going. The best husband, best father, best brother, best friend, and best person I have ever known.

Shahbaz Asad Siddiqi: my pride and joy, my sunshine, my hero. Every day I hope to be worthy of the honor of being your Amma.

And finally, I would like to acknowledge myself. Through personal and professional challenges, I have persevered and have come out stronger because of it.

Table of Contents

List of Tables

List of Figures

List of Abbreviations

AC: Articular Cartilage

AF: Annulus Fibrosus

ANOVA: Analysis of Variance

APS: Ammonium Persulfate

ATR-FTIR: Attenuated Total Reflection – Fourier Transform Infrared Spectroscopy

BC: Bacterial Cellulose

CEP: Cartilaginous Endplate

CMC: Carboxymethyl Cellulose

CNC: Cellulose Nanocrystals

Col II: Type II Collagen

CS: Chondroitin Sulfate

DP: Degree of Polymerization

DS: Degree of Substitution

DSC: Differential Scanning Calorimetry

ECM: Extracellular Matrix

GAG: Glycosaminoglycan

HA: Hyaluronic Acid

hMSC: Human Mesenchymal Stromal Cell

^{1}H-NMR: Proton Nuclear Magnetic Resonance

HEMC: Hydroxyethyl Methylcellulose

HPMC: Hydroxypropyl Methylcellulose

IVD: Intervertebral Disc

IVDD: Intervertebral Disc Degeneration

Ma-CMC: Methacrylated Carboxymethylcellulose

Ma-MC: Methacrylated Methylcellulose

MC: Methylcellulose

MFC: Microfibrillated Cellulose

MMP: Matrix Metalloproteinase

MSC: Mesenchymal Stem Cell

NC: Notochordal Cell

NFC: Nanofibrillated Cellulose

NP: Nucleus Pulposus

NPC: Nucleus Pulposus Cell

PG: Proteoglycan

sGAG: Sulfated Glycosaminoglycan

sMC: Sulfonated Methylcellulose

TEMED: N,N,N',N'-Tetramethylethylenediamine

TGF-β3: Transforming Growth Factor-β3

Chapter 1: Introduction to Intervertebral Disc – From Structure and Function to Regeneration and Repair

1.1 An Unmet Clinical Need: Low Back Pain and the Intervertebral Disc

The intervertebral disc (IVD) is a fibrocartilaginous tissue that exists between vertebral bones within the spinal column. Its primary function is loadbearing, as it provides crucial shock absorption to the spine during motion (Neidlinger-Wilke et al. 2013). The IVD is a composite organ made up of three primary tissues: the nucleus pulposus (NP), annulus fibrosus (AF), and cartilaginous endplates (CEP), which together provide support and range of motion to the spine (Humzah and Soames 1988). Injury and degeneration of the IVD critically impair the IVD's ability to perform that function (Raj 2008). Intervertebral disc degeneration (IVDD) is linked to chronic low back pain and neck pain, the leading cause of disability worldwide (Hartvigsen et al. 2018). Although IVDD and low back pain are not life threatening, the personal and economic burdens of chronic pain are enormous; in 2016 low back and neck pain accounted for the highest amount of healthcare spending in the US, totaling approximately $134.5 billion in total spent on care, and is responsible for 60.1 million disability adjusted life years (DALYs) globally, which translates to hours of lost work opportunities and lost wages (Dieleman et al. 2020).

Degeneration generally begins in the NP, where altered loading or injury can initiate aberrant cellular catabolism and breakdown of the proteoglycan-rich matrix that mediates NP hydration and hydrostatic pressure (Urban, Roberts, and Ralphs 2000). Loss of hydration and pressure leads to altered loading on the total disc, placing increased stress on the AF, giving rise to bulging, fissures, and even herniation of the NP out of the AF, as well as calcification and fracture of the CEP, and osteophyte formation (Iatridis et al. 2013; Setton and Chen 2006; Urban, Roberts, and Ralphs 2000). Pain management and physical therapy remain the standard of care for early to mid-stage symptomatic degeneration, while eventually late-stage degeneration can necessitate a complete discectomy and spinal fusion (Desmoulin, Pradhan, and Milner 2020). Because the IVD

is mainly avascular, it has little to no capacity for repair, and so IVDD is a progressive condition for which there remains no effective treatment that addresses the cause of the degeneration or prevents progression of the disease.

Tissue engineering solutions aim to address this issue by combining cell therapy with a scaffold that will both restore IVD mechanics and support further tissue repair. Because IVDD is understood to begin in the NP, the degenerate NP and mid-stage degeneration are the preferred targets for early intervention. The ideal tissue engineering construct attempts to recapitulate nature in an engineered implant by mimicking the environmental cues (i.e. mechanical and chemical) found in the natural tissue, to promote the differentiated phenotype of the incorporated cells. The construct must withstand the mechanical loads of the native NP, as well as allow for fluid and nutrient transport in a manner similar to the native IVD. Additionally, delivery of a tissue-engineered system must be minimally invasive; injury to the AF can further IVDD by causing a reduction in the pressurization of the IVD, and therapeutic delivery must be injectable through a fine gauge needle to prevent further disruption of the AF. The combination of mechanical demands, limited nutritional and regenerative capacity, and need for minimally invasive and disruptive delivery present unique challenges for tissue engineering repair of the IVD. In the current chapter, physiology of the healthy and pathological IVD will be discussed, with emphasis on the NP as the therapeutic target, and current existing and investigative solutions for NP replacements will be outlined. Components of traditional tissue engineering – scaffold materials, cell source, and instructive signaling cues – will then be reviewed, in addition to the critical design criteria for evaluating success in NP tissue engineering. Finally, the scope and aims of the present investigation will be introduced.

1.2 Intervertebral Disc Anatomy and Physiology

1.2.1 Anatomy and function

The spinal column is made up of repeating vertebral bones separated by a unique connective tissue of the IVD that allows for a broad range of motion (**Figure 1.1.A**). The function of the IVD is mechanical, as it transmits loads through the spine. The IVD allows for 6 degrees of freedom in motion: compression, anterio-posterior and lateral shear, flexion, and torsion (Buckwalter et al. 2000; Neidlinger-Wilke et al. 2013; Iatridis et al. 2013). It does so by virtue of its composite structure: the NP, a gel-like structure, resists vertical compression via hydrostatic pressure, and is surrounded by the annulus fibrosus (AF), which resists the radial stress from the expanding NP via circumferential tension. The NP and AF are sandwiched superiorly and inferiorly by the CEP, thin strips of cartilage which provide adhesion to the adjacent vertebral bodies and allow nutrition transport (Buckwalter et al. 2000; Raj 2008). The healthy IVD is avascular and mostly aneural.

The NP is a highly hydrated, gelatinous structure. Water makes up approximately 80% of the wet weight of the NP; the rest of the wet weight is made up of proteoglycans (PGs) (15%), collagens (4%), and other extracellular matrix proteins (Raj 2008; Buckwalter et al. 2000). It is similar to hyaline cartilage in that the major collagen in the NP is collagen type II, and the most common PGs in the NP are aggrecan and versican (Raj 2008; Hayes, Benjamin, and Ralphs 2001). Aggrecan is high in chondroitin sulfate and keratan sulfate glycosaminoglycans which are covalently attached to its protein core in an arrangement that resembles a bottlebrush formation. The high negative charge of the sulfated glycosaminoglycan (sGAG) chains promote the influx of positive ions and water into the NP, creating hydrostatic pressure within the tissue (Buckwalter et

al. 2000; Hayes, Benjamin, and Ralphs 2001; Pattappa et al. 2012). The arrangement of fibers within the NP is isotropic, which enables uniform distribution of compressive loads.

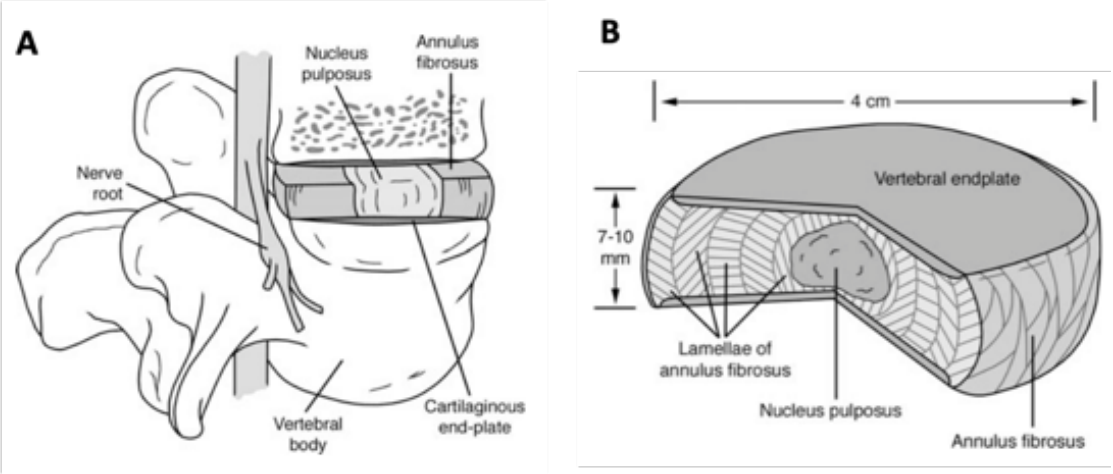

Figure 1.1: Schematic of the anatomy of the IVD and surrounding tissues.
A) The spinal segment consisting of two vertebral bodies and an intervertebral disc sandwiched between them. B) A sectioned portion of a normal human disc, displaying the location of the NP, lamellae of the AF, and vertebral endplate (CEP). Adapted from Raj, (2008).

Surrounding the NP is the AF, which consists of circumferential lamellae comprising the outer region of the IVD. The AF is also highly hydrated, although less so than the NP, with water making up 70% of the wet weight. Collagen is the next most abundant component of the AF, making up 15% of the wet weight of the AF (70% of the dry weight). The AF contains both type I and type II collagen, with type I being more abundant in the outer AF, and elastin between lamellae. PGs make up only 5% of the wet weight of the AF (Raj 2008; Hayes, Benjamin, and Ralphs 2001; Bruehlmann et al. 2002). The lamellae of the AF are highly anisotropic and are arranged in concentric rings which maintain circumferential hoop stresses that resist the outward pressure created by the compressed NP (**Figure 1.1.B**). The collagen fibers in the lamellae are arranged parallel within each lamella and approximately 60° to the vertical axis, and alternate in direction between lamellae, which allow it to resist crack propagation in the case of injury (Raj 2008; Iatridis et al. 2013; Bruehlmann et al. 2002). The CEPs form the superior and inferior interface of the disc

and the vertebral bones. Thin strips of hyaline cartilage, the CEPs are also composed mainly of water (58% of total tissue weight), although less than each of the other two IVD tissues. Additionally, the CEP contains collagen and PGs at different weight percentages than the NP and AF, containing 60-80% collagen/dry weight and only 17%/dry weight of PGs (Roberts, Menage, and Urban 1989). Viscous fluid flow through the CEP allows for nutrient exchange via diffusion and convection from capillary beds in the subchondral plate through the CEP to the central portions of the disc and back (Urban, Smith, and Fairbank 2004).

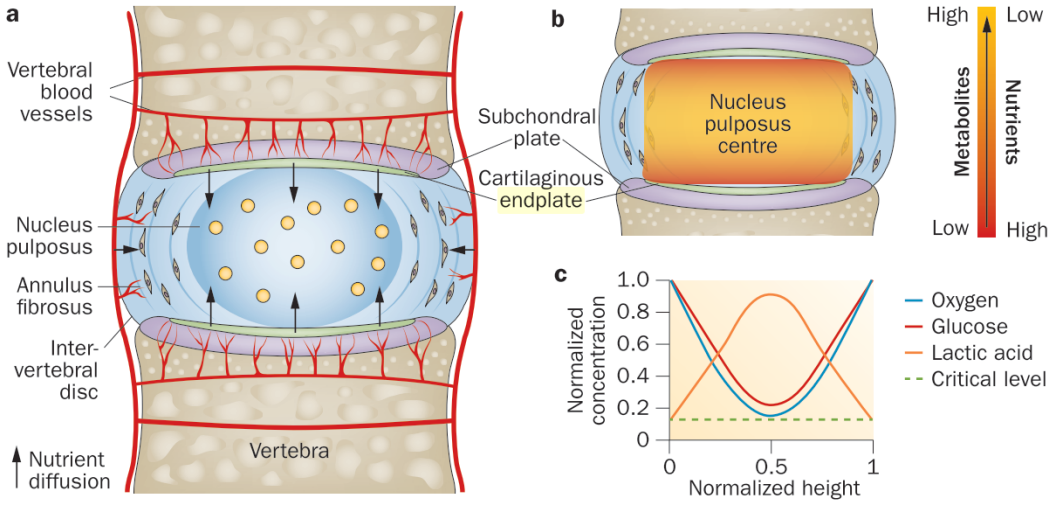

Figure 1.2: Pathways of nutrient supply in the healthy IVD.
A) Cells of the avascular NP and inner AF are supplied by nutrients via capillary beds emerging from the vertebrae. B) The center of the disc has the lowest level of nutrients and highest amount of metabolites. C) Schematic of the nutrient gradients from endplate (0) to endplate (1). Adapted from Huang et. al. (2014).

The IVD is mostly avascular, and blood supply in the healthy IVD is restricted to the subchondral plate and the outermost portions of the AF that experience only a few millimeters of capillary penetration from the surrounding tissue (**Figure 1.2.A**) (Huang, Urban, and Luk 2014). Because nutrient and metabolite exchange occurs primarily via diffusion, concentration gradients exists as a product of the rate of supply and consumption within the IVD, leading the IVD, and in particular the NP, to be generally a hypoxic, acidic environment with low glucose (**Figure 1.2.B-**

C) (Horner and Urban 2001; Raj 2008). Even though the cells of the disc are uniquely differentiated to thrive in this environment (Guehring et al. 2009), a critical threshold exists beyond which cells will not remain active or viable, as well as a limit to the number of cells that can be supported within the tissue.

1.2.2 Cells of the IVD

The adult IVD has a very low cell density, at approximately 0.25-0.5% total tissue volume (Urban, Roberts, and Ralphs 2000). The NP contains ~4 x 10^6 cells/cm^3 and the AF has a slightly higher cell density at ~9 x 10^6 cells/cm^3 (Pattappa et al. 2012; Raj 2008). The cells of the outer AF are fusiform and fibroblast-like and are aligned with the collagen fibers in the AF lamellae. Moving towards the center of the IVD, the AF cells become more oval shaped (Bruehlmann et al. 2002; Johnson and Roberts 2003). The cells of the NP are rounded and are often referred to as chondrocyte-like cells, or IVD-chondrocytes; however, despite many similarities between NP cells and articular chondrocytes, there are key differences. The NP structure originates from the notochord in development, and the young NP is populated with large, highly vacuolated notochordal cells (NCs) (Urban, Roberts, and Ralphs 2000; Rodrigues-Pinto, Richardson, and Hoyland 2014); by approximately 10 years, these cells are replaced by smaller, more chondrocyte-like NP cells (NPCs) (Rodrigues-Pinto, Richardson, and Hoyland 2014; Yang et al. 2009). There has been debate as to whether the NCs differentiate into NPCs or if they simply disappear and are replaced by the NPCs through an unknown mechanism (Rodrigues-Pinto, Richardson, and Hoyland 2014). Histological observations have shown chondrocyte migration from the endplate towards the central regions of the IVD (Yang et al. 2009; Kim et al. 2003; Kim et al. 2009). However, recent fate mapping experiments have shown that throughout the aging process of the NP, the cells within the NP remain notochordal in lineage (Choi and Harfe 2011; Choi, Cohn, and

Harfe 2008; McCann et al. 2012). It has been hypothesized that the phenotypic shift from highly vacuolated notochord-like cells to smaller, chondrocyte-like cells contributes to aging and degeneration of the disc (Risbud and Shapiro 2011; Chen, Yan, and Setton 2005).

The cells of both the NP and AF exist within a dense pericellular matrix (PCM) high in collagen type VI, similar to the cells of articular cartilage (AC) (Cao, Guilak, and Setton 2007; Wilusz, Sanchez-Adams, and Guilak 2014). This matrix is both biochemically and morphologically distinct from the surrounding territorial matrix. NPCs exist both alone and in groups of 2 to 4 in the NP, and in longitudinal arrangements of up to 10 in the AF. The PCM is thought to have a mechanoregulatory function, and studies suggest that the pericellular matrix plays a critical role in both transmitting and attenuating mechanical forces experienced by the whole IVD to the cells (Cao, Guilak, and Setton 2011; Cappello et al. 2006; Cao, Guilak, and Setton 2009).

1.3 Mechanics of the Disc

The role of the IVD is purely mechanical: it functions to allow support and motion to the body. IVDs, along with small amounts of hyaline cartilage between the facets (the zygapophyseal joint) of two adjacent vertebral bodies, compose a motion segment that allows bending and twisting of the neck, torso, and waist. The disc thus must withstand compressive loads from both body weight and muscle tension. While standing, the posterior spinal muscles exert force to balance the flexion moment caused by body weight (Neidlinger-Wilke et al. 2013). In the healthy IVD, compressive loads are evenly borne and distributed by the NP. Hydrostatic pressure in the adult human NP measures at about 0.1-0.2 MPa while in supine position at rest, around 0.5 MPa when standing, and as high as 2.3 MPa while carrying a weight in a flexed position (**Figure 1.3.A**) (Neidlinger-Wilke et al. 2013). The wide range of motion allowed by the spine combined with

carrying extra weight can significantly alter the load on the spine and create much more complex loads on the disc (Hsieh and Twomey 2010; Wilke et al. 1999).

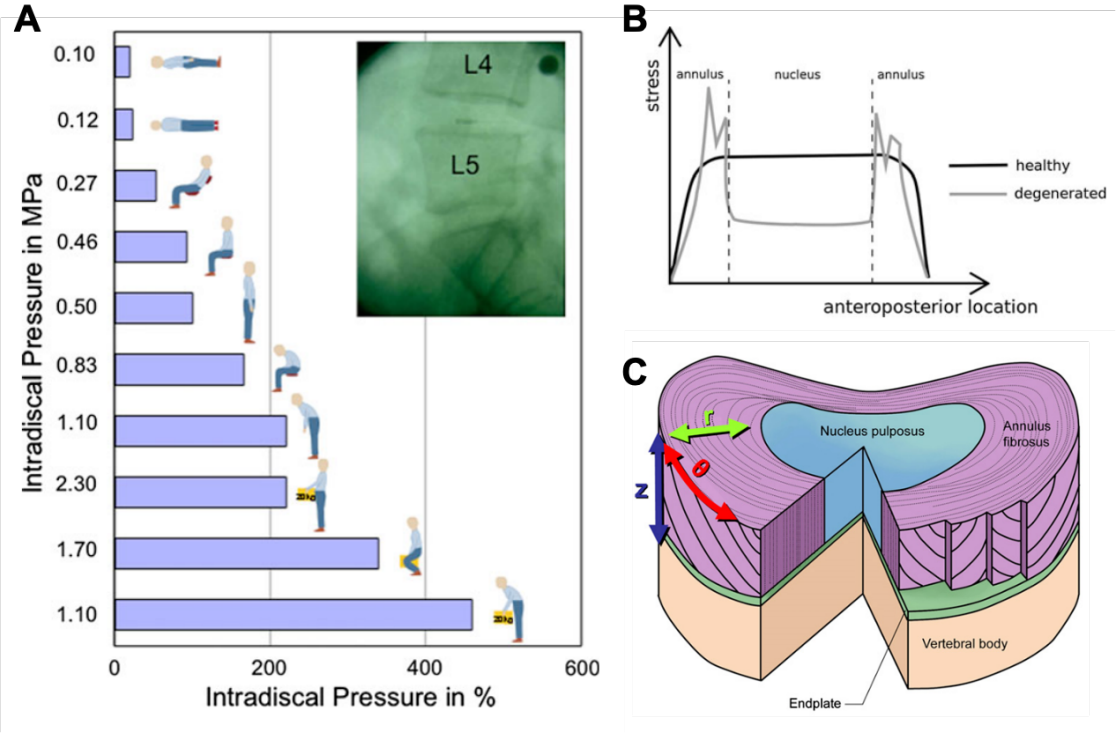

Figure 1.3: Forces acting on the IVD.
A) *In vivo* values of intradiscal pressure at different postures and daily activities. B) Representative stress profiles in the lumbar IVDs in healthy and degenerative conditions. Adapted from Neidlinger-Wilke et al. (2013). C) Schematic representation of the multiscale architecture of the IVD and the axes of force distribution. Adapted from Nerurkar, Elliott, & Mauck (2011).

Load distribution in the IVD is dependent on its composition (**Figure 1.3.C**). The high hydrostatic pressure within the NP resists compression from body weight and motion. As the NP undergoes compression, the AF stretches in tension and provides resistance to expansion, thereby maintaining high pressure within the NP. The AF also resists strains during twisting and bending (Buckwalter et al. 2000; Iatridis et al. 2013; Neidlinger-Wilke et al. 2013). When the NP degenerates and loses hydration, it also loses height, which shifts abnormal loads to the AF, creating stress peaks which further promote disc degeneration and fissures (**Figure 1.3.B**). The figure is simplified in that it represents the stress distribution measured *in vitro* and does not

consider the varied loading conditions involved *in vivo*. It also only represents compressive stress and not tensile or shear stress.

There is a wide range of both organization and composition of the ECM environment within the IVD; this contributes to the wide variety of forces experienced by the cells within the IVD. The cells in the NP are exposed to predominantly uniform hydrostatic stress (**Figure 1.4**). Conversely, the cells of the AF lie along collagen fibers in the lamellae and are exposed to tensile strain and shear stress as a result of the stretching and sliding of the fibers within the lamellae. NP cells also undergo compressive stress and fluid shear stress caused by convective flow of water during loading (Neidlinger-Wilke et al. 2013). The cells of the IVD have been shown to be sensitive to both magnitude and frequency of stimuli, in what is known as a threshold effect (Setton and Chen 2006). For example, static compression (0.4-1.3 MPa) has been shown to promote disc degeneration in a dose-dependent fashion, whereas cyclic loading (0.01- 0.1 Hz) has shown to balance anabolic and catabolic processes within the disc at the same peak stresses (Lotz et al. 2002). Static compressive load has been reported to increase PG and collagen synthesis in IVD cells at low stresses of 0.2-0.4 MPa, and gene expression for matrix proteins is stimulated at stresses even lower than that (~0.1 MPa) (Ohshima, Urban, and Bergel 1995; Chen, Yan, and Setton 2004). Cellular response to hydrostatic pressure is much the same, with an increase in synthesis of collagen, PG, and tissue inhibitor of metalloproteinase 1 (TIMP1) under low to moderate hydrostatic pressures (<0.3MPa), while higher pressures were shown to inhibit PG synthesis and increase nitric oxide (NO) and matrix metalloproteinase 3 (MMP-3) production (Handa et al. 1997; Liu et al. 2001).

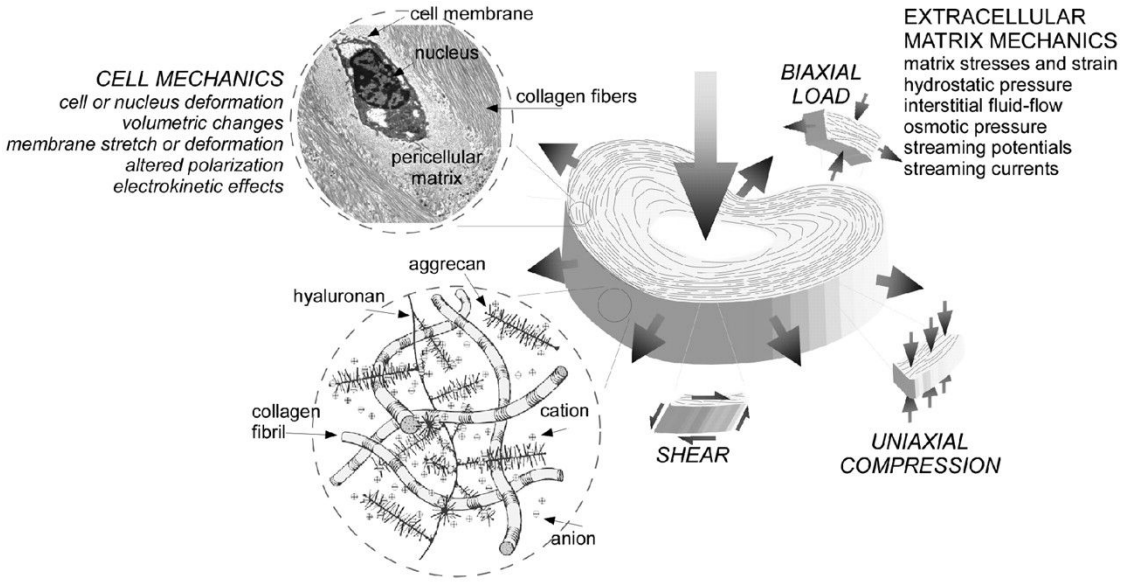

Figure 1.4: Complex physical changes that may be transduced as mechanical stimuli to the cells. Axial compressive loading (represented by the large arrow) of the disc is shown to induce shearing and tensile stresses as well as radial expansion that results in compression in both axial and radial directions. These loads will be distributed to the PG-collagen extracellular matrix (inset, bottom left) and the interstitial fluid phase that undergoes changes in hydrostatic pressure. The physical effects may be transduced from the matrix and contained fluid to cells that re-side in and interact with the extracellular matrix (inset, top left). Adapted from Setton & Chen (2006).

1.4 Development, Aging, and Degeneration

1.4.1 Development of the IVD

During vertebrate embryonic development, the cells of the early embryo arrange into three distinct germ layers, the ectoderm, the mesoderm, and the endoderm, in a process known as gastrulation, and together they give rise to all the various tissues of the body. The mesoderm is the germ layer from which most connective tissues are derived. The mesoderm further separates into subdivisions: the axial mesoderm, paraxial mesoderm, intermediate mesoderm, and lateral plate mesoderm. The notochord develops from the axial mesoderm while somites form from the paraxial mesoderm, and together they go on to form the primitive skeleton. The notochord is a rod-shaped structure in the developing embryo of vertebrates that defines the primitive axis of the

embryo. This notochord eventually becomes segmented and forms the NP (Sivakamasundari and Lufkin 2012; Pattappa et al. 2012; Rodrigues-Pinto, Richardson, and Hoyland 2014).

When the embryo begins to undergo organogenesis, the notochord directs the somites to migrate. Some of these cells differentiate into sclerotome and migrate towards and encircle the notochord and neural tube to begin to form the spine (Rodrigues-Pinto, Richardson, and Hoyland 2014; Pattappa et al. 2012). These cells begin to condense around the notochord, forming a peri-notochordal sheath (Pattappa et al. 2012). Internal pressure within the vacuolated notochordal cells causes the structure to elongate along the midline axis. The sclerotome begins to condense in segmented areas, and will eventually become the AF, while the non-condensed sclerotome forms the cartilaginous precursor to the vertebral bodies and the CEPs. The segmentation and condensation of the sclerotome causes the notochord to segment and expand, forming the NP (Pattappa et al. 2012; Rodrigues-Pinto, Richardson, and Hoyland 2014). Hedgehog signaling is responsible for pattern regulation and cell proliferation in the developing IVD (Sivakamasundari and Lufkin 2012; Risbud and Shapiro 2011; Choi and Harfe 2011; Dahia et al. 2009a). Development of the notochordal sheath depends on this signaling to provide mechanical constraint to the notochord and aid in its segmentation into distinct discs.

Postnatally, the cells of the NP are notochordal in phenotype, being relatively large (~30 μm diameter) and containing large vacuoles which enable the cells to generate a large osmotic swelling pressure within the NP. The matrix of the infant IVD is highly gelatinous, with a clearly demarcated border between the NP and AF. Within 10 years of birth, the IVD undergoes numerous changes in matrix composition and cell phenotype (Raj 2008; Roughley 2004). The NCs decline in number and slowly give way to the more chondrocyte-like NPCs (Rodrigues-Pinto, Richardson, and Hoyland 2014; Dahia et al. 2009b). Furthermore, there is a reduction in cell clusters, which

may have an impact on cell-cell signaling and matrix maintenance (Hunter, Matyas, and Duncan 2003; 2004). How this vacuolated NC population is lost to a smaller, chondrocytic phenotype is still under investigation; elucidation of the mechanism of change might give insight into the process of NP degeneration (Risbud and Shapiro 2011; Chen, Yan, and Setton 2005; Sivakamasundari and Lufkin 2012). Blood vessels which populated the CEP and AF regress in the first two years postnatally as well, minimizing the capacity for nutrient exchange and waste removal, and thus also cell proliferation and matrix production (Nerlich, Schleicher, and Boos 1997). NPCs are adapted to the low oxygen environment; however, buildup of waste increases the concentration of lactic acid, making the IVD, and in particular the NP, a more acidic environment. This acidity enhances proteolytic activity, driving enzymatic breakdown of the matrix (Roughley 2004). While these processes are a normal process of IVD aging, degeneration of the IVD is characterized as an accelerated progression of this breakdown, mediated by an aberrant cellular response (Smith et al. 2011).

1.4.2 Degenerative Pathology

The IVD undergoes enormous physiological changes throughout the aging process. Discs begin to degenerate far earlier than most other skeletal tissues. Signs of structural changes in the lumbar discs of humans can be found as early as 10 years of age; by 50 years, 10% of discs show signs of severe degeneration, and this increases to 60% by 70 years of age (Nerlich, Schleicher, & Boos, 1997; Raj, 2008; Urban et al., 2000). The causes of IVDD can be a multifactorial combination of aging, trauma, and lifestyle influences (high fat diet, smoking) (Adams and Roughley 2006; Hartvigsen et al. 2018). Altered loading, either via injury or aging, is strongly implicated in the degenerative cascade within the IVD. Injury may be dramatic, like disc herniation, or subtle, such as annular fissures. Studies have shown that violation of the AF as small

as a needle puncture can induce degenerative changes as a result of loss of IVD pressurization (Korecki, Costi, and Iatridis 2008; Iatridis et al. 2013). End plate fracture and radial fissures are also subsequent injuries of the IVD that can occur due to degeneration. Altered loading in one disc affects the surrounding tissue as well; osteophytes begin to grow in the vertebrae neighboring the degenerate disc, and ligamentous thickening can contribute to spinal stenosis (**Figure 1.5**).

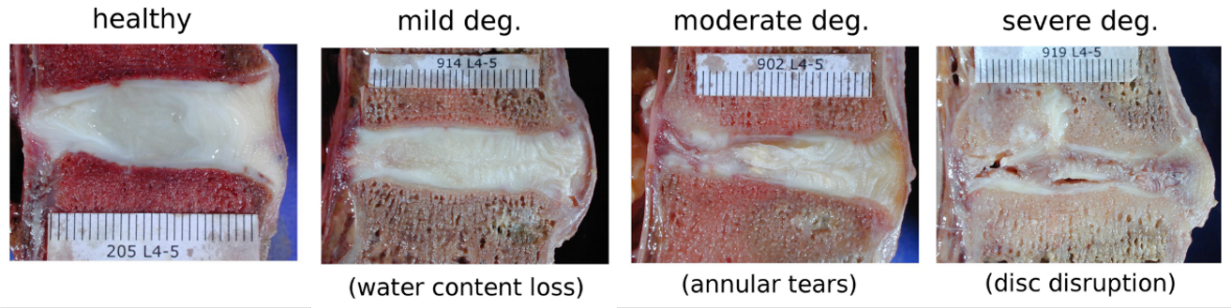

Figure 1.5: Sagittal sections of human lumbar discs in various stages of degeneration.
Adapted from Galbusera et al. (2014).

Change in matrix components are the most characteristic changes, as matrix composition dictates mechanical function. Both normal aging and pathologic degeneration are characterized by a loss of hydration and height. GAG content in the NP at 40-60 years of age is half that of what it was as a toddler; similar trends are seen in progressive stages of degeneration. Loss in % of water content is strongly correlated with loss of sGAGs, and as aging and degeneration progress, the distinction between both sGAG and hydration of the NP and AF blurs (Antoniou et al. 1996). PGs are aggregate molecules made up of sGAGs around a core protein, making a bottle-brush structure, which allows for maximal exposure of negatively charged sulfates for interaction with positively charged ions and water molecules. Aggrecan is the primary PG of the NP as well as AC and is often bonded to hyaluronic acid via link proteins, forming large proteoglycan aggregates. Throughout the aging process, these aggregates break down, reducing the compressive strength of the NP (Sivan, Wachtel, and Roughley 2014). Along with the decrease in hydration, the NP also

becomes more fibrotic, with increasing collagen content. Although type II collagen is the predominant collagen in the NP, it is highest in absolute value/dry weight in the inner AF, giving way to type I collagen in the outer AF; age-related changes see a reduction in type II collagen as well as an increase in type I collagen, further blurring the distinction between NP and AF. Nonenzymatic glycation causes cross-linking of collagens, which stiffens the usually gelatinous material, and further stimulates enzyme and cytokine release in the degenerating disc (Weber et al. 2015; Rodrigues-Pinto, Richardson, and Hoyland 2014). This transition in matrix composition is illustrated in **Figure 1.6**, where the shift in ECM from mostly PGs to increasing collagen is accompanied by the temporal break down of PG aggregates (Roughley, 2004).

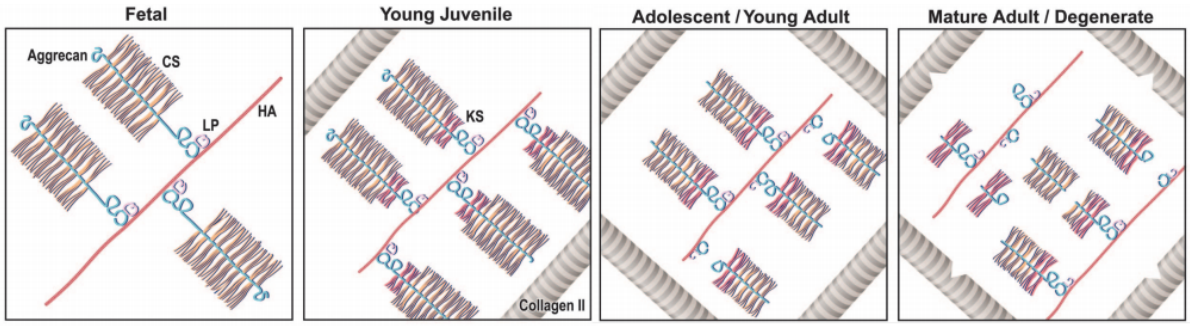

Figure 1.6 Human NP collagen II fibril and aggrecan proteoglycan composition with age.
(CS – Chondroitin Sulfate, KS – Keratin Sulfate, LP – Link Protein, HA – Hyaluronic Acid).
Adapted from Roughley (2004).

In the healthy disc, there is a constant balance of matrix degradation and synthesis by the IVD cells. It is still not clear what causes the phenotypic shift that throws off the balance between the two. Altered loading conditions have been shown to increase the catabolic response of NP cells, with an increased production of matrix metalloproteinase (MMPs), cathepsins, and aggrecanases (Rodrigues-Pinto, Richardson, and Hoyland 2014; Urban, Roberts, and Ralphs 2000). Mechanotransduction is the process by which cells sense mechanical stimuli and convert it to electrochemical activity (Discher, Janmey, and Wang 2005). Given the complex mechanical loads

experienced in the disc, numerous studies have investigated how the cells of the IVD sense and respond to their environment (Fearing et al. 2018; Hsieh and Twomey 2010). Guehring et al. (2010) showed that NCs are less resistant to mechanical loading than NPCs, suggesting that the increased loading during growth and aging may contribute to the disappearance of NPCs. Both integrin binding with the ECM (Gilchrist and Chen 2007; Le Maitre et al. 2009; Nettles, Richardson, and Setton 2004) and cadherin-mediated traction forces between cells (Hwang, Jing, et al. 2014) have been implicated in IVD mechanotransduction. The reduction in cell-cell interactions and subsequent loss of direct cell communication as the NP decreases in cellularity may be associated with further aberrant cell responses to stress. Indeed, the appearance of protrusions from the usually round cell bodies of NPCs may be indicative of cells both responding to increased matrix tension as well as attempting to respond to neighboring cells (Errington et al. 1998; Johnson and Roberts 2003).

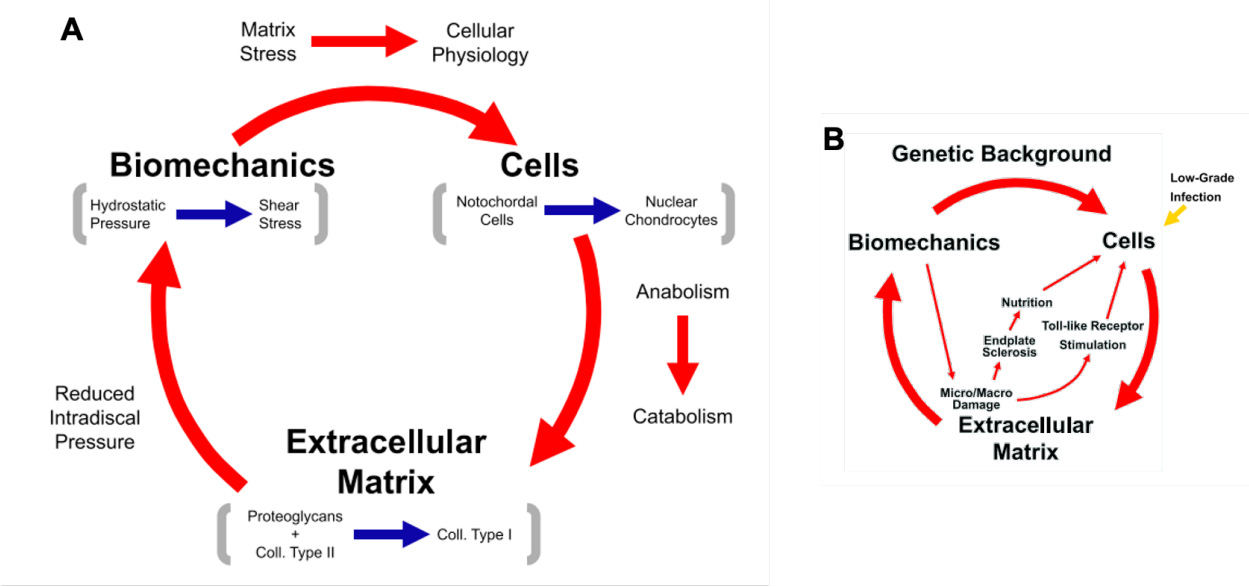

Figure 1.7: The degenerative cycle of IVD degeneration.
A) Homeostasis of the intervertebral disc is dependent on the interaction of cells, extracellular matrix and biomechanical stress, and alterations to the balance at any point can set off a degenerative cascade. B). Additional factors impacting the degenerative cycle including genetic predisposition to IVDD, infection, and alterations in nutrition. Adapted from Vergroesen et al. (2015).

It is becoming increasingly evident that disc degeneration creates a "vicious cycle" wherein cell-mediated catabolism causes fundamental changes in the matrix, which results in altered loads on the IVD, and further stimulates cellular pathology (Vergroesen et al. 2015). Because these factors are connected and amplify each other, researchers have proposed a model wherein these interrelated factors exist in a cycle that can be entered at any point, all leading to the same pathology (**Figure 1.7**).

1.4.3 IVDD Associated Pain

Degenerative changes to the disc are strongly correlated with low back pain (Adams and Roughley 2006). Vascularized granulation tissue extending from the NP to fissures in the AF have been associated with low back pain (Peng 2013). Inflammation has also been linked to symptomatic and painful IVDD (Molinos et al. 2015; Khan et al. 2017). Release of inflammatory cytokines from within the disc has been implicated in painful neural ingrowth into the AF (Ohtori, Miyagi, and Inoue 2018). Additionally, dynamic loading of the IVD has been shown to drive the influx of inflammatory cytokines, such as TNFα, into the disc, furthering cell-mediated degeneration (B. A. Walter et al. 2015; Molladavoodi, McMorran, and Gregory 2020). Non-discogenic sources of pain are also common. Hypermobility of the disc subsequent to degeneration destabilizes the entire spine and requires the local musculature to overwork in compensation (Iatridis et al. 2013; Ohtori, Miyagi, and Inoue 2018). Furthermore, radicular pain and radiculopathy (also known as sciatica) frequently occurs due to spinal stenosis, itself a result of loss of disc height, osteophyte formation, facet joint hypertrophy, and disc herniation (Hartvigsen et al. 2018; Vassilaki and Hurwitz 2014). Interestingly, IVDD is not always symptomatic. Medical imaging in the form of magnetic resonance imaging (MRI) is still the standard mode of identifying IVD injury or degeneration, and usually only called for with symptomatic pain. This presents a

challenge in timing when disc degeneration is addressed, and the conservativeness or aggressiveness of the proposed therapy (Wu, Kim, and Jang 2020; Adams, Stefanakis, and Dolan 2010).

1.5 Current Clinical Repair Strategies

Low back pain is a nearly ubiquitous condition, affecting up to 80% of the world's adult population, and is highly associated with IVDD (Hoy et al. 2014) and results in $134.5 billion in healthcare spending in the US alone (Dieleman et al. 2020); IVDD is implicated in nearly 40% of these patients (Ohtori, Miyagi, and Inoue 2018; L. Zhao et al. 2019). Early non-surgical treatment strategies usually involve pain management via oral analgesics or non-steroidal anti-inflammatory drugs (NSAIDs) and physical therapy (Raj 2008; Adams, Stefanakis, and Dolan 2010). However, discogenic pain is often not noticeable until the disease has progressed considerably. The extent of intervention varies with the severity of the condition (**Figure 1.8**). Intradiscal steroid injections used to suppress inflammation and reduce pain has gone out of favor due to associated chondral degradation, but epidural injections of steroid are still commonly used for pain management and inflammation reduction (Nguyen et al. 2017; Schoenfeld and Weiner 2011). Intradiscal electrothermal annuloplasty (IDEA) and biacuplasty are minimally invasive thermal treatments for radiofrequency ablation of nociceptive nerve ingrowth, but have shown limited efficacy, and are focused strictly on resolving discogenic pain (L. Zhao et al. 2019).

Surgical intervention becomes necessary in the case of severe, unremitting symptoms. Discectomy, or the removal of all or part of the NP, is the most common procedure for symptomatic herniation, but does not replace the NP, and so does not restore disc height or mechanics, leaving the AF vulnerable to further degradation (Kim, Park, and Kim 2009). AF defects are associated with 5-25% of post-operative re-herniation (Ambrossi et al. 2009; Long et

al. 2016; Shepard and Cho 2019). AF closure and repair is performed in cases of high risk for reherniation but the quest for a successful biomaterial AF sealant is still undergoing investigation (Bouma et al. 2013; H. J. Wilke et al. 2013; Thomé et al. 2018; Hom et al. 2019; Likhitpanichkul et al. 2014; Distefano et al. 2020).

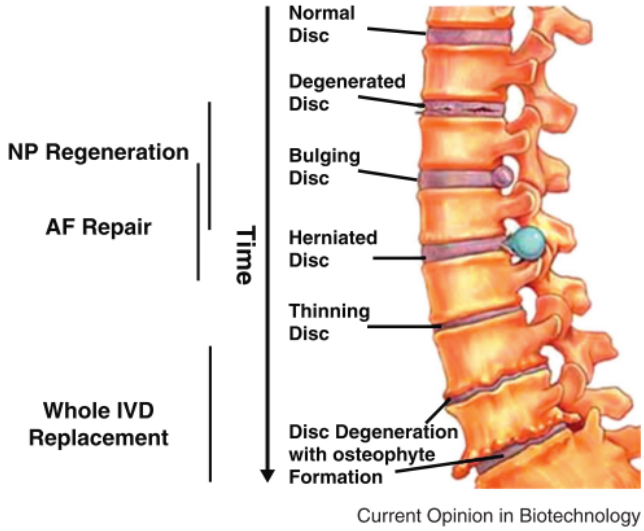

Figure 1.8: Schematic of the progression of IVD degeneration highlighting the traditional timing of interventions.
Adapted from Hudson et al.(Hudson et al. 2013)

Severe degeneration in which the integrity of the AF has been obliterated may be treated by spinal fusion, in which the whole disc is removed, and adjacent vertebral bodies are fused together. These interventions alter the range of motion and consequently negatively impact the mechanics of the adjacent discs (Iatridis et al. 2013; Yang, Langrana, and Lee 1986; Nunley et al. 2013). Prosthetic disc replacement of either the nucleus or whole disc has been explored as an alternative to spinal fusion. NP replacements require the AF to remain intact, while late-stage degeneration may require total disc replacement (TDR) or disc arthroplasty (Brophy and Hoh 2018). The efficacy of TDR is still under consideration; while some studies have shown TDR to be safe and effective, with greater patient satisfaction regarding mobility and short-term efficacy at least equal

to fusion (Bai et al. 2019; Ding et al. 2017), there have been reports of prosthetic induced osteolysis (Serhan et al. 2006).

As the origin of IVD degeneration is generally understood to begin in the NP, repair or replacement of the NP has garnered increased therapeutic interest, with the goal of restoring biomechanics, thereby interrupting the degenerative cascade. Prosthetic implants such as Prosthetic Disc Nucleus (PDN-SOLO, Raymedica, Inc., Bloomington, MN) and NeuDisc™ (Replication Medical Inc., New Brunswick, NJ), fully formed implantable hydrogels, have shown promise in restoring disc mechanics, but do not sufficiently integrate with the complex geometry of the NP void space, and ultimately fail by device migration (Di Martino et al. 2005). DASCOR™ *in situ* forming polyurethane "balloon" showed promise in restoring disc height and motion segment stability, but has a preformed shape that does not integrate with the remaining tissue that surrounds it (Ahrens et al., 2009). Some of these materials have received CE Mark for marketing in Europe but have yet to receive FDA approval due to safety concerns.

Research efforts have increasingly shifted towards biomaterial and regenerative engineering strategies for NP repair. As pre-formed NP replacements have largely failed due to device migration, *in situ* curing injectable materials are increasingly of interest as they can successfully integrate with the surrounding tissue and resist migration and extrusion (Lewis, 2012). Acellular injectable biomaterials focus on the restoration of disc height, mechanics, and hydration, and can also be used to deliver therapeutics directly to the disc for pain management or biological repair (Bowles and Setton 2017). Biologic therapy is an appealing alternative to end-stage surgical treatment, as it attempts to address early and mid-stage degeneration and mitigate further degeneration before the effects become too severe and spread to adjacent structures (Hudson et al. 2013). Such therapies can include drugs or biomolecules to stimulate anabolic repair processes in

the remaining native cells or introduce cells in hydrogel carriers in order to drive tissue regeneration. Current ongoing clinical trials involving both cellular and acellular hydrogels for NP replacement have focused on patients with symptomatic discogenic pain without bulging or herniation (indicating gross AF damage) and moderate loss in disc height (30-50%), as more advanced damage would likely result in extrusion and failure of the implanted material (Amirdelfan et al. 2021; Ceylan et al. 2019). The subsequent sections will thus focus on injectable biomaterial-based strategies for NP replacement and repair.

1.6 Polymeric Biomaterials for Nucleus Pulposus Replacement

Biomaterial replacement of the NP aims to repair the IVD by recapitulating the mechanical behavior of the healthy NP. Hydrogels are a class of biomaterials with high swelling capacity and highly tunable properties. The high water content in hydrogels allows them to behave like many natural soft tissues (Peppas et al. 2006). As such, hydrogels have been investigated for a wide variety of applications, from contact lenses to drug depots and cell scaffolds (Censi et al. 2012; Gaharwar, Peppas, and Khademhosseini 2014; Lin et al. 2021; Muir and Burdick 2021; Anseth, Bowman, and Brannon-Peppas 1996; Kretlow, Klouda, and Mikos 2007) Hydrogels may be synthetic or natural polymers, but they are all characterized as mesh networks swollen with water, much like the proteoglycan rich network of the NP. The ability to form *in situ*, conform to the complex void space in a degenerated or injured IVD and resist migration are all key factors in the design of a potential NP replacement biomaterial. In addition, biocompatibility and long-term stability in an acellular scaffold are necessary if the replacement is to persist in the IVD and restore mechanical function. Biomaterials for cell-based therapies may be biodegradable, and the rate of degradation must be tuned to match the rate of de-novo tissue development to maintain structural stability of the repaired IVD; additionally, the degradation byproducts must not be cytotoxic.

Synthetic hydrogels that have been used include poly(ethylene glycol) (PEG) and poly(N-isopropylacryl-amide) (PNIPAAm) (Yang and Li 2009; Francisco et al. 2014; Thomas et al. 2010). Synthetic polymers are generally bio-inert, in that they do not illicit an immune response. They are also very well controlled as there is minimal variation between batches, and so are easily characterized. While synthetic polymers are usually readily modified and can be delivered with other natural materials, they themselves are not bioactive. Some polymeric scaffolds, like PGA/PLA/PLGA are degradable through hydrolysis of the ester linkages (Sahoo et al. 2008; Jeong, Wang, and Gutowska 2001). Others, such as PEG are not readily degraded, but can be chemically modified to degrade (Vernengo et al. 2008; Zhu 2010; Buxton et al. 2007).

Natural materials include animal-derived molecules that mimic the native structure of or are present in the IVD, such as collagen (types I or II) and hyaluronic acid (Neidlinger-Wilke et al. 2005; Cloyd et al. 2007; Bian, Guvendiren, et al. 2013). Scaffolds have also been produced directly by decellularizing IVD tissue (Liu et al. 2014). Other natural materials have been derived from plant or animal sources, and are chosen based on their similarity to proteoglycans in the NP as well as their ability to create swollen networks, such as chitosan (Sukarto et al. 2012; J. Li et al. 2012), plant-derived agarose, alginate (DiMicco et al. 2007; Chang and Poole 1996; Horner and Urban 2001), methylcellulose and carboxymethylcellulose (Reza and Nicoll 2010a; 2010b; Gupta, Cooper, and Nicoll 2011; Lin et al. 2016; Varma, DiNicolas, and Nicoll 2018), all of which are long-chain polysaccharides. Cellulose, chitosan, and alginate are naturally-derived polysaccharides that mimic the GAGs of the NP, but because they are not animal derived, they resist enzymatic degradation, unlike other natural hydrogels like hyaluronic acid and chondroitin sulfate. This characteristic is important as the degenerate disc space contains an increased amount of matrix metalloproteinases that can degrade animal-derived polymers. Additionally, animal-

derived polymers can be immunogenic. Recently, peptide-based hydrogels have also come into investigation, as researchers use the very building blocks of native tissues to design highly specialized materials for many biomedical applications (Moss et al. 2011; Leckie et al. 2012).

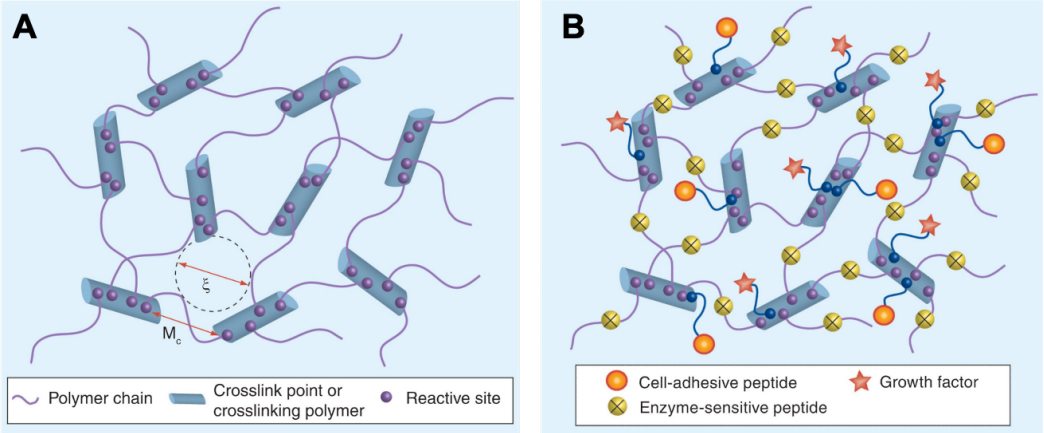

Figure 1.9: Schematic of hydrogel structure.
A) Polymer chains connected at crosslink point or crosslinking polymers. Mc = Number average molecular weight between two adjacent crosslinks, directly related to n (degree of crosslinking). x = mesh size, related to the distance between crosslinks. B) Common hydrogel modifications in tissue engineering including cell-adhesive ligands, enzymatically degradable crosslinks, and immobilized or sequestered growth factors. Adapted from Zhu & Marchant, (2011).

1.6.1 Tunability

Hydrogels are highly tunable platforms in which scaffold stiffness, porosity (and thus permeability), and swelling properties can be easily tuned by molecular weight, macromer concentration and crosslinking density (Zhu and Marchant 2011). The creation of polymeric networks that can swell many times their dry weight is due to crosslinking between macromers. Crosslinks can be physical in nature, mediated by temperature, pH, or ionic stimuli, or chemical, in which permanent covalent bonds are made between macromers. Crosslinking density itself can be modified by adjusting the concentration and size of the macromer, (Jeon et al. 2009; Gupta and Nicoll 2014) or density of functional crosslinking moieties. Crosslinking efficiency is affected by molecular weight as well; longer polymer chains are more likely to form chain entanglements that

can aid or inhibit crosslink formations depending on the type of crosslinking occurring (Ferry 1980). The theory of rubber elasticity states that the strength of a hydrogel increases with increasing crosslinking density, which also decreases the swelling ratio (Flory and Rehner 1943a; 1943b; Rehmann et al. 2017). Swelling ratio and crosslinking density are directly related to the mesh size (ξ) (**Figure 1.9**) (Canal and Peppas 1989), which affects the diffusion of solutes into and out of the hydrogel, as well as influences the movement of cells through the gel (Brazel and Peppas 2000).

Equilibrium swelling behavior is a balance between the elastic properties of the polymer and the water content of the hydrogel. As such, hydrogels are viscoelastic materials with mechanical behavior that is both like an elastic solid and viscous fluid (Anseth, Bowman, and Brannon-Peppas 1996). The NP is a highly viscoelastic structure as well, in that it relaxes and behaves in a fluid-like manner under transient loading, but under dynamic loading it behaves more like a solid (Iatridis et al. 1996). Thus, hydrogels are the ideal class of biomaterials for NP replacement, and polymer choice is dictated only by the extent of control available over each polymer's properties.

1.6.2 Injectability

Of particular interest for NP replacement and IVD repair applications is the delivery mechanism. As mentioned earlier, an ideal NP replacement strategy would be deployed in an IVD where the AF was mostly intact. As such, in order to prevent further violation of the AF and exacerbate the degenerative cascade further, it is necessary that any intradiscal therapeutic be able to be delivered through a fine gauge needle (Korecki, Costi, and Iatridis 2008). Initial viscosity of a material will determine the ease of its delivery. Upon injection, it must begin crosslinking quickly, increasing in viscosity rapidly so as not to extravasate from the injection site, which is critical in the high-pressure disc space. If cells are being deployed within the hydrogel then an

ideal hydrogel would also protect cells from shear-induced damage (Marquardt and Heilshorn 2016; Burdick, Mauck, and Gerecht 2016).

In situ curing polymers that form covalently crosslinked hydrogels upon injection satisfy this description, as they have not gone through their crosslinking reaction prior to injection (**Figure 1.10**). Free-radical polymerization is one of the most common methods for chemical crosslinking and produces strong and highly stable inter-chain bonds. Radical-initiated reactive groups commonly used include acrylate (Buxton et al. 2007), methacrylate (Stalling, Akintoye, and Nicoll 2009; Erickson et al. 2009), methacrylamide (H. Shin, Olsen, and Khademhosseini 2012), and styrene moieties (Chen et al. 2009), all of which contain a vinyl group that is the target of free-radical crosslinking (Muir and Burdick 2021). Photopolymerization, in which an initiator molecule is cleaved by light of a certain wavelength (UV, visible light) to generate the free radical, is widely used, however, does not lend itself to injectable applications due to the limited penetration of light through tissue. Oxidative-reductive (redox) reactions can be used to generate free radicals in injectable systems by separating the two initiators into separate barrels of a dual-barrel syringe and injecting via a mixing tip. As the reaction begins upon mixing, this is a very useful system for injectable applications. Still, the potential cytotoxicity of initiators, and in particular the leaching of unreacted initiators, should be monitored and titrated. Ammonium persulfate (APS) with N,N,N',N'-tetramethylethylenediamine (TEMED) or ascorbic acid are common redox initiators for biomedical applications (Temenoff et al. 2003). Redox initiators can also be used to initiate "click" reactions, named thus because of the speed and specificity of the reactions. Thiol-ene radical crosslinking is one such mechanism that uses dithiol crosslinkers. The most common of these is norbornene, a bridged cyclic hydrocarbon with a vulnerable carbon-carbon double bond (Rehmann et al. 2017). Michael addition crosslinking occurs between thiol-enes without the need

for free-radical initiators. The elimination of redox initiators as a potential source of cytotoxicity makes these excellent crosslinking systems for injectable applications, however, are limited by the need for high macromer concentrations to produce efficient reactions. These reactions can take from seconds to hours, depending on their reactivity, and so the system needs to be tuned to the application (Liang et al. 2016). Tyramine crosslinking is another covalent crosslinking mechanism that lends itself well to injectable systems, where oxidation of the phenol group of tyramine is mediated by the enzymatic reaction between horseradish peroxidase (HRP) and H_2O_2 (Ren et al. 2016).

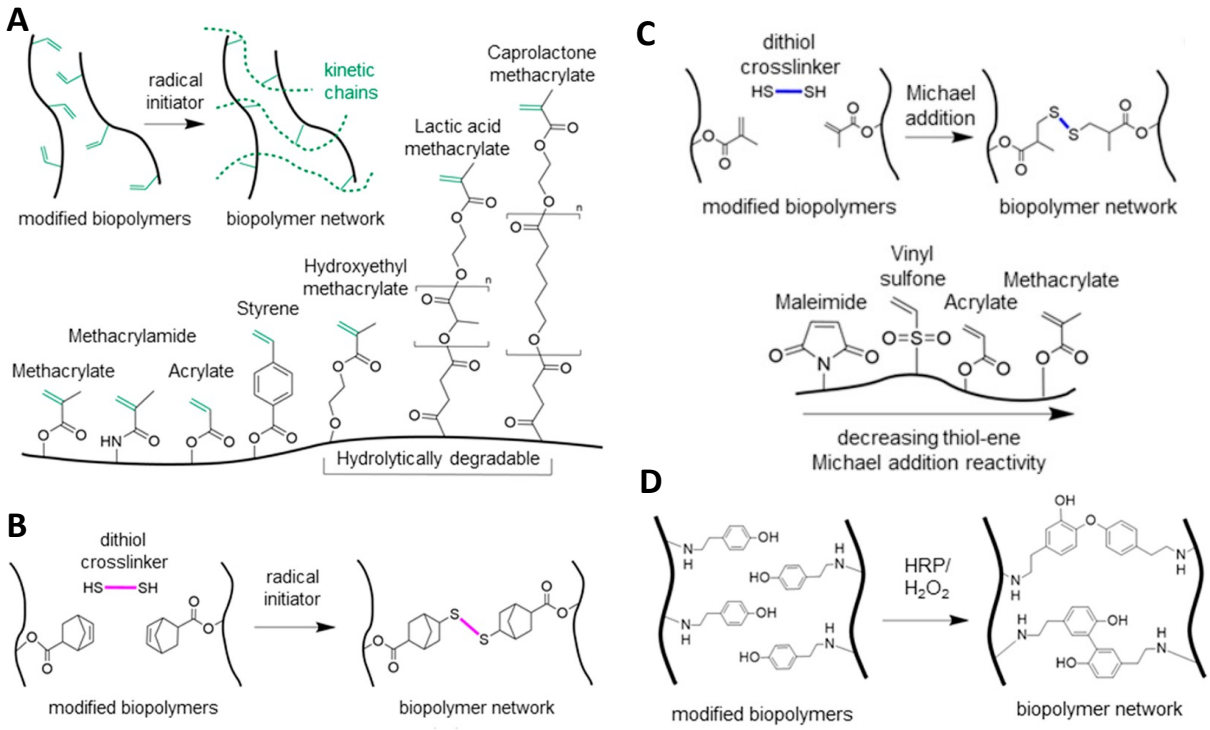

Figure 1.10 Schematic representation of various injectable *in situ* curing chemical crosslinking systems.

A) Free-radical chain polymerization B) Thiol-ene radical addition C) Thiol-ene Michael addition and D) Tyramine-based enzymatic crosslinking. Adapted from Muir & Burdick, (2021).

An alternative to chemical crosslinking systems for injectable hydrogels is physically crosslinked systems. Physically crosslinking hydrogels are stimuli responsive, forming crosslinks in response to changes in temperature, pH, and ionic concentration, which makes them useful for

injection into the body where the environment has very specific cues. Thermogelling polymers are of specific interest for the disc because of their tunable gelation. Although ionic and pH- sensitive hydrogels have been studied in the context of the disc, since the pH and ionic quality of the IVD is highly variable depending on degenerative stage, as opposed to temperature which is relatively constant, they will not be explored here. Thermogelling polymers include naturally- derived chitosan, (Alinejad et al. 2019) and cellulose derivatives including methylcellulose (MC), (Choi et al., 2020) and hydroxypropylmethylcellulose (HPMC), (Buchtová et al. 2018), animal-derived gelatin, (Cheng et al. 2010) and synthetic poly N-isopropylacrylamide (pNiPAAm) (Ji et al. 2009). Thermogelling hydrogel systems exhibit a lower critical solution temperature (LCST) below which the polymers are soluble; as temperature rises above the LCST, the polymers become increasingly hydrophobic. Instead of coming out of solution altogether, the hydrophobic moieties form networks which trap water within the gel (Klouda and Mikos 2008). Tuning thermogelling polymers so that the transition from solution to gel, or sol-gel transition, occurs at or below physiologic temperature (37°C) is ideal for injection into the human body. The reversibility of physical crosslinks has pros and cons. Physically crosslinked hydrogels are more permissive to cell growth and matrix deposition, as their structure can change in response to cells. The most obvious con of physically crosslinked gels is that the crosslinks are reversible and sensitive to deformation. Because of this, physically crosslinked gels alone would not perform well as NP replacements. Physical crosslinking systems can, however, be combined with other systems to form dual-polymer networks (DPN) and dual crosslinking hydrogels, where the thermoresponsive nature of the physical gel works in conjunction with covalent crosslinks to form a stronger gel.

Shear thinning is another material behavior that is highly sought after for injectable applications (Loebel et al. 2017). Materials that exhibit high viscosity or even gel like behavior in

the absence of deformation in shear, but quickly decrease in viscosity with increasing shear rates, hold great appeal for injectable systems. Such materials are less likely to cure and set within a mixing tip or needle upon delivery, and rapidly recover to their original gelled state once the force upon them is removed, a feature known as "self-healing" (Zhang et al. 2020; Yeo and Park 2021). Shear-thinning gels are frequently physically crosslinked, and lack sufficient mechanical integrity as previously mentioned. Therefore, secondary crosslinking is often applied to set the gel once it has been injected in the location and forms the desired shape. These systems are also gaining interest as polymer inks for 3-D printing applications.

Rheology is a critical tool in assessing the viscoelastic properties of materials, and in particular, the injectability and gelation kinetics of crosslinking hydrogels (Chen, Wen, Janmey, Crocker, & Yodh, 2010). Small amplitude oscillatory shear (SOAS) allows for stress and strain to be measured under controlled oscillations, where the complex modulus G^* is given by

$$G^* = \sigma_{max}/\gamma_{max} \tag{1.1}$$

where σ_{max} is the maximum stress and γ_{max} is the maximum strain. Purely elastic materials exhibit maximum stress at maximum strain, where both are in phase ($\delta \rightarrow 0$), and in a purely viscous material, the maximum stress occurs when the strain *rate* is greatest, and stress and strain are out of phase by 90°. Thus, the relationship between the complex modulus and its elastic and viscous components (*G'* and *G"*, respectively) of a given viscoelastic material is given by the relationship in **Figure 1.11**:

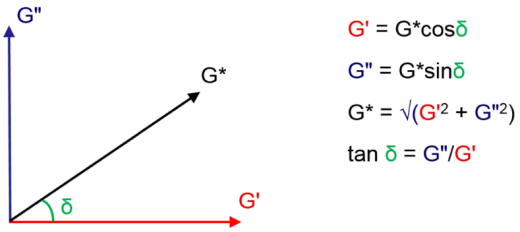

Figure 1.11: Geometric relationship between G* and its components G' and G".
(Malvern Instruments 2016)

This fundamental concept allows us to utilize the rheometer to ascertain a large amount of information, including the complex viscosity, η^*, from its relationship with G^* and the angular frequency ω:

$$\eta^* = G^*/\omega \tag{1.2}$$

The linear viscoelastic region (LVER), or region where stress and strain are proportional, can be determined via strain sweep. The point at which the material begins to yield, known as the yield strain (γ_{yield}), defines where *G'* becomes strain dependent, and is the upper limit of the parameters for where most SAOS testing occurs. Strain sweeps, and the resulting γ_{yield} also determine strain yielding/shear-thinning behavior (Chen et al., 2017; Loebel et al., 2017). Materials that exhibit gradual yielding with increasing strain are more likely to be easily injected than those that "rupture" by exhibiting a precipitous drop in *G'* at higher strains. This rupture indicates that a large shearing force is necessary to achieve material yielding, which likely translates to material bursting forth from the injection needle, and very limited control. While physically crosslinked biopolymers such as agarose and methylcellulose exhibit shear thinning, many biological polymers display strain stiffening and rupture (Zuidema et al. 2014). Cyclic strain tests in which the apparatus is rapidly switched between high and low strain regimes can also be performed to assess shear-thinning behavior. Low viscosity or *G'* measurements at high strains followed by rapid recovery, as well as high viscosity or *G'* values at low strain, indicate not only that the material is shear thinning, but that it recovers quickly and is less likely to extravasate from the injection site once it has exited the syringe.

Throughout these tests, the relationship between *G'* and *G"* is indicative of whether the material is exhibiting mostly elastic or mostly viscous behavior, respectively, as the relationship *G'>G"* is traditionally considered the "gel point." Subsequently, this point also corresponds to the

δ=45°. Rheometry can also be used to determine the kinetics of free-radical polymerization over time (Temenoff et al. 2003; Gold et al. 2014), as well as thermoresponsiveness, both by measuring the response to steadily increasing temperatures (usually at a ramp rate of 1-2°C/min) to determine the temperature at which a polymer rapidly begins to aggregate into a gel (Bain et al. 2012; Nasatto et al. 2015), or to instantaneous thermoresponsiveness by rapidly increasing the platform temperature (usually to 37°C) and holding for a prescribed amount of time to measure the time course of gelation behavior when introduced to physiologic temperatures (Caicco et al. 2013).

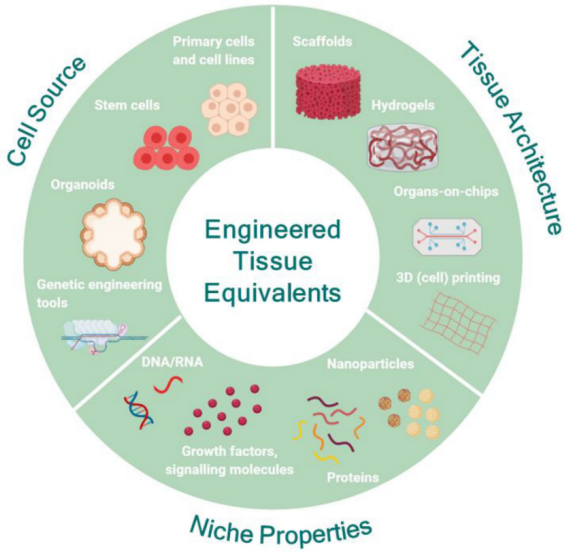

Figure 1.12: The tissue engineering paradigm: Cells, Scaffold (Tissue Architecture), and Signals (Niche Properties).
Adapted from Moysidou, Barberio, & Owens (2021).

1.7 Tissue Engineering and Biological Repair

While acellular biomaterial approaches to IVD repair hold promise for restoring disc hydration and mechanics, biologic therapy is an increasingly appealing alternative to end-stage surgical treatment, as it attempts to mitigate the cause of IVDD before the effects become too severe and spread to adjacent structures. Partial or full NP replacement seeks to rehydrate the disc and restore hydrostatic pressure lost during nucleotomy. The goal of tissue-engineered disc

replacements is not only to restore hydration, pressure, and overall mechanical function, but also biological function, so that the replaced disc can maintain itself.

Tissue engineering aims to combine cells with engineered environments in an attempt to replicate, heal, and/or replace injured or diseased tissues, and thus, is a promising strategy for alleviating the effects of IVDD (O'Halloran and Pandit 2007; Henry et al. 2018; Hudson et al. 2013). Targeting the NP where IVDD begins, tissue engineering strategies attempt to address degeneration before the effects spread irreversibly to the surrounding tissues of the AF, CEP, and adjacent vertebral bodies. Depending on the severity of the disease state, various regenerative approaches may be taken. In early degeneration, direct growth factor delivery may be sufficient to stimulate matrix production in the native cells (Singh, Patel, and Singh 2021). Platelet-rich plasma (PRP) is an appealing therapy utilized by clinicians because it is an autologous treatment that requires little to no manipulation and can be produced quickly, avoiding many regulatory hurdles of regenerative therapies, however, clinical efficacy is highly variable and there is no strong consensus on whether the resultant effects are regenerative or palliative. (Urits, Viswanath, et al. 2019). If the native cells are not responsive, or the existing matrix is too degenerated, a nucleotomy may be performed and the void space may be filled with cells in an engineered scaffold. Both of these treatments depend on the remaining structural stability of the AF; if the AF is damaged and can no longer provide mechanical support to withstand the pressure within the NP, then a whole disc replacement will be necessary, with both NP and AF portions of the IVD engineered (Bowles et al. 2011; Gullbrand et al. 2018). The traditional tissue engineering paradigm is a triad that consists of cells, scaffold, and signals (**Figure 1.12**): the appropriately terminally differentiated cells or stem cells with potential to differentiate to the target cell type must be delivered with a scaffold material to provide structure and mechanical cues, while soluble factors like growth

factors and cytokines, as well as bound factors such as integrin binding peptides can be utilized to further direct cell behavior. The following sections will outline the three traditional components of tissue engineering and the current state of the art of NP tissue engineering.

1.7.1 Cell Source

Cell source is one of the first questions that must be answered when tissue engineering the NP, as the unique characteristics of the cell will dictate what type of environment is necessary to produce a *de novo* healthy NP. Various animal sources of NP cells have been used in *in vitro* and preclinical *in vivo* studies, including rat (Bowles et al., 2011; Maidhof et al., 2012; O'Halloran & Pandit, 2007), and bovine cells (Chou and Nicoll 2009; Reza and Nicoll 2010a; 2010b; Feng et al. 2014). While these cells are useful model systems, development of translational therapeutics has focused on allogeneic and autologous cells. Autologous or cadaveric NP cells have been considered as an option; however, their functionality and availability is problematic. Given that the loss of the large, vacuolated notochordal cells (NCs) and the rise of small, chondrocytic cells in the NP is regarded as a precipitator of degeneration, autologous adult NP chondrocytes are generally not used as a tissue replacement. Conversely, NCs are known to regulate NP matrix early in life and are an appealing option, however, cell density in the native disc is so low that harvesting enough cells to expand in culture and produce a clinically viable tissue-engineered construct is difficult. NCs almost entirely disappear from the human NP by 10 years of age, which also contributes to the problem of acquisition of cells (Chen, Yan, and Setton 2005). Still, NCs, and NC-conditioned media have been shown to promote NP matrix elaboration in other cells in co-culture, which may be useful for *in vitro* organ development (Korecki et al. 2010; Aguiar, Johnson, and Oegema 1999).

Significant developments in stem cell research make such progenitor cells an appealing choice for NP tissue engineering. Potential sources of stem cells include induced pluripotent stem cells (iPSCs) (Tang et al. 2018) and adult mesenchymal stromal cells (MSCs). Embryonic stem cells (ESCs) from animal sources are available for study, however, human embryonic stem cells are difficult to obtain and face ethical and political challenges for use (Urits, Capuco, et al. 2019). Autologous adult MSCs have shown promise in differentiating into NP-like cells (Gou et al. 2014; Risbud et al. 2004; Steck et al. 2005). These multipotent, non-hematopoietic progenitor cells have proven ability to differentiate into all connective tissue lineages, and are easily harvested from a patient, either from bone marrow (Zhang et al. 2021; Gupta and Nicoll 2014) or adipose tissue (Zhu et al. 2019; Minogue et al. 2010), and expanded in culture.

Recently, a subset of mesenchymal stem cells within the IVD have been identified, showing nearly identical differentiation capabilities as bone marrow-derived MSCs (all except adipocytes) (Blanco et al. 2010; Henriksson et al. 2009). Although the population is likely too small to harvest and use for tissue engineering, they do have the potential for direct stimulation by growth factor delivery in the early stages of disc degeneration, as well as being target cells for cell-homing strategies that use diffusion of growth factors to induce chemotaxis, such that the local stem cell population will populate a cell-free scaffold themselves (Illien-Jünger et al. 2012; Sakai and Grad 2015).

Identifying the phenotype of the cells chosen for the tissue engineering construct is critical in determining the success of the biological therapy. Many attempts have been made at identifying NP specific gene and protein markers. The primary matrix components of the NP are similar to those of AC, namely proteoglycans (in particular, aggrecan) and type II collagen, although the proportions of proteoglycan to collagen (as well as total water content) differ. NP cells and AC

cells both highly express *COL2A1, ACAN,* and *SOX9*. Minogue et al. (2010) explored gene expression in NP and AC cells and identified a number of NP positive and NP negative (AC positive) genes. The NP-positive genes were *PAX1, FOXF1, HBB, CA12,* and *OVOS2;* the AC-positive genes were *GDF10, CYTL1, IBSP,* and *FBLN1*. Lee et al. (2007) found that in rat NP, annexin A3, glypican 3 (*GPS3*), keratin 19 (*K19*), pleiotrophin (*PTN*), and vimentin (*VIM*) were expressed significantly more than in the AF and AC, while cartilage oligomeric matrix protein (*COMP*) and matrix gla protein (*MGP*) were higher in AC than NP; they did note, however, that there were no clear "on/off" markers to distinguish NP from AF or AC cells. Lv et al. (2014) reviewed many different studies on phenotypic markers in multiple species and concluded that N-cadherin (*CDH2*) and keratin 19 (*K19)* are potential NP markers, as they distinguish healthy NP from AF, AC, and degenerate NP. Although these and other genes have been described as NP markers because they identify NPCs in non-human species, Thorpe et al. (2015) have cautioned that KRT-19, KRT-18, CD24 and laminin genes, LAM-5 and LAM-11, do not distinguish between NPC and AC cells in humans. Gene expression is a useful tool in determining cell differentiation and lineage, however, protein expression has more direct functional application, as it is not only indicative of successful transcription of the genes but results in gross biological and mechanical changes in the tissue.

1.7.2 Growth Factor Delivery

When engineering new tissues, and particularly when using stem cells, growth factors are often necessary to direct cells towards the appropriate phenotype. These factors may influence the production of matrix molecules, decrease the production of catabolic enzymes, or a combination of both effects (Yang and Li 2009). Many of the growth factors used in engineering NP tissues are from the transforming growth factor-β (TGF-β) superfamily, including TGF-β1, TGF-β3, and bone

morphogenetic proteins-2, -7 and -12 (BMP-2, -7, -12) (Li et al. 2017), as well as others, such as insulin-like growth factor 1 (IGF-1) (Chon et al. 2013; Shim et al. 2016), and growth/differentiation factor-5 (GDF-5) (Yang and Li 2009; O'Halloran and Pandit 2007; S Chen et al. 2019). In particular, numerous studies have utilized TGF-β1 and TGF-β3 to differentiate stem cells towards a chondrogenic and NP-like phenotype *in vitro* (Steck et al. 2005; Cox et al. 2014; Gupta, Cooper, and Nicoll 2011). Studies have shown that short term TGF-β3 treatment of encapsulated bone-marrow derived MSCs was sufficient to promote long-term differentiation and tissue maturation (Steck et al. 2005; Cox et al. 2014; Gupta, Cooper, and Nicoll 2011). Long-term efficacy of growth factor stimulation and delivery is limited, however, due to their short half-lives (Wang et al. 2017). Growth factor stimulation has been shown to be critical for the differentiation of encapsulated hMSCs; in the absence of growth factor stimulation, cells fail to clearly differentiate and synthesize new matrix (Madry et al. 2014; Johnstone et al. 2013; Gupta, Cooper, and Nicoll 2011). Various delivery vehicles have been developed to protect and prolong the bioavailability and bioactivity of growth factors for tissue engineering, with a particular focus on *in vivo* translation.

In vivo, exogenous growth factor supplementation is not feasible, and so growth factor delivery mechanisms must be utilized to supply growth factors with the injectable scaffold material and sustain their bioavailability long enough to direct stem cell differentiation. Prolonged growth factor delivery can be difficult to control and expensive to maintain. Direct loading of growth factors into hydrogels usually results in a burst release due to the rapid influx of water into the hydrogel pushing out the payload (Lin and Metters 2006; Silva et al. 2009). Sequestration or delivery of growth factor remains an area that many are attempting to address through such methods as modification of the scaffold material via covalent tethering (Mann, Schmedlen, and

West 2001; Schneider et al. 2019; McCall, Luoma, and Anseth 2012), encapsulated microparticles (Holland, Tabata, and Mikos 2003; Bian et al. 2011), and affinity-based sequestration (**Figure 1.13**) (Benoit and Anseth 2005; Tae et al. 2006; Bian et al. 2011; Lee, Silva, and Mooney 2011). Covalent immobilization of growth factors or growth factor mimics can lead to sustained signaling, but can be susceptible to hinderance by steric factors, or conversely can provide permanent stimulation, which is not always desirable (Mann, Schmedlen, and West 2001). Secondary carriers such as microparticles have also been used in growth factor delivery, however, this approach requires multiple steps for particle and hydrogel preparation, and presents a less direct route for delivery since the factor must be released from the microparticles to reach encapsulated cells, potentially delaying stimulation (Bian et al. 2011).

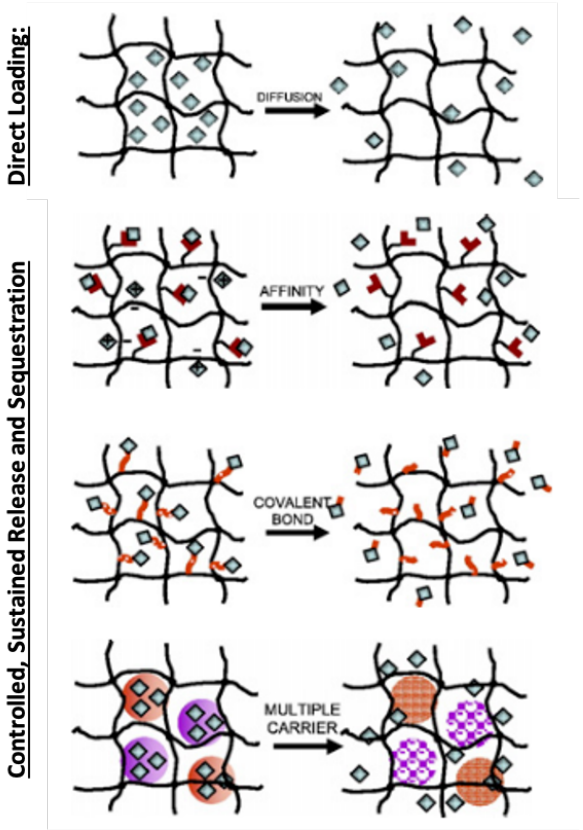

Figure 1.13: Schematic representation of growth factor delivery mechanisms from hydrogels. (Blue squares represent growth factors). Adapted from Censi et al. (2012).

Affinity-based growth factor sequestration is a promising method that utilizes affinity between molecules to attract and reversibly bind growth factors. These affinity molecules can be ligand mimetic peptides, guest-host interactions (cyclodextrin), or more fundamental intermolecular attractions like Van der Waals forces, hydrogen bonding, electrostatic and hydrophobic interactions (Wang & Von Recum, 2011). Electrostatic interactions are one such affinity sequestration mechanism of particular interest because it mimics the natural behavior of the native ECM. Specifically, negatively charged sulfates on GAGs, such as heparin and chondroitin sulfate, are known to act as depots for charged growth factors, maintaining their availability and prolonging their activity, with some growth factors showing greater resistance to proteolysis and thermal denaturation when bound to heparin or heparan sulfate (McCall, Lin, and Anseth 2011; Soares Da Costa, Reis, and Pashkuleva 2017). Heparin-based growth factor delivery systems have been investigated due to the affinity of many growth factors such as BMP, bFGF, and TGF-β to heparin, thus enabling sustained release of the encapsulated growth factors (Jeon et al. 2011; Lei, Trevino, and Temenoff 2016; Lei et al. 2014; Nie et al. 2007; Liang and Kiick 2014; Hachim et al. 2019).

Scaffolds that mimic the sulfation of native matrix GAGs by artificially incorporating sulfate groups have also been investigated (Purcell et al. 2014; Feng et al. 2017; Hintze et al. 2012; Yan et al. 2018; Portocarrero Huang et al. 2017; Waghmare et al. 2018). Sulfated alginate gels have shown to sequester heparin-binding proteins bFGF, VEGR, IGF and TGF-β1 (Freeman, Kedem, and Cohen 2008; Re'em et al. 2012). Many of these artificially sulfated polymers have been referred to as "GAG mimetics" as they aim to mimic highly sulfated GAG-rich matrices in a controllable fashion (Arslan, Guler, and Tekinay 2016; Sivan et al. 2014). These studies utilize SO_3-dimethyl formamide complexes, pentosan sulfates, carbodiimide chemistry with sulfuric acid,

and other mechanisms for covalently sulfating the base polymer (Hintze et al. 2012; Frith et al. 2013; Freeman, Kedem, and Cohen 2008).

1.7.3 Biomaterials for NP Tissue Engineering

Biomaterials under consideration for tissue engineering of the NP must satisfy the same requirements as acellular NP replacement biomaterials (injectability, *in situ* gelling, and swelling and mechanical properties matching the healthy NP) as described earlier in section 1.6. In addition, there are a number of considerations specific to carrying and supporting cell differentiation and tissue growth (Huang, Hu, Li, & Luk, 2018). Firstly, cytocompatibility of the material must extend beyond not releasing cytotoxic factors (the response to which is noticeable within 24-72 hours) but should promote cell survival and differentiation. Proliferation is often seen as a marker of cell health, however, studies have shown that proliferative phenotypes are different than "biosynthetic" phenotypes that lay down matrix, so increasing cell number may not be indicative of biomaterial success (Strehl et al. 2002). Secondly, ideally the scaffold should break down at a rate concurrent with matrix deposition by the cells, such that mechanical integrity of the construct is not lost, but void space is created within the gel to be permissive for neomatrix elaboration (Bryant and Anseth 2003; Chung et al. 2009).

Integrin binding moieties like RGD (fibronectin derived) or direct conjugation of cell attachment matrix proteins (like laminin) have been utilized to harness the cell's responsiveness to its environment (Bridgen et al. 2017; Francisco et al. 2013). Immature NP cells preserve their phenotype and matrix-production on soft gels (Hwang, Chen, et al. 2014). Similarly, studies with both NPCs and hMSCs in chemically crosslinked carboxymethylcellulose (CMC) yield better results in NP gene expression and matrix elaboration on softer substrates, even in the absence of any cell-binding sites (Reza and Nicoll 2010a; Gupta and Nicoll 2014; Lin et al. 2016). Hyaluronic

acid and type II collagen-based hydrogels have been studied extensively for NP tissue engineering, as they are found natively in the NP, and provide an excellent mimic for the native tissue that promotes NP-like differentiation (Calderon et al. 2010; Cloyd et al. 2007). However, because they are animal derived and specifically found in the NP, these materials are susceptible to enzymatic degradation, which is upregulated in the degenerative disc. Hydrogels composed of alginate, a natural polysaccharide derived from kelp, have also shown the ability to support NP-like matrix elaboration (Chou and Nicoll 2009; Bron et al. 2009). Nevertheless, these ionically crosslinked gels are not mechanically stable enough for long-term culture, and certainly less so for *in vivo* application. Synthetic materials have also been investigated for NP tissue engineering, although less so than naturally derived substrates. Synthetic hydrogels that are designed with hydrolytically degradable portions in particular, like poly(lactic-co-glycolic acid) (PLGA) have shown promise as they are permissive to NP-like matrix elaboration, although they are otherwise "bioinert" in that they do not directly interact with encapsulated cells (Fraylich et al. 2010).

As stated in earlier sections, injectability is a critical factor for both acellular biomaterial and cell-based NP replacement materials. Injectability in the IVD possesses a unique challenge, not only because delivery must be through a fine gauge needle, but because the IVD and NP void space are naturally high-pressure regions, and the void space created by nucleotomy is irregular, all of which puts the injectable at risk for extravasation. This not only directly leads to failure of the NP replacement but can have deleterious effects to neighboring tissues *in vivo*. It is critical that "injectable" systems that pass injectability tests in the laboratory be validated, either *in vivo* or in *ex vivo* motion segment models. Work in our lab has shown very promising results for NP-like differentiation and matrix elaboration in soft, CMC-based hydrogels (Reza and Nicoll 2010b; Gupta, Cooper, and Nicoll 2011; Gupta and Nicoll 2014; Lin et al. 2016). Recently, we were able

to transition the photocrosslinked CMC hydrogel system to one that polymerizes *in situ* without the need for ultraviolet light exposure using a redox-initiated crosslinking system with APS/TEMED in dual-barrel syringes (Varma, DiNicolas, and Nicoll 2018). These scaffolds showed robust and uniform distribution of NP matrix components Col II and sGAGs. However, preliminary *ex vivo* motion segment studies showed that despite redox-initiated polymerization and rheological studies that indicated rapid gelation, the viscosity of the gel did not increase enough to resist extravasation from the disc upon injection. CMC was mixed with MC in order to combine the high swelling capacity of CMC and the intrinsic thermogelling capacity of MC to form an *in situ* gelling acellular NP replacement that restored disc height and range of motion (Varma et al. 2018). However, the effective macromer concentration of this system is 6%, which is far from the low macromer concentrations that are most permissive to cell differentiation (1.5-2%). Thus, future work aims to shift the development of this cellulose-based hydrogel system, such that it maintains the ability to support cell differentiation and matrix production, while also providing translational potential of an *in situ* forming hydrogel.

1.7.4 Cellulosic Biomaterials

Cellulose is a naturally occurring polysaccharide and is the most abundant polymer on earth (Klemm et al. 2005). It is renewable and biodegradable, making it an ideal biomaterial in the age of sustainability. It is also easily chemically modified and is highly tunable, making it an ideal material for biomedical applications (Fox et al. 2011; Kamide 1977). Cellulose is primarily derived from the cell walls of plants but can also be synthesized by bacteria and tunicates (Klemm et al. 2005; Gorgieva and Trček 2019). Consisting of repeating β(1,4) linked D-glucose units, each glucan ring has 3 hydroxyl groups, which allows for strong hydrogen bonding between cellulose chains. The hydrogen bonding makes cellulose resistant to dissolution in water and many other

organic solvents. However, cellulose can be solubilized in ionic solutions and processed by means such as casting, molding, or electrospinning. Degree of polymerization (DP), or the number of repeating monomeric units, is highly dependent on source, and can affect the mechanics and viscosity of the polymer solution (Klemm et al. 2005).

The three hydroxyl groups on each glucan unit can easily be substituted with functional groups, changing the solubility of the polymer, and making it suitable for a variety of applications in biomedicine. Esterification of the hydroxyl groups is a common modification that results in a number of cellulose derivatives that have widely been used as biomaterials (**Figure 1.14**) (Fox et al. 2011). Methylcellulose (MC) is the simplest of these derivatives, in which hydroxyl groups are replaced by methoxy groups (Desbrières, Hirrien, and Ross-Murphy 2000; Nasatto et al. 2015). These methoxy groups create hydrophobic regions within the cellulose polymer while still rendering it water soluble (Nasatto et al. 2015; Haque and Morris 1993). The result is a thermosensitive polymer that can form reversable, physically crosslinked hydrogels upon heating. The addition of ionic salts and other components in solution can be used to tune the thermogelation temperature of MC, making it useful for injectable systems that go from lower ambient temperatures to physiologic temperatures (Caicco et al. 2013; Gupta, Tator, and Shoichet 2006; Zheng et al. 2004). Hydroxypropyl methylcellulose (HPMC) displays similar thermoresponsiveness that varies depending on the percentage of methoxyl and hydroxypropyl substitutions (Joshi 2011). CMC is another cellulose ether in which hydroxyl groups are replaced by highly negatively charged carboxylmethyl groups (Ogushi, Sakai, and Kawakami 2007; Reeves et al. 2010). The increased negative charge makes CMC highly hydrophilic, and an excellent material for applications in which a high affinity for water is critical. CMC is highly sensitive to pH and ionic concentration, which results in tunable swelling behavior. All these cellulose ethers

are commonly used in the pharmaceutical and food industries, are biocompatible and are FDA approved for several biological applications. Cellulose sulfates (CS) have also been investigated, both for their highly anionic character, like CMC, as well as their similarity to sulfated glycosaminoglycans found in many animal tissues (Wang et al. 2007; Zhang, Lin, and Yao 2015; Portocarrero Huang et al. 2018; Portocarrero Huang et al. 2017)

Cellulose microparticles are another form of cellulose that have also recently gained interest for biomaterial applications. They include microfibrillated and nanofibrillated cellulose (MFC and NFC, respectively), and cellulose nanocrystals (CNC). MFC and NFC are cellulose microfibers formed by defibrillation of plant cellulose and are noted to possess high stiffness and strength (Borges et al. 2011; Eyholzer et al. 2011). CNC is formed via acid hydrolysis of naturally occurring crystalline cellulose fibers (Bhat et al. 2019). The resulting material consists of rod-like crystals with unique rheologic properties. CNC is comprised of an isotropic suspension that then forms a liquid crystal structure depending on concentration, and is highly dependent on temperature, ionic strength, and pH of the solution (Qiao et al. 2016). Micro- and nano-celluloses can be used on their own or can be incorporated into hydrogels and other biomaterial matrices in order to increase their physical properties (McKee et al. 2014; Stevanic et al. 2012; Haghpanah et al. 2013; Dai et al. 2019; Markstedt et al. 2015; Bhat et al. 2019).

Cellulose-derived biomaterials have been used for a variety of applications, such as soft tissue fillers (Varma et al. 2014; Gold et al. 2015; 2014), ophthalmic lubricants, and hemostats (Lewis et al., 2013). In addition to its tunability, cellulose is not enzymatically degradable by the human body, as humans do not naturally produce cellulose or the enzyme that degrades it (i.e., cellulase). This creates the potential for continuous structural support but may be undesirable in the case of tissue engineering solutions where the scaffold should eventually degrade at the approximate rate

of new tissue development. The introduction of functional groups can tune cellulosic susceptibility to hydrolytic degradation. Bacterial cellulose (BC) has become increasingly popular for various biomedical applications. Cellulose fibers formed by bacteria, particularly those formed by the genus *Acetobacter,* have high appeal due to their superior purity (they are not associated with other substances such as hemicellulose or lignin which are present in plant sources) and are able to achieve a much higher DP than plant cellulose, resulting in greater crystallinity as well as increased mechanical properties (Rajwade, Paknikar, and Kumbhar 2015).

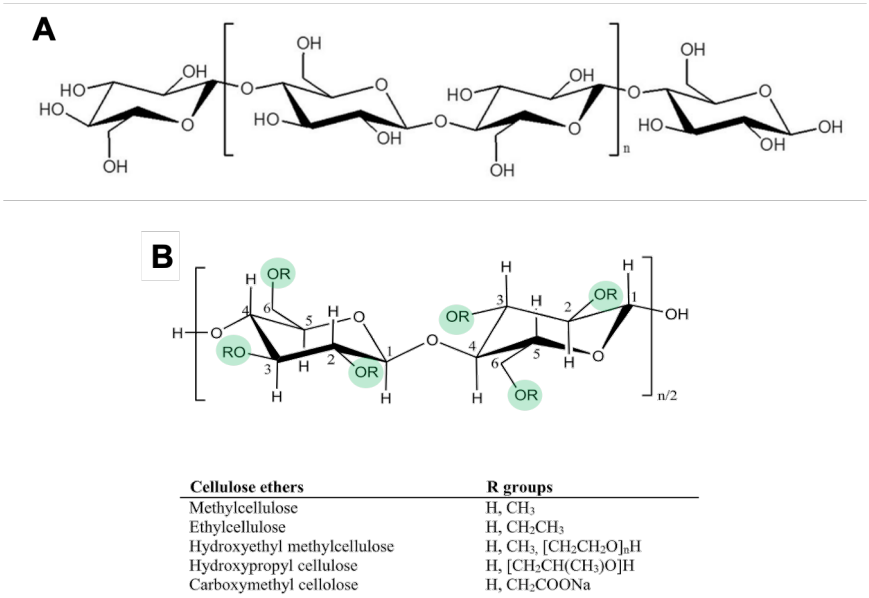

Cellulose ethers	R groups
Methylcellulose	H, CH_3
Ethylcellulose	H, CH_2CH_3
Hydroxyethyl methylcellulose	H, CH_3, $[CH_2CH_2O]_nH$
Hydroxypropyl cellulose	H, $[CH_2CH(CH_3)O]H$
Carboxymethyl cellolose	H, CH_2COONa

Figure 1.14: A) Cellulose and B) its ether derivatives.
Available locations for ether modifications highlighted in green. Adapted from Kabir et al. (2018).

The variety of sources, chemical and physical modifications, and micro- and nano- structures of cellulose make it an ideal material for a wide range of biomedical uses, including for IVD repair (Klemm et al. 2005; Courtenay, Sharma, and Scott 2018).

1.7.4.1 Cellulosics for Disc Repair – Acellular Biomaterials

Several forms of cellulose are being used to develop cell-free, structural reinforcement to the IVD, especially for early stages of the disease and post microdiscectomy. Acellular repair or

replacement of IVD tissue is a promising approach that faces much fewer regulatory hurdles than cell-based tissue engineering. These strategies focus on the mechanical strength of the material, their durability over repeated cycles of physiological loading and resistance to herniation during complex loading.

Borges et al. (2010, 2011) developed composite photocrosslinked hydrogels containing Tween 20 trimethacrylate, N-vinyl-2-pyrrolidone, and nanofibrillated cellulose (NFC) and assessed the gelling behavior, compressive mechanical properties, and swelling behavior along with the morphology and biocompatibility. Here, NFC was chosen as a component of the composite hydrogel due to its high water retention value as well as its previous use as a reinforcing additive in other polymer matrices. Inclusion of 1.6 wt% of NFC led to a 30-fold increase in the compressive strength of the hydrogels. However, despite NFC having a high water-retention value, it actually resulted in a lower swelling ratio compared to hydrogels without NFC included. To address this, the same group created carboxymethylated NFC (c-NFC), introducing negatively charged carboxymethyl groups to increase the hydrophilicity of the composite hydrogel. Increasing degree of carboxymethylation resulted in shear thinning behavior by the hydrogel mixture, which is promising for injectable applications. Swelling ratio increased within each concentration of NFC added, however, none were able to achieve the swelling ratio of the hydrogels without c-NFC. Similarly, static compression showed that while the addition of NFC increased compressive modulus of the hydrogels, carboxymethylation reduced the modulus within a respective % NFC, likely due to the same loosening of the polymer network. A dynamic compression protocol comprised of cyclic compression between 0.5-1 kPa using a testing protocol mimicking a 16-hour workday. Here, gels with NFC demonstrated highest stiffness and percent recovery post testing (Eyholzer et al. 2011).

More recently, similar implant strengthening behavior of NFC was also delineated in an *ex vivo* bovine motion segment model using polyethylene glycol dimethacrylate (PEGDMA) hydrogels (Khoushabi et al. 2015; Schmocker et al. 2016; Karami et al. 2018). Photopolymerized PEGDMA hydrogels were reinforced with NFC, increasing the stiffness 2-3.5-fold without compromising the toughness. The high crystallinity and aspect ratio of NFCs provided mechanical reinforcement to the hydrogels while lowering gelation time. Additionally, *ex vivo* biomechanical assessment of NFC-chitosan hydrogels implanted in porcine discs demonstrated disc height restoration along with relaxation parameters similar to native IVD (Doench et al. 2018). Currently, these NFC-chitosan gels form over an hour, which limits their ability to gel *in situ* for minimally invasive IVD procedures. Another interesting nano-sized form of cellulose consists of cellulose nanocrystals, which were recently tested in ionically crosslinked gellan gums for AF repair. Similar to NFCs, the nanocrystals increased hydrogel stiffness and complex modulus while also aiding the gelation process. However, the gelation kinetics of this platform is slow, requiring close to 10 minutes to obtain fully formed hydrogels. Further, degradation studies indicated poor stability of the gels, with 15% mass loss in 30 days of incubation in PBS (Pereira et al. 2018).

CMC, a cellulose ester with high water absorbing capacity due to the substitution of anionic carboxyl groups for some of the hydroxyls on the cellulose backbone has been methacrylated to allow for free-radical crosslinking of the polymer chains resulting in hydrogels with tunable material properties (Varma et al. 2014; Gupta, Cooper, and Nicoll 2011). Recently, the Nicoll lab has combined methacrylated CMC with thermosensitive MC to obtain thermogelling, injectable, redox-polymerized hydrogels capable of forming rapidly (within 4 min.) *in situ,* with swelling and compressive mechanical properties akin to native NP tissue (Varma et al. 2018). Cyclic compressive loading of bovine motion segments injected with CMC/MC hydrogels restored a

range of compressive biomechanical parameters to healthy values, including the disc height, range of motion and neutral zone parameters. Additionally, fatigue testing of this formulation in bovine motion segments revealed that the CMC/MC hydrogel improved fatigue endurance of the discs compared to the injured condition, but performed similar to the nucleotomy control group, a clinical standard for IVD herniation. Although, the implanted and nucleotomy groups presented similar herniation risks during the failure test, a majority of the failure parameters (failure strength, subsidence to failure and stiffness) were similar between the implanted and intact discs (Lin et al. 2019).

1.7.4.2 Cellulosics for Disc Repair – Cell-based Strategies and Tissue Engineering

While biomaterial-based acellular replacements may be able to relieve pain and partially restore mechanical functionality of the spine, lack of cells limits their use for biological repair of disc tissue. Therefore, in the long run, a cell-based therapy may serve as a better solution for disc degeneration (O'Halloran and Pandit 2007; Yang and Li 2009; Hudson et al. 2013). Roughley et al. (2006) explored a composite hydrogel containing chitosan, glycerophosphate, and hydroxyethyl cellulose (HEC) for its potential as an NP tissue engineering scaffold. These hydrogels with encapsulated disc cells showed deposition and retention of GAGs. To the best of our knowledge, we are the only group to have successfully demonstrated the use of cellulose as the primary scaffold material for NP tissue engineering. Reza and Nicoll (2010a) demonstrated that photocrosslinked carboxymethylcellulose hydrogels can support NP-like matrix elaboration by encapsulated bovine NP cells, thus establishing CMC as a promising biomaterial for NP tissue engineering. Gupta et al. (2011) further explored the utility of photocrosslinked CMC hydrogels for the encapsulation of human mesenchymal stem cells (hMSCs). These cells showed NP-like differentiation under TGF-β3 treatment, as determined by assessment of gene expression and

relevant matrix macromolecular deposition. Furthermore, the resulting tissue engineered constructs possessed compressive mechanical properties similar to that of the human NP. That study was a critical step forward as hMSCs are a more clinically relevant cell source compared to either autologous or allogeneic NP cells. In subsequent studies, our group evaluated the impact of photocrosslinked CMC scaffold composition and TGF-β3 exposure duration on the NP-like differentiation of encapsulated hMSCs, further elucidating scaffold microenvironmental effects on hMSCs, leading to improved CMC hydrogel systems (Gupta and Nicoll 2015; Lin et al. 2016; Gupta and Nicoll 2014). As UV light has limited tissue penetration, photocrosslinking restricts clinically relevant, minimally-invasive delivery of CMC hydrogels. Thus, the Nicoll group has recently been exploring redox-initiated crosslinking in CMC hydrogels to achieve *in situ* gelation with an injectable material, moving closer to clinical translation. (Varma, DiNicolas, and Nicoll 2018) successfully demonstrated that redox-polymerized CMC hydrogels support NP-like differentiation of encapsulated hMSCs, leading to relevant matrix deposition and functional mechanics *in vitro*.

Successful tissue engineering of whole IVDs will be a big step forward in the spine field, especially for patients who present late stage IVDD requiring full discectomy. The angle-ply architecture of the AF and integration of the inner AF to the NP are largely responsible for maintaining the disc pressure, height and preventing herniation of the NP in healthy discs, however, this complex structure is challenging to replicate in tissue-engineered constructs. Yang et al. (2018) presented an interesting approach to tissue engineer whole IVDs by micropatterning bacterial cellulose to re-create the angle-ply structure of the AF, further rolling the cellulosic sheets embedded with AF cells, and combining a central collagen gel to create disc-shaped organs. Integration of these tissue-engineered units with native tissue was evaluated *in vivo* in rat tails. The

resulting 3-month data demonstrated successful integration and inter-lamellar neo-tissue formation along with disc height and mechanical strength similar to native, healthy discs. This study utilized micropatterning to achieve aligned cells and matrix components - a novel, scalable approach to obtain tissue-engineered whole IVDs. Although successfully demonstrated in animal studies, the isolation and use of healthy human AF and NP cells poses several challenges, which can be countered by using adipose or mesenchymal stem cells. In addition, this strategy is also dependent on successful delivery of growth factors, either via scaffolds or gene-delivery. Growth factors, such as GDF-5, TGF-β1, are some of the most studied proteins for NP differentiation and identified as critical to sustain the differentiated state of stem cells in the NP. Henry et al. (2017) demonstrated the use of pullulan microbeads to enable sustained release of these growth factors in injectable silanized hydroxypropylmethylcellulose (HPMC) hydrogels. Further investigation of the microbead system in an *ex vivo* degenerative disc model showed that sequential release of the chemokine CCL-5, followed by TGF-β1 and GDF-5, could recruit MSCs into the NP and induce matrix elaboration, although they have not yet reported data on tissue elaboration within the HPMC hydrogels.

Recently, an injectable hyaluronic acid-methylcellulose (HAMC) hydrogel carrier with Wharton's jelly-derived MSCs (WJ-MSCs) was reported for repair of degenerate discs in a rat model (Choi et al., 2020). This hydrogel has been previously used for various neurological repair strategies, but this is the first report of its use in orthopedic tissues (Gupta, Tator, and Shoichet 2006; Caicco et al. 2013). The hydrogel promoted retention and survival of the WJ-MSCs, and together showed superior matrix elaboration, restoration of disc hydration, and down regulation of catabolic enzymes that frequently matched that of the uninjured control. It should be noted, however, that the rat-tail model is extremely small, and retention within a disc of that size does not

necessarily translate to retention of cells or elaboration within larger species (i.e., human). Furthermore, mechanical properties were not reported, and from previous studies of physically crosslinked gels, it can be surmised that the HAMC hydrogel system would not likely contribute to the restoration of disc height or mechanics.

1.7.5 Design Criteria and Functional Outcomes

The goal of NP tissue engineering is to restore the mechanical function of the degenerate disc to healthy levels and promote the ability of the incorporated cells to actively maintain the healthy tissue. In addition, delivery of a tissue-engineered therapeutic for NP repair must minimize any disruption to the neighboring structures to limit further damage and disease progression. As such, the endpoints of the tissue-engineered construct should be clearly defined and aim to achieve characteristics as close to the native, healthy disc as possible.

As the NP and IVD's function is purely mechanical, a tissue-engineered NP replacement must attempt to meet the mechanical specifications of the NP (Nerurkar, Elliott, and Mauck 2011). Several studies have been conducted on the native tissue mechanics of the healthy IVD, as a composite structure, as well as the individual portions of the AF and NP. **Table 1.1** below shows a summary of the mechanical benchmarks for the NP relevant for NP tissue engineering. Additionally, swelling behavior is a critical component of NP material behavior. Though to the best of our knowledge the equilibrium weight swelling ratio (Q_w) of healthy human NP tissue has not been reported in the literature, our laboratory has previously measured Q_w of healthy bovine NP tissue to be ~19 (Reza and Nicoll 2010b).

Table 1.1: Summary of native tissue mechanics benchmarks of the NP.
Modified from Nerurkar et al. (2011)

Testing Modality	Benchmark	Native Value
Confined Compression (Johannessen and Elliott 2005)	Swelling Stress P_{sw}	0.138 MPa
	Aggregate Modulus H_A^{eff}	1.01 ± 0.43 MPa
	Permeability k_o	0.9×10^{-15} m^4/Ns
Unconfined Compression (Cloyd et al. 2007)	Equilibrium Young's modulus E_y	5 kPa
	Poisson's ratio	0.62
	Percent relaxation	~65%
Torsional shear (Iatridis et al. 1997)	Complex shear modulus $\|G^*\|$	7.4-19.8 kPa
	Phase shift δ	23º-30º

The similarities between AC and the IVD are many, particularly in the make-up of the matrix. The cells of the mature IVD are so similar to articular chondrocytes that they are often referred to as NP chondrocytes. Still, the IVD and AC are two distinct tissues that have key differences to be mindful of while tissue engineering either one of them. The function of the IVD as a whole is to resist compression and allow motion; separately, the NP resists compression while the AF resists tension. Cartilage resists compression but also provides lubrication for articulating joints (Chen et al. 2017). Both AC and NP are characterized as having high proteoglycan content, particularly of aggrecan, as well as collagen type II. A critical difference lies in the ratio of these molecules, as the glycosaminoglycan to collagen ratio is 2:1 in cartilage, and 27:1 in the NP (GAG:Hydroxyproline) (Mwale et al. 2004; Yang and Li 2009). Absolute values of GAG and collagen in the NP are approximately 250 µg/mg dry weight and 525 µg/mg dry weight, respectively (Antoniou et al. 1996; Mwale et al. 2004). Type II collagen outnumbers type I in the NP 60:1 (Antoniou et al. 1996). The relative proportions of these matrix components are what distinguish NPCs from AC cells, however, it is not necessarily accurate to apply this proportion to gene expression (Mwale et al. 2004; Risbud et al. 2015).

In addition to the functional outcomes of mechanics and biochemistry/matrix elaboration, clinical translation must be considered. Primary considerations include the material be sterilizable,

cytocompatible, injectable, and retained *in situ* upon injection. The ideal NP replacement delivered minimally invasively, to limit disruption of the AF. Low initial viscosity can allow for injection through fine gauge needles (Boyd and Carter 2006). Injectable dermal fillers, which similarly require delivery through a fine gauge needle (27-30 ga) have been reported to range in initial viscosity from 58-1199 Pa·s (Falcone and Berg 2008). In addition, because the center of the IVD is a high-pressure space, the injectable material must rapidly increase in viscosity and shear modulus as it cures *in situ* in order to resist extravasation from the void space. Previous work from our lab using a CMC-MC DPN system reported initial viscosity (within 30 seconds of injection) to be 440.7 Pa·s, followed by a rapid 10-fold increase in viscosity by gelation completion (Varma et al. 2018). Previous work with CMC alone achieved a final gelation viscosity of ~160 Pa·s, though this was found not to be retained within the disc when injected in an *ex vivo* bovine disc model. Thus, while rheological analysis can be used to quantify the viscosity and shear modulus, secondary validation in a constrained space, or better yet, an *in vivo* or *ex vivo* nucleotomy model is useful for qualitatively confirming gelation and retention (Frith et al. 2013; Varma et al. 2018). Gelation time should also be taken into consideration, such that the physician has enough time to work with the pre-gelled material and fill void spaces, but short enough that the material does not extravasate and the procedure time is not prolonged. The current ISO standard for injectable biomaterials is 4-15 minutes (ISO Standard 5833:2002).

1.8 Motivation and Research Overview

Tissue-engineered NP replacements are a promising solution that can address the immediate mechanical needs of a damaged disc; however, clinical translation is hindered by a number of factors. As the goal of tissue engineering repair is to minimize further injury to the degenerated or herniated disc, delivery of the constructs must remain minimally invasive. Injectability, *in situ*

formation and retention are necessary for any acellular or cell-laden biomaterial approach. CMC has been methacrylated to form stable, chemically-crosslinked hydrogels that support growth of NP cells (Reza and Nicoll 2010b; 2010a) and the differentiation of hMSCs towards an NP-like phenotype when treated with TGF-β3 (Gupta, Cooper, and Nicoll 2011; Gupta and Nicoll 2014; Lin et al. 2016). However, recent work has demonstrated that even when utilizing redox-initiated crosslinking methods, methacrylated CMC does not gel *in situ* in the disc space due to diffusion away from the injection site (Varma et al. 2018). Recently a dual-polymer network (DPN) hydrogel consisting of methacrylated CMC and MC was investigated as a potential acellular NP replacement. MC afforded the construct additional thermogelling capacity, which allowed for *in situ* retention and restoration of disc height and mechanics, however, the effective polymer concentration was too high to support encapsulated cell viability. To reduce the effective macromer concentration while maintaining injectability and intradiscal retention, the overall objective of this thesis was to identify a lower macromer concentration of a single polymer network consisting of MC that would be retained *in situ* while serving as a potential cell scaffold. MC hydrogels have been well characterized for their mechanical and material properties once chemically crosslinked and for rheological properties during redox-initiated gelation (Gold et al. 2014; 2015), but the influence of this chemical modification on the intrinsic thermogelation of MC is unclear. Therefore, the first objective of this thesis was to investigate the effect of methacrylation on MC thermogelation and its role in the rheologic properties of a dual-crosslinked MC hydrogel network. Although methylcellulose is a water-soluble cellulose derivative, its thermosensitive nature is derived from the presence of hydrophobic methoxy groups on its backbone, which also results in a lower swelling capacity than CMC. Incorporation of negatively charged sulfonate groups to the polysaccharide backbone of MC would allow the polymer to mimic the charged

proteoglycan-rich matrix of the NP, which can enhance the water uptake and swelling capacity and potentially promote differentiation of stem cells towards an NP-like phenotype. Thus, the second objective of this thesis was to develop a sulfonated MC hydrogel and characterize its material properties relevant to NP replacement. Furthermore, matrix sulfation has been shown to promote sequestration and presentation of growth factors. Clinical translation of a potential injectable, cell-based scaffold material requires the ability to retain and deliver TGF-β3 (Purcell et al. 2014; Lei, Trevino, and Temenoff 2016; Merceron et al. 2012). Accordingly, we also aimed to characterize the sustained release or sequestration of encapsulated TGF-β3 from within these scaffolds. Multiple studies have now shown CMC hydrogels successfully support NP-like differentiation and matrix elaboration of hMSCs (Varma, DiNicolas, and Nicoll 2018; Lin et al. 2016; Gupta and Nicoll 2014; Gupta, Cooper, and Nicoll 2011); however, methacrylated MC hydrogels have not been investigated as scaffolds for hMSCs. Thus, the final objective was to characterize hMSC survival, differentiation, and matrix elaboration within dual-crosslinked MC hydrogels. As matrix sulfation has been shown to be critical to the development of healthy skeletal tissues, the effect of added sulfonation to the matrix was also investigated (Cho et al. 2004; Mertz et al. 2012; Cortes, Baria, and Schwartz 2009; Klüppel et al. 2005).

The tissue engineering paradigm centers on three factors: scaffolds, signals, and cells; previous studies have combined these *in vitro* using exogenous delivery of growth factors via cell culture media. A clinically translatable tissue engineering solution would need to deliver all three together, as exogenous growth factor is not clinically feasible. In addition, previous work in our lab has shown promise for robust acellular *in situ* gelling biomaterials that aim to restore disc mechanics, and for soft, cell-laden constructs that promote hMSC differentiation, but not materials that achieve both desirable outcomes. As such, the **global hypothesis of this thesis is that an MC-**

based hydrogel system can be utilized as a thermogelling, injectable and *in situ* gelling system capable of serving as a clinically translatable method of tissue engineering NP repair. Specifically, chemical modifications of MC via controlled methacrylation percentage and sulfonation may be employed to direct injectability and sequestration of soluble factors to support hMSC differentiation towards an NP-like phenotype.

The specific aims to test this hypothesis are as follows:

Specific Aim 1: Investigate the influence of the degree of methacrylation modification on thermogelation and rheological properties of MC.

MC polymer solutions will be modified with methacrylate groups resulting in varying methacrylation percentages, and the rheological properties of methacrylated MC without redox-initiated chemical crosslinking (thermogelation onset temperature, storage and loss modulus, complex viscosity, phase angle, and shear thinning behavior) will be assessed in relation to varying temperature, shear rate, and time. Storage and loss modulus upon completion of redox-initiated chemical crosslinking and time to completion will also be investigated after gelation at room temperature (20ºC) and physiologic temperature (37ºC) to assess the role of the thermoresponsive behavior in chemically crosslinked hydrogel behavior, and to determine if gelation at physiologic temperature results in a dual-crosslinked hydrogel.

Specific Aim 2: Develop sulfonated MC hydrogels for injectable NP replacement with tunable swelling and mechanical properties, as well as a means for retaining incorporated TGF-β3 to serve as a clinically relevant, tissue engineering scaffold.

Negatively charged monomers, 2-sulfoethyl methacrylate (2SEM), will be covalently incorporated into MC hydrogels during free-radical polymerization. The effects of 2SEM incorporation on bulk material properties (equilibrium swelling, mechanics) and long-term

stability of acellular hydrogels will be assessed. Injectability will be evaluated by investigating thermogelation and redox-initiated gelation of sulfonated gels via rheometry, and *in situ* gelation will be assessed via injection into an *ex vivo* nucleotomized bovine motion segment model. The electrostatic interaction of sulfonated MC hydrogels with proteins will be characterized by quantifying serum protein adsorption, and more specifically, its ability to sequester incorporated TGF-β3 over the course of two weeks via electrostatic affinity will be interrogated.

<u>Specific Aim 3:</u> Investigate the ability of redox-polymerized MC hydrogels (with and without the addition of sulfonates) to support human mesenchymal stromal cell (hMSC) differentiation towards an NP-like phenotype with TGF-β3 supplementation in cell culture media or direct incorporation into hydrogel constructs.

Human MSCs will be encapsulated within MC hydrogels with and without sulfonates, and survival and differentiation will be assessed *in vitro*. TGF-β3 will either be incorporated directly into the hydrogels or supplemented exogenously via cell culture media to assess the impact of the hydrogel sulfonation on the bioavailability of TGF-β3 to encapsulated hMSCs. Human MSC viability and differentiation will be determined based on DNA content, ECM content (sGAGs and Collagen type II) and distribution and construct mechanical properties over the duration of the culture period.

Successful completion of the above Specific Aims will result in the development of a fully self-contained, injectable system for tissue engineering repair of the injured or degenerate NP. This thesis work will provide greater insight into the influence of chemical modifications (i.e., methacrylation, sulfonation) on the thermoresponsive behavior of MC and functional network formation. Moreover, it will establish the feasibility of chemically-crosslinked MC hydrogels as cell-instructive scaffolds for minimally invasive, clinically-relevant, tissue engineering therapies.

1.9 Overview of Present Investigation

The global objective of this thesis is to engineer an injectable MC-based hydrogel system as a functional NP replacement for both cell-based and acellular therapies for IVDD. Previous studies have shown successful NP-like differentiation of encapsulated hMSCs but were unsuccessful in forming gels directly in the disc, and the combination acellular cellulosic gel developed subsequently (CMC-MC) was not permissive for hMSC encapsulation and differentiation. It was found that the thermogelling capacity of MC combined with redox-initiated covalent crosslinking is necessary for *in situ* gel formation. Even though we have seen that the thermogelling behavior is preserved in methacrylated MC, the effect of methacrylate modification and percent modification on the thermoresponsive behavior of MC has not been investigated. Additionally, we have observed previously that methacrylation percentage surprisingly did not have a strong effect on swelling and network properties (i.e., mesh size, crosslinking density) of MC, contradictory to most polymer studies (including CMC), which showed increasing the availability of potential crosslinking sites leads to increased crosslink formation and modified physical properties. This motivated the more in depth rheometric investigation of MC at varying methacrylation percentages. Thus, thermogelation onset temperature, thermoresponsive gelation and shear thinning behavior at physiologic temperature, and redox-initiated crosslinking kinetics were investigated for various methacrylation percentages and are presented in Chapter 2. This study demonstrated that the addition of methacrylate groups lowers the thermogelation onset temperature and increases the thermoresponsiveness of MC hydrogels, potentially affecting the injectability and handling of MC solutions, but did not have a major additive effect on the complex modulus of redox-polymerized gels at room temperature or physiologic temperature.

Previous studies comparing CMC hydrogels to MC hydrogels favored CMC hydrogels because of the higher swelling capacity afforded by the negatively charged carboxyl groups. An additional translational challenge has been delivery of TGF-β3 within the hydrogel system. As such, Chapter 3 aimed to address both issues by incorporating sulfonates into the MC hydrogel system, with the goal of creating an *in situ* gelling GAG mimetic that increased MC swelling capacity and sequestered incorporated TGF-β3 for delivery in a single hydrogel system. Sulfonated MC hydrogels were investigated for injectability, swelling, mechanical behavior, long-term stability, and cytocompatibility in a factorial design comparing three macromer concentrations (2%, 3%, and 4%) and four sulfonate concentrations (0 mM, 1 mM, 5 mM, and 10 mM). Sulfonate incorporation did not increase the water capacity of MC hydrogels but did sequester TGF-β3 in a tunable fashion. In addition, *ex vivo* bovine motion segment models for injection and retention showed that a minimum of 3% MC crosslinked with 10 mM APS and TEMED each was necessary to form hydrogels *in situ*. Therefore, this formulation was used to investigate bioactivity and capacity to support hMSC differentiation in Chapter 4.

The results of Chapter 3 demonstrated the successful creation of an *in situ* gelling, sulfonated MC that sequestered TGF-β3 in a tunable fashion. We selected 5 mM sulfonate concentration, as this afforded no significant difference in sequestration from 10 mM, both of which displayed the strongest sequestration of encapsulated TGF-β3 over 2 weeks. Bone marrow-derived MSCs were encapsulated in redox-polymerized MC hydrogels with and without sulfonates, and TGF-β3 delivery was administered either within the hydrogel or through media supplementation, and growth factor-free conditions served as controls. Over 6 weeks of culture, the MSC-laden constructs showed moderate matrix deposition, with clear superiority in the groups that were both sulfonated and received TGF-β3 stimulation, regardless of delivery route. However, the measured

values of ECM content did not approach reported native NP levels. Mechanical and swelling properties did not change over time, indicating that MC remained resistant to hydrolytic degradation as previous studies had shown. Cell viability decreased over time in all groups except those with both sulfonate and TGF-β3 supplementation, indicating a potentially synergistic effect. Overall, the study showed that sulfonation and encapsulated TGF-β3 delivery hold promise for cellulose-based hydrogels for NP tissue engineering, but that the low swelling capacity and lack of scaffold breakdown may have prevented robust matrix elaboration and cell survival, and that further optimization is necessary to develop an *in situ* gelling cellulosic hydrogel that can repair and replace the degenerating NP.

Chapter 2: Rheological Analysis of the Effect of Methacrylation on the Thermoresponsive Gelation of Methylcellulose in Aqueous Solutions

The following chapter was presented in part at the American Chemical Society National Meeting and Exposition (2020):

Haq-Siddiqi N.A., Nicoll, S.B. (2020). Effect of methacrylation on the thermoresponsive sol-gel transition of methylcellulose. (Poster Presentation) Paper No. CELL 71, *American Chemical Society Spring 2020 National Meeting and Exposition*, Philadelphia, PA. doi.org/10.1021/scimeetings.0c05990

2.1 Introduction

Hydrogels are a broad class of biomaterials composed of highly hydrated polymer networks. These materials have a wide array of biomedical applications, due to their tunability and water content, from cell-laden tissue engineering scaffolds to cell-free prostheses and fillers (Peppas et al. 2006; Sivashanmugam et al. 2015; Raucci et al. 2020). *In situ* forming injectable hydrogels are increasingly necessary for a number of minimally invasive biomedical interventions, including soft tissue fillers (Gold et al. 2015; Varma et al. 2014; Li et al. 2019; Falcone and Berg 2008), orthopedic implants (Raucci et al. 2020; Lin et al. 2021), and drug delivery depots (Mathew et al. 2018). These biomaterials must have a low starting viscosity in order to be easily injected through small gauge needles but must also exhibit an increase in viscosity upon injection in order to not lose mechanical integrity or extravasate from the injection site. Physical, ionic, and covalent crosslinking of polymeric biomaterials are all means by which an injectable material can form a gel *in situ* in order to be retained at the site of injection. Physical crosslinking of polymers is frequently mediated by environmental changes like temperature and pH. This is very useful in biological applications, where the introduction of physiological temperature (37°C) or pH (7.4) can direct the formation of gels. Physical crosslinks driven by environmental changes are also reversible, as they are dependent on specific environmental stimuli, which may fluctuate.

Methylcellulose (MC) is one such polymer that exhibits temperature-dependent physical crosslinking to produce thermoreversible hydrogels. MC is a water-soluble derivative of cellulose, a naturally occurring plant-derived polysaccharide and the most abundant natural polymer on earth (Klemm et al. 2005). Cellulose is a linear polymer made up of repeating β(1,4) linked D-glucose units with three hydroxyl groups on each glucan ring, which allows for strong inter- and intra-chain hydrogen bonding, resulting in a rigid crystalline structure and resistance to water solubility.

Substitution of the hydroxyl groups on cellulose by methoxy groups in MC disrupts the crystalline structure, thereby improving its affinity for water and enabling it to be dissolved in aqueous solutions (Nasatto et al. 2015). The methoxy groups themselves are hydrophobic, and thus, while the polymer chain is made water-soluble, the methoxy groups form aggregations as temperature increases, resulting in a reversible, physically crosslinked hydrogel. Unmodified MC has been reported to show a thermogelation onset temperature ranging from 50°C to 70°C, depending on degree of substitution (DS) of cellulose hydroxyls by methoxy groups and weight % concentration (Haque and Morris 1993; Lin Li 2002). The ability to form hydrophobic aggregates in response to increasing temperature is dictated by the concentration of hydrophobic moieties. A DS of 1.7-1.9 out of 3 possible substitutions of methoxy groups for hydroxyls on cellulose has been shown to be optimal for solubility and thermoresponsiveness; higher or lower than this limits the water solubility of MC (Sarkar 1979). Other additions to MC such as hydrophobic stearyl groups and hydrophilic carboxyl, amino, and acylamino modifications have been used to decrease and increase the thermogelation temperature, respectively (Wu et al. 2021; Lee, Cho, and Park 2005; Li et al. 2012).

Although MC readily forms thermoreversible hydrogels, the mechanical properties of the gels are generally not sufficient to withstand the forces experienced in many biomedical applications (i.e., movement, touch, load-bearing joints). As such, MC is frequently used as an additive in dual polymer networks to provide thermogelling capacity, but not on its own as a primary scaffold material (Gupta, Tator, and Shoichet 2006; Payne et al. 2017; Choi et al. 2020; Oğuz and Ege 2018; Jung, Kim, and Ho Park 2019; Mihardja et al. 2013). In order to enhance the mechanical properties of MC, we previously coupled methacrylate groups to the MC backbone to allow for free-radical crosslinking and the formation of mechanically stable hydrogels via

photopolymerization (Stalling, Akintoye, and Nicoll 2009). The injectability of methacrylated MC (Ma-MC) hydrogels was later achieved by introducing redox initiators to form covalently crosslinked hydrogels *in situ* (Gold et al. 2014; 2015). In that prior work, Ma-MC hydrogels were formed *in vitro* using redox-initiated, free radical polymerization at room temperature, but the influence of temperature on Ma-MC gelation, was not explored. Methacrylate groups are strongly hydrophobic and have been shown to decrease the cloud point temperature of the cellulose derivative, hydroxypropyl cellulose, in a manner proportional to the degree of methacrylate substitution (Marsano, Bianchi, et al. 2000). Thus, it was hypothesized that methacrylation would augment the hydrophobically-driven physical crosslinking of MC, thereby lowering the thermogelation onset temperature and enhancing the chemical crosslinking of methacrylate moieties, leading to more robust, dual-crosslinked hydrogels.

Numerous studies have also shown that the solvent constitution of the MC solution (i.e., water versus saline) can alter the thermogelation temperature of MC (Zheng et al. 2004; Xu, Li, et al. 2004; Xu, Wang, et al. 2004). Ionic solutes in aqueous MC solutions can modify both the temperature and strength of thermogelation by altering the water solubility of the polymer in "salting-out" or "salting-in" effects, depending on the ion(s), in accordance with the Hofmeister series (Xu, Wang, et al. 2004; Hofmeister 1888). The effect is tunable and can be seen to vary depending on the mixture and concentration of ions, including those in physiologically relevant solutions (Xu, Li, et al. 2004; Zheng et al. 2004). This is particularly relevant for MC hydrogels containing cellulose nanocrystals, which require specific solvents (i.e., water) for complete resuspension and dispersion in MC solutions (Hynninen et al. 2018). Therefore, in this study the effect of methacrylate pendant groups on the thermoresponsive behavior of MC in water and saline solutions, and the effect of gelation temperature on redox-initiated polymerization were

characterized. This investigation has important implications for surgical implementation of the injectable biomaterial, interrogating how the rate of thermogelation and strength of physical crosslinks formed at physiologic temperature impact the efficiency of redox-initiated chemical crosslinking.

2.2 Materials and Methods

2.2.1 Macromer Preparation

Methylcellulose was methacrylated by esterification of hydroxyl groups with methacrylic anhydride (Sigma-Aldrich) according to previously described protocols (**Figure 2.1**) (Gold et al. 2014; Stalling, Akintoye, and Nicoll 2009; Varma et al. 2018). Briefly, 15kDa (15 cP viscosity at 2 wt%, 20°C) and 41kDa (400 cP viscosity at 2 wt%, 20°C) MC powder (Sigma-Aldrich, degree of substitution of methoxy groups 1.8) was mixed 1:1 and then added to deionized H_2O (diH_2O) at 1% (w/v) at 80°C until it was evenly disbursed, after which the temperature was lowered to 4°C and allowed to continue to dissolve fully for ~24 hours. The mixture of low and medium viscosity MC was used for optimal viscosity and handling, as previously described for injectable tissue replacement applications (Varma et al. 2018; Lin et al. 2019). The solution was then reacted with methacrylic anhydride with a molar excess of 20 at 4°C with periodic adjustments of pH between 8-9 for 48 hours. The reaction product was purified by dialysis (Spectra/Por, MWCO 6-8 kDa) over 3 days to remove unreacted methacrylic anhydride. Purified solution was lyophilized and stored at -20°C. Unmodified MC was treated in the same method as Ma-MC, by dissolving 1:1 low-medium viscosity MC and dialyzed and lyophilized but without reacting with methacrylic anhydride.

2.2.2 *Nuclear Magnetic Resonance*

Polymer samples were acid hydrolyzed as previously described for ^{1}H NMR analysis (500 MHz, Varian Mercury 500) (Stalling, Akintoye, and Nicoll 2009; Reza and Nicoll 2010a). Percent methacrylation was determined via relative integrations of methacrylate protons to carbohydrate protons:

$$\%\, methacrylation = \frac{(A_{Methyl}/P_{Methyl})}{(A_{MC}/P_{MC})} \times 100 \quad (2.1)$$

$$DS_M = \%\, methacrylation \times 3 \quad (2.2)$$

where A_{Methyl} is the peak area of the protons (P_{Methyl} = 3) in the methyl of the methacrylate group and A_{MC} is the peak area of the protons (P_{MC} = 14) on the disaccharide subunit of MC, and degree of methacrylate substitution (DS_M) was determined based on a maximum DS of 3 (Gold et al. 2015).

2.2.3 *Rheology*

Methacrylated methylcellulose and unmodified methylcellulose (uMC) were dissolved in either diH_2O or Dulbecco's Phosphate Buffered Saline (DPBS) at 3% w/v and stored at 4ºC until use. All rheometric analyses were performed on an AR2000ex Rheometer (TA Instruments) with a cone and plate geometry (2º, 20mm) under oscillatory conditions. Preliminary strain and frequency sweep measurements on non-gelled methacrylated MC polymer solutions established the optimal test parameters (1% strain, 1 Hz) based on the linear viscoelastic region (Gold et al. 2015; Varma et al. 2018). A solvent trap apparatus with diH_2O was used to prevent sample dehydration. Results were analyzed using the TA Data Analysis software (Advantage v.5.4.0). Shear storage modulus (G'), shear loss modulus (G''), and phase angle (δ) were measured against temperature, time, and strain % (γ) (Kim et al. 2016; Gold et al. 2015; 2014).

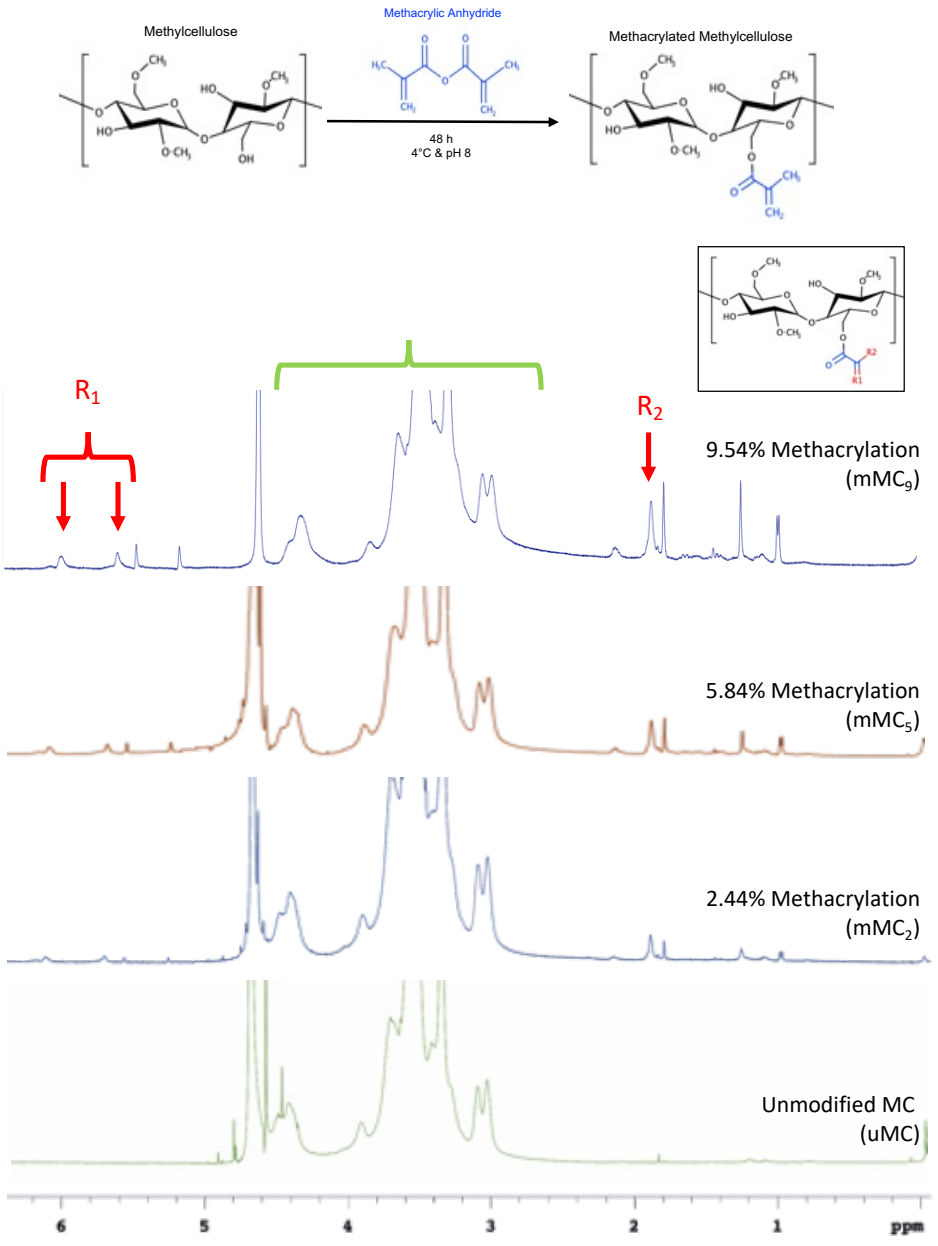

Figure 2.1: Reaction scheme of the esterification of methylcellulose with methacrylic anhydride, and subsequent ^{1}H- NMR spectra.

2.2.3.1 Determination of Thermogelation Onset Temperature

A temperature ramp was performed from 4ºC to 80ºC with a ramp rate of 1ºC/min to determine the temperature of thermogelation onset. Onset temperature was measured using three different methods (**Figure 2.2**) to account for the variation in methodology reflected in the literature (Li

2002; Arvidson et al. 2013; Knarr and Bayer 2014). Method 1 employed the most commonly used definition of gelation onset as the point at which *G'>G"*, indicating the elastic component of the complex modulus was dominant over the viscous component (Desbrières, Hirrien, and Ross-Murphy 2000; Winter and Chambon 1986; Payne et al. 2017; Caicco et al. 2013; Oğuz and Ege 2018). Method 2 defined thermogelation as the point at which the rate of increase in *G'* was greater than 2% for 4 or more consecutive points, used to determine the inflection point of G' which corresponds to a rapid increase in stiffness (Xu and Li 2005; Haque and Morris 1993; Tate et al. 2001; Xu, Li, et al. 2004; Almeida, Rakesh, and Zhao 2018). The final method defined thermogelation onset by the local maximum of the first derivative of log(*G'*) with respect to temperature, corresponding to the steepest slope in the curve of G', indicating rapid gel formation (Zheng et al. 2004; Li et al. 2002; Wang and Li 2005).

2.2.3.2 Strain Sweep and Timed Temperature Hold at Physiologic Temperature

The response to instantaneous increase in temperature, as is experienced during injection into the body, was determined via time sweep at physiologic temperature, 37ºC. Polymer solution was equilibrated at 4ºC for 5 minutes, after which the temperature was immediately raised to 37ºC and held for 15 minutes (1 Hz, 1% strain). Logarithmic strain sweeps from 0% to 100% were performed at 4ºC and 37ºC, before and after the timed temperature hold, respectively.

2.2.3.3 Strain Recovery

Recovery of the MC formulations after cyclic deformation was investigated by applying strain and cyclically switching from low strain (0.2%) to high strain (500%) for 2 minutes each over the course of 14 minutes, at 37ºC and 1 Hz throughout the experiment (Chen et al. 2017; Loebel et al. 2017).

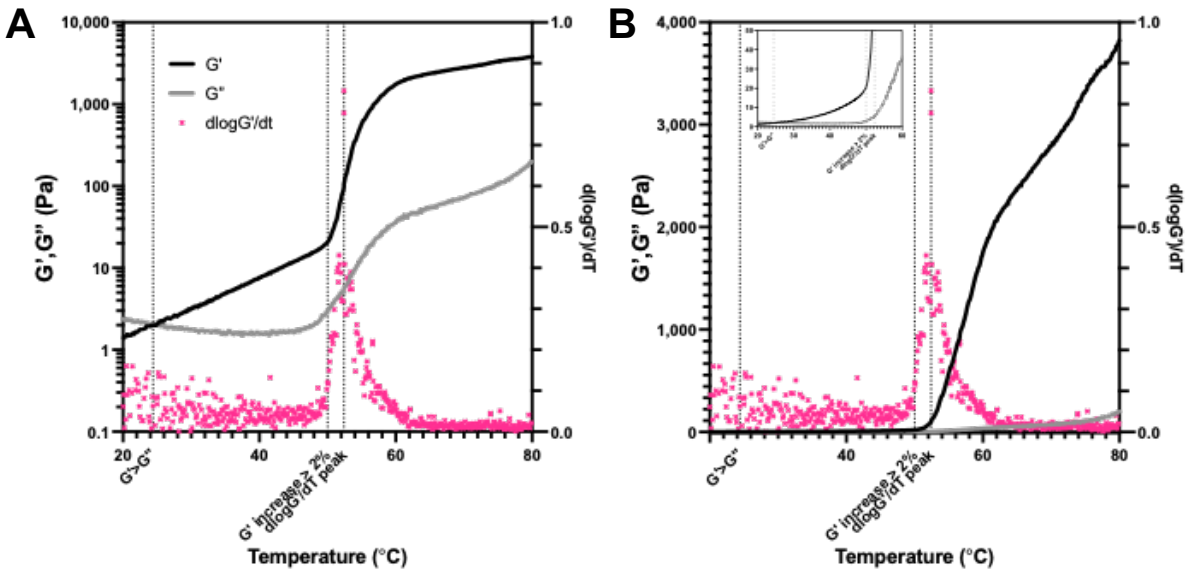

Figure 2.2: Methods of determining thermogelation temperature via rheometric analysis. A) Log plot and B) standard plot of the same data set (G' and G") with three commonly used methods for defining thermogelation onset marked accordingly. Method 1 uses the Winter-Chambon criteria of G'>G" and equates the formation of a gel with thermogelation. Method 2 selects the point of sharp increase in G' (corresponding to an increase in G' of greater than 2% for 4 consecutive points over 30 seconds). Method 3 displays the derivative of logG' with respect to T, exhibiting a clear maximum at the inflection point of logG', where increase in G' is at its maximum.

2.2.3.4 Thermogelation Effect on Redox-Initiated Crosslinking of Methacrylated MC

The influence of temperature during redox-initiated crosslinking of injectable MC hydrogels was measured via time sweep. MC solutions were dissolved as previously described in in dual-barrel syringes, at a final concentration of 3% w/v (Gold et al. 2014). Redox initiators ammonium persulfate (APS) (Sigma) and N,N,N,N-tetramethylethylenediamine (TEMED) (Sigma) were each added in opposing sides of the dual-barrel syringe (Pac-Dent) at 10 mM final concentration for free-radical polymerization. Mixing tips (1:1) were used to mix polymer precursors during ejection onto the pre-warmed (20ºC or 37ºC) peltier plate. T=0 was defined as the point at which 10 mM TEMED was added to the MC/10 mM APS solution. Gelation onset, determined by oscillation time sweep, was identified at the point at which *G'>G"*. Gelation completion was established as

the first time at which four consecutive data points exhibited less than a 2% change in the growth of *G'* (Gold et al. 2014; Temenoff et al. 2003).

2.2.4 Statistical Analysis

All analyses were performed in triplicate unless otherwise noted. Data are represented as mean ± standard deviation. A two-way ANOVA was used to determine the effect of methacrylation percentage and solvent on thermogelation onset temperature, and the effect of methacrylation percentage and temperature on the properties of redox-polymerized gels. A three-way ANOVA was used to determine the effect of methacrylation percentage, solvent, and temperature on rheological properties of thermally crosslinked gels. Significance was set at $p<0.05$.

2.3 Results

2.3.1 Structural Characterization

^{1}H-NMR confirmed the methacrylation of MC via the presence of methylene and methyl protons of the methacrylate at $\delta \approx 6.1$ and 5.7 ppm and $\delta \approx 1.9$ ppm respectively, which are not present on the unmodified MC (**Figure 2.1**). The broad stretch from ~2.8-4.6 ppm corresponding to protons on the disaccharide MC subunit was integrated with respect to the methyl peak, and relative methacrylation calculated based on the relative ratio of methyl protons (3) to disaccharide protons (14).

Table 2.1: Methacrylation percentage and degree of methacrylate substitution

	% Methacrylation	Degree of Substitution by Methacrylates
uMC	0%	0
mMC$_2$	2.44%	0.07
mMC$_5$	5.84%	0.18
mMC$_9$	9.54%	0.29

2.3.2 Determination of Thermogelation Onset Temperature

Thermogelation curves of MC of varying methacrylation percentage from 4ºC to 80ºC (**Figure 2.3A**) showed a wide range of moduli (*G', G"*) as well as rates of increase (**Figure 2.3C**).

The effect of methacrylation percentage on thermogelation onset temperature was significant across all three methods of calculation, with gelation onset temperature decreasing with increasing methacrylation percentage (**Figure 2.3B**). The effect of the solvent on thermogelation was only statistically significant when measured by the first derivative of log(*G'*) or by the sharp increase of *G'*; for thermogelation onset temperature measured by *G'*>*G"*, the effect of the solvent was not considered significant. For mMC_9, *G'* was greater than *G"* from the onset of the experiment, and therefore, onset temperature was calculated as 0ºC.

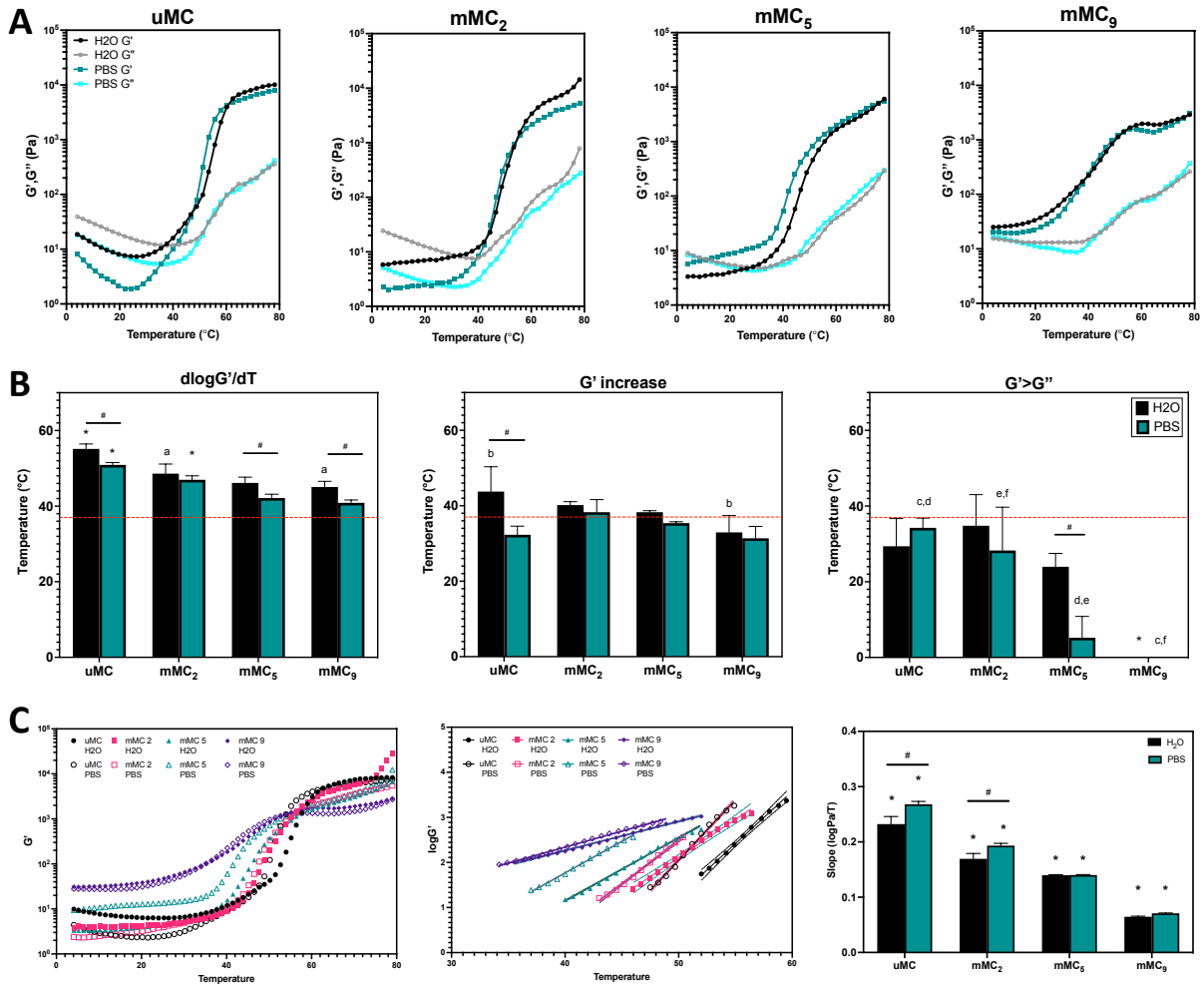

Figure 2.3: Temperature-dependent gelation of MC formulations with increasing temperatures. A) Representative temperature ramp curves of various Ma-MC (and unmodified MC) formulations in H2O and PBS. B) Gelation onset temperatures as determined by differing mathematical criteria. C) Determination of thermogelation rate and comparison of slopes. # — Significant difference between solvents. * — Significantly different from all other methacrylation % within the same solvent. a,b,c,d,e,f — Significantly different from other methacrylation % within the same solvent. Significance set at $p < 0.05$.

2.3.3 Thermoresponsive Gelation at Physiologic Temperature

Strain sweeps were conducted at 4ºC and 37ºC to simulate the behavior of the polymer solutions at refrigerated storage temperature and physiologic temperature, respectively. Representative curves of each group are shown in **Figure 2.4** for polymer solutions in H_2O and **Figure 2.5** for polymer solutions in PBS. Quantitative values for each group were taken at 1% strain (**Figure 2.6**). Strain sweeps at 4ºC showed that *G"* was consistently greater than *G'* for almost all methacrylation percentages, indicating the polymer solutions were more viscous than elastic. Only mMC_9 showed *G'* as slightly greater than *G'* until the yield strain was reached. This was corroborated by the phase angle *(δ)* which was near 90º for most groups at 4ºC, characteristic of viscous fluid-like behavior, while mMC_9 had a phase angle less than 45° in both solvents. At 37ºC, all groups had achieved "gelation" in that *G'>G"* from the onset of the strain sweep. Only mMC_9 exhibited *G'* and $|\eta^*|$ significantly greater than groups of lower methacrylation percentage at 4ºC (**Figures 2.6A, B**). At physiologic temperature, all groups underwent thermogelation as shown by δ less than 45º indicating more elastic than viscous behavior (**Figure 2.6C**). All samples displayed δ significantly lower than those at 4ºC. Despite this, uMC and mMC_2 showed no significant change in *G'* or $|\eta^*|$ in either solvent, while mMC_5 and mMC_9 displayed significantly higher *G'* and $|\eta^*|$, with solutions in PBS resulting in even stiffer/more viscous gels.

Physical crosslinks are reversible and can break under deformation and then reform when the force is released. This can be observed by the decrease in *G'* with increasing γ (**Figures 2.4 and 2.5**). Yield strain (γ_{yield}) is typically described as the strain at which *G'* becomes less than *G"*, indicating the strain-dependent gel-sol transition (Shih, Shih, and Aksay 1999). Unmodified MC mMC_2 and mMC_5 did not display yield according to this definition, although a decrease in *G'* can be observed between 1 and 10% strain. Yield strains were observed for uMC and mMC_2 (H_2O and

PBS) at 37ºC (**Figures 2.4** and **2.5, Table 2.2**). mMC_5 and mMC_9 displayed strain stiffening behavior rather than thinning as shown by an increase in both *G'* and *G"*, which for mMC_9 resulted in rupture of the gel at high γ, as shown by a sharp drop in both *G'* and *G"* **(Figures 2.4** and **2.5)**.

Table 2.2: Yield strain (γ_{yield}) from strain sweeps performed at 4°C and 37°C (1 Hz)

		Yield Strain	
		4ºC γ_{yield} (%)	37ºC γ_{yield} (%)
uMC	H_2O	—	15.25 ± 21.50
	PBS	—	12.88 ± 6.38
mMC_2	H_2O	—	18.64 ± 15.24
	PBS	—	14.84 ± 15.43
mMC_5	H_2O	0.097 ± 0.12[a]	—
	PBS	—	—
mMC_9	H_2O	5.51 ± 3.48[a]	—
	PBS	6.26 ± 0.82	—

[a] – Significantly different from other yield strain within the same solvent. Significance set at $p < 0.05$.

Between strain sweeps, temperature was increased from 4ºC to 37ºC rapidly and held for 15 minutes to simulate the temperature change upon injection. Onset of gelation here was defined as the time at which *G'>G"* (sol-gel transition) and completion of the thermogelling process at 37ºC was defined as the point at which *G'* increased by less than 2% for 4 or more consecutive points, corresponding to a plateauing of the increase in *G'*. Thermogelation onset time ranged from 0:13 ± 0:05 to 0:45 ± 0:22 minutes; thermogelation completion was achieved between 2:40 ± 0:20 and 6:09 ± 1:12 minutes (**Table 2.3**).

Table 2.3: Onset and completion times of thermogelation at 37°C (1%, 1 Hz).

		Thermogelation Onset Time (min)	Thermogelation Completion Time
uMC	H_2O	00:19 ± 00:22	03:25 ± 01:08
	PBS	00:43 ± 00:04	02:55 ± 00:39
mMC_2	H_2O	00:40 ± 00:42	03:12 ± 01:08
	PBS	00:36 ± 00:28	02:42 ± 01:26
mMC_5	H_2O	00:28 ± 00:15	02:40 ± 00:20[#]
	PBS	00:45 ± 00:22	06:09 ± 01:12*
mMC_9	H_2O	00:13 ± 00:05	03:00 ± 00:10
	PBS	00:17 ± 00:04	02:50 ± 00:04

* - Significant difference from all other methacrylate percentages. # - Significant difference from PBS with the same methacrylation % and temperature. Significance set at $p < 0.05$.

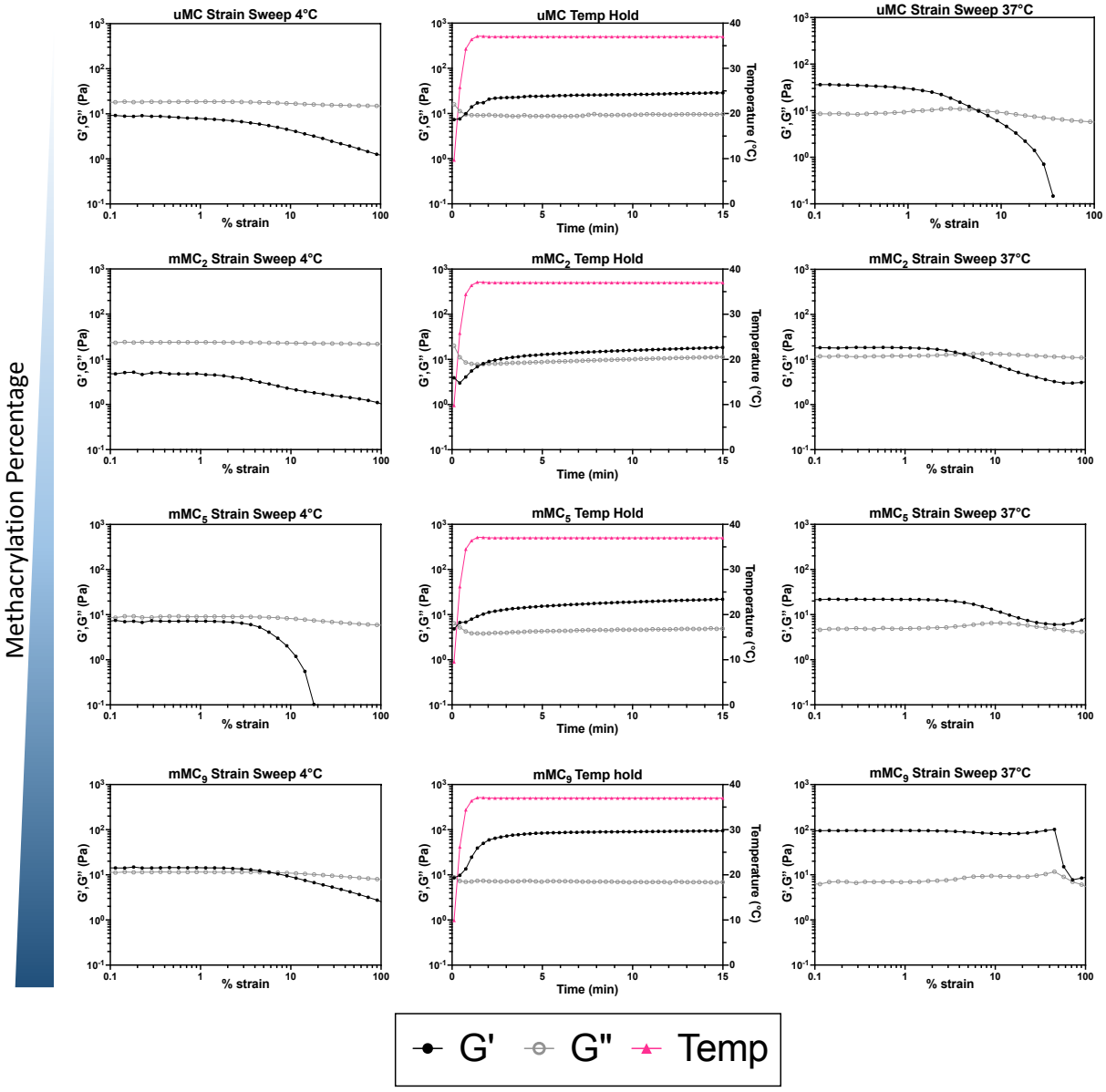

Figure 2.4: Temperature-dependent gelation and strain behavior of MC formulations in H_2O. MC formulations were equilibrated at 4°C and then underwent a strain sweep, followed by an immediate ramp up to 37°C that was held for 15 minutes, after which a subsequent strain sweep at 37°C was conducted, displaying time, temperature, and deformation-dependent mechanical behavior of physically crosslinked MC gels.

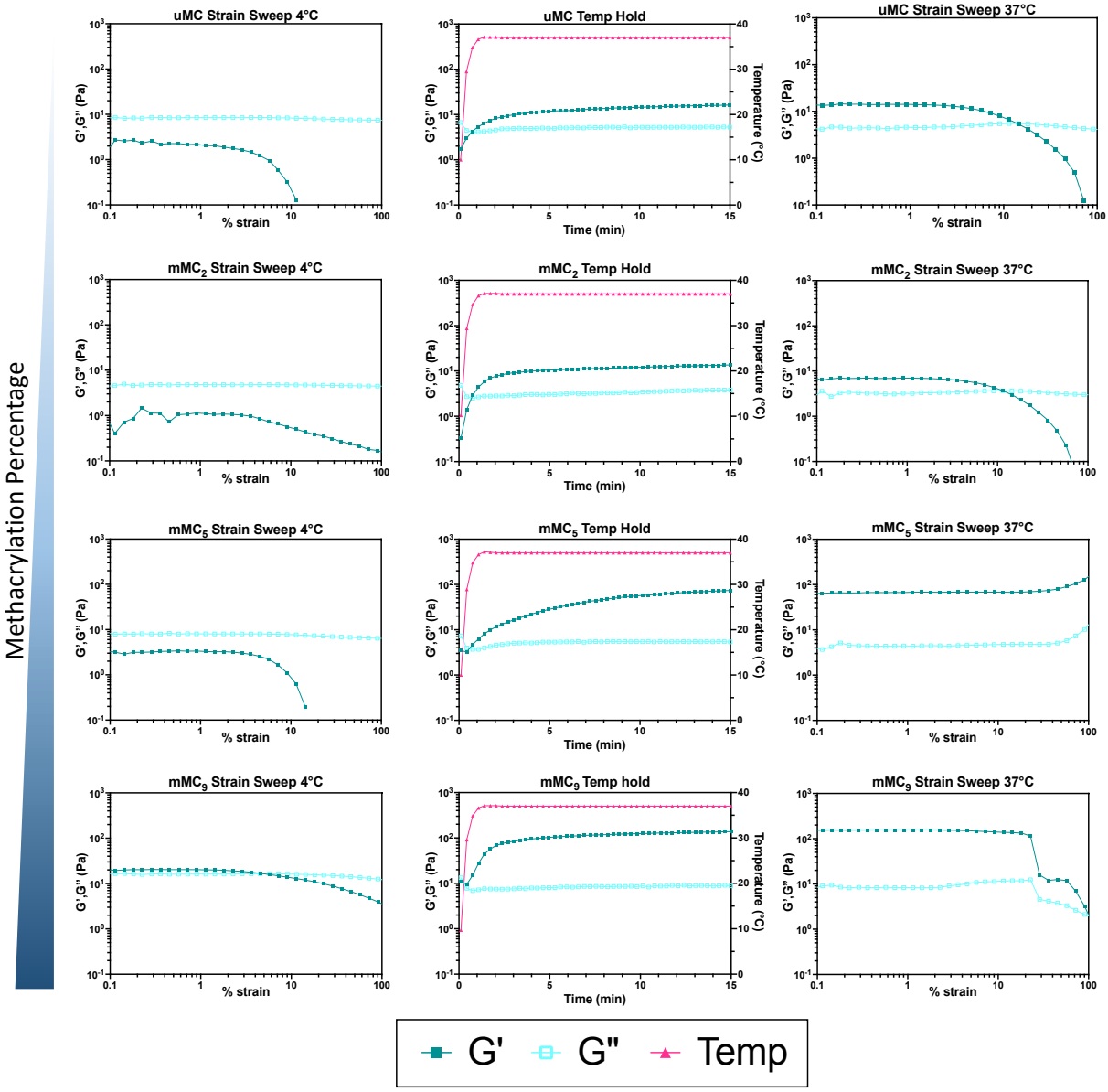

Figure 2.5: Temperature-dependent gelation and strain behavior of MC formulations in PBS. MC formulations were equilibrated at 4°C and then underwent a strain sweep, followed by an immediate ramp up to 37°C that was held for 15 minutes, after which a subsequent strain sweep at 37°C was conducted, displaying time, temperature, and deformation-dependent mechanical behavior of physically crosslinked MC gels.

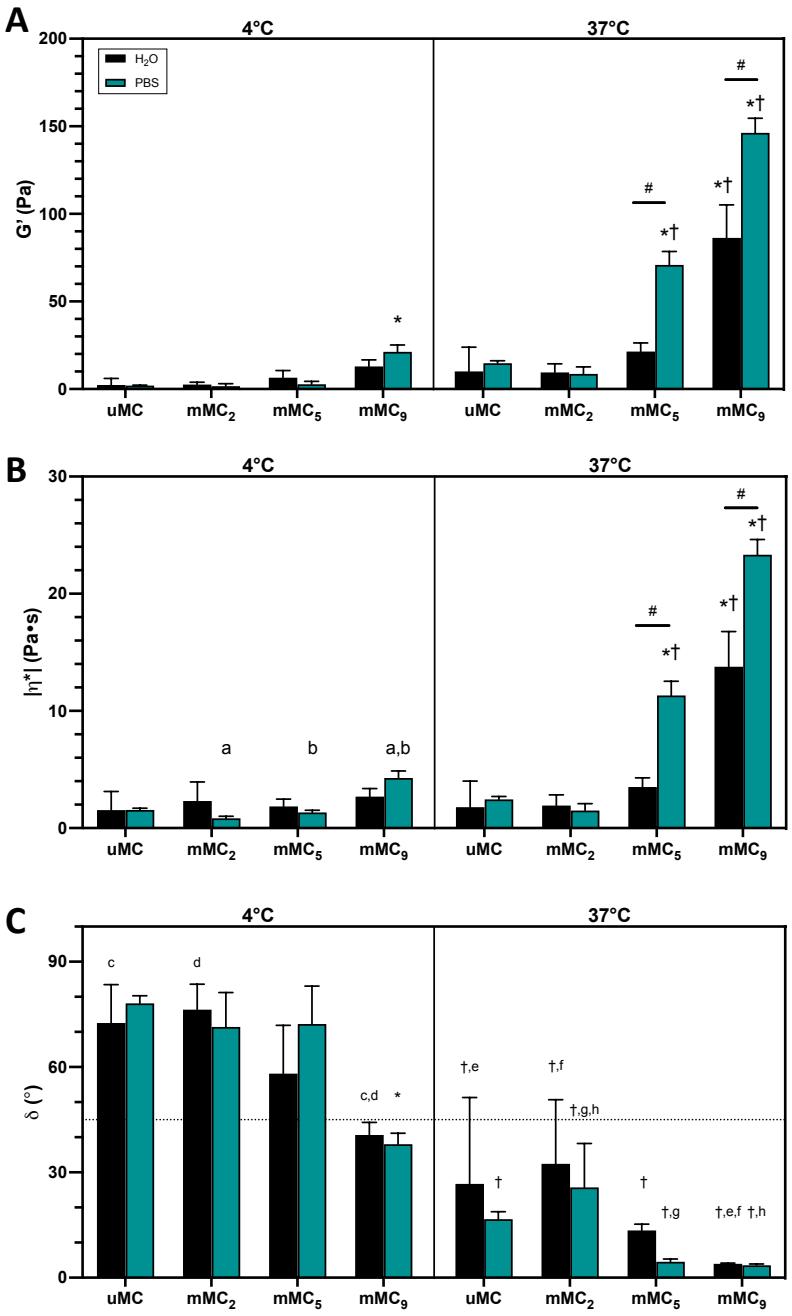

Figure 2.6: Behavior of thermogelling MC solutions at storage and physiologic temperatures (1% strain, 1 Hz).

A) Storage modulus G', B) complex viscosity |η*| and C) phase angle δ for varying MC formulations at 4ºC and 37ºC. * - Significant difference from all other macromer % within the same solvent and temperature. # - Significant difference between solvents within the same methacrylation % and temperature. † - Significant difference from 4°C within the same methacrylation % and solvent. a,b,c,e,f,g,h – Significant difference between the same letters. Significance set at $p < 0.05$.

2.3.4 Strain Recovery

The rapid breaking and recovery of physical crosslinks was demonstrated via cyclic strain time sweep. Application of extremely high strain (500%) resulted in fluid-like behavior where *G'<G"* and immediate removal of the high strain (strain % of ~0.2%) returned the MC solution to a "gel" with *G'>G"* (**Figure 2.7**). Recovery at low strain included characteristic thixotropic behavior, wherein a gradual increase in *G'* is attributed to the time-dependent reordering of hydrophobic aggregate crosslinks within the MC chains. The recovery profile for mMC_9 in H_2O is shown in **Figure 2.7** as a representative profile; all other groups showed similar results.

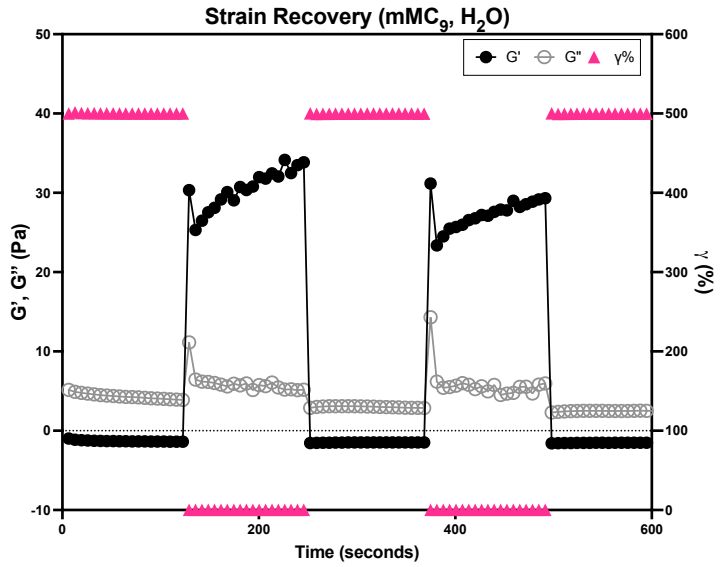

Figure 2.7: Representative graph of gel recovery under cyclic strain.

2.3.5 Effect of Temperature on Redox-Initiated Crosslinking of Methacrylated MC

Gelation of methacrylated MC hydrogels with redox initiators APS and TEMED was performed at 20ºC and 37ºC to compare the gelation kinetics and modulus of thermosensitive, chemically crosslinked gels. Characteristic gelation curves (**Figure 2.8A**) showed a toe region where chemical crosslinking and polymerization was not dominant within the gel system at 20ºC that lasted an average of 3:39 ± 0:36 minutes across all methacrylated groups (not significantly

different). This lag time was eliminated when gelation occurred at 37ºC. Gelation initiation time was significantly different across all methacrylation percentages at 20ºC (**Figure 2.8B**), with gelation onset occurring more rapidly with increasing methacrylation, ranging from 0:34 ± 00:06 to 04:37 ± 00:32 minutes for all methacrylated groups. With mMC_9, gelation onset was nearly instantaneous even at 20ºC, however, there was still a toe region. There was no significant difference between gelation onset time for all groups at 37ºC, with *G'>G"* occurring at or prior to the first recorded point, ranging from 26 ± 4 seconds to 42 ± 14 seconds. Unmethacrylated MC was mixed with redox initiators and prepared exactly as the methacrylated MC to investigate any effect the redox initiators might have on gelation characteristics of the unmodified polymer. Unmodified MC did not achieve consistent gelation initiation at 20ºC, as *G'* became equal to *G"* at a few points but never crossed over. Gelation completion, defined as the point at which *G'* increased by less than 2% for 4 or more consecutive points (**Figure 2.8A**, dotted red line) and coinciding with a plateauing of the gelation reaction, was significantly different between 20ºC and 37ºC for all methacrylated MC, with an average difference of 5:33 ± 00:51 minutes between temperatures.

Initial *G'* ranged from 0.773 ± 0.271 to 16.416 ± 4.786 Pa and was significantly influenced by both methacrylation percentage and temperature. Upon gelation completion, *G'* was two orders of magnitude greater in the methacrylated MC gels (1,046.63 ± 139.84 to 3,722.67 ± 474.21 Pa) than uMC (0.842 ± 0.093 to 8.383 ± 6.169 Pa), due to the formation of chemical crosslinks by the redox initiation of methacrylate crosslinking. Viscosity behaved similarly, with initial $|\eta^*|$ for mMC_9 higher than all other groups, although values were on the same order of magnitude for all samples (under 5 Pa•s), and $|\eta^*|$ at completion ranging from 166.60 ± 22.30 to 592.5 ± 75.54 Pa•s. *G'* and $|\eta^*|$ were higher in all gels formed at 37ºC than those formed at 20ºC except for mMC_9.

Although gelation completion had been achieved as defined previously by the plateauing of *G'*, gels continued to stiffen as the final remnants of free radicals and methacrylates reacted to form crosslinks, and by the true end of the reaction, each methacrylated MC group was significantly stiffer than at "completion." Gels from mMC_2 and mMC_5 formed at 20ºC were no longer significantly softer than those formed at 37ºC, as the reactions had essentially "caught up" with those at 37ºC. However, while mMC_9 gels also continued to increase in *G'*, the increase at 20ºC was significantly higher than at 37ºC (**Figure 2.9**). The phase angles for all chemically crosslinked gels were less than 1 (0.341º ± 0.065 to 0.856º ± 0.033) indicating the formation of strongly crosslinked elastic solids, while uMC reached a δ of 65.553º ± 8.095 at 20ºC and 20.190º ± 8.072 at 37ºC, consistent with a viscous fluid at room temperature and a weak elastic gel at physiologic temperature.

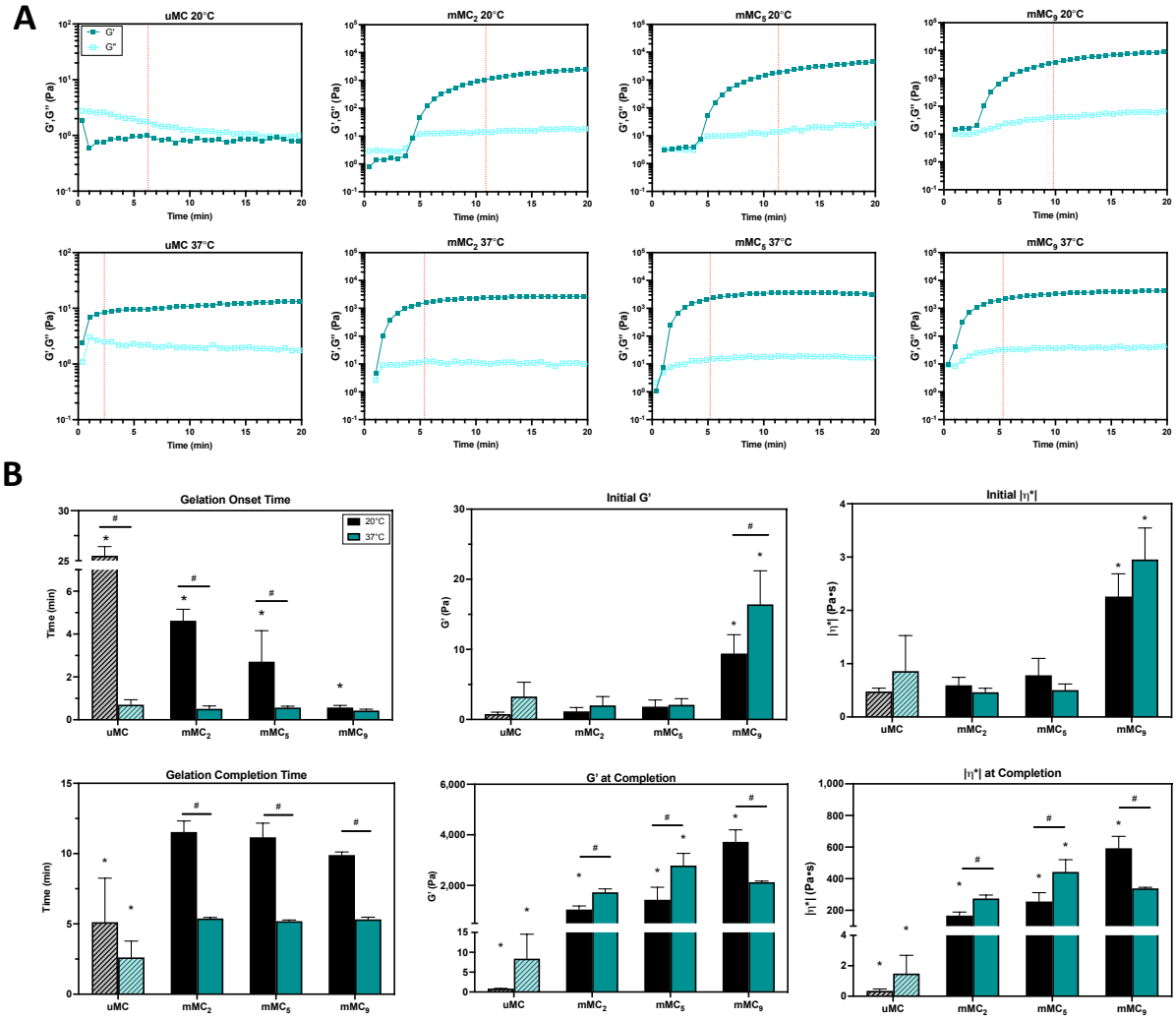

Figure 2.8: Free-radical polymerization of MC formulations with redox initiators APS and TEMED (10 mM each) in PBS at room temperature (20ºC) versus physiologic temperature (37ºC). A) Representative gelation curves over 20 minutes. B) Values measured from gelation curves for gelation onset and completion time, and storage modulus *G'* and complex viscosity |η*| at the initiation and completion of the redox polymerization reactions. (uMC included for comparison but did not react with redox initiators as it does not have methacrylate groups). * - Significant difference from other methacrylation % within temperature # - Significant difference between temperature within the same methacrylation %. Significance set at $p < 0.05$.

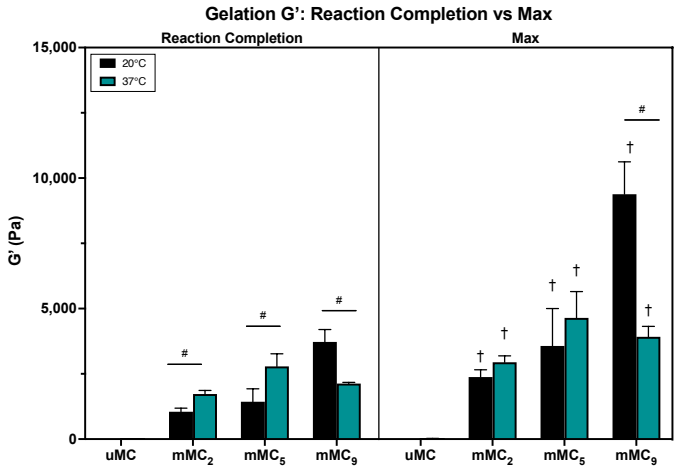

Figure 2.9: Continued increase in storage modulus G' after completion of free-radical polymerization reaction.

[#] - Significant difference between gelation temperature within the same methacrylation %. [†] - Significant difference from "reaction completion" within the same methacrylation % and temperature. Significance set at $p < 0.05$.

2.4 Discussion

Thermogelling hydrogels have immense utility in biomedical applications, as they take advantage of the difference between ambient temperatures and physiologic temperatures to form gels *in situ,* allowing minimally invasive delivery of therapeutics, drug depots and cell-laden scaffolds. In order to achieve robust mechanical properties that withstand physiological stresses and strains *in situ,* high macromer concentrations may be necessary, however, rendering injectability more difficult, as increased macromer concentration even at low temperatures is often accompanied by high viscosity. We have previously shown that MC, a thermogelling derivative of cellulose, can be chemically modified with methacrylate groups to enable the formation of stable, chemically crosslinked hydrogels via photopolymerization (Stalling, Akintoye, and Nicoll 2009). The use of redox initiators in a dual-barrel syringe system further enables injectability of these chemically crosslinking gels, which have been characterized extensively for their material properties including swelling, compressive mechanics, long-term stability, and cytocompatibility

(Gold et al. 2014; 2015). Here, we investigated the influence of hydrophobic methacrylate substitutions on the thermogelation of MC via rheometric analysis. It was found that the combination of thermally mediated physical crosslinks and redox-initiated chemical crosslinks influences the rate and efficiency of gel formation as well as the final gel strength in relation to the percent methacrylation of MC. This has implications for ease of use in surgical implementation, as well as tuning hydrogel formulations for a variety of indications.

Physiologic applications for thermogelling polymers require a threshold of 37ºC for onset of gelation, above which a polymer solution is generally considered less than ideal for biomedical applications, because it implies that the change in temperature upon injection would not elicit a gelation response. There is, however, no consensus in the literature for determining the temperature of thermogelation. Rheology has widely been used as a tool to measure the gelation properties of MC. While other analytical methods like differential scanning calorimetry (Haque and Morris 1993; Li et al. 2002) and turbidimetry (Arvidson et al. 2013; Zheng et al. 2004) have also successfully been used to measure thermogelation onset temperature, rheology provides data relevant to the physical behavior of the material, such as shear modulus, phase angle, and viscosity, which are of particular interest in the characterization of an injectable material for clinical applications. Within the available rheometric studies of thermogelling materials, numerous definitions of thermogelation onset temperature have been used, making comparison across studies difficult. The most common and traditional definition for gelation is point at which *G'* becomes greater than *G"*, indicating the elastic component of the modulus dominating over the viscous component (Desbrières, Hirrien, and Ross-Murphy 2000; Winter and Chambon 1986; Payne et al. 2017; Caicco et al. 2013; Oğuz and Ege 2018; Almdal et al. 1993). This method works reasonably well where the difference between *G'* and *G"* grows rapidly, however, frequently there is no

physical significance as both *G'* and *G"* remain within an order of magnitude of each other for a considerable range of temperature increase beyond that point, and the rapid increase in *G'* indicative of molecular aggregation has not yet been reached (**Figure 2.3B**). This is particularly evident at lower concentrations of MC. The temperature at which *G'* exhibits a sharp increase has also frequently been used as the definition of thermogelation onset, although there is no consensus on a numerical method to identify it (Knarr and Bayer 2014; Xu and Li 2005; Haque and Morris 1993; Tate et al. 2001; Xu, Li, et al. 2004; Almeida, Rakesh, and Zhao 2018). Here, we have proposed a method of defining the rapid increase in *G'* by identifying the point at which *G'* consistently increases by greater than 2% for 4 or more consecutive points (at a sampling rate of 6.5 s), thus resulting in a more physically relevant increase in *G'*. Zheng *et al.* (2004) have previously showed that the first derivative of *LogG'* with respect to temperature, *T*, is a reliable mathematical method for rheologically determining the sol-gel transition of thermally gelling MC, as it represents the highest rate of increase in *G'*. This has also been shown to correspond with the endothermic peak in calorimetric measurements of MC thermogelation and the cloud point measured by turbidimetry (Li 2002; Wang and Li 2005).

Temperature ramps of MC samples showed that "thermogelation onset temperature" decreased with increasing methacrylation percentage across all methods of determination. The derivative of *LogG'* gave the most consistent results both with respect to the effect of saline solution and the effect of methacrylation percentage on reduction of thermogelation temperature. It was observed that due to the initial decrease in *G'* at increasing temperatures of unmodified MC, the >2% increase in *G'* occurred at a much lower temperature than *dLogG'*. This initial decrease in *G'* with increasing temperature is characteristic of most liquids, and the disappearance of that behavior from methacrylated MC samples is indicative of the increased intermolecular aggregation

between macromolecular chains in the presence of methacrylate groups even at low temperatures. The crossover point where *G'* > *G"*, which is most commonly used as an indicator of gelation, was shown to have the greatest variability between groups. Indeed, mMC_9 and occasionally mMC_5 in PBS never displayed such a crossover, as *G'* began higher than *G"* even at 4ºC. As the polymer solution was able to flow and be extruded through a micropipette, the material had not formed a strong gel despite meeting the technical definition of having achieved sol-gel transition, thus supporting the conclusion that *G'*>*G"* is not a fully accurate physically descriptive criterion for identifying thermoresponsive aggregation, particularly at low concentrations. Here, it can be observed that between the three criteria, a given sample may or may not meet the threshold for thermogelation at physiologic temperature: if *dLogG'/dT* is used, none of the samples achieve thermogelation at 37ºC, however, the other criteria show that the thermal response does begin at or below 37ºC. The Winter-Chambon criterion describes the point at which the elastic component of the shear modulus becomes dominant over the viscous component, thus behaving in a more "gel-like" manner. Nevertheless, this does not necessarily correlate with the thermal response of the material, as some formulations displayed gel-like behavior at the lowest temperature recorded, indicative of strong inter-chain bonds, but the rapid response of *G'* to increasing temperatures did not occur until later in the temperature sweep. As such, the thermoresponsive behavior of polymer solutions and particularly thermogelation onset should be clearly regarded as distinct from the Winter-Chambon criteria for the shift to more gel-like behavior of viscoelastic materials.

To examine the thermoresponsive behavior of MC in a physiologically relevant test, MC was equilibrated at 4ºC and then the temperature was rapidly raised to 37ºC and held constant for 15 minutes, simulating the rapid increase in temperature from refrigerated storage to injection *in vivo* and its development over time. Despite the fact that not all groups achieved a thermogelation onset

temperature of 37ºC or less (according to any of the aforementioned definitions), all MC formulations underwent some thermogelation when the temperature was raised to 37ºC (**Figure 2.3**). This indicates that the temperature-dependent gelation response of MC is not binary, in that the solution can display thermoresponsive behavior below the "thermogelation onset temperature". All groups started at 4ºC with *G'<G"* and rapidly increased in *G'*, undergoing sol-gel transition before plateauing. Thermogelation at 37ºC did not result in strong gels, however; across all groups, *G'* increased by only one order of magnitude, with the maximum storage modulus achieved by mMC_9 in PBS at 146.27 ± 8.29 Pa (**Figures 2.4-2.6**). These values are on the order of other reported MC thermogels at 37ºC including those of higher macromer percentage, further exhibiting that increasing methacrylate percentage increases hydrophobic interactions, thereby strengthening the gels (Shin et al. 2020; Jung, Kim, and Ho Park 2019; Gupta, Tator, and Shoichet 2006; Caicco et al. 2013; Stabenfeldt, Garcia, and LaPlaca 2006).

There was also a marked effect of solvent on the temperature-dependent, strain response of the gels (**Figures 2.4-2.6, Table 2.2**). In both H_2O and PBS, mMC_9 formed very weak gels even at 4ºC, which displayed shear thinning behavior. Interestingly, uMC and mMC_2 gels exhibited shear thinning behavior at 37ºC, while mMC_5 and mMC_9 did not. In H_2O, mMC_5 briefly yielded and decreased in *G'* at increased strain but then underwent strain stiffening and did not experience a gel-sol transition, while in PBS, it did not yield at all and only displayed strain stiffening. In H_2O, very transient strain stiffening behavior in mMC_9 was followed immediately by rupture of the gel; there was no stiffening prior to rupture in PBS. The formulations that underwent true strain yielding experienced it at moderate strain percentages (1.53 ± 2.64% to 12.88 ± 6.38%) whereas the rupture of mMC_9 occurred at much higher strains (21.22 ± 2.84% and 51.49 ± 9.178% in PBS and H_2O, respectively). As has been previously shown, PBS likely strengthened the hydrophobic

interactions at the higher methacrylation percentages, rendering the gels more brittle, and for mMC_9, resulting in rupture at a lower strain percentage than in H_2O (Thirumala, Gimble, and Devireddy 2013; Zheng et al. 2004). Similar strain stiffening behavior is seen in many biopolymers, including type I collagen, actin, and fibrin (Erk, Henderson, and Shull 2010; Motte and Kaufman 2013).

Concern over whether strain stiffening could potentially make injectability more difficult for an *in situ* polymerizing biomaterial motivated investigating the recovery behavior of the MC thermogels. These tests showed that MC deformed and recovered under rapidly cycling changes at high strains (**Figure 2.7**). The strain stiffening seen in the sweep experiments, in which a graded increase in strain was applied, can be attributed to the gradual ordering of the polymer chains and associated increases in chain alignment and polymer crystallinity. In contrast, the rapid recovery at high cyclic strains likely did not allow for increased chain organization, with the material retaining its amorphous structure.

Having shown the effect of methacrylates on the thermal response of physically crosslinked gels, further studies focused on characterizing the influence of the thermal response on chemically crosslinked gels. MC solutions were mixed with redox initiators APS and TEMED in dual-barrel syringes and extruded via mixing tips onto the rheometer peltier plate at either 20ºC or 37ºC. Unmodified MC was used as a control to assess the influence of the redox initiators on thermogelation, as the absence of methacrylates prevents any chemical crosslinking from occurring. As was expected, uMC did not undergo thermogelation at 20ºC in H_2O but did undergo thermogelation at 37ºC; there was no significant difference when compared to the behavior of uMC in PBS as presented in **Figure 2.5**, suggesting that 10 mM concentrations of APS and TEMED do not strongly influence the thermoresponsiveness of the base polymer (data not shown).

Redox-initiated gelation resulted in shear moduli 1-2 orders of magnitude greater than physically crosslinked gels alone, without raising the macromer concentration (**Figure 2.8**). Increasing the macromer concentration increases viscosity, which would make injection of high macromer concentration cellulosic solutions difficult for minimally invasive procedures using fine gauge needles.

The ability to rapidly transition from a viscous fluid to an elastic solid at physiologic temperature is a highly appealing feature that combines ease of delivery with structural stability. It was shown that redox-initiated chemical gelation was accelerated at 37ºC versus 20ºC across all methacrylated groups (**Figure 2.8A**). The toe region of the gelation curves observed at 20ºC appear to indicate where physical interactions were dominating the reaction, as the MC polymer chains intermixed and arranged in such a way that free radicals produced by the initiators had yet to substantially crosslink the methacrylates at that point. Thermogelation onset temperature measurements shown in **Figure 2.4** demonstrated that the *G'>G"* point occurred prior to 20ºC for mMC_9 (< 4ºC) and mMC_5 (5.20 ± 5.64ºC), and that for mMC_2, 20ºC was within one standard deviation of the mean (28.26 ±11.46ºC). The gelation onset time of redox-polymerized gels at 20ºC reflected that pattern, with the onset time for $mMC_2 > mMC_5 > mMC_9$, confirming that the methacrylate contribution to thermogelation plays a role even when redox initiators are present (**Figure 2.8B**). At 37ºC, all formulations began gelation instantaneously, which could be a result of both thermogelation onset at 37ºC (which occurred within 1 minute for nearly all formulations) and heat-mediated acceleration of the redox-initiated chemical reaction. Once the redox reaction began to dominate, there was no effect of the interplay between methacrylation percentage and thermogelation on completion.

Redox-polymerized gels increased in stiffness with increasing methacrylation percentage at 20ºC, which is not unexpected (assuming complete conversion of all available methacrylates during crosslinking), as the theory of rubber elasticity states that hydrogel strength and stiffness increase with increasing crosslinking density (Flory and Rehner 1943a). Interestingly, this pattern was not evident at 37ºC, with mMC_9 exhibiting lower *G'* at completion than mMC_5. Additionally, by gelation completion, all groups except mMC_9 achieved higher *G'* at 37ºC vs 20ºC. Although gelation was complete by the accepted definition of reaction completion (Temenoff et al. 2003; Gold et al. 2014), gels continued to stiffen, and by the end of the reaction, there was no significant difference in *G'* between gels made at 20ºC and 37ºC for both mMC_2 and mMC_5 (**Figure 2.9**). However, the difference between the moduli of gels formed at 20ºC and 37ºC for mMC_9 persisted, with the gels formed at 20ºC continuing to stiffen for an extended period. Not only was *G'* significantly lower for mMC_9 when gelation occurred at physiologic temperature, but it was also found not to be significantly different from the two lower methacrylation percentages at the same temperature. This disproves the hypothesis that thermogelation and redox-initiated gelation would have an additive effect, resulting in stiffer gels. Moreover, it suggests that there is a point at which temperature directed network structure formation at 37ºC prevents efficient or complete chemical crosslinking reactions between methacrylate groups. While it is generally understood that chemical crosslinks are much stronger than physical crosslinks, steric influences of physical crosslinking can dictate how many chemical crosslinks are able to actually form. Phase separation and syneresis may prevent mixing and penetration of free radicals produced by the redox initiators (Sarkar 1979; Wu et al. 2021; Arvidson et al. 2013; Nasatto et al. 2015). While these effects appear to be negligible in mMC_2 and mMC_5, the strength of the hydrophobic aggregate formation in mMC_9 demonstrated by *G'>G"* (even at 4ºC), the lack of shear thinning behavior, and rupture during

strain sweeps at 37ºC appears to be causing syneresis-driven inefficiency in free-radical crosslinking at physiologic temperature. Morozova et al. (2019) have also shown that allyl-modified MC hydrogels result in softer gels when chemically crosslinked at a higher temperature versus low temperature, based on the permanent chemical crosslinking of the MC network/fibrils formed by physical aggregation at higher temperatures.

As tunability is a highly desirable factor in biomaterial development, understanding the interaction of the thermosensitive nature of MC and the reaction efficiency of redox-initiated crosslinking will be important for predicting the behavior of these gels when injected and formed *in vivo*. It is well established that macromer concentration, degree of methoxy substitution, and solvent all influence the thermoresponsive behavior and rheo-mechanical properties of MC solutions (Nasatto et al. 2015; Sarkar 1979). In addition, it was previously shown that chemically crosslinked Ma-MC can produce highly tunable chemically crosslinked hydrogels for a variety of applications (Stalling, Akintoye, and Nicoll 2009; Gold et al. 2014; 2015; Varma et al. 2018). Here, it was demonstrated that increasing methacrylation percentage gave rise to increased inter-chain hydrophobic interactions, further resulting in lowered thermogelation onset temperature (**Figure 2.3**) and stiffer physically crosslinked gels (**Figure 2.6**). Formulations with higher methacrylation percentages (i.e., mMC_5 and mMC_9) showed very strong interchain interactions, particularly in PBS, which was reflected by G'>G" at 4ºC (**Figure 2.3B** and **Figure 2.5**), as well as strain stiffening behavior. These solutions exhibited significant increases in viscosity at 37°C (relative to values at 4ºC) without the addition of redox-initiated crosslinking (**Figure 2.6B**). This suggests that these specific formulations are less likely to rapidly migrate or diffuse from the injection site. Further tuning of the methacrylation percentage and a wider range of strain measurements would provide more in-depth information regarding control of the injectable

system. Initial complex viscosity of all groups tested was on the lower end of commercially available dermal fillers (i.e., Teosyal Meso, 0.942 Pa·s), while final viscosity for physically and dual-crosslinked gels was comparable to medium and high viscosity commercial fillers (Belotoro (32.9 Pa·s) and Restylane (532.4 Pa·s), respectively), all of which are injectable via 27-30 gauge needles (Falcone and Berg 2009).

Previous studies in our lab have employed the use of "pre-gelling" redox-initiated crosslinked systems by warming the dual-barrel syringe containing mMC and redox initiators to 37ºC prior to injection (Varma et al. 2018). Anecdotal observation has shown that while the thermogelled system remains injectable (as corroborated here by strain sweep and strain recovery), a large amount of force is required to eject the pre-gelled solution, which can interfere with handling, particularly in situations where careful volume control is necessary such as dermal fillers. In addition, the present data indicate that at high methacrylation percentages, not only is injection of a pre-gelled solution more difficult (due to strain stiffening), but it may also interfere with complete redox-initiated crosslinking efficiency. Still, the increase in thermoresponsiveness of mMC at higher methacrylation percentage is indicative of rapid *in situ* gelation that would likely resist extravasation at physiologic temperatures and supports the use of pre-cooled solutions for injectable applications.

Beyond injectable applications, dual-crosslinked injectable hydrogels show great potential for 3D printing and bioinks (Loebel et al. 2017). Similar dual-crosslinked MC hydrogels have recently been formulated with tyramine-modified MC, which possess initial storage moduli (uncrosslinked) on the same order of magnitude as mMC but require higher MC concentrations (8%) (Shin et al. 2020). These formulations resulted in softer thermogelled constructs (G' ≈ 11 Pa) that maintained fidelity of the printed shape when extruded at 37ºC, and were then able to be photocrosslinked and

cured to form gels with moduli up to 250 Pa. As shown previously, mMC can successfully form stable, biocompatible hydrogels via photo-initiated crosslinking (Stalling, Akintoye, and Nicoll 2009), resulting in much stiffer gels (3-8 kPa) at lower concentrations (2-4%), which holds promise for future studies that might use cell-laden mMC as a bioink for 3D printing of tissues.

2.5 Conclusion

In this study, increasing methacrylation of MC was shown to increase intermolecular attraction via hydrophobic interactions, which in turn decreases thermogelation onset temperature and enhances the strength of the thermal response. Moreover, the methacrylate contribution to MC thermogelation accelerates the redox-initiated crosslinking reaction and contributes to matrix stiffening at physiologic temperatures. Nevertheless, there is a limit after which thermal aggregation of hydrophobic groups prevents efficient chemical crosslinking due to phase separation. This behavior is not only critical in assessing the injectability of potential thermoresponsive, dual-crosslinking biomaterials, but also in predicting the *in situ* behavior of the gels. Future studies will further characterize the molecular mechanisms and long-term mechanical behavior of these dual-crosslinked hydrogels.

2.6 Acknowledgements

This work was supported in part by a grant from the National Science Foundation (IIP 1701120). The authors wish to thank Dr. Padmanava Pradhan for technical assistance with ^{1}H-NMR spectroscopy, and Dr. Jeff Morris for the use of the AR2000ex Rheometer.

Chapter 3: Injectable Sulfonated Methylcellulose Hydrogels with Tunable Growth Factor Sequestration as Potential Nucleus Pulposus Replacements

The following chapter was presented in part at the Orthopaedic Research Society Annual Meeting (2018) and the Society for Biomaterials Annual Meeting and Exposition (2019):

Haq-Siddiqi N.A., Nnadi W.O., Lin H.A., Nicoll S.B. (2018). Characterization of a novel injectable, thermogelling sulfated methylcellulose hydrogel system for nucleus pulposus repair. (Poster Presentation) *Trans. Orthop. Res. Soc*., **43**: 1232. *64th Annual Meeting of the Orthopaedic Research Society*, New Orleans, LA.

Haq-Siddiqi N.A., Bunde K., Nnadi W.O., Iatridis J.C., Nicoll S.B. (2019). Injectable sulfonated methylcellulose hydrogels for growth factor sequestration and nucleus pulposus repair. (Podium Presentation) *Trans. Soc. for Biomater.*, **40**: 10. *42nd Annual Meeting and Exposition, Society for Biomaterials,* Seattle, WA.

3.1 Introduction

Degeneration of the intervertebral disc (IVD) has been implicated as a primary cause of lower back and neck pain, which are responsible for 12-14% of all adult medical visits in the United States (not counting physical therapy and chiropractic visits) (Bone and Joint Initiative USA 2015). IVD degeneration is characterized as an aberrant, cell-mediated response to structural failure, wherein diminished nutrient transport, cellular senescence, increased enzymatic activity, and changes in matrix composition and hydration progressively and rapidly contribute to the breakdown of the disc (Adams and Roughley 2006). The etiology of the disease is thought to begin with the loss of hydration in the central nucleus pulposus (NP) region, which causes a decrease in IVD height and increased loading on the circumferential annulus fibrosus (AF). This leads to AF bulging, fissures, and potentially herniation of the NP through the AF, in addition to vertebral changes such as endplate calcification and osteophyte development (Adams & Roughley, 2006). Symptomatic degeneration is associated with discogenic pain, which is caused by the infiltration and subsequent stimulation of nociceptive nerve fibers in the AF, or by radiculopathy, which results from compression of spinal nerve roots, inducing pain, numbness and tingling throughout the lower back and legs (Peng 2013). Medical treatment for degenerative disc disease is conservative and generally involves physical therapy, pharmaceutical pain management, or a combination of the two, although these methods are purely palliative and do not address the progressive degenerative state. Eventually late-stage degeneration can be treated surgically via spinal fusion, however, this alters spinal loading further, and does not reduce the progression of degeneration in adjacent IVD segments (Zhao et al. 2019; Natarajan and Andersson 2017).

Biomaterial replacement of the degenerate NP has been proposed in order to restore IVD height and mechanical properties and to promote the biological repair of the injured tissue by

directing cellular behavior within a biomaterial scaffold (Choi, Park, and Lee 2019; Stergar et al. 2019; Tendulkar et al. 2019; Pelletier et al. 2016; Goins et al. 2005). Hydrogels, water-swollen polymeric matrices, are an ideal class of material for NP repair, as they resemble the highly hydrated network properties of the native tissue (Peppas et al. 2006; Guan et al. 2017; D'Este, Eglin, and Alini 2018; Bowles and Setton 2017). Several natural and synthetic hydrogels have been shown to support NP-like matrix deposition by encapsulated NP cells and mesenchymal stem cells (MSCs) (Tsaryk et al. 2014; Illien-Jünger et al. 2016; Thorpe et al. 2017; Wang et al. 2019; Kumar et al. 2016; Gupta, Cooper, and Nicoll 2011). Recent clinical trials exploring such hydrogels as acellular NP replacements or as cell delivery vehicles for NP regeneration have had some success targeting patients exhibiting discogenic pain without disc bulging or herniation, and with no more that 30% to 50% loss of disc height at the treatment level (Amirdelfan et al. 2021; Ceylan et al. 2019).

Cellulose-derived scaffolds are a unique class of materials in that they are naturally-derived, plant polysaccharides with similar structure to glycosaminoglycans (GAGs) that are the most abundant dry constituent of the NP. Moreover, since they are not animal derived, cellulosic materials are not susceptible to enzymatic degradation by the elevated levels of matrix metalloproteinases that may be present in the injured and degenerate IVD (Sivan, Wachtel, and Roughley 2014). Cellulose ethers such as methylcellulose (MC) and carboxymethylcellulose (CMC) are water-soluble cellulose derivatives that have been FDA-approved for a number of biomedical and food applications (Rohowsky et al. 2016). We have demonstrated previously that methacrylation of both CMC and MC allows for the formation of stable, covalently crosslinked hydrogels via free radical polymerization. The resulting gels exhibit a very mild foreign body response and can be used for various clinical indications (Gold et al. 2015; 2014; Varma et al.

2014; Stalling, Akintoye, and Nicoll 2009; Reza and Nicoll 2010a). In particular, photocrosslinked hydrogels fabricated from methacrylated CMC (Ma-CMC) were investigated for NP tissue engineering due to the negatively charged carboxyl groups on the CMC backbone, which contribute to its high swelling capacity and similarity to the polyanionic sulfated GAG-rich network of the native NP. These Ma-CMC-based hydrogels were shown to promote NP-like matrix elaboration by encapsulated cells with exogenous delivery of transforming growth factor-beta 3 (TGF-β3) *in vitro* (Gupta, Cooper, and Nicoll 2011; Gupta and Nicoll 2015). In follow-up studies employing redox polymerization to impart superior injectability and *in situ* gelation properties (in contrast to photopolymerization systems) (Varma, DiNicolas, and Nicoll 2018), Ma-CMC was not retained within the high-pressure IVD space and extravasated before gelation completion (Varma et al. 2018). In order to be an effective minimally invasive therapy, the replacement material (with or without biologics or therapeutics) must remain localized at the injection site and be delivered via a small gauge needle so as not to compromise the mechanics and pressurization of the IVD (Elliott et al. 2008; Iatridis et al. 2013). MC has a unique thermogelation capacity, which allows it to increase in viscosity at increasing temperatures (Sarkar 1979; Haque and Morris 1993). Here, we propose the use of a thermoresponsive, cellulosic formulation that undergoes redox-initiated crosslinking within the IVD void space may provide improved intradiscal retention *in situ*.

The degenerate NP is marked by extremely limited nutrient availability due to the diminished concentration of sulfated GAGs, which drive the influx of nutrients and cytokines into the IVD (Huang, Urban, and Luk 2014; Loibl et al. 2019; Ohnishi, Novais, and Risbud 2020; Walter et al. 2016). Artificial sulfation by the addition of negatively charged sulfate (SO_4^{2-}) or sulfonate (SO_3^-) groups directly onto a candidate biomaterial may be used to mimic the mechanism by which

growth factors and other proteins are localized by sulfated GAGs in native tissues (Zhu and Marchant 2011; Censi et al. 2012; Belair, Le, and Murphy 2014; Wang and Von Recum 2011). For example, heparin-based growth factor delivery systems have been investigated due to the affinity of many growth factors such as bone morphogenetic proteins, basic fibroblast growth factor, and TGF-β to heparin, thus enabling sustained release of the incorporated growth factor (Liang and Kiick 2014; Jennifer Lei, Trevino, and Temenoff 2016; Park et al. 2012; Hettiaratchi et al. 2014; Jeon et al. 2011). Interaction of growth factors with matrix macromolecules has also been shown to enhance growth factor bioavailability, with some growth factors showing greater resistance to proteolysis and thermal denaturation when bound to heparin or heparan sulfate (Ji et al. 2009; Park et al. 2008). Previous work has demonstrated that exogenous transforming growth factor-β3 (TGF-β3) supplementation supports the differentiation of encapsulated NP and bone marrow-derived stromal cells in cellulosic hydrogels *in vitro* (Gupta, Cooper, and Nicoll 2011; Gupta and Nicoll 2014; 2015; Lin et al. 2016; Varma, DiNicolas, and Nicoll 2018). However, exogenous supplementation of growth factors in culture media is not translatable for an *in situ* curing system. A viable therapy utilizing an injectable scaffold would need to deliver the signaling factors by directly incorporating them into the biomaterial. Recently, polysaccharides such as alginate (Freeman, Kedem, and Cohen 2008), hyaluronic acid (Feng et al., 2017; Purcell et al., 2014), and cellulose (Portocarrero Huang et al. 2018; Arora, Mahajan, and Katti 2017; Waghmare et al. 2018) have been artificially sulfated for affinity-based growth factor delivery, with promising results, and suggest a similar approach may be employed with MC.

This study presents the characterization of an injectable, *in situ*-gelling NP replacement biomaterial capable of growth factor sequestration. Specifically, hydrogels comprised of Ma-MC macromers at low effective concentrations (2%, 3%, and 4%) were sulfonated with the addition of

2-sulfoethyl methacrylate (2SEM), which can react with free methacrylate groups on Ma-MC during redox-initiated, free radical polymerization (**Figure 3.1**). This method of sulfonation takes advantage of the hydrogel polymerization reaction and negates the need for extra processing steps. The addition of charged methacrylate monomers in the formulation may support serum protein adsorption and enable growth factor sequestration but may also hinder the gelation process during injection and formation via competition for pendant methacrylate groups. Therefore, the objectives of this study were to assess the effects of sulfonate modification on the injectability, gelation, functional material properties (i.e., mechanics, swelling), and TGF-β3 sequestration capability of MC hydrogels as potential NP replacements.

3.2 Materials and Methods:

3.2.1 Methacrylation of Methylcellulose

Methacrylated methylcellulose (Ma-MC) was synthesized through esterification of hydroxyl groups based on previously described protocols (**Figure 3.1A**) (Stalling, Akintoye, and Nicoll 2009; Gold et al. 2014). A 1:1 ratio of 15 kDa and 41 kDa MC (degree of substitution of methoxy groups: ~1.5-1.9) (Sigma-Aldrich, St. Louis, MO) was dissolved at 1% (w/v) total macromer concentration in deionized H_2O (diH_2O) and reacted with methacrylic anhydride (Sigma-Aldrich, St. Louis, MO) in 20-fold excess (based on a theoretical 10% modification) for 48 hours at 4°C with periodic adjustments of pH with NaOH to maintain a pH of 8.0 (Varma et al., 2018). The combination of low and medium molecular weight MC was employed to balance the need for ease of handling (i.e., mixing and injectability) with producing hydrogels of sufficient structural integrity (Gold, 2017; Varma et al., 2018). The modified Ma-MC solution was purified of excess methacrylic anhydride via dialysis using Spectra/Por 1 dialysis tubing (MWCO 6-8 kDa, Spectrum Laboratories, Rancho Dominguez, CA) against deionized water for three days. During dialysis,

membranes were changed once daily and diH_2O changed twice daily to drive purification. Purified Ma-MC was recovered via lyophilization, and stored at -20°C.

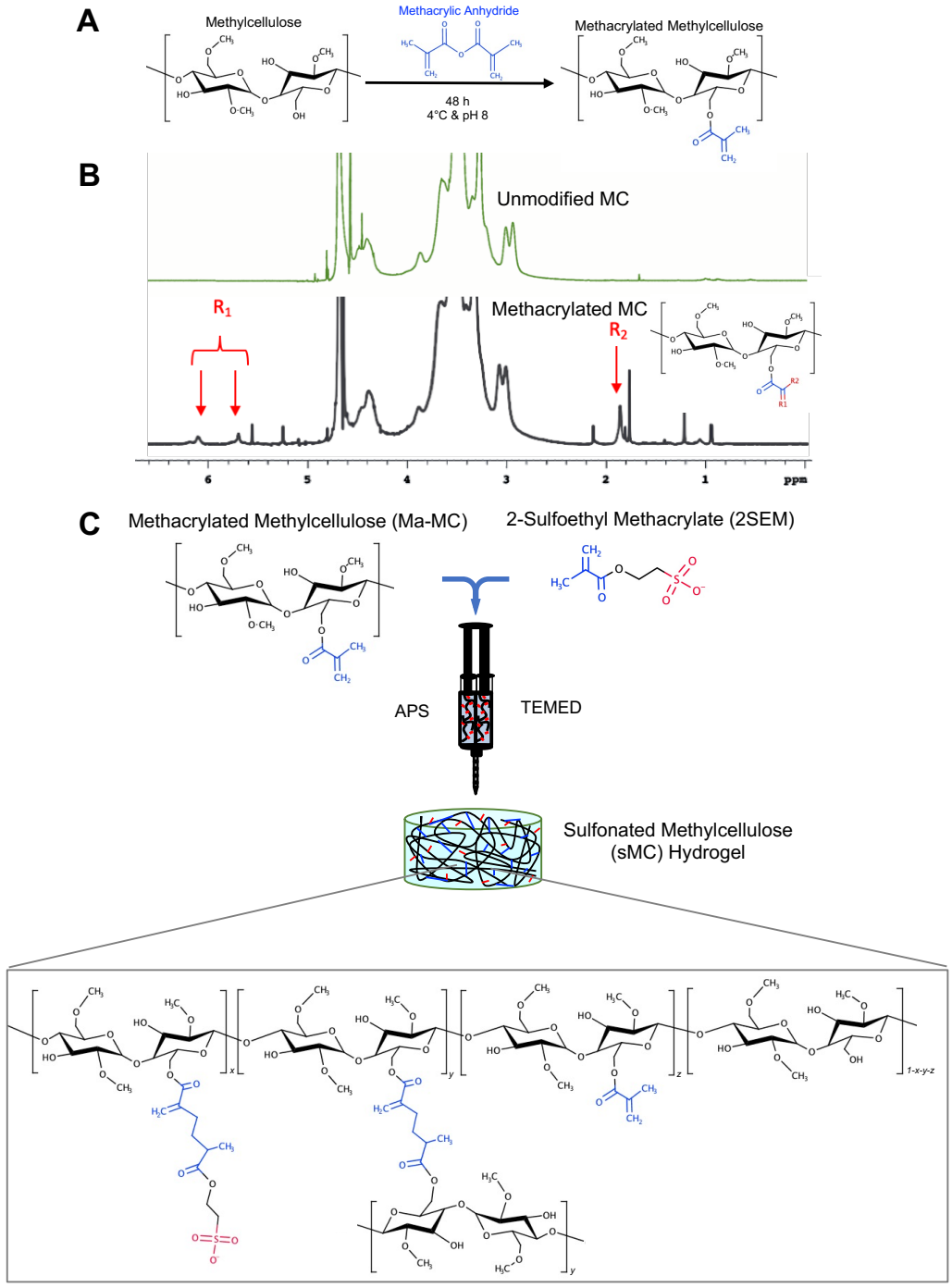

Figure 3.1: Synthesis and characterization of sulfonated methylcellulose (sMC) hydrogels. A) Methacrylation of MC and B) 1H-NMR spectra confirming methacrylate proton peaks. C) Hydrogel fabrication via redox-initiated crosslinking. sMC hydrogels were fabricated with 1, 5, or 10 mM 2SEM, and MC alone hydrogels were fabricated identically, without the addition of 2SEM.

3.2.2 Proton Nuclear Magnetic Resonance Spectroscopy (^{1}H-NMR)

Purified Ma-MC was acid hydrolyzed and ^{1}H-NMR (Varian 500 MHz, Agilent Technologies, Santa Clara, CA) was conducted to verify and quantify the degree of methacrylation. The relative integrations of methacrylate proton peaks (methylene, δ=6.2 and 5.8 ppm; methyl peak, δ=2.0 ppm) to protons on the methylcellulose backbone were used to determine the molar percentage of methacrylation.

3.2.3 Hydrogel Fabrication

Hydrogel constructs were fabricated by mixing polymer precursor solutions in dual-barrel syringes. Ma-MC was dissolved in Dulbecco's phosphate-buffered saline (DPBS) (Gibco) at final macromer concentrations of 2%, 3%, and 4% (w/v). Redox initiators ammonium persulfate (APS) (Sigma) and tetramethylethylenediamine (TEMED) (Sigma) were added at 10 mM final concentration each in opposing barrels of the syringe for free radical polymerization.

Sulfonation was achieved during polymerization through the addition of 2-sulfoethyl methacrylate (2SEM) (Polysciences) at 0 mM, 1 mM, 5 mM, and 10 mM final concentrations (**Figure 3.1C**). Mixing tips (1:1) were used to mix polymer precursors during ejection to create hydrogels in custom casting devices; polymer was allowed to cure for 15 min at room temperature to form cylindrical gels (5-mm diameter, 2-mm height).

3.2.4 Sulfonation Quantification

Hydrogel sulfonation was evaluated via 1,9-dimethylmethylene blue (DMMB) staining and quantification (n=5). Gels were swollen overnight in DPBS at 37°C and then stained with DMMB dye overnight. Unbound DMMB stain was removed by rinsing stained gels 2x in PBS. Gross images of stained gels were captured using a stereomicroscope (Stemi 2000-C) with Zeiss AxioVision software. Gels were then de-stained using a 4M Guanidine Hydrochloride (GuHCl)

solution overnight at 37°C with gentle agitation. Desorbed stain was quantified via absorbance at 656 for relative sulfonation (Barbosa et al. 2003).

3.2.5 Mechanical Testing

Compressive mechanics were measured by unconfined compression testing of the hydrogels on a custom apparatus as previously described (n=5) (Soltz and Ateshian 2000; Gold et al. 2014). Hydrogels were formed in molds as described in 2.3 and stored at -20°C until testing. Gels were thawed and equilibrated at room temperature in PBS for 2 hours prior to testing. The testing protocol consisted of an initial creep test (tare load = 1 g) at a ramp speed of 10 μm/s held at 2700 s until equilibrium was reached (equilibrium criterion: <10 μm displacement in 10 min), which was followed by a multi-ramp stress relaxation test, consisting of three 5% strain ramps with a 2000 s relaxation period between ramps (equilibrium criterion: <0.5 g change in 10 min. Equilibrium Young's modulus (E_Y) was determined as the slope of the equilibrium stress (calculated at each ramp) versus applied strain curve. Peak stress (σ_{pk}) and equilibrium stress (σ_{eq}) were calculated at the third ramp corresponding to 15% strain, and percent relaxation was calculated by the formula

$$Percent\ Relaxation = \left(1 - \frac{\sigma_{eq}}{\sigma_{pk}}\right) \tag{3.1}$$

3.2.6 Swelling Properties and Hydrogel Network Characterization

Equilibrium weight swelling ratio (Q_w) was measured for all hydrogel formulations (2%, 3%, 4% w/v Ma-MC; 0, 1, 5, 10 mM 2SEM) (n=4). Freshly made hydrogels were swollen in PBS overnight at 37°C. Gels were removed from PBS and blotted to remove excess liquid and then placed in pre-weighed 1.5 mL microcentrifuge tubes. Wet weight, (W_s) was taken prior to freezing at -80°C. Frozen gels were lyophilized and dry weight measured (W_d). Equilibrium weight swelling ratio was calculated as:

$$Q_w = \frac{W_s}{W_d} \tag{3.2}$$

and volumetric swelling (Q_v) was determined from the weight swelling ratio by

$$Q_v = 1 + \left(\frac{\rho_p}{\rho_s}(Q_w - 1)\right) \tag{3.3}$$

where ρ_p is the density of the dry polymer (0.276 g/cm^3) (Leach et al. 2003; Marsano, Gagliardi, et al. 2000), and ρ_s is the density of the solvent (PBS = 1.01 g/cm^3). The average molecular weight between crosslinks ($\bar{M}_c$) was calculated using a modified Flory-Rehner equation (Flory and Rehner 1943b; Mason et al. 2001; Gold et al. 2015; Leach et al. 2003):

$$Q_v^{5/3} \cong \frac{\bar{\nu}\bar{M}_c}{V_1}\left(\frac{1}{2} - \chi\right) \tag{3.4}$$

where $\bar{\nu}$ is the specific volume of the dry polymer, V_1 is the molar volume of the solvent (PBS ≅ water 18.0 mol/cm^3), and χ is the Flory polymer-solvent interaction parameter (0.473) based on the assumption that χ for MC is comparable to that of other polysaccharides such as hyaluronic acid and dextran due to similar chemical structures (Gold et al. 2014; 2015; Leach et al. 2003).

The Flory-Rehner model was then used to calculate effective crosslinking density, ν_e, and mesh size, ξ, of the swollen hydrogels using the following equations:

$$\nu_e = \frac{\rho_p}{\bar{M}_c} \tag{3.5}$$

$$\xi = \sqrt{\bar{r}_0^{\,2}}\left(\frac{\sqrt{\bar{M}_c}}{\sqrt{M_n}}\right) Q_v^{1/3} \tag{3.6}$$

where $\sqrt{\bar{r}_0^{\,2}}$ is the root-mean-square distance between crosslinks (Canal and Peppas 1989; Leach et al. 2003; Lin et al. 2016). The root-mean-square end-to-end distance previously reported for CMC (Cleland 1970) as

$$\sqrt{\frac{\bar{r}_0^{\,2}}{2n}} \cong 2.1\text{nm} \tag{3.7}$$

was used as an approximation for MC, as the polymer backbones are nearly identical (Gold et al. 2014; 2015). Here *n* represents the degree of polymerization:

$$n = \frac{M_n}{M_o} \tag{3.8}$$

where M_n is the number average molecular weight of the polymer and Mo is the molecular weight of the monomer unit (186.67 g/mol). In this study, a 1:1 ratio of 15 kDa and 41 kDa MC was used in order to facilitate handling, so we have taken the average, 28 kDa, as the M_n for mesh calculations, giving an average n of 150. The values calculated for νe, and ξ are considered approximations due to the assumptions made in the Flory-Rehner calculations.

3.2.7 Gelation Properties

Rheometric analysis was conducted on 2%, 3% and 4% w/v Ma-MC using an AR2000ex Rheometer (TA Instruments) equipped with a cone and plate geometry (2°, 20mm). Optimal test parameters (1% strain, 1 Hz frequency) were selected via strain and frequency sweep measurements on the base polymer solution (3% (w/v)) in DPBS.(Gold et al. 2015; D. M. Varma et al. 2018; Gold et al. 2014) Storage modulus *(G')*, loss modulus (*G"*), complex viscosity ($|\eta^*|$), and dynamic shear modulus *(|G*|)* were measured for each test. Results were analyzed using TA Data Analysis software (Advantage v5.4.0).

3.2.8 Thermogelation Onset Temperature

A temperature ramp from 4°C to 40°C (ramp rate: 1°C/min) was conducted to determine the temperature of thermogelation onset of the polymer solution (n=3). Polymer solutions were prepared without redox initiators in order to isolate the effect of temperature-sensitive physical crosslinking of MC polymer. Thermogelation onset was defined as the temperature at which the storage modulus (G') increased greater than 2% for 4 or more consecutive points.

3.2.9 Redox-Initiated Gelation

To assess gelation kinetics of the injectable, redox-polymerized system, a time sweep was conducted on polymer samples with redox initiators APS and TEMED (10 mM each) mixed into separate sides of 1:1 dual-barrel syringes (Pearson Dental Supply Co) (n=3). To simulate *in vivo* injection, syringes were maintained at ~4°C and the polymer mixture was dispensed directly onto the pre-heated Peltier plate at 37°C. Time zero was considered as the point at which the initiators were mixed. Gelation onset, determined by oscillation measurement, was defined as the point at which the elastic modulus (*G'*) and viscous modulus (*G"*) were equal, or *G'/G"* = 1 (Winter and Chambon 1986). Gelation completion was defined as the first point at which four consecutive values of *G'* increased by less than 2% (Gold et al. 2014; Temenoff et al. 2003).

3.2.10 In Situ Gelation

Ma-MC and sMC (10 mM 2SEM) hydrogels were evaluated for their ability to gel and be retained *in* situ in an *ex vivo* bovine motion segment model (n=3). Bovine coccygeal bone-disc-bone motion segments (cc1-2 and cc3-4) were harvested from healthy, skeletally mature bovine tails acquired from a local abattoir (Lin et al. 2019; Varma et al. 2018; Likhitpanichkul et al. 2014). Extraneous musculature and ligaments were removed with a scalpel, vertebrae were cut proximal and distal to vertebral endplates, and facet and transverse processes were removed with a bone band saw, after which motion segments were wrapped in PBS hydrated tissue to preserve hydration and frozen at -20°C until future use. Segments were thawed at 37°C in PBS prior to use. Cruciate incision was created posterolaterally with a #15 blade through the AF and nucleotomy was performed by removing 0.15-0.20 g (~ 60%) of the NP tissue with a pituitary ronguer via the incision.(Malhotra et al. 2012) Ma-MC (2%, 3%, and 4% w/v), redox initiators (APS and TEMED, 10mM each), and 2SEM (0 or 10mM) were prepared in dual-barrel syringes as previously described. Trypan blue stain was added to aid in hydrogel visualization. Polymer solution and

motion segments were warmed to 37°C and polymer solution was injected with a 20G needle into the NP void space via the injury site. Initial gross gelation was assessed after incubation at 37°C for 30 minutes (Varma et al., 2014).

3.2.11 In Vitro Stability

In vitro stability of sMC hydrogel constructs was determined by measuring the dry weight of hydrogels over an 8-week period (n=3-4). 3% (w/v) MC hydrogels (0, 1, 5, and 10 mM 2SEM) were fabricated in molds as described in 2.3. Samples were incubated in PBS at 37°C on an orbital shaker for the duration of the experiment in order to mimic the temperature and fluid flow of the native IVD environment. PBS buffer was changed 3 times weekly, and at 4 and 8 weeks, gels were collected and lyophilized, and measured for dry weight (Varma et al. 2014; Lin et al. 2019; Gold et al. 2015). In addition, stereomicrographs of the gels were captured at each timepoint for visual assessment.

3.2.12 Cytocompatibility

Human dermal fibroblasts (hDFs) were encapsulated within MC and sMC hydrogels to assess construct cytocompatibility. Hydrogels were prepared as described in section 2.3 with the addition of hDFs in the prepolymer mixture. Lyophilized Ma-MC polymer was sterilized under germicidal UV light for 30 min and dissolved in sterile PBS (3% (w/v)) (Lin et al. 2016). Redox initiators APS and TEMED (10 mM each) and sulfonate monomer 2SEM (0, 1, 5, and 10 mM) were prepared as previously described with the additional step of sterilization via syringe filtration (0.22 μm filter size) (Lin et al. 2019). Sterile polymer precursors were prepared in dual-barrel syringes with the addition of hDFs at a final cell concentration of 4 x 10^6 cells/mL. Gels were formed as detailed earlier and cultured for 5 days at 37°C and 5% CO_2 in high glucose DMEM with 1% Penicillin/Streptomycin and 10% fetal bovine serum (FBS). Fibroblasts were used as a general

screen for cytocompatibility of sMC as the material can also be used for other applications (such as soft tissue fillers) (Varma et al. 2018; Shin, Olsen, and Khademhosseini 2012).

Total DNA content was measured to assess cell proliferation on days 1 and 5. Gels were frozen and lyophilized, homogenized and digested in pepsin based on previous protocols (Gupta, Cooper, and Nicoll 2011). Briefly, lyophilized gels were digested in a pepsin (Sigma) solution in 0.05N acetic acid for 48 hrs. at 4°C, after which the solution was neutralized with 10x tris-buffered saline. Samples were analyzed using the PicoGreen assay (Invitrogen, ThermoFisher Scientific, USA) according to manufacturer's protocol using calf thymus DNA (Sigma) as a standard, at an excitation/emission of 480/520 nm on a BioTek Instruments plate reader (Synergy 4, Winooski, VT, USA) (n=5). Cell viability was also assessed visually at 1 and 5 days of culture using the Live/Dead assay kit (Invitrogen, ThermoFisher Scientific, USA), staining with calcein AM and ethidium homodimer-1 (0.75 μM each) for live and dead cells, respectively (n=2).

3.2.13 Protein Adsorption

Freshly made hydrogel constructs (3% MC; 0, 1, 5, 10 mM 2SEM) were swollen in PBS for 1 hour and then incubated in sterile FBS at 37°C for 2 hours on an orbital shaker. Gels were rinsed 3x in PBS to remove non-adherent proteins. Gels were then placed in extraction buffer (1% SDS, 1 mM EDTA, and 10 mM Tris, pH 8.0) on an orbital shaker at 37°C for 1 hour. Release buffer was analyzed using the Bicinchoninic Acid (BCA) protein assay (Pierce, Thermo Fisher Scientific) according to the manufacturer's protocol using bovine serum albumin (BSA) as a protein standard for total protein content (n=4).

3.2.14 Growth Factor Release

Sequestration of TGF-β3 within sMC hydrogels was assessed by encapsulating growth factor within hydrogels and measuring cumulative release over 14 days. Hydrogel precursors were

prepared as described in section 2.3, with the addition of rhTGF-β3 (R&D Systems, Minneapolis, MN). UV-sterilized Ma-MC polymer (3% w/v) was dissolved in sterile PBS and mixed with sterile redox initiators (10 mM) and 2SEM (0, 1, 5, and 10 mM) in dual-barrel syringes. TGF-β3 was added to the TEMED side of the dual-barrel syringe only for a final concentration of 2000 ng/mL (~80 ng/gel), corresponding to the total amount of TGF-β3 that would be supplemented via cell culture media for 2 weeks based on previous studies (M. S. Gupta and Nicoll 2015). Preliminary studies showed that direct exposure to oxidizing agent APS denatures the TGF-β3 and reduces its bioactivity rendering it undetectable via enzyme-linked immunosorbent assay (ELISA). Growth factor-laden hydrogels were maintained in release buffer (sterile PBS with 1% BSA) for 2 weeks at 37°C on an orbital shaker for the duration of the experiment. Release buffer was collected and replaced at various time points and frozen at -20°C for future quantification. The DuoSet TGF-β3 ELISA (R&D systems) was used according to manufacturer's instructions to quantify total growth factor released (n=4).

Release behavior was characterized via the Korsmeyer-Peppas power-law model:

$$\frac{M_t}{M_\infty} = kt^n \tag{3.9}$$

where M_t/M_∞ is the fractional release of the solute at time t, k is a constant representing structural and geometric characteristics of the system, and n is the diffusional exponent indicative of the release mechanism. Cylindrical gels used in this study had an aspect ratio of 2.5 (diameter/height), and therefore, n was taken to be 0.43 based on modeling the system as a tablet exhibiting release via Fickian diffusion (Ritger and Peppas 1987a). Swelling effects were assumed to be negligible (swelling < 25% of the original volume) (Ritger and Peppas 1987b).

3.2.15 Statistics

A two-way ANOVA was used to determine the effects of macromer concentration and 2SEM concentration on hydrogel properties. One-way ANOVA was used to determine effects of sulfonate concentration on protein adsorption. Two-way repeated measures ANOVA was used to determine effects of sulfonate concentration and time on cumulative release of TGF-β3. Tukey's post-hoc tests were used in all cases to assess significance ($p<0.05$). Data represent mean ± SD.

3.3 Results

3.3.1 Spectroscopy and Methacrylation Quantification

The percentage of methacrylate substitutions via esterification of hydroxyl groups on the MC backbone was found to be 5.25%, as determined by relative integrations of methacrylate proton peaks to protons on the MC backbone (**Figure 3.1B**).

3.3.2 Sulfonation Quantification

Hydrogels were formed by crosslinking using redox initiators APS and TEMED (10 mM each) and with the addition of 2SEM in the prepolymer mixture. Sulfonation of sMC formulations was assessed qualitatively and quantitatively via DMMB stain. Hydrogels showed increasing intensity of blue stain with increasing 2SEM concentration, with 0 mM 2SEM gels staining faintly blue, 1 mM 2SEM gels staining a moderate blue, and 5 and 10 mM 2SEM gels staining deep indigo for all macromer concentrations (**Figure 3.2A**). For all macromer percentages (2%, 3%, and 4%), hydrogel sulfonation by inclusion of 2SEM during polymer crosslinking resulted in a dose-dependent increase in DMMB staining intensity, as quantified by GuHCl destaining and spectroscopic analysis (**Figure 3.2B**). DMMB staining was significantly higher in 5 and 10 mM 2SEM gels than 0 and 1mM gels at 3% and 4% macromer concentration, and significantly higher in all 2SEM containing groups (1 mM, 5 mM, and 10 mM) at 2% macromer concentration. All 2SEM concentrations showed significantly higher sulfonation relative to gel weight in the 2%

macromer concentration compared to the equivalent 2SEM concentrations in the other two macromer concentrations.

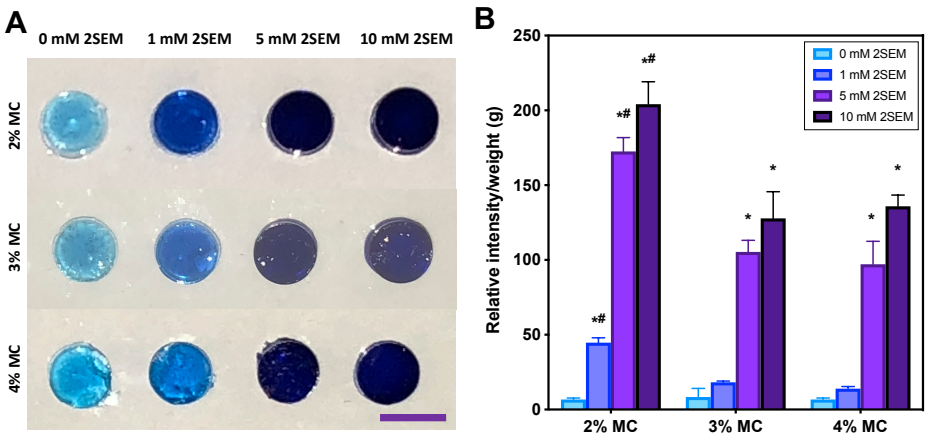

Figure 3.2: Quantification of sulfonation.
A) Relative quantification of DMMB staining exhibiting an increase in staining intensity with increasing 2SEM (i.e., sulfonate) concentration. B) Stereomicrographs of DMMB stained hydrogels. Scale bar represents ~5 mm. Significance set at $p < 0.05$ * — significantly different w.r.t. 0 mM 2SEM within macromer concentration. # — significantly different w.r.t. same 2SEM concentration of different macromer concentration.

3.3.3 Compressive Properties

Equilibrium mechanical properties were determined via unconfined compression. Constructs with the highest macromer concentration (4% w/v) showed the highest E_Y (24.97 ± 6.79 to 31.60 ± 3.80 kPa) (**Figure 3.3A**) as well as peak stress (σ_{peak}) (**Figure 3.3B**) which were all significantly higher than those of 2% and 3% w/v hydrogels. Percent relaxation was not significantly different across all groups, averaging 46.00 ± 11.77%. Sulfonate concentration had no significant effect on all measured mechanical properties.

3.3.4 Equilibrium Swelling and Hydrogel Mesh Characterization

Equilibrium weight swelling (Q_w) was measured for all gels, and crosslinking density (ν_e) and mesh size (ξ) calculated from the acquired data using the Flory-Rehner model (**Table 3.1**). Q_w was significantly different across all macromer concentrations. The range of Q_w was from 16.05 ±

1.53 to 26.40 ± 0.61 with increasing macromer concentration resulting in decreasing swelling ratio. Similarly, ν_e increased with macromer concentration, ranging from 4.75 x 10^{-5} ± 1.65 x 10^{-6} to 1.00 x 10^{-4} ± 1.36 x 10^{-5} mol/cm^3, and ξ was inversely associated with macromer concentration, ranging from 19.79 ± 1.89 to 33.07 ± 0.81 nm. Sulfonate concentration had no significant effect on the swelling behavior or corresponding crosslinking density and mesh size.

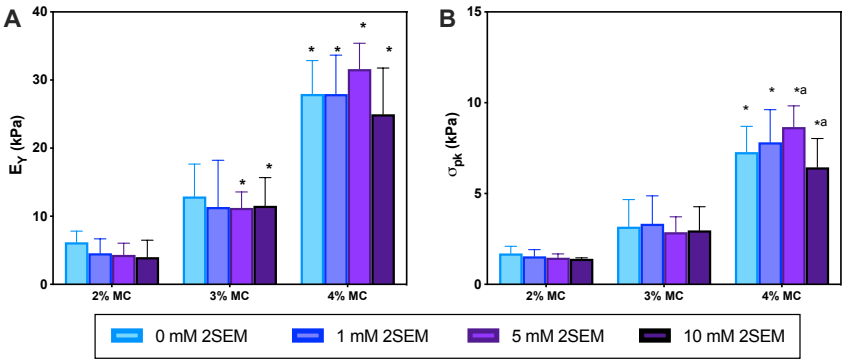

Figure 3.3 Equilibrium mechanical properties of MC and sMC hydrogels.
A) Equilibrium Young's modulus, and B) peak stress, σ_{pk}. Significance set at $p<0.05$ * — significantly different from all other macromer concentrations of corresponding 2SEM concentration, $^{\#}$ — significantly different from corresponding 2SEM concentration w.r.t. 2% MC, ^{a} — significantly different from each other.

Table 3.1: Swelling ratio and related physical properties of sulfonated MC hydrogels.

Macromer Concentration (w/v)	2SEM Concentration (mM)	Q_w	ν_e (mol/cm^3)	ξ (nm)
2%	0	22.82 ± 1.52	5.94x10^{-5} ± 5.76x10^{-6}	28.37 ± 1.98
	1	26.40 ± 0.61	4.75x10^{-5} ± 1.65x10^{-6}	33.07 ± 0.81
	5	24.96 ± 1.34	5.18x10^{-5} ± 4.31x10^{-6}	31.17 ± 1.75
	10	24.88 ± 0.92	5.20x10^{-5} ± 2.87x10^{-6}	31.06 ± 1.22
3%	0	20.21 ± 1.50	7.12x10^{-5} ± 7.58x10^{-6} $^{\#}$	25.02 ± 1.93$^{\#}$
	1	20.43 ± 2.68*	7.13x10^{-5} ± 1.41x10^{-5} *	25.31 ± 3.42*
	5	19.08 ± 1.29$^{a\#}$	7.74x10^{-5} ± 7.18x$10^{-6\#}$	23.58 ± 1.64$^{\#a}$
	10	22.95 ± 0.76^{a}	5.87x10^{-5} ± 2.93x10^{-6}	28.54 ± 0.99^{a}
4%	0	16.69 ± 2.97*	9.74x10^{-5} ± 2.61x10^{-5}*	20.61 ± 3.68*
	1	16.05 ± 1.53*	10.00x10^{-5} ± 1.36x10^{-5}*	19.79 ± 1.89*
	5	16.41 ± 1.13$^{\#}$	9.63x10^{-5} ± 9.18x$10^{-6\#}$	20.25 ± 1.40$^{\#}$
	10	17.96 ± 2.41*	8.60x10^{-5} ± 1.68x10^{-5}*	22.19 ± 3.03*

Q_w = equilibrium weight swelling ratio; ve = effective crosslinking density; ξ = hydrogel mesh size; Significance set at $p<0.05$ ^{a} – significantly different from other sulfonate concentration within macromer concentration * – significantly different from corresponding sulfonate concentration w.r.t. 2% MC concentration $^{\#}$ – significantly different from corresponding sulfonate concentration w.r.t. all other MC concentration

3.3.5 Gelation Properties

3.3.5.1 Thermogelation Onset Temperature

The effect of macromer and sulfonate concentration on thermal behavior of the prepolymer mixture was measured via temperature ramp. Thermogelation onset temperature was defined as the temperature at which G' of the polymer solution (without chemical crosslinking agents) increased by 2% or more for 4 or more consecutive points (**Figure 3.4A**, arrow indicates thermogelation onset). This point more accurately identifies the sharp increase in G' at the onset of thermally induced physical crosslinking than when G'=G", which occurs at much lower temperatures where the rate of increase in G' is still quite low (not shown). Thermogelation onset occurred within the physiologic range (<37°C) for all concentrations tested, ranging from 24.6 ± 0.52°C to 34.23 ± 2.40°C (**Figure 3.4B**). All 2% MC formulations began to gel at a significantly higher temperature than 3% and 4% gels. There was no significant effect on thermogelation due to the addition of sulfonate groups to the polymer solution. G' and |η*| were closely mirrored throughout the temperature ramp as shown in the representative graph (**Figure 3.4A**).

3.3.5.2 Redox-Initiated Gelation

Redox polymerization of the prepolymer mixtures with the addition of redox initiators APS and TEMED (10 mM each) was measured via time sweep. Time zero was defined as the moment the MC/TEMED mixture was combined with the MC/APS mixture in the mixing tip of the dual-barrel syringe. Gelation onset, when *G'* and *G"* were equal, occurred under 30 seconds for all polymer solutions at 37°C (**Figure 3.4C**), followed by a sharp increase in *G'*. Gelation completion, defined as the point at which increase in *G'* was less than 2% for 4 or more points was achieved between 4.22 ± 0.45 and 6.61 ± 1.46 minutes for all formulations (**Table 3.2**). As with the thermogelation without initiators, |η^*| was closely associated with *G'* throughout the measured

gelation time. Initial $|\eta^*|$ and $|\eta^*|$ at gelation completion were dependent on macromer concentration; at both time points viscosity was significantly different based on the concentration of MC. Similarly, upon gelation completion, $|G^*|$ increased with increasing macromer concentration. The concentration of sulfonate monomer did not have a significant effect on the $|\eta^*|$ or $|G^*|$ at either timepoint measured.

Table 3.2: Rheological properties of redox-polymerized sulfonated MC hydrogels.

Macromer Concentration (w/v)	2SEM Concentration (mM)	Initial $\|\eta^*\|$ (Pa·s)	$\|\eta^*\|$ at Gelation Completion (Pa.s)	$\|G^*\|$ at Gelation Completion (Pa)	Gelation Completion Time (min)
2%	0	0.58 ± 0.39*	148.62 ± 104.4 *	993.93 ± 656.54*	5.07 ± 0.17
	1	0.53 ± 0.39*	151.33 ± 61.83*	950.63 ± 388.42*	6.61 ± 1.46
	5	0.53 ± 0.23#	156.27 ± 5.40#	981.80 ± 33.82#	5.51 ± 0.46
	10	0.81 ± 0.34#	145.47 ± 14.45*	913.80 ± 90.66*	5.58 ± 0.41
3%	0	3.10 ± 0.52	564.70 ± 10.05*	3,548.00 ± 63.17*	5.39 ± 0.52
	1	3.28 ±0.70*	480.63± 20.32*	3,019.67 ± 127.60*	5.80 ± 0.84
	5	2.47 ± 0.70#	387.77 ± 138.85#	2,436.33 ± 871.85#	6.37 ± 1.51
	10	1.27 ± 0.44#	603.23 ± 118.87	3,790.00 ± 747.35*	5.20 ± 0.29
4%	0	4.89 ± 1.97*	970.17 ± 81.76*	6,095.00 ± 513.36*	5.11 ± 0.58
	1	6.60 ± 0.90*	1,172.33 ± 133.28*a	7,289.67 ± 755.74* a	4.86 ± 0.36
	5	5.42 ± 2.12*	952.87 ±138.85*	5,987.00 ± 2206.9*	5.59 ± 1.86
	10	6.24 ± 1.70*	865.13 ± 40.78 a	5,435.67 ± 256.14* a	4.22 ± 0.45

$|\eta^*|$ = complex viscosity; $|G^*|$ = dynamic complex modulus; Significance set at $p<0.05$ * – significantly different w.r.t. corresponding sulfonate concentration in all other macromer concentrations # – Significantly different w.r.t. corresponding sulfonate concentration at 4% MC [a] – significantly different from other sulfonate concentration within macromer concentration.

3.3.6 In Situ Gelation

MC formulations (2%, 3% and 4% w/v) with and without sulfonate (0 or 10 mM 2SEM) and redox initiators were screened for their ability to form stable hydrogels *in situ* within the void space of bovine IVD motion segments post-nucleotomy. Transverse dissection of the motion segments after gelation was allowed to take place for 30 minutes at 37°C showed that 2% MC formulations were not retained in situ (not shown), while 3% (**Figure 3.4D**) and 4% (not shown) formulations with and without added sulfonates were both retained within the disc space.

Based on the material characterization data, 2% and 3% MC hydrogels exhibited a modulus and swelling behavior that were closest to the native human NP (Cloyd et al. 2007; Reza and Nicoll

2010b). The 3% and 4% MC formulations gelled *in situ* but 4% gels were stiffer than the target tissue, so 3% MC was selected for further characterization.

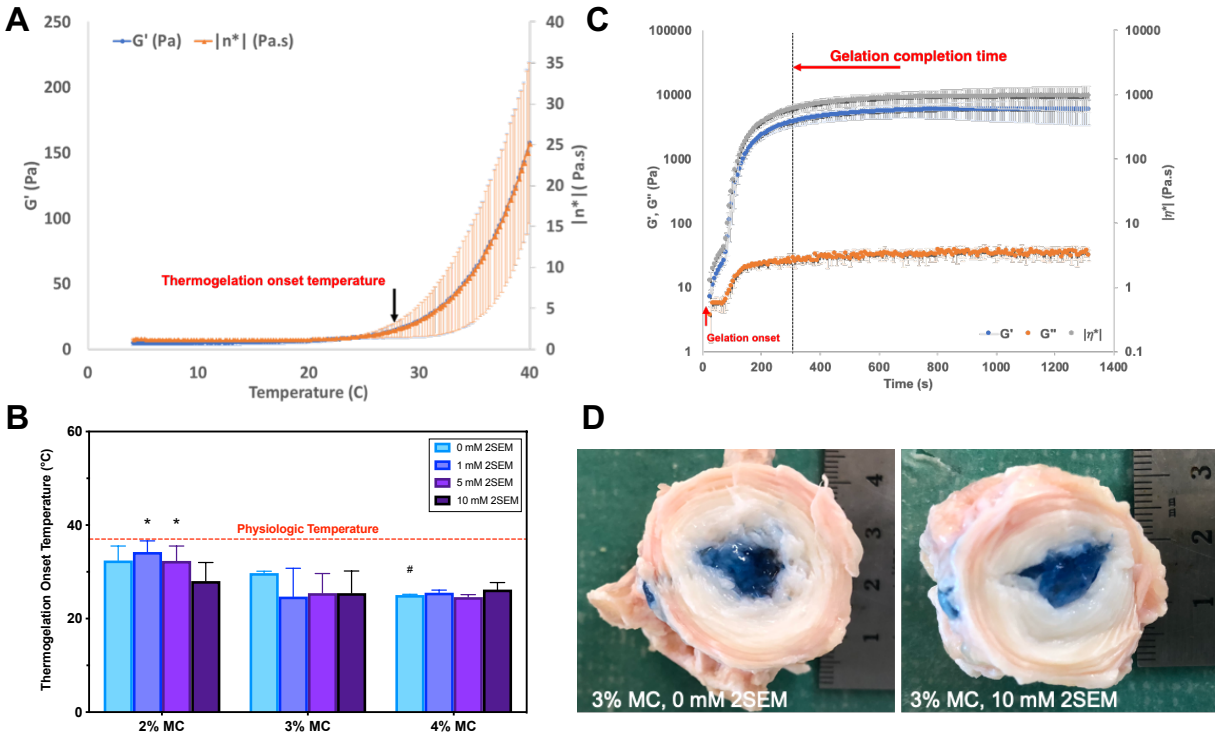

Figure 3.4: Gelation kinetics and in situ gelation.

A) Representative rheometric graph of uncrosslinked MC solution showing G' and |η*| over a temperature ramp from 4°C to 40°C. Arrow indicates point of thermogelation onset. B) Thermogelation onset temperature of MC polymer solutions with 2SEM of varying concentrations. Red dashed line indicates physiologic temperature, 37°C. C) Representative rheometric graph of redox-initiated gelation behavior of Ma-MC with 10 mM redox initiators APS and TEMED and varying concentrations of 2SEM, showing G', G", and |η*| over time. Red arrow indicates redox-initiated gelation onset, which occurs nearly instantaneously before the first data point is collected. Dashed black line indicates redox-initiated gelation completion. A,C) Representative graphs both show 3% MC, 10 mM 2SEM as examples. D) Gross images of 3% MC hydrogels with 0 mM 2SEM (left) and 10 mM 2SEM (right) injected into the void space of nucleotomized bovine caudal IVDs. Hydrogels are stained blue with trypan blue for visualization. Significance set at $p<0.05$ * — significantly different from other macromer concentrations.

3.3.7 In Vitro Stability

Mass loss studies of 3% hydrogels with varying sulfonate content demonstrated that all material formulations maintained their structure (**Figure 3.5A**) and dry weights (**Figure 3.5B**) over 8 weeks in aqueous solution *in vitro*.

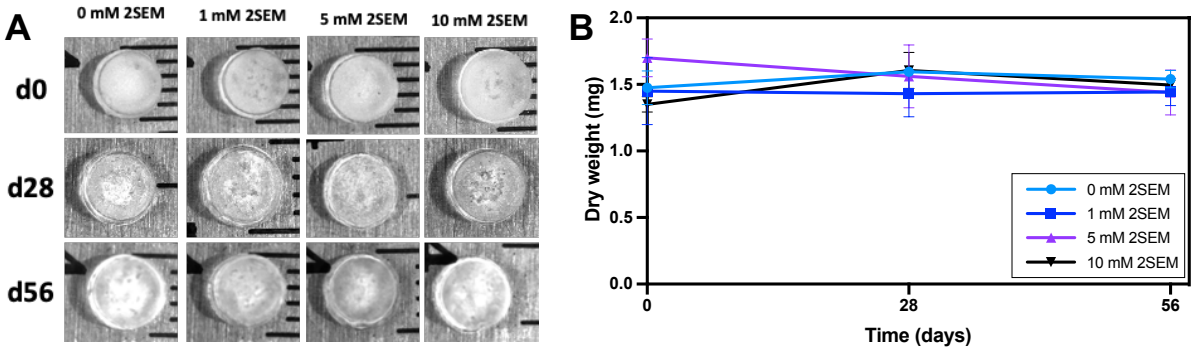

Figure 3.5: In vitro stability of 3% MC hydrogels of varying 2SEM concentration (0, 1, 5, 10 mM) over 8 weeks.

A) Stereomicrographs of representative gels at 0, 4, and 8 weeks after initial casting. B) Dry weight of gels showing no significant change in mass over 8 weeks. Significance set at $p<0.05$

3.3.8 Cytocompatibility

Human dermal fibroblasts were encapsulated within 3% w/v sMC hydrogels for 5 days as model cells for characterizing scaffold cytocompatibility. PicoGreen analysis of encapsulated hDFs showed a significant increase in cell DNA content between day 1 and day 5 (**Figure 3.6A**). The inclusion of sulfonate monomers had no significant effect on fibroblast viability. Live/dead staining (**Figure 3.6B**) confirmed cell survival with minimal cell death.

3.3.9 Protein Adsorption

3% MC gels were incubated for 2 hours in FBS, and adsorbed proteins were extracted and quantified via BCA assay. Protein quantification showed significantly higher protein adsorption on 5 mM and 10 mM 2SEM gels in comparison to 0 and 1 mM 2SEM gels (**Figure 3.7A**), with protein deposition strongly correlating with sulfonate content ($R^2 = 0.9546$).

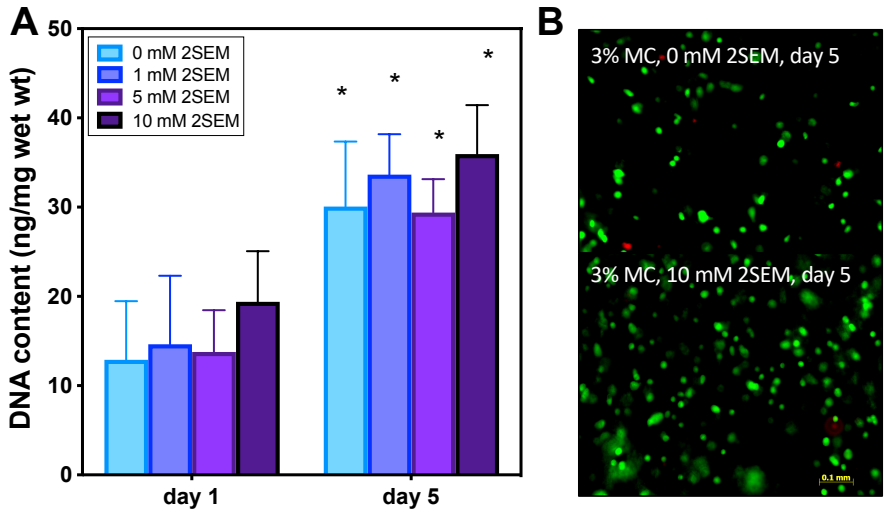

Figure 3.6: Cytocompatibility of 3% MC hydrogels with varying concentrations of 2SEM (0, 1, 5, 10 mM) with encapsulated human dermal fibroblasts (hDFs).
A) DNA content of hDFs cultured within hydrogels on day 1 and day 5, and B) representative images of live/dead staining of encapsulated hDFs in MC only gels (top) and sMC gels prepared with 10 mM 2SEM (bottom). Significance set at $p<0.05$ * — significantly different from corresponding 2SEM concentration w.r.t. day 1.

3.3.10 Growth Factor Release

TGF-β3 was incorporated within hydrogels during gel formation, and cumulative release measured over 14 days. Release data showed a burst release of growth factor within the first 24 hours from all groups, likely due to initial swelling of the hydrogel. By 24 hours, the growth factor released from all sulfonated groups was significantly less than the unsulfonated MC hydrogels (**Figure 3.7B**). At the end of 2 weeks, the 0 mM 2SEM hydrogels released 52.6 ± 6.9% of the total loaded growth factor (**Figure 3.7C**) while the 10 mM 2SEM gels released only 10.6 ± 3.9% of the total growth factor loaded within the gels. There was no significant difference between the release from 5 mM and 10 mM 2SEM gels for all time points beyond 24 hours. Because the total loaded growth factor was not released from any of the constructs, fractional release was calculated as total mass of TGF-β3 released normalized to the total average released from unsulfonated MC gels (0 mM 2SEM). Under the assumptions for the Korsmeyer-Peppas model, equation (3.9) is applicable

for the first 60% of solute release. When plotted against t^n where $n = 0.43$ for the given geometry and aspect ratio of the system, the data for each system show a linear fit with strong R^2 values, indicative of Fickian diffusion (**Figure 3.7D**). The slopes of the lines, representing k and directly proportional to the diffusion coefficient, were all significantly different, with the steepness of the lines (i.e., absolute value of the slopes) inversely proportional to sulfonate concentration.

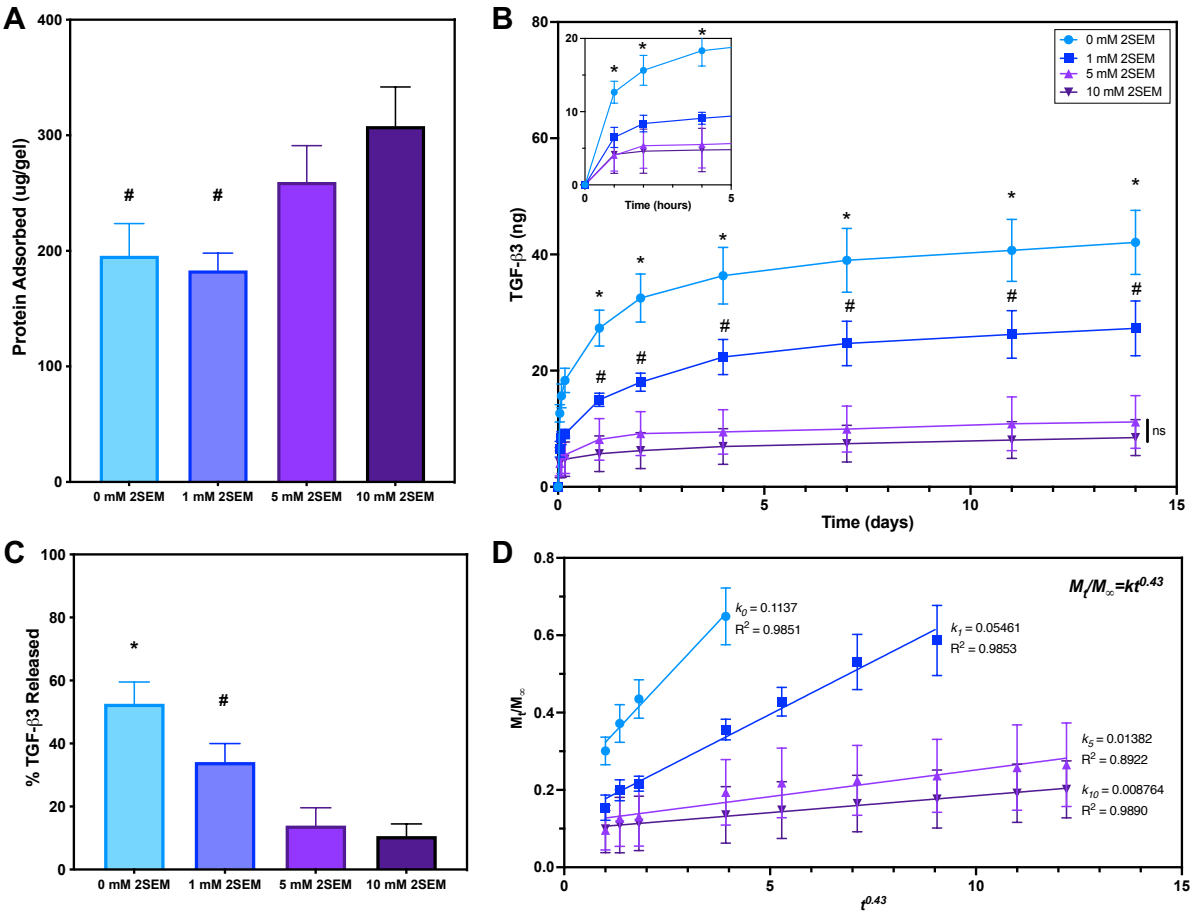

Figure 3.7: Protein adsorption and TGF-β3 release from 3% MC hydrogels of varying sulfonate concentration (0, 1, 5, and 10 mM 2SEM).

A) Serum protein adsorption on hydrogels after 2-hour incubation in sterile FBS as quantified by BCA assay. B) Cumulative release profile of encapsulated rhTGF-β3 from hydrogels over the course of 2 weeks, as quantified by ELISA. C) Percent of total loaded growth factor released at the end of 2 weeks. D) Korsmeyer-Peppas model of Fickian release from sMC gels. Significance set at $p<0.05$ * — significantly different from all other sulfonate concentrations. # — significantly different w.r.t. 5 and 10 mM 2SEM.

3.4 Discussion

Affinity-based sequestration of signaling molecules via sulfonation of biomaterials has the potential to deliver soluble growth factors in the local vicinity of host and seeded cells to promote sustained matrix elaboration. However, modification of NP replacement biomaterials for growth factor sequestration has not been investigated. MC has previously been utilized in its methacrylated, chemically-crosslinked form for soft tissue reconstruction applications due to its tunable mechanics and resistance to enzymatic degradation *in vivo* (Stalling, Akintoye, and Nicoll 2009; Gold et al. 2014; 2015). Similarly crosslinked polyanionic Ma-CMC hydrogels have shown promise as tissue engineering scaffolds for NP regeneration (Reza and Nicoll 2010b; 2010a; Varma, DiNicolas, and Nicoll 2018), yet despite redox initiators rendering them injectable, the lack of thermoresponsiveness resulted in incomplete retention *in situ* and extravasation from the IVD void space. Therefore, a dual-polymer network (DPN) combining MC along with CMC was investigated as a biomaterial for NP repair, combining the high swelling capacity of CMC with the thermogelation feature of MC (Varma et al. 2018). The incorporation of MC was found to be critical, as the thermogelation property allowed for a rapid increase in viscosity and improved polymer retention upon injection into the intradiscal void space post nucleotomy (Lin et al. 2019; Hom et al. 2019). The CMC-MC DPN system, while serving as a promising acellular repair strategy, is not as favorable for cellular delivery due to its high effective macromer concentration (6% (w/v)). Numerous studies have shown that increasing macromer concentration is deleterious to cell proliferation and chondrogenic differentiation of encapsulated MSCs (Erickson et al. 2009; Gupta and Nicoll 2014; Burdick et al. 2005; Panebianco et al. 2020). Thus, the present study aimed to explore the effectiveness of sulfonated MC-based gels alone as injectable NP replacements, as well as potential scaffolds for future cell-laden, tissue-engineered constructs. Sulfonates were

added to increase hydration of the MC network and more closely mimic the sulfated GAG-rich matrix of the native NP.

The facile method of sulfonation described here using 2SEM takes advantage of the methacrylate modification present on the MC macromers to covalently bind sulfonates to the polymer chains. Alternate techniques for sulfation and sulfonation of cellulosics and other polysaccharides have been investigated, such as reaction of available hydroxyls with chlorosulfonic acid, but require further processing, purification, and characterization (Portocarrero Huang et al., 2017; Wang et al., 2007; Zeng, Groth, & Zhang, 2019). In addition, direct chemical modification of the MC backbone with charged groups can potentially alter or disrupt the mechanism of thermoresponsiveness, which relies on the aggregation of hydrophobic methoxy groups at increasing temperatures (Sarkar 1979; Wu et al. 2021). Usage of sulfonated monomers as detailed in this study allowed for reliable and controlled tuning of sulfonate content. The coupling of the sulfonates occurs during the redox-initiated polymerization process to form the hydrogels, utilizing some of the pendant methacrylates functionalized onto the MC backbone to attach 2SEM. DMMB staining showed that sulfonates were successfully incorporated into the MC gels and that staining intensity increased in a dose-dependent manner.

Mechanical and material properties of the sMC constructs were tested to investigate their potential as NP replacement materials. Since the NP plays a critical role in spine mechanics, it is necessary to recapitulate the physical behavior of the healthy native NP. Unconfined compression testing was used to investigate the influence of added sulfonates and macromer concentration to the elasticity of the Ma-MC hydrogels. The utilization of methacrylate monomers to couple sulfonates via available methacrylate groups on the modified MC backbone potentially consumes methacrylates that might be used for crosslinking, thereby altering hydrogel mechanics.

Unconfined compression demonstrated that, as previously reported, E_Y may be tuned by varying macromer concentration (Gold et al. 2014; 2015). Data also showed that the addition of 2SEM at the concentrations tested did not have a statistically significant effect on the hydrogel elasticity. Similarly, σ_{pk} increased with increasing macromer concentration but was unaffected by the incorporation of sulfonate monomers. E_Y of 2% gels measured between 3.99 ± 2.49 and 6.18 ± 1.64 kPa, within the range of the native human NP (~5 kPa), and all formulations studied exhibited elasticity in the range of other injectable hydrogels under investigation for NP replacement (Cloyd et al. 2007; Smith et al. 2014; Francisco et al. 2013; Kumar et al. 2014). E_Y values higher than that of healthy native NP may be necessary to resist matrix breakdown within the degenerative environment *in vivo* (Roughley 2004). In addition, our recent study using a similar redox-polymerized cellulosic hydrogel system revealed that injection into the IVD void space results in a lower E_Y in comparison to gelation in a casting device *in vitro* (16.62 ± 3.59 kPa *in situ* gelation versus 34.27 ± 4.53 kPa *in vitro*) (Varma et al. 2018). This is likely due to the casting device being rigid and constricted, in contrast to the soft tissue of the IVD void space, potentially resulting in less efficient mixing and crosslinking, with free radicals lost due to reaction with ambient oxygen in the air. With this in mind, the proposed material at the concentrations studied is well within the range of the mechanical properties of the native human NP.

In addition to altering the compressive mechanical properties, the presence of sulfonates in the MC gels has the potential to alter the swelling behavior of the materials. It was hypothesized that negatively charged sulfonates would increase the attraction and influx of water molecules into the hydrogel in a manner similar to sGAGs, which would potentially alter the swelling and hydrostatic pressure within the gel network. NP hydration is regulated by the abundance of sGAGs within the tissue, and the addition of sulfonates to MC was intended to replicate the chemistry and

function of native sGAGs. Previous studies artificially sulfating polysaccharides have shown increased water retention and swelling ratio in response to the added negative charge (Rother et al. 2017; Liang et al. 2016; Purcell et al. 2014). However, equilibrium weight swelling measurements on sulfonated MC constructs demonstrated that the addition of sulfonate groups had no effect on the swelling behavior of the gels. This may be due to the dominating effect of interchain covalent crosslinks between methacrylate groups, which stabilize the gel network and prevent any further swelling caused by the anionic sulfonates attracting water. Interestingly, based on the calculations of crosslinking density using a modified Flory-Rehner model, the addition of the 2SEM monomers did not significantly affect the number of crosslinks formed, and thus, the overall mesh size. This seems to indicate that at the concentrations of 2SEM and redox initiators used in this study, the available methacrylate groups on the MC backbone are not fully saturated. This may be a result of temperature-dependent formation of physical crosslinks via aggregation of hydrophobic moieties within MC, which create rigid structural assemblies that only permit interchain coupling reactions between methacrylate groups that are accessible and in close proximity. Indeed, this phenomenon was also observed in the lack of significant differences in swelling behavior and related network properties (i.e., crosslinking density and mesh size) between redox-polymerized Ma-MC hydrogels of varying methacrylation percentage (Gold et al. 2014). Conversely, increased methacrylation percentage did significantly affect swelling ratio and mesh size in Ma-CMC hydrogels, suggesting that the process of redox-polymerized network formation is influenced by the formation of hydrophobic aggregates within the MC polymer, a characteristic which is not shared with CMC (Gold et al. 2014; Lin et al. 2016). This might indicate that within redox-polymerized Ma-MC hydrogels, a number of unsaturated pendant methacrylate groups remain available to react with methacrylate monomers such as 2SEM. The evidence that sulfonate

monomer concentration had no effect on swelling ratio, crosslinking density or mesh size is consistent with the lack of 2SEM monomer concentration influence on MC hydrogel mechanical properties. This is supported by the theory of rubber elasticity, which predicts a proportional relationship between crosslinking density and hydrogel stiffness (Canal and Peppas 1989; Anseth, Bowman, and Brannon-Peppas 1996).

One of the primary advantages of MC as a biomaterial is its thermoresponsive character. Aqueous solutions of MC form thermoreversible hydrogels upon heating, due to the aggregation of the hydrophobic methoxy groups at higher temperatures (Desbrières, Hirrien, and Ross-Murphy 2000; Haque and Morris 1993). As such, the influence of sulfonates on the temperature-sensitive behavior of MC was characterized given that this is the first known study to functionalize MC with charged moieties in this manner. The addition of other solutes, in particular ionic groups such as sulfates, has previously been shown to alter the thermogelation point of MC (Xu, Li, et al. 2004; Xu, Wang, et al. 2004). Xu and colleagues have shown that the sol-gel transition of MC can be shifted to lower or higher temperatures based on the Hofmeister series, an order of ions ranked based on how strongly they affect the hydrophobicity of a solute in water (Hofmeister 1888). In this series, SO_4^{2-} is one of the lowest of the kosmotropes, ions that enhance the hydrophobicity of a solute or cause a "salt-out" response. This accelerates the sol-gel transition as temperature increases, effectively lowering the onset temperature of thermogelation. They also showed that this salt-assisted effect is concentration dependent. Therefore, 2SEM was added to Ma-MC, and the thermoresponsiveness of the polymer solution was characterized via temperature ramp to determine whether the presence of negatively charged sulfonated monomers in solution would have a similar effect on the thermogelation properties of the MC hydrogel. Rheological properties were measured from 4°C to 40°C, as this was the relevant temperature range to capture for a

material stored in a standard 4°C refrigerator and injected into physiologic temperature. Thermogelation onset temperature was defined as the temperature at which *G'* increased for 2% or more for at least 4 consecutive points. This measure was chosen as a true indicator of the increase in viscosity caused by the aggregation of hydrophobic moieties on MC. The crossover point of *G'* and *G"*, where the elastic portion of the shear modulus *G'* becomes dominant over the viscous portion *G"*, is the classical definition of gelation onset in rheometry of viscoelastic materials (Winter and Chambon 1986; Ferry 1980). However, in cases such as this where the magnitude of the change is very low (under 10 Pa), the cross-over point is of limited physical relevance, as the solution does not behave like a gel. In addition, the point of sharp increase in *G'* has been shown to more closely correlate with the onset of the endothermic peak when thermal capacity of MC solutions are measured using differential scanning calorimetry, indicating the rapid, temperature-dependent aggregation of hydrophobic regions (Li 2002; Xu, Li, et al. 2004; Zheng et al. 2004). The addition of sulfonated monomers had no significant effect on the thermogelation of the Ma-MC base polymer, maintaining thermogelation onset temperature above room temperature but below physiologic temperature (24.6°C ± 0.0°C to 34.23± 2.4°C), an ideal characteristic for maintaining injectability. It should be noted that the polymer solutions used for thermogelation experiments were dissolved in 1X PBS (as were all polymer solutions in this study). The concentration of salts in PBS are an order of magnitude higher than the highest concentration of 2SEM studied here (137 mM NaCl being the highest salt concentration), and may likely dominate the thermogelation behavior of the solutions (Zheng et al. 2004).

Sulfonated MC hydrogel solutions were then assessed for injectability and gelation kinetics in the context of a minimally invasive NP repair strategy. When redox initiators were added to the polymer solution, gelation onset (*G'/G"* =1) at 37°C was nearly instantaneous, occurring under

30 seconds from initial injection. Prepolymer solutions were maintained on ice prior to injection onto the pre-warmed platform to simulate the instantaneous temperature change of injection into the body. The thermogelation component of MC without the influence of initiators allows for rapid aggregation of hydrophobic methoxy groups on the MC backbone; this in turn promotes more rapid and efficient mixing and reaction between methacrylate groups when in the presence of redox initiators. In contrast, pilot studies showed that the gelation time (initiation and completion) was delayed by nearly 6 minutes when the same samples were measured at 20°C. Gelation completion, defined as the point at which *G'* increased less than 2% for 4 consecutive points (<0.3% change/second), occurred between 4.22 ± 0.45 and 6.61 ± 1.46 minutes for all groups, within ISO Standard 5833:2002 for injectable acrylic materials (4-15 min). The initial $|\eta^*|$ of all formulations was on the order of 0.53 ± 0.23 to 6.60 ± 0.90 Pa·s, predicting ease of delivery through a fine gauge needle (usually 18-20G). In comparison, $|\eta^*|$ of commonly used polysaccharide-based dermal fillers range from 0.942 to 1,199.0 Pa·s, using even finer needles of 27-30 gauge (Falcone and Berg 2009). By gelation completion, $|\eta^*|$ increased by two orders of magnitude over the initial $|\eta^*|$, indicating likelihood that the injectable material would resist extravasation. The dynamic shear modulus $|G^*|$ also increased with increasing macromer concentration, with 4% Ma-MC gels approaching the reported range of $|G^*|$ for non-degenerate human NP (~7.4 kPa), and all concentrations were comparable to other injectable constructs under development (Iatridis et al. 1996; 1997; Chen et al. 2013; Frith et al. 2013).

The measured rheological parameters indicate that the sulfonated MC gel can be rapidly injected and solidify within the time frame of a spinal microdiscectomy procedure and can therefore be implemented within a clinical workflow. Still, rheometric analysis alone cannot determine whether the injectable material will form and be retained within the void space. Previous

work in our laboratory showed that CMC (2% w/v) with 10 mM redox initiators APS and TEMED initiated gelation in under 90s (the first point of recorded data) and reached gelation completion at ~12 min with a corresponding complex shear modulus, G^*, of ~758 Pa (Varma, DiNicolas, and Nicoll 2018). When injected into bovine motion segments, even with higher macromer content and initiator concentration (3% w/v, 20 mM initiators), CMC was not retained *in situ* and required the addition of MC to provide the necessary thermogelation capacity and allow the hydrogel to remain localized within the IVD at physiologic temperature (Varma et al. 2018). Therefore, *in situ* injections were performed with Ma-MC and sMC (10 mM 2SEM) at all three macromer concentrations (2%, 3% and 4%) in order to verify that rheometric results were translatable into a clinically relevant *ex vivo* model. Pilot studies showed formulations at 2% were not retained *in situ*, likely due to the low $|\eta^*|$ upon gelation completion (145.47 ± 14.45 to 156.27 ± 5.40), however, 3% and 4% were both retained within the IVD space. To strike a balance between mechanical properties, clinical translatability, and potential future use as cell delivery scaffold, 3% Ma-MC constructs of varying sulfonate concentration were investigated in subsequent studies (Panebianco et al. 2020).

Long-term structural integrity of NP replacement materials is important for maintaining IVD mechanical function. Cellulose-based hydrogels are not susceptible to enzymatic degradation in the human body, as humans do not produce the enzyme cellulase. This provides an advantage over other constructs generated from animal-derived ECM components, particularly when considering the degenerate IVD setting which exhibits higher levels of matrix-degrading enzymes (Rodrigues-Pinto, Richardson, and Hoyland 2014). Previous studies have shown that Ma-MC hydrogels are generally stable and resist degradation in aqueous environments, whereas Ma-CMC hydrogels lose significant amounts of their dry weight over time under the same conditions (Gold et al. 2015;

Varma et al. 2014). Here, Ma-MC-based hydrogels were found to retain their weight and structural stability and were not significantly impacted by the incorporation of charged sulfonates over 8 weeks in an aqueous environment. This corroborates the swelling results, which showed sulfonation did not increase hydration or swelling capacity of the construct, and thereby does not increase susceptibility to hydrolytic degradation. Further study in a clinically relevant *ex vivo* motion segment model or *in vivo* testing, which would incorporate mechanical and biochemical cues, would be necessary to confirm long-term stability of the constructs (Lin et al. 2019).

Another concern for clinical translation is cytocompatibility. Ma-MC hydrogels have exhibited robust cytocompatibility *in vitro* and elicit a minimal immune response *in vivo* in subcutaneous rodent models (Stalling, Akintoye, and Nicoll 2009; Gold et al. 2014; 2015; Gold 2017). However, the incorporation of methacrylate monomers in the pre-gel solution adds a potential source for cytotoxicity (Ansteinsson et al. 2013). As such, the survival of cells encapsulated within sMC hydrogels was investigated. Human dermal fibroblasts were mixed directly into the pre-polymer mixture, and thus, were exposed to unreacted 2SEM for a short amount of time before gels were injected into molds and redox polymerization consumed the methacrylate monomers. Dermal fibroblasts were used as a general screen for connective tissue cytocompatibility as the sMC material holds potential for other clinical applications (i.e., soft tissue reconstruction, dermal fillers, drug delivery vehicle), and as a comparison to our previous studies with similar cellulosic gels (Varma et al. 2018; Gold et al. 2014; 2015). Studies were conducted over 5 days in accordance with ISO standard 10993-5:2009 for biological evaluation of medical devices, which stipulate that cytotoxicity assessments should be performed for 24-72 hours. Live/dead staining showed that there were negligible cells dead at either day 1 or day 5. Moreover, PicoGreen DNA analysis revealed that there was no significant effect of sulfonate

content on cell proliferation over the 5-day culture period. Further, proliferation of encapsulated hDFs demonstrates the potential use of sMC hydrogels for cell encapsulation-based regenerative therapies.

Aside from influencing the hydration of polymeric constructs, artificial sulfation has been used as a method of protein attraction and sequestration. Electrostatic interactions between positively-charged growth factors and negatively-charged sulfates and sulfonates have been widely utilized as affinity binding methods for growth factor delivery for a variety of tissue engineering applications, including cartilage repair, but to the best of our knowledge this is the first study to utilize this method in IVD repair (Jeon et al. 2011; Freeman, Kedem, and Cohen 2008; Waghmare et al. 2018; Re'em et al. 2012; Purcell et al. 2014). Charged polymer scaffolds can influence adsorption of proteins from the surrounding media, which can alter surface chemistry, cell-material interactions, and immune responses *in vivo* (Lin et al. 2014; Freeman, Kedem, and Cohen 2008; Hartvig et al. 2011; Hoven et al. 2007). Gels were incubated in FBS to simulate early serum protein adsorption on an *in vivo* implant. Protein adsorption correlated with sulfonate concentration ($R^2 = 0.9621$), as MC gels modified with 5 and 10 mM 2SEM exhibited significantly more adsorbed serum protein than samples polymerized with 0 and 1 mM 2SEM. In the degenerate IVD, decreased nutrient transport mediated by changes in the cartilaginous endplates and vertebral vasculature contribute to altered metabolism, which may be exacerbated by the loss of hydration and osmotic pressure caused by matrix breakdown, and regenerative repair strategies may require increased nutritional demand (Huang, Urban, and Luk 2014). The ability of a charged scaffold such as sMC to attract and bind local proteins has the potential to increase nutrient and cytokine bioavailability to drive endogenous repair.

Sulfonation of MC hydrogels enabled the sequestration of growth factor encapsulated within the hydrogels in a manner similar to its adsorption of serum proteins. TGF-β3 was incorporated within the hydrogels during formation, and release was measured over the course of two weeks. Previous studies have shown similar methods of growth factor sequestration of heparin-binding proteins like TGF-β3, however, many do so by taking advantage of the ability of the pre-formed charged material to absorb proteins into the hydrogel bulk (Waghmare et al. 2018; Portocarrero Huang et al. 2017). For hydrogels that form *in situ*, such post-polymerization growth factor loading is not possible. The pre-polymerized material must contain the growth factor, sequester it within the forming hydrogel, and protect it from denaturation during polymerization and thereafter. This may necessitate protection of the growth factor from polymerizing agents (McCall, Lin, and Anseth 2011). In pilot studies of this project, exposure of TGF-β3 to APS, a powerful oxidizing agent, denatures the growth factor and renders it unable to be detected by ELISA. Thus, TGF-β3 was mixed only into the TEMED containing barrel of the dual-barrel syringe system, to avoid overexposure to APS.

TGF-β3 release over two weeks showed decreasing release rate with increasing concentration of sulfonates. Varying the mesh size is a well-established method of controlling diffusivity of proteins from within a hydrogel network, which scales relative to diffusivity in a pure solvent by $(1-R_h/\xi)$, where R_h is the Stokes radius of the protein and ξ network mesh size (Mason et al. 2001; McCall, Lin, and Anseth 2011). Although the hydrodynamic diameter of TGF-β3 has not been published, it can be approximated based on the molecular weight of its dimeric form (25.5 kDa) in comparison to other proteins of similar weight, such as PDGF-BB (24.3 kDa, 7 nm), to have a diameter of ~ 3.0 - 7.0 nm (Rehmann et al. 2017; McCall, Lin, and Anseth 2011). Given that there was no statistically significant difference in mesh size calculated from swelling data for gels of the

same macromer concentration regardless of sulfonate concentration (23.58 ± 1.64 to 28.54 ± 0.99 nm for 3% w/v MC gels), and that the calculated mesh size was much larger than the encapsulated growth factor, it can be inferred that any changes in the release profile of TGF-β3 were due to chemical differences in the hydrogel composition and not to structural differences in the hydrogel mesh network (Amsden 1998). This suggests that sulfonated MC hydrogels interact with the encapsulated growth factor via electrostatic affinity, retarding the overall diffusive release and sequestering growth factor within the construct, similar to the mechanism by which growth factors are sequestered within sGAG rich tissues. Affinity-controlled release from hydrogels is driven by the reversible association (k_{on}) and dissociation (k_{off}) rates between affinity binding groups (Hettiaratchi and Shoichet 2019). In this study, the affinity-binding moiety 2SEM was the same between groups, thus it can be surmised that the association/dissociation constants did not change. Instead, the increasing concentration of 2SEM increased the number of binding sites, promoting the rapid re-association of TGF-β3 with the hydrogel network, thus limiting the diffusion of dissociated TGF-β3 outside of the hydrogel (Vo and Meere 2013). Indeed, modulation of sulfation concentration in heparin-based microparticles has been shown to tune protein release from 5% to 60% (Tellier et al. 2015).

The ability to sequester cationic proteins such as TGF-β3 suggests sulfonated MC hydrogels may be well suited as scaffolds for cell-based therapies to improve growth factor bioavailability to encapsulated cells. The amount of TGF-β3 loaded into the hydrogels was calculated based on the total growth factor that is delivered exogenously to encapsulated cells via cell culture media (at a concentration of 10 ng/mL) over the course of 2 weeks. Previous studies have shown that spatiotemporal control of TGF-β3 stimulation is critical for both chondrogenic and NP-like differentiation of cells *in vivo* (Martin et al. 2017; Gupta and Nicoll 2015; Huang et al. 2009). The

precise dosing of sequestered TGF-β3 for direct or extended stimulation of MSCs varies in the literature and will require titration studies; however, the present investigation shows that growth factor concentration within the hydrogel system and release rate can be easily tuned by adjusting sulfonate concentration.

3.5 Conclusions

The results presented here demonstrate the successful fabrication of injectable, sulfonated MC hydrogels, which form and are retained *in situ* in a bovine nucleotomy model. The addition of sulfonates had no significant impact on gelation or mechanical properties, resulting in a sulfonated biopolymer scaffold with tunable properties relevant to NP replacement. The materials were not cytotoxic and supported cell proliferation. Moreover, the sulfonated MC hydrogels displayed affinity for adsorbed serum proteins and encapsulated growth factor, which was proportional to the concentration of sulfonate incorporated into the constructs. Taken together, these results show that sMC hydrogels are a promising scaffold material for nucleus pulposus repair. Future studies will investigate the utility of the sulfonated scaffolds for cell-based, NP tissue engineering strategies.

3.6 Acknowledgements

This work was supported in part by grants from the National Science Foundation (IIP 1701120, S.B.N.), a Harvey L. Karp Discovery Award (S.B.N.) and the National Institutes of Health (R01AR057397, J.C.I.). The authors wish to thank Dr. Padmavana Pradhan, Dr. Devika Varma, Dr. Gittel Gold, and Dr. Huizi Anna Lin for technical guidance, Jesse A. Martin for assistance in preparing motion segments, and Tyler DiStefano for valuable scientific discussions. Authors also wish to thank Dr. Jeffrey Morris and Dr. Mitchell Schaffler for the use of equipment.

Chapter 4: TGF-β3 Sequestering, Sulfonated Methylcellulose Hydrogels Support Nucleus Pulposus-Like Matrix Elaboration by Encapsulated Human MSCs

The following chapter was presented at the Biomedical Engineering Society Annual Scientific Meeting (2021):

Haq-Siddiqi N.A., Iatridis, J.C., Nicoll, S.B. (2021). MSC-laden Sulfonated Methylcellulose Hydrogels for Nucleus Pulposus Tissue Engineering. (Podium Presentation) *Biomedical Engineering Society Annual Fall Scientific Meeting*, Orlando, FL.

4.1 Introduction

Low back and neck pain continue to be among the leading causes of disability, with up to 80% of the world's adult population affected by it in their lifetime (Tamrakar et al. 2021). This has enormous social and economic repercussions, with low back and neck pain ranking as the most expensive health conditions in the United States, resulting in $134.5 billion in healthcare spending in 2016 alone (Dieleman et al. 2020). The prevalence of low back pain has increased by over 50% between 1990 and 2015, and with continually aging populations, both the number of sufferers and economic cost is only set to grow (Hartvigsen et al. 2018). A large majority of this disability is caused by degeneration and injury to the intervertebral disc (IVD), the complex fibrocartilaginous tissue situated between the vertebral bones of the spine (Peng 2013). Degeneration of the IVD results in loss of disc height, limited mobility, and often discogenic pain associated with ingrowth of nerves into the IVD, or impingement of spinal nerve roots, causing radiculopathy (Peng 2013).

IVD degeneration is understood to begin in the central nucleus pulposus (NP) region of the disc. Aberrant cellular responses to loading lead to matrix breakdown, decreased transport of nutrients and metabolites, and cellular senescence (Zhao et al. 2007). In particular, increased catabolism and breakdown of the negatively charged proteoglycans that maintain the high water content of the NP causes a reduction in hydrostatic pressure and the ability of the NP to resist compressive loads (Sivan, Wachtel, and Roughley 2014). This shifts stress to the outer lamellar portion of the IVD, the annulus fibrosus (AF) (Adams, McNally, and Dolan 1996), leading to further IVD degeneration and injury such as bulging, fissures, and potential herniation of the NP through the AF (Galbusera et al. 2014). Because the IVD is generally avascular, with low cellularity, it has very little ability for self-repair. Nutrient supply in the healthy adult IVD is limited mainly to diffusion via the cartilaginous endplates (CEP) that sandwich the disc, which

receive blood supply from adjacent vertebral bones. This becomes further limited by the compounding effects of aging and degeneration, which include endplate calcification as well as regression and occlusion of the vessels originating in the vertebral bones (Huang, Urban, & Luk, 2014). Although prevalence of symptomatic IVD degeneration continues to rise, therapeutic options have largely not improved. Current treatments largely involve palliative care and pain management, ranging from over-the-counter pain relief to steroidal injections and physical therapy; however, these treatments address pain and not the underlying issue, allowing the degenerative cascade to progress (Zhao et al., 2019).

Tissue engineering strategies incorporating cells, materials and biological signaling molecules have been explored to restore mechanical function of the IVD and to reverse the existing tissue damage (Bowles and Setton 2017; Hudson et al. 2013; Tendulkar et al. 2019). In particular, NP replacements have been investigated as interventions for early-stage degeneration to prevent further disease progression and the development of more serious injuries (i.e., herniation). Hydrogels are a class of polymeric scaffold that are ideal for NP tissue engineering, as they mimic the highly hydrated network of the native NP (Gupta, Cooper, and Nicoll 2011; Halloran et al. 2008; Showalter et al. 2015; Tsaryk et al. 2015; Alinejad et al. 2019; Iatridis et al. 2013; Lewis 2012). Many studies have investigated stem cell-laden hydrogels for NP regeneration, however, the vast majority of tissue engineering studies are validated first *in vitro* wherein the constructs receive nutrients and differentiation cues from cell culture media, which is not readily translatable to the clinical setting (Risbud et al. 2004; Steck et al. 2005; Kregar Velikonja et al. 2014; Sakai and Andersson 2015). For example, previous reports have shown promising results with cellulosic hydrogels as scaffolds for mesenchymal stromal cells (MSCs) that differentiate towards NP-like phenotypes and elaborate NP-like matrix components (Varma, DiNicolas, and Nicoll 2018; Lin et

al. 2016; Gupta and Nicoll 2015; 2014). These studies required exogenous delivery of the growth factor, transforming growth factor-β3 (TGF-β3), a cytokine which is critical for differentiation of chondrogenic tissues such as cartilage and NP (Chen et al. 2019; Mackay et al. 1998; Madry et al. 2014). Hydrogels, while excellent carriers for cell encapsulation, frequently exhibit burst release of such soluble factors loaded within them, due to the influx of water into the polymer network (Lin and Metters 2006; Brazel and Peppas 2000; Ritger and Peppas 1987a; 1987b). To drive clinical translation, growth factors must be retained within the construct long enough to stimulate cell differentiation. Studies have shown that transient TGF-β stimulation is sufficient to initiate chondrogenic differentiation from MSCs, thus a system that maintains growth factor concentration within the vicinity of encapsulated cells long enough to initiate differentiation is desirable (Huang et al. 2009; Gupta and Nicoll 2015; Kim et al. 2012).

Recently, we developed and characterized an injectable, *in situ* forming sulfonated methylcellulose (sMC) hydrogel that sequesters encapsulated TGF-β3 (Chapter 3). Methylcellulose (MC) is a thermoresponsive, water-soluble derivative of cellulose, the most abundant polysaccharide on earth. The addition of sulfonates to the polysaccharide backbone of MC mimics the structure of the sulfated glycosaminoglycans (sGAGs) that comprise the matrix of the healthy NP. In addition to facilitating tissue hydration, part of the essential function of sGAGs is acting as depots for growth factors, extending their bioavailability and functionality via electrostatic interactions between cationic growth factors and anionic sulfates (Soares Da Costa, Reis, and Pashkuleva 2017). Similarly, the sMC hydrogels electrostatically sequester loaded growth factor over the course of 2 weeks of *in vitro* culture. The release rate of loaded TGF-β3 can be tuned by controlling the concentration of sulfonates added to the MC scaffold. Moreover,

the resultant scaffold delivers growth factor directly incorporated into the pre-gelled polymer solution, which can be injected via fine-gauge needle and form stable hydrogels *in situ*.

The present study aimed to investigate the ability of this growth factor-sequestering hydrogel system to support MSC growth and differentiation towards the NP-cell phenotype. Bone marrow-derived MSCs were thus encapsulated within the sMC hydrogels and evaluated for functional NP-like differentiation by quantifying characteristic matrix elaboration (type II collagen and sGAGs) and the development of functional construct material and mechanical properties over time. The potential for the sMC scaffold to drive differentiation in the absence of growth factor was also investigated in order to evaluate the influence of charged sulfonates on MSC differentiation, as matrix sulfation has been shown to be critical for the development of healthy skeletal tissues (Cortes, Baria, and Schwartz 2009; Mertz et al. 2012; Paganini et al. 2020). We hypothesized that the combination of matrix sulfonation and stimulation by sequestered TGF-β3 would support functional NP-like differentiation and matrix elaboration by encapsulated MSCs resulting in a clinically translatable, injectable tissue-engineered construct for NP replacement.

4.2 Materials and Methods

4.2.1 Macromer Preparation

Methacrylated methylcellulose (Ma-MC) was fabricated by esterification of hydroxyl groups with methacrylic anhydride (Sigma-Aldrich) according to previously described protocols (Gold et al. 2014; Stalling, Akintoye, and Nicoll 2009; Varma et al. 2018). Briefly, 15 kDa (low viscosity) and 41 kDa (medium viscosity) methylcellulose powder (Sigma-Aldrich, degree of substitution of methoxy groups ~1.5-1.9) was mixed 1:1 (for ease of handling and control for injectable applications) (Varma et al. 2018; Lin et al. 2019) and then added to deionized H_2O (diH_2O) at 1% (w/v) at 80°C until it was evenly disbursed, after which the temperature was lowered to 4°C and

allowed to continue to dissolve fully for ~24 hours. The solution was then reacted with methacrylic anhydride with a molar excess of 20 (based on theoretical 10% modification) at 4°C and pH 8 for 48 hours. The reaction product was purified by dialysis (Spectra/Por, MWCO 6-8 kDa) over 3 days to remove unreacted methacrylic anhydride. Purified solution was lyophilized and stored at -20°C. Polymer samples were acid hydrolyzed as previously described by ^{1}H-NMR spectroscopy (500 MHz, Varian Mercury 500) (Stalling, Akintoye, and Nicoll 2009; Reza and Nicoll 2010a). The relative integrations of methacrylate protons (δ = 6.1 and 5.7 ppm; methyl, δ = 1.9 ppm) to carbohydrate protons were used to determine the molar percentage of methacrylation (Stalling, Akintoye, and Nicoll 2009).

4.2.2 Human Mesenchymal Stromal Cell (hMSC) Culture

Cryopreserved bone marrow-derived hMSCs were acquired from RoosterBio (Frederick, MD) and expanded according to the manufacturer's protocol using proprietary high-performance expansion media (RoosterBasal™ -MSC medium with RoosterBooster™-MSC supplement). Cell lots from three healthy biological donors (MSC00115, MSC00175, and MSC00179) were used to reduce donor variability (**Table 4.1**). Each lot of hMSCs was expanded separately, to an average population doubling level (PDL) of 16.24 ± 0.27. Cell lots were passaged according to the manufacturer's protocol and then pooled at equal cell number for encapsulation as mixed donor samples. All cell culture was performed at 37°C and 5% CO_2, under normoxic (18.6% O_2) conditions.

Table 4.1: RoosterBio™ hMSC donor lot characterization and differentiation potential profiles

	Donor information		Differentiation Potential		
MSC Lot #	Age	Sex	Adipogenic	Osteogenic	Chondrogenic
00115	20 y.o.	Female	Yes	Yes	Yes
00175	25 y.o.	Male	Yes	Yes	Yes
00179	21 y.o.	Male	Yes	Yes	Yes

4.2.3 Hydrogel Preparation and Culture

Lyophilized Ma-MC was sterilized under germicidal UV light for 30 minutes and dissolved in sterile DPBS for a final concentration of 3% (w/v). Additional polymer precursors, redox initiators ammonium persulfate (APS) and N,N,N′,N′-tetramethylethylenediamine (TEMED), and 2-sulfoethyl methacrylate (2SEM) were prepared at 200 mM and 500 mM working concentration, respectively, and sterilized via syringe filtration (0.22 μm filter size). APS and TEMED (Sigma-Aldrich) were added to separate barrels of dual-barrel syringes (Pac-Dent) for a final working concentration of 10 mM each. Sulfonated gels were formed by including 2SEM (Polysciences) in the prepolymer mixture for a final concentration of 5 mM. Gels containing directly incorporated TGF-β3 were formed by adding rhTGF-β3 (R&D Systems, Minneapolis, MN) to the TEMED side of the dual-barrel syringe only, for a final concentration of 2 μg/mL (~80 ng/gel) corresponding to the total amount of TGF-β3 to be supplemented via cell culture media for 2 weeks (when maintained at a concentration of 10 ng/mL) (Gupta and Nicoll 2015). Pooled-lot hMSCs were mixed directly into the prepolymer solution for encapsulation in redox-polymerized MC hydrogels at 20 x 10^6 cells/mL. Hydrogels were formed by injecting the polymer solution through a 1:1 mixing tip into custom casting devices and allowed to cure for 15 minutes at room temperature to form cylindrical gels (5-mm diameter, 2-mm height).

Cell-laden hydrogels were cultured *in vitro* in chemically defined medium (CDM), consisting of high-glucose DMEM (Gibco), 1% insulin-transferrin-selenium-A (with sodium pyruvate) (Gibco), 100 U/mL penicillin + 100 μg/mL streptomycin (Gibco), 40 μg/mL l-proline (Fisher Scientific), 50 μg/mL ascorbic acid 2-phosphate (Sigma-Aldrich), and 100 nM dexamethasone (ACROS Organics). Negative controls for growth factor supplementation were maintained without TGF-β3. Positive control gels received media supplemented with 10 ng/mL TGF-β3 (CDM+).

Culture conditions are outlined in **Figure 4.1**. Media were changed three times weekly. Hydrogels were isolated at 1, 7, 21, and 42 days for various forms of analysis. Used media were collected and stored at -20°C for analysis (n=4).

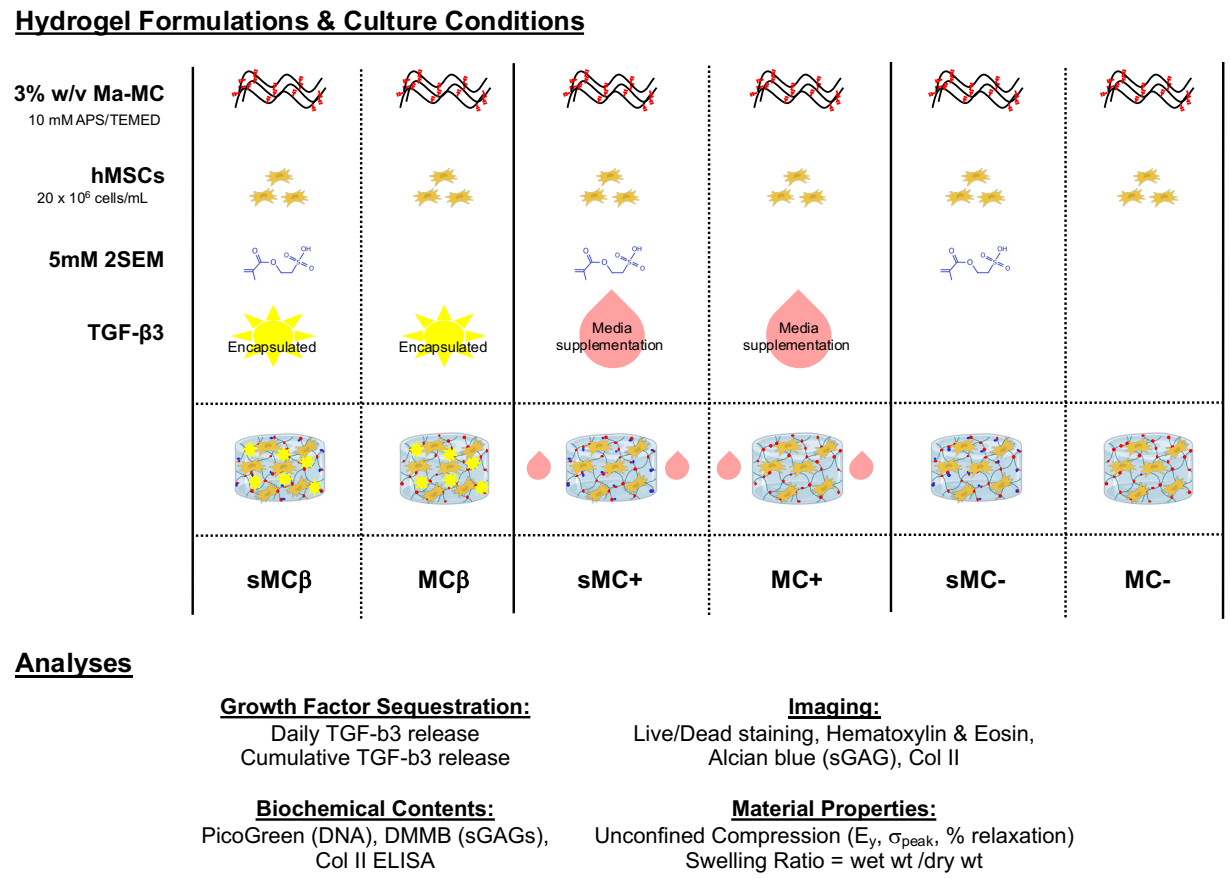

Figure 4.1: Schematic of hydrogel formulations, culture conditions and outcome measures
All hydrogels were cultured in chemically defined medium (CDM). Media supplemented with exogenous TGF-β3 referred to as CDM+. Constructs were cultured for 42 days total and collected at 1, 7, 21 and 42 days for analysis. CDM was collected after each media exchange for analysis of growth factor release.

4.2.4 TGF-β3 Release

Cumulative release of active TGF-β3 from hydrogels fabricated with incorporated growth factor (MCβ and sMCβ) was quantified over the first 3 weeks of culture. CDM was collected after each media exchange and stored at -20°C until quantification. Solid phase sandwich DuoSet ELISA (R&D systems) was used according to the manufacturer's instructions to quantify total

active growth factor released (n=4). Any potential latent growth factor produced by the cells was not quantified by skipping the activation step (rhTGF-β3 loaded within gels at fabrication was already in its active form). Unused CDM was used as a negative control.

4.2.5 Cell Viability

Cell-laden hydrogels were examined for viability and proliferation over the 42-day culture period. Hydrogels isolated for quantitative analysis were lyophilized, homogenized and digested with 4560 units/mL pepsin (from porcine gastric mucosa, Sigma-Aldrich) in 0.05N acetic acid (pH 2.8) (Sigma-Aldrich) for 48 hours at 4°C with constant agitation, after which pepsin activity was neutralized by adding 10x Tris-buffered saline (pH 8.0) (Gupta, Cooper, and Nicoll 2011; Reza and Nicoll 2010b). Total DNA content was quantified via Quant-iT™ PicoGreen™ Assay (Invitrogen Molecular Probes, Eugene, OR) against calf thymus DNA (Sigma-Aldrich) standard curve and analyzed with a BioTek Instruments microplate reader (Synergy 4, Winooski, VT) at excitation and emission of 480 nm and 520 nm, respectively (n=6). Cell viability was assessed visually by Live/Dead staining (Invitrogen) using calcein AM (green, indicative of live cells) and ethidium homodimer-1 (red, indicative of dead cells) (n=2) and imaged on a Zeiss Axio Imager Z1 (Carl Zeiss, Inc., Thornwood, NY) optical microscope and ZenBlue software (Carl Zeiss, Inc.).

4.2.6 Biochemical Analysis

Hydrogels were isolated on days 7, 21, and 42 to quantitatively measure matrix elaboration. Gels were homogenized and digested in pepsin as described in the previous section. Sulfated GAG content was quantified using the 1,9-dimethylmethylene blue (DMMB) assay (Sigma-Aldrich). DMMB assay reagent was prepared as previously described, with pH 1.5 to minimize the confounding effects of scaffold and DNA interference (Zheng and Levenston 2015). Absorbance

was measured at 525 nm and 595 nm against a chondroitin-6 sulfate standard (Sigma-Aldrich) and the difference in optical density (OD) used to quantify total sGAG present (OD_{525}-OD_{595}).

Collagen production was quantified via indirect enzyme-linked immunosorbent assay (ELISA), using monoclonal antibodies to type II collagen (Col II, II-II6B3, Developmental Studies Hybridoma Bank, University of Iowa, Iowa City, IA) as previously described (Gupta et al., 2011; Lin et al., 2016). Protein values were determined using human type II collagen standards (Chondrex, Inc., Redmond, WA). Absorbance was measured at 450 nm. Total GAG and collagen content were normalized to wet weight of the gels (n=6).

4.2.7 Histological/Immunohistochemical Evaluation

Hydrogels were rinsed in DPBS and fixed in a buffered zinc-formalin solution (Z-fix, Anatech, Battle Creek, MI) overnight at room temperature, and then stored in ethylene glycol monoethyl ether (EGME, Fisher Scientific). Samples were then dehydrated in a graded series of ethanol and then embedded in paraffin. Embedded constructs were sectioned to a thickness of 8 μm using a Thermo Scientific Rotary Microtome (MC HC325, Walldorf, Germany) and then sections were mounted on charged slides and dried at 37°C overnight. Slides were deparaffinized with Citrisolv™ Hybrid Solvent and rehydrated in graded ethanol. Cellular morphology and distribution were visualized with Hematoxylin & Eosin Y (alcoholic) (Sigma-Aldrich) staining. Distribution of sulfated GAGs was determined by staining with 1% Alcian Blue (pH = 1.0) (Pastewka 1974).

Immunohistochemistry was used to visualize specific matrix macromolecules. Clearer visualization of Col II and Col VI was achieved by first exposing collagen epitopes by 30-minute treatment of samples in hyaluronidase (type IV-S, Sigma-Aldrich) at 37°C to remove interfering GAGs. Sections were further swollen in 0.5 N acetic acid (Sigma-Aldrich) for 2 hours at 4°C to

increase access to epitopes. Slides were blocked in 10% horse serum for 20 minutes at room temperature, followed by incubation in primary antibodies (1 μg/mL in 10% horse serum) overnight at 4°C (Col II II-II6B3 monoclonal mouse IgG, Developmental Studies Hybridoma Bank (DSHB)). Non-specific mouse IgG was used as a control. Alexa Fluor™ 488 (Invitrogen) Goat anti-Mouse IgG (H+L) secondary antibody was applied at 1:200 dilution and 4′,6-diamidino-2-phenylindole (DAPI, Sigma-Aldrich) was used to counterstain cell nuclei. All stained sections were imaged and captured using the Zeiss Axio Imager optical microscope and AxioVision software (Carl Zeiss) (n=2-3).

4.2.8 Swelling Behavior

Equilibrium weight swelling ratio (Q_W) of cell-laden hydrogels was measured at day 1, 7, 21 and 42 (n=3-6). Constructs were isolated and blotted to remove excess liquid, and then weighed to determine the wet weight (W_s), after which gels were frozen at -80°C, lyophilized and weighed again to measure the dry weight (W_d). Equilibrium weight swelling ratio was calculated as

$$Q_w = \frac{W_s}{W_d} \tag{4.1}$$

4.2.9 Mechanical Testing

Cell-laden hydrogels were characterized for their mechanical properties under unconfined compression using a custom-built apparatus as previously described (n=5) (Soltz and Ateshian 2000; Gold et al. 2014). Gels were isolated at days 1, 7, 21 and 42 and stored at -80°C until testing. Gels were thawed and allowed to equilibrate completely in PBS overnight at 4°C prior to mechanical testing. The testing protocol consisted of a creep test (tare load = 1 g) at a ramp speed of 10 μm/s held at 2700 s until equilibrium was reached (equilibrium criterion: <10 μm displacement in 10 min), followed by a multi-ramp stress relaxation test, consisting of three 5% strain ramps with a 2000 s relaxation period between ramps (equilibrium criterion: <0.5 g change

in 10 min). Equilibrium Young's modulus (E_Y) was determined as the slope of the equilibrium stress (calculated at each ramp) versus applied strain curve. Peak stress (σ_{pk}) and equilibrium stress (σ_{eq}) were calculated at the third ramp corresponding to 15% strain, and percent relaxation was calculated by the formula

$$Percent\ Relaxation = \left(1 - \frac{\sigma_{eq}}{\sigma_{pk}}\right) \quad (4.2)$$

4.2.10 Statistical Analysis

Data are represented as the mean ± standard deviation. A two-way ANOVA with a Tukey's post-hoc test was used to determine the effects of sulfonation and growth factor supplementation at each time point, and subsequent one-way ANOVA of time across each group on hMSC-laden hydrogel constructs. Two-way repeated measures ANOVA was used to determine the effect of sulfonation and time on TGF-β3 release. All statistical analyses were carried out using GraphPad Prism v.9 (GraphPad Software, San Diego, CA) with significance set at $p < 0.05$.

4.3 Results

Methylcellulose was methacrylated to enable redox-initiated crosslinking at 5.84% modification as confirmed by ^{1}H-NMR (not shown).

4.3.1 Growth Factor Release from Sequestering Hydrogels

TGF-β3 that was incorporated into hydrogels during formation was measured during media exchange to track sequestration in sulfonated vs sulfonate-free gels (sMCβ vs. MCβ, respectively). Each media change was collected and assayed for TGF-β3 present in the media, and daily and cumulative release was calculated for the duration of the culture. Both conditions experienced a burst release in the first day (42.62 ± 11.59 ng, MCβ and 21.71 ± 5.77 ng, sMCβ), with the unsulfonated gels releasing significantly more TGF-β3 per day over the first 5 days (**Figure 4.2A**).

Cumulative release from sMCβ reached a plateau by day 3, while MCβ gels continued to release growth factor until reaching a plateau by day 16, **Figure 4.2B** shows sulfonate-free gels released the total amount of calculated TGF-β3 loaded (indicated by dotted grey line). The wide standard deviation (shown by the shaded region) is indicative of the variability in loading efficiency during hydrogel fabrication (78.73 ± 18.66 ng/gel). Sulfonated gels released 37.35 ± 6.87% of the calculated total amount of TGF-β3 loaded within the gels over the time measured (29.33 ± 5.39 ng/gel).

4.3.2 Cell Viability, Distribution, and Morphology

hMSC-laden MC hydrogels were fabricated at a seeding density of 20 x 10^6 cells/mL (~800,000 cells/gel) and exhibited DNA values ranging from 51.33 ± 23.54 ng/mg to 77.01 ± 19.67 ng/mg (DNA/wet weight). There was a statistically significant decrease in cellularity over time, as indicated by decreasing DNA content (**Figure 4.3A**), for all groups except sMCβ and sMC+. Significant differences in cellularity between groups were seen at day 21, with nonsulfonated constructs displaying DNA levels significantly lower than sulfonated constructs (24.45 ± 9.30 ng/mg to 29.08 ± 7.52 ng/mg versus 41.77 ± 11.11 ng/mg to 48.04 ± 9.51 ng/mg, respectively). By the end of the 6-week culture, there were no significant differences in cell density across all groups (ranging from 48.65 ± 18.16 ng/mg to 30.04 ± 9.86 ng/mg). These findings were corroborated by the decrease in staining of live cells over the course of the 6-week study (**Figure 4.3B**).

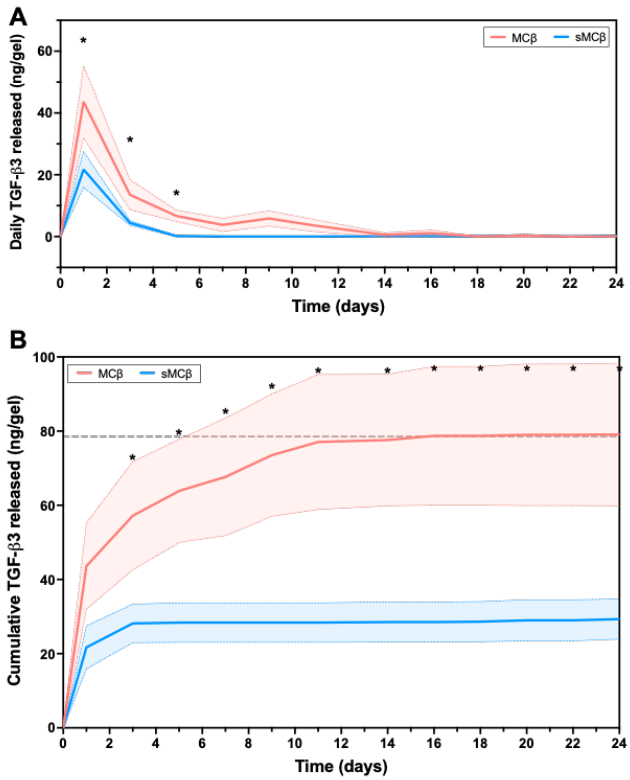

Figure 4.2: Daily A) and cumulative B) release of encapsulated TGF-β3 from hMSC-laden hydrogels.

Shaded regions indicate SD. * - Significant difference in amount of TGF-β3 released between groups. Significance set at $p < 0.05$.

Hematoxylin and eosin staining (**Figure 4.4**) also confirmed the decrease in cellularity, showing much more sparsely populated constructs on day 42 versus day 7 across all groups. Although fewer in number and distribution, cells in sulfonated gels at day 42 still displayed a large, rounded cell morphology, characteristic of an NP-like phenotype. Conversely, the majority of cells seen in MC only gels at day 42 appeared small or showed evidence of membrane disruption and cellular lysis.

4.3.3 NP Matrix Elaboration and Distribution

The sGAG content in the hydrogels increased over time only in groups with both sulfonates and growth factor supplementation (sMCβ and sMC+) (**Figure 4.5A**). By day 42, sMCβ produced

significantly more sGAGs (836.24 ± 181.89 ng/mg) than sulfonate-free constructs with and without exogenous growth factor delivery, and sMC+ constructs produced more sGAG than all other groups (1,242.35 ± 286.11 ng/mg). Alcian blue staining of day 42 samples was strongest in sMCβ and sMC+ sections, consistent with the DMMB results, and concentrated pericellularly, rather than spreading diffusely throughout the bulk of the construct (**Figure 4.6A**). Not all cells in those constructs were producing sGAG, however, as smaller, unstained cells can be seen adjacent to larger cells that did stain positively for sGAGs. Alcian blue staining of the charged sulfonated constructs unrelated to sGAG production was observed, as seen in the staining of sMC- gels, where cells were clear of any blue dye. Faint blue staining was seen diffusely around the cells in MC only constructs, which were smaller and less rounded.

Type II collagen production increased in all groups over time except in MC+ (averaging 25.83 ± 6.58 ng/mg over all time points) (**Figure 4.5B**). Col II production peaked at 21 days of culture in sulfonated gels (82.68 ±16.91 ng/mg, 70.93 ±4.38 ng/mg, and 57.26 ± 10.68 ng/mg in sMCβ, sMC- and sMC+, respectively), with a decrease in Col II accumulation in sMC- constructs (43.42 ± 6.31 ng/mg) and no significant change between day 21 and 42 for sMCβ and sMC+ constructs (67.26 ± 30.92 ng/mg and 62.14 ± 13.60 ng/mg, respectively). At 21 days, each sulfonated group showed significantly greater Col II accumulation compared to all non-sulfonated constructs. By day 42, MCβ and MC- had increased Col II elaboration and values were not statistically different from the sulfonated gels (48.34 ± 16.34 ng/mg and 49.17 ± 9.93 ng/mg, respectively).

Immunohistochemical staining of day 42 constructs for Col II showed positive staining in all constructs, although not all cells in each construct elaborated matrix (**Figure 4.6B**). Faint pericellular staining was evident in MCβ gels, and few cells demonstrated staining in MC- conditions. Staining was more abundant in MC+ and sMC- constructs, but still faint. Consistent

with results of the Col II ELISA, staining in sMCβ and sMC+ gels was more abundant pericellularly, with some staining in the interterritorial space.

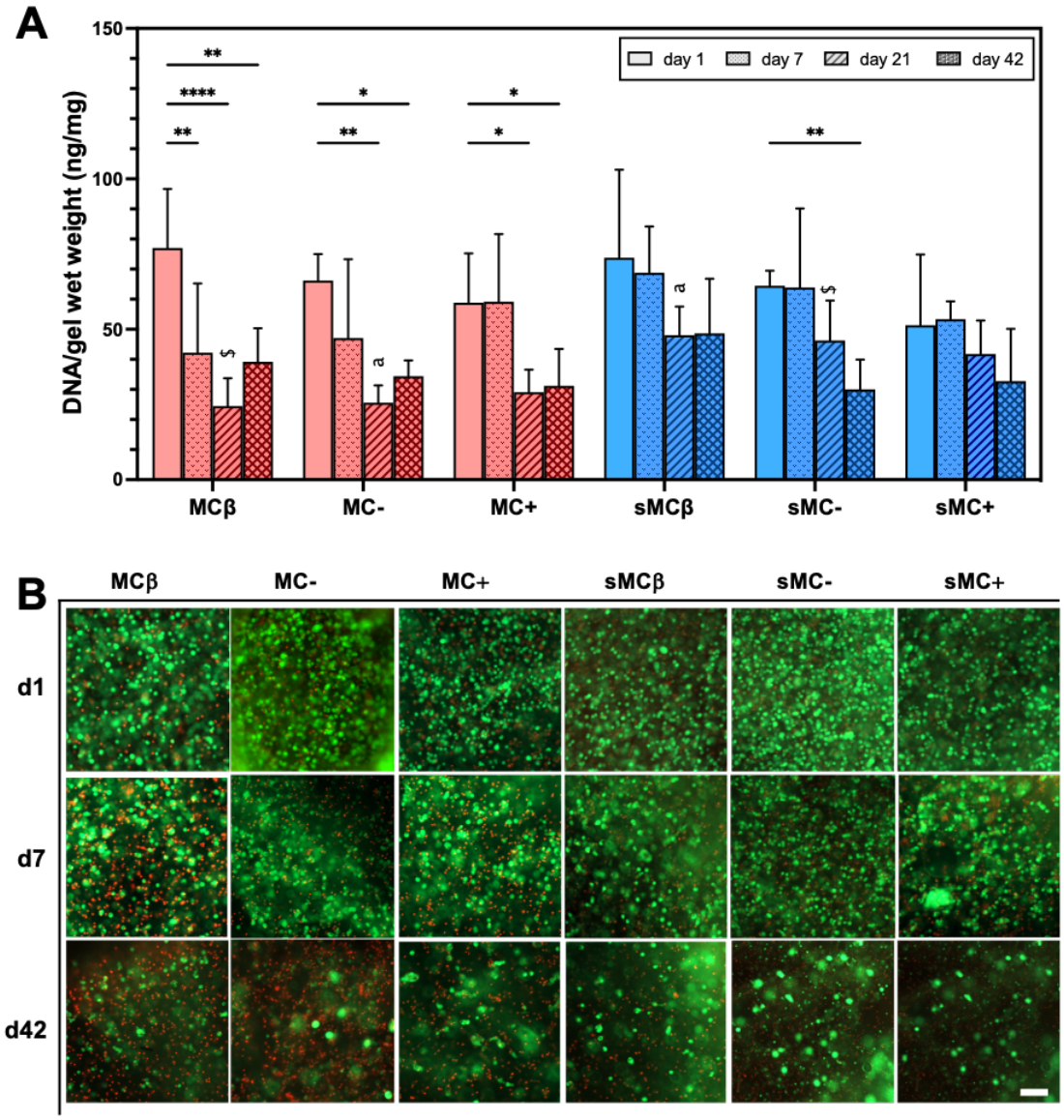

Figure 4.3: Viability and survival of hMSCs encapsulated within MC and sMC hydrogels. A) DNA content over 42 days as quantified by PicoGreen assay. Significant difference between time points within the same group: *– $p < 0.05$, **– $p < 0.01$, ***– $p < 0.0005$, ****– $p < 0.0001$, $^{\$}$– significantly different from all other constructs of different scaffold sulfonation within the same time point. ^{a}– significantly different from each other. Significance set at $p < 0.05$. B) Representative Live/Dead stained images of hMSCs in hydrogels over time (Live = green; Dead = red). Scale bar = 100 μm.

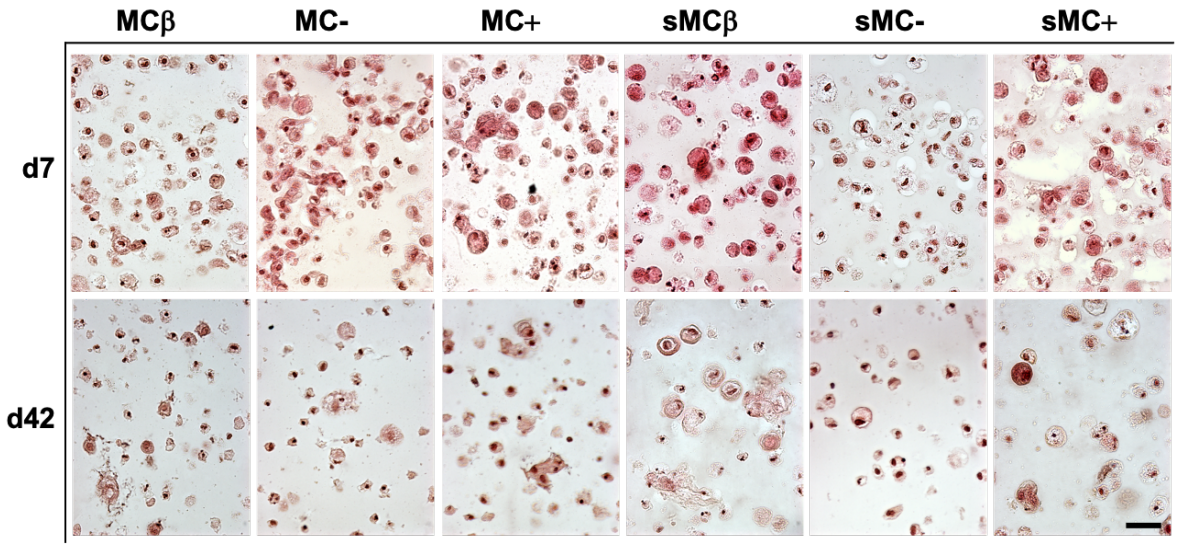

Figure 4.4: Hematoxylin & Eosin staining of hMSC-laden hydrogels at day 7 and day 42.
Scale bar = 50 μm.

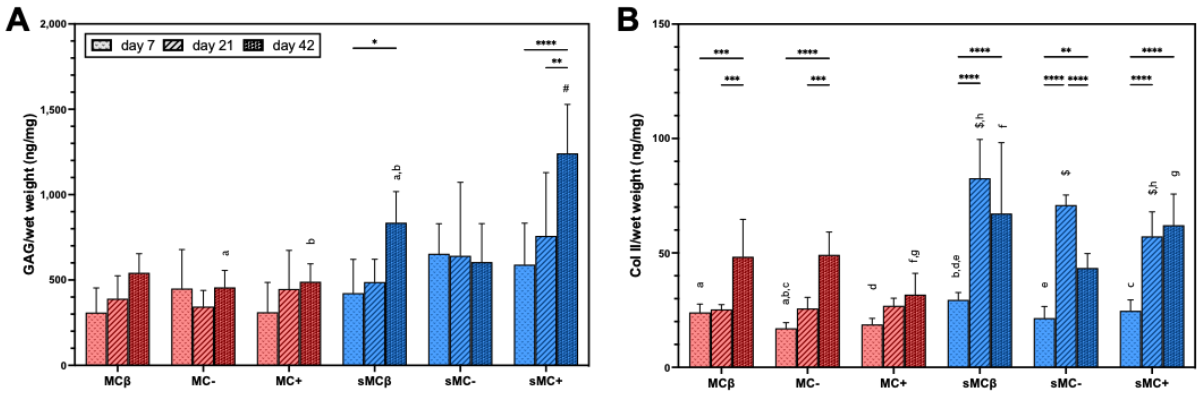

Figure 4.5: Biochemical content of hMSC-laden MC hydrogels over time.
A) Sulfated GAG and B) Col II. Significant difference between time points within the same group: *– $p < 0.05$, **– $p < 0.01$, ***– $p < 0.0005$, ****– $p < 0.0001$, $^{\$}$– significantly different from all other constructs of different scaffold sulfonation within the same time point. ^{a,b,c,d,e,f,g,h}– significantly different from each other. Significance set at $p < 0.05$.

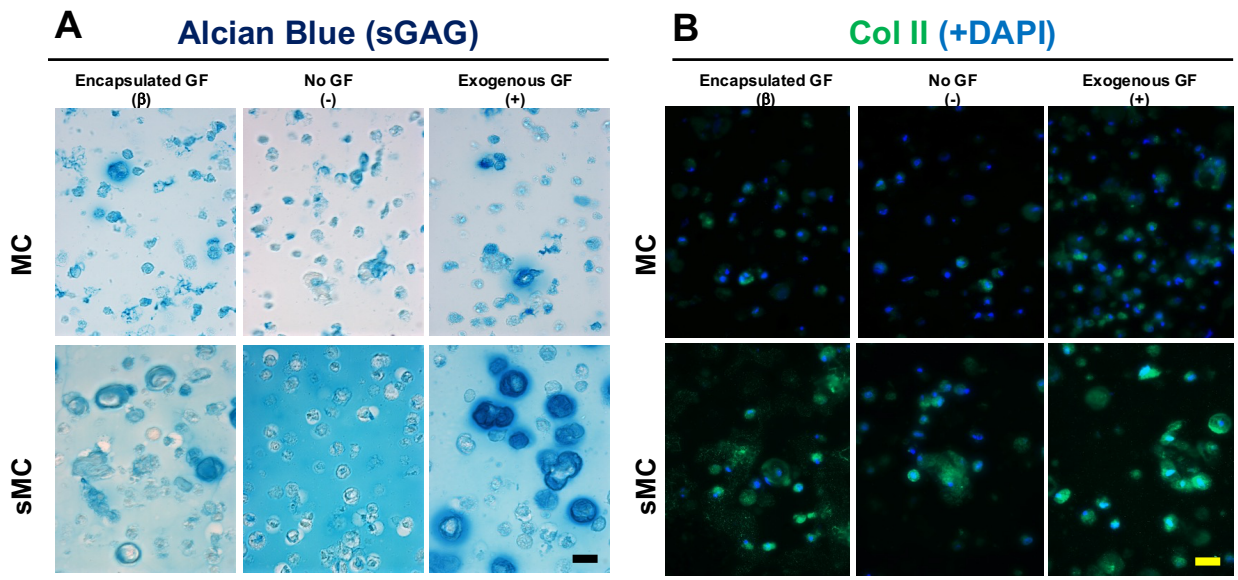

Figure 4.6 ECM localization within hMSC-laden MC hydrogels at 42 days.
A) Alcian blue staining of sGAGs, and immunofluorescence of B) Col II and C) Col VI localization (green), with nuclei stained with DAPI (blue). Scale bar = 50 μm..

4.3.4 Material Properties of Constructs

Construct mechanics were stable and showed very little change over time. There was no significant change in E_Y between day 1 and day 42 for all groups studied (**Figure 4.7A**). Final E_Y for all groups ranged from 7.57 ± 2.02 kPa (MCβ) to 12.34 ± 1.55 kPa (sMC-). At day 21, sMC+ and sMC- (but not sMCβ) were significantly stiffer than all unsulfonated constructs, regardless of growth factor delivery. By day 42, sulfonated gels without growth factor supplementation (sMC-) exhibited a significantly greater equilibrium Young's modulus than unsulfonated gels with encapsulated growth factor (MCβ) and without growth factor supplementation (MC-, 8.42 ± 1.67 kPa). Similarly, at intermittent time points sulfonated gels achieved greater σ_{peak} than unsulfonated samples, irrespective of growth factor supplementation. However, by day 42 there were no significant differences in the σ_{peak} achieved by any groups, ranging from 1.83 ± 0.45 kPa (MCβ) to 2.60 ± 0.52 kPa (sMC-) (**Figure 4.7B**). Growth factor delivery and scaffold sulfonation had no

significant effect on % relaxation. Despite % relaxation decreasing within MC- and MC+ groups over time, relaxation behavior was also relatively stable, with an average % relaxation of 35.23 ± 4.49% across all groups (**Figure 4.7C**).

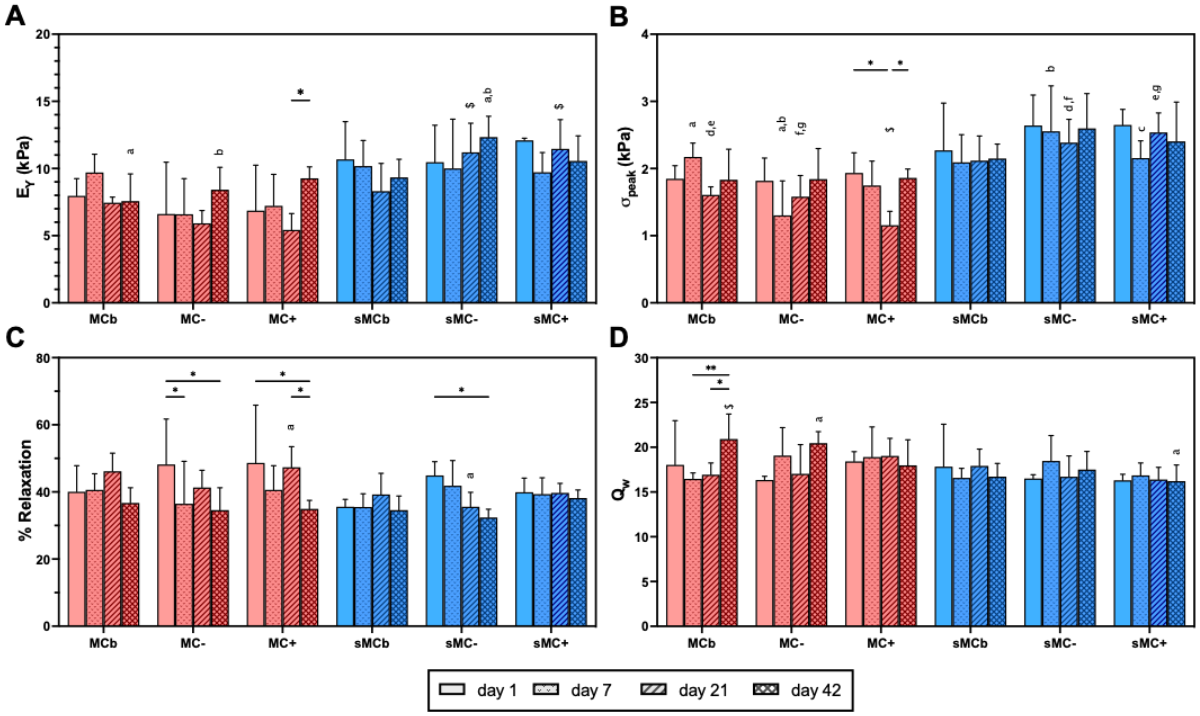

Figure 4.7: Material properties of hMSC-laden MC hydrogels over time.
A) Equilibrium Young's modulus (E_Y), B) peak stress (σpeak), C) % relaxation, and D) equilibrium weight swelling ratio (Q_w). Significant difference between time points within the same group: *– $p < 0.05$, **– $p < 0.01$, $^{\$}$– significantly different from all other constructs of different scaffold sulfonation within the same time point. ^{a,b,c,d,e,f,g}– significantly different from other group within the same time point. Significance set at $p < 0.05$.

Swelling ratio (Q_w) did not change significantly over time for most groups, with MCβ showing the only significant change in swelling ratio by 42 days (**Figure 4.7D**). Growth factor delivery method and scaffold sulfonation had no effect on swelling ratio over the first 3 weeks of culture; by 6 weeks, however, MCβ and MC- displayed higher equilibrium swelling ratio (20.77 ± 2.82 and 19.95 ± 0.51, respectively) than the sulfonated constructs (14.9 ± 1.82 to 16.66 ± 2.23).

4.4 Discussion

Tissue engineering repair of the NP is a promising strategy for treatment of IVD degeneration that aims to prevent further downstream breakdown of the disc by restoring the mechanical and biological function of the healthy NP. A clinically-viable tissue-engineered replacement for the NP requires that the traditional triad of tissue engineering components – scaffold, cells, and signals – are delivered together in a minimally invasive manner, such that differentiation and development of the replacement tissue can proceed *in situ*. To this end, we recently developed a GAG-mimetic cellulosic biomaterial system that is injectable, forms robust hydrogels *in situ*, and sequesters TGF-β3 directly within the scaffold for ease of delivery (Chapter 3). By incorporating negatively charged sulfonates onto the backbone of the physically and chemically crosslinked MC scaffold, we have been able to sequester TGF-β3 via electrostatic interactions to serve as a depot for growth factors in a mechanism similar to sGAGs found in the native NP. TGF-β is critical in the development of the IVD and other cartilaginous tissues (Chen et al. 2019; Reza and Nicoll 2010b; Haberstroh et al. 2009; Gupta, Cooper, and Nicoll 2011; Barry et al. 2001; Mackay et al. 1998). Thus, the present study aimed to investigate the ability of this scaffold to support differentiation and NP-like matrix elaboration of encapsulated MSCs. The effect of TGF-β3 sequestration and enhanced bioavailability was examined with and without the influence of sequestering sulfonates, while TGF-β3 delivered exogenously through supplemented media was included as a positive control. Studies have shown that artificially sulfated scaffolds can promote early chondrogenic differentiation in the absence of soluble differentiating factors, therefore, constructs with and without sulfonates were also cultured without TGF-β3 in order to isolate the effect of matrix sulfonation on MSC growth and differentiation (Kwon et al. 2010; Kwon 2012).

Artificially sulfated scaffolds and sGAG-mimetics have become increasingly popular methods of sustained growth factor delivery for tissue engineering applications, but to the best of our knowledge, this is the first study to utilize the method specifically for IVD tissue engineering (Zeng, Groth, and Zhang 2019; Arslan, Guler, and Tekinay 2016; Yaylaci et al. 2016; Freeman, Kedem, and Cohen 2008; Portocarrero Huang et al. 2017; Waghmare et al. 2018; Feng et al. 2017). Sulfonated MC gels successfully sequestered incorporated TGF-β3 for the duration of the culture, with characteristic burst release on the first day of culture, followed by sustained release for all gels. The concentration was loaded at 2 μg/mL, the equivalent of 2 weeks of supplementation at 10 ng/mL in chondrogenic medium (Madry et al. 2014). Previous studies have shown transient exposure to TGF-β for 2 weeks is sufficient to stimulate chondrogenic differentiation in MSCs (Kim et al. 2012; Huang et al. 2009; Gupta and Nicoll 2015). The wide disparity in release from non-sulfonated gels may be due to variations in mixing while loading or to variability in individual gel network formation; if it is not the former, it is conceivable that some gels maintained trace amounts of TGF-β3 within them. Release from these gels reached a plateau corresponding to the total theoretical loaded growth factor within 2 weeks, crossing below the threshold for therapeutic concentration at approximately 1 week. Sulfonated gels also experienced a burst release that was significantly lower than the non-sulfonated gels. Interestingly, the release quickly plateaued and did not appreciably increase beyond the 27.5 ng/mL released, indicating true sequestration rather than delayed or sustained release. Preliminary data (not included) have shown that 2SEM does not denature or reduce the detectability of TGF-β3 by the ELISA, and as all the theoretical load was released from the unsulfonated gels, we are able to discern that the loaded growth factor was not denatured. Because affinity-based sequestration techniques rely on association-dissociation reactions between the therapeutic and binding ligand, release behavior is dependent on the strength

of the affinity between the ligand and therapeutic, with diffusion-based release kinetics driven by the amount of unbound therapeutic at a given time (Vulic et al. 2015). The data here suggest very strong binding interactions between the sulfonates and TGF-β3.

Based on the release data alone, it is not immediately obvious whether sequestration translates into increased presentation to encapsulated cells or to reduced bioavailability due to over-sequestration. Strong sequestration of growth factors has been observed in chondroitin sulfate- and heparin-containing biomaterials, in which selective de-sulfation increased the release of encapsulated growth factors (Lei, Trevino, and Temenoff 2016; Lim and Temenoff 2013). In prior studies, we showed that sequestration of TGF-β3 is tunable by titrating the sulfonate concentration. Fluorescence recovery after photobleaching (FRAP) is a technique that has been previously employed to determine the ratio of mobile to immobile TGF-β by visualizing the rate of influx of fluorescently-labeled growth factor into an area of interest that had been photobleached (Jha, Mathur, et al. 2015). Further investigation of the movement and distribution of TGF-β3 within the sulfonated scaffolds using FRAP may provide greater insight into the bioavailability of the sequestered growth factor. It is important to note that tethered TGF-β3 has successfully been used to induce chondrogenesis in encapsulated MSCs (McCall, Luoma, and Anseth 2012), demonstrating that even immobilized growth factor can promote differentiation, provided the spacer arm of the tethering polymer is long enough to prevent steric hinderance from impeding cellular access and ligand binding.

The combined effects of sulfonation and TGF-β3 appear necessary for maintaining cell survival within this crosslinked MC hydrogel system. This is evidenced by the finding that DNA content decreased over time in all groups except for those with both sulfonate and TGF-β3 supplementation (sMCβ and sMC+). Neither scaffold sulfonation nor TGF-β3 supplementation

alone (sMC-, or MCβ and MC+, respectively) were sufficient in preventing significant decrease in cellularity. The reduction in cellularity was clearly visualized both in live/dead staining and H&E histological sections. H&E staining showed those cells that remained in the sulfonated constructs displayed a large, rounded morphology, typical of the chondrocytic cell phenotype, but that the vast majority of cells in the non-sulfonated gels were shriveled and seemed unhealthy, appearing to have disrupted membranes or have lysed. Similar results were observed in heparin-modified hyaluronic acid hydrogels, where heparin-bound TGF-β1, but not unbound incorporated or exogenous delivery of TGF-β1, enhanced survival and proliferation of encapsulated cardiac progenitor cells by retaining the active form of the growth factor in close proximity to the cells for an extended amount of time (Jha, Tharp, et al. 2015). In our development of the sMC hydrogel (Chapter 3), there was no indication of cell death, and in fact, there was evidence of proliferation over the course of the study. Nevertheless, the focus of that cell study was on cytocompatibility, in accordance with ISO standard 109935:2009, and lasted 5 days to assess the cytotoxic potential of the hydrogel components during and immediately following gel formation, and not on long-term survival. The fact that a significant decrease in cell number was observed in MCβ gels as early as 7 days of culture despite direct encapsulation of TGF-β3 was surprising, as TGF-β has been shown to inhibit disc cell apoptosis (Ni et al. 2014; Xie et al. 2020). The burst release of TGF-β3 from the unsulfonated hydrogel seen in the release study may be responsible for the lack of response. MC+, which received continuous exogenous TGF-β3 delivery, did not display significant cell loss until 21 days. Still, sulfonated MC gels without TGF-β3 supplementation (sMC-) showed a significant drop in cellularity only by day 42, suggesting that the sulfonation of the scaffold alone may have assisted in maintaining cell survival. Qualitative inspection of live/dead staining showed an obvious decrease in the density of live cells across all groups,

although there was no statistically significant change in cell number. From morphological analysis alone it is not possible to discern whether cell death was caused by apoptosis or necrosis. In the absence of phagocytic cells to engulf apoptotic bodies, apoptotic cells go through secondary necrosis (Silva 2010). Staining of cleaved caspase-3, an apoptotic marker, was not performed, but could be used in the future to elucidate whether apoptosis or necrosis was the cause of cell death in these scaffolds.

The decrease in cell viability and proliferation observed in most of the MC hydrogel formulations may be due to subtle alterations in gel material properties (i.e., stiffness, hydration, nutrient transport) attributed to the hydrophobic character and thermoresponsive nature of the biomaterials. Earlier studies directly encapsulating bovine NP cells into similar hydrogels of photocrosslinked methacrylated MC (3% w/v) reported only 20-30% survival by 21 days of culture (culture medium contained serum and no TGF-β3 supplementation), which is comparable to the survival at day 21 in sulfonate-free gels (MC-) in the present investigation (Reza, Stalling, and Nicoll 2006). We hypothesized that this may have been caused by the limited hydration of MC that results from the presence of hydrophobic methoxy substitutions on its backbone. When MC is in solution, the methoxy groups (as well as the methacrylates on modified MC) aggregate at increasing temperatures to form thermoreversible physical crosslinks. Few studies have investigated dual-crosslinked MC systems similar to the one presented here, wherein the reversible thermally induced physical crosslinking of MC is combined with permanent redox-initiated chemical crosslinks to form more stable and mechanically robust hydrogels (Pakulska et al. 2015; Morozova et al. 2019; Shin et al. 2020). Morozova et al. (2019) have recently shown that allyl-modified, photocrosslinked MC formed at lower temperatures (~20°C) form amorphous crosslinked hydrogels that retain some of their thermoresponsive nature, with increasing storage

modulus and decreasing volumetric swelling with increasing temperatures, but it was not clear if this increase was significant within the range of 20°C to 37°C. Shin et al. (2020) have also recently formulated tyramine-modified photocrosslinkable MC for use as a bioink and found that dual-crosslinked MC (chemically and thermally at 37°C) result in stiffer gels than those chemically crosslinked at room temperature, regardless of the order of stimuli. While the chemical and material specifics of these studies are different, they exhibit the strength of the hydrophobic interactions in MC, even when chemical crosslinking dominates the material behavior. In the present study, hydrogels were chemically crosslinked for 15 minutes at room temperature, as maintaining the developing system at 37°C was not feasible while ensuring sterile conditions. It is possible that once the hydrogels were moved to 37°C, the gels contracted or stiffened, which has implications both on the mechanical stimuli experienced by the cells, as well as on the transport of fluid and nutrients within the constructs. We have generally operated under the assumption that the methacrylate-derived crosslinks dominate the properties of the gels, as these permanent chemical bonds result in storage moduli 1-2 orders of magnitude higher than gels stabilized solely by physical thermal crosslinks (see Chapter 2). Nevertheless, the thermally driven contributions to the network structure may still influence the viability of cells encapsulated within the cellulosic scaffolds.

Despite evidence that cells were not apparently proliferating within the constructs and cell death was observed across many of the groups, metabolic activity via production of matrix components in all constructs suggests the observed cell death was apoptotic rather than necrotic, as necrotic cells would not be actively producing matrix components (Strehl et al. 2002). As might be expected, the groups that produced the most NP specific matrix components (sGAG and Col II) were also the groups with the best cell survival. Both sMCβ and sMC+ exhibited increasing sGAG

accumulation over the course of culture, with the greatest amount of sGAG accumulation exhibited in constructs with exogenous growth factor delivery. The finding that all sulfonate-free groups, even with TGF-β3 stimulation, did not display a significant increase in sGAG accumulation over time indicates that the inclusion of the negatively charged moieties was necessary for matrix stimulation. This is likely attributed to the sequestration and presentation of TGF-β3 in the vicinity of the cells, as growth factor-free, sulfonated constructs (sMC-) showed no significant increase in sGAG production, nor any improvement over any of the non-sulfonated constructs. Interestingly, sMC- gels presented with intense non-specific Alcian blue staining not localized to cells. As Alcian blue dye is cationic and attracted to negative charges, the stronger blue staining throughout the sMC- gels may be interpreted as uniform staining of the construct with evenly distributed fixed charge distribution. In contrast, the sMC+ and sMCβ gels that produced more sGAGs (as confirmed by the DMMB assay) presumably had a higher concentration of negatively charged sulfates and associated fixed charge density in the vicinity of the pericellular neomatrix. This would result in the observed sequestration of Alcian blue dye in the pericellular space and less non-specific staining of the sulfonated scaffold. Moreover, this was confirmed via Alcian blue staining of all day 7 sulfonated gels, which also exhibited stronger non-specific background staining, as did acellular sulfonated gel sections (not shown).

With respect to Col II production, there was a significant increase in all groups except MC+ over the course of the 6-week culture. All sulfonated groups exhibited marked, significant increases in Col II production between days 7 and 21, regardless of growth factor stimulation. However, sMC- demonstrated an equally significant drop in Col II content by 42 days. The decrease in accumulated Col II may be relative to the loss of cellularity; when normalized to DNA, Col II in sMC- gels was not significantly different at day 42 than 21. Even though Col II

production was more rapid in the sulfonated gels, the non-sulfonated gels did catch up, and by 42 days there was no significant difference between Col II production in non-sulfated and sulfated gels, except for those where TGF-β3 was delivered exogenously. Data normalized to DNA suggest again that the combination of scaffold sulfonation and continuous exogenous TGF-β3 stimulation resulted in the most robust anabolic activity, as well as the most consistent increase in Col II over time.

The distribution of dead cells and elaborated matrix did not exhibit any spatial pattern that would indicate nutrition or diffusional constraints, as has been exhibited in previous studies (Gupta and Nicoll 2015; Varma, DiNicolas, and Nicoll 2018). As mentioned earlier, labeling of TGF-β3 to image distribution, motility, and consumption may be useful in determining whether sequestration played a role in limiting the growth and differentiation of the encapsulated cells. Additionally, this study used a pooled batch of 3 distinct hMSC donors. Pooled-donor usage has been shown to have no negative effects on viability, proliferation, or differentiation when compared to single donor studies, and is intended to eliminate the need for biological replicates (Hejretová et al. 2020; Widholz et al. 2019). However, lack of an evident pattern in the distribution of dead cells and metabolically active cells (as exhibited by GAG and Col II staining around some, but not all cells) raises the question of whether one or more donor cell source was exhibiting a more robust response than others. Pooling donors eliminates the ability to discern minute biological differences that could influence cellular response, and future studies may need to take that into account. Yet, this issue has not been raised in other NP tissue engineering studies that used pooled donors (Thorpe et al. 2010; Frith et al. 2014; Potier and Ito 2014).

In this study, matrix production was analyzed to provide evidence of NP-like differentiation, as the goal of tissue engineering is to develop *de novo* healthy tissue. Hence, the production of the

major matrix components responsible for healthy NP functionality were the primary outcome measures to assess cell-driven repair. Type II collagen and proteoglycans, specifically aggrecan, are the most abundant matrix components of the NP as well as hyaline cartilage. Indeed, differentiation of NP cells is often somewhat loosely referred to as chondrogenesis despite the two tissues being distinct. The mechanical role and behavior of the two tissues are quite different, which is reflected in the ratio of these matrix components. The high hydration and soft viscoelastic behavior of NP tissue is afforded by the abundance of sGAGs, which appear at a ratio of 27:1 to hydroxyproline, as opposed to ~2:1 in healthy adult cartilage (reaching a maximum of 5:1 in degenerate cartilage) (Risbud et al. 2015; Mwale et al. 2004). As the mass ratio of hydroxyproline to collagen has been reported as 1:7.5, the effective sGAG:Collagen ratio was calculated as 3.6:1 in healthy adult NP and 1:1.5 to 1:3.75 in cartilage. Type II collagen accounts for nearly 100% of the collagen content in the NP (other collagens like type VI, IV, and XI are present but their relative quantities are so much lower as to be negligible for the current approximation) (Antoniou et al. 1996). Due to the slower apparent collagen production in sulfonate-free MC constructs, the sGAG:Col II ratio was significantly higher in MC-only constructs versus sMC constructs (~34-40:1 versus 16-19:1, respectively) at day 21 but by day 42 the differences in ratio were no longer significant between groups, averaging ~22:1. While relative matrix production is a useful tool in phenotypic distinction, absolute quantity allows for better assessment of the regenerative potential of the system. By 42 days of culture, sGAG production was nearly 50-fold lower than the native NP (525 μg/mg dry weight) at 2.33% across all conditions, and collagen production was lower still, at 0.36% (250 μg/mg dry weight) (Antoniou et al. 1996).

The production of sGAG and Col II were evaluated as the primary endpoints for successful differentiation and tissue regeneration in the present study. NP-specific gene markers have been

identified such as N-cadherin (*CDH2*), keratin 19 (*K19)* (Lv et al. 2014) *, PAX1, FOXF1, HBB,* and *CA12* (Minogue et al. 2010)*,* and can be useful in determining early differentiation. However, in the absence of downstream protein translation, gene expression profiles provide limited functional information. Given the limited matrix deposition and cell survival exhibited in this study, further genetic characterization was not pursued. As future studies optimize the system for cell survival, gene expression will become a more relevant tool for identifying differentiated NP cells.

Histological images showed that matrix accumulation was generally limited to the pericellular area for both Col II and sGAGs. Only sMCβ constructs showed some faint interterritorial staining for Col II. The limited diffusion of matrix components into the hydrogel is likely due to the combined effects of the low swelling capacity of MC and lack of matrix degradation. Numerous studies investing the effects of hydrogel material properties have shown that matrix deposition by cells is a function of the available volumetric space and diffusivity (Bian, Hou, et al. 2013; Erickson et al. 2009; Lin et al. 2016; Gupta and Nicoll 2014). The effective mesh size of these MC based hydrogels has been previously calculated from equilibrium swelling ratio to be on the order of ~20 nm (Chapter 3). Bryant and Anseth (2002) first reported that diffusion and distribution of elaborated sGAGs in hydrogels requires a mesh size of a minimum 9 nm. While these hydrogels satisfy that requirement, this assumes uniform distribution of the mesh and no steric or electrochemical interference that would limit Fickian diffusion of sGAG molecules. The largest mesh size of the poly(ethylene glycol diacrylate) hydrogels investigated in that study was 14 nm; despite being fairly close to the size of the matrix molecules, the construct showed good diffusion and distribution of sGAGs throughout the hydrogel. Given that the MC hydrogels have a mesh size that is permissive for sGAG diffusion, it is not clear why elaborated sGAGs would remain

within the pericellular region. Degrading hydrogels have shown promise as scaffolds for cartilage and NP tissue engineering as controlled breakdown of the scaffold is conducive to the elaboration of matrix, particularly larger matrix molecules like collagen (~300 nm fibril diameter) (Bryant and Anseth 2003; Chung et al. 2009; Reza and Nicoll 2010a). Ma-MC-based hydrogels exhibit excellent long-term stability and are typically not susceptible to hydrolytic degradation, both *in vitro* and *in vivo* (Stalling, Akintoye, and Nicoll 2009; Gold et al. 2015; Lin et al. 2019). Ester bonds formed between the methacrylate groups are susceptible to hydrolytic cleavage, however, actual hydrolysis is dependent on the hydration of the network and steric factors, with higher water content (and frequently larger mesh size) corresponding to increased exposure of the ester linkage to water (Reza and Nicoll 2010a; Varma et al. 2014; Jeon et al. 2009). The low swelling capacity of MC hydrogels due to the hydrophobic methoxy groups supports the long-term stability of the gel, but also prevents the hydrolysis-mediated creation of void space necessary for accumulation of neomatrix (Chung et al. 2009; Bryant and Anseth 2003).

There was virtually no net change in compressive properties or swelling in any of the constructs over time. Given the limited matrix deposition shown via histology, it can be assumed that the stability of the mechanical properties is derived from the lack of scaffold breakdown. Some significant differences were observed in percent relaxation of MC-, MC+ and sMC- gels over time, however, this cannot readily be explained by the limited matrix accumulation. It may be an artifact of variability between gel casting, which could be reduced in further studies by increasing the sample size. All constructs were within the range of the mechanical and material properties reported for NP, which has been reported as having an E_Y of 5.39 ± 2.56 and percent relaxation of 34.23% ± 11.30% (as calculated in Eq. 4.2) for human tissue in unconfined compression, and an equilibrium weight swelling ratio of 19.94 ± 3.09 for bovine tissue (Cloyd et al. 2007; Reza and

Nicoll 2010b). From the perspective of mechanical replacement and restoration in the IVD, the stability of the constructs is promising, as it is not ideal to have an NP replacement that is too soft to withstand the compressive forces of the disc. Having a compressive modulus slightly higher than the native NP in unconfined compression has shown promising results for the restoration of motion segment mechanics in ex vivo models (Varma et al. 2018). Nevertheless, it has been well established that increasing scaffold stiffness by modulating macromer concentration and crosslinking density has negative effects on differentiation and matrix elaboration of cartilaginous tissues (Erickson et al. 2009; Gupta and Nicoll 2014; Lin et al. 2016). In the previous study (Chapter 3), it was determined that although the components of the sMC hydrogel system are tunable and allow for a wide range of mechanical properties, a minimum of 3% w/v macromer concentration was necessary to form stable hydrogels that gelled *in situ* and were retained when injected into the void space of a bovine disc explant model. Thus, this was the formulation employed for the current cellular investigation.

The goal of a clinically translatable formulation for an NP replacement material is that it must be injectable and minimally invasive in order to preserve AF integrity, as well as immediately able to restore mechanical deficiencies of the degenerate disc. The challenge for *in situ*-based, tissue engineering strategies is that soft substrates that mimic the developmental milieu and promote NP cell differentiation (Navaro et al. 2015; Francisco et al. 2014; Francisco et al. 2013) provide little to no immediate biomechanical support or restoration of disc height, range of motion, and most importantly, reduction in pain for patients suffering from degenerative disc disease. Panebianco et al. (2020) have recently presented a systematic review of cell-based injectable biomaterials for IVD repair highlighting the ongoing competitive balance that exists between biomechanical and biological performance and asserted that materials that are able to combine high modulus with

controlled degradation and ability for cellular remodeling are likely to be the best candidates for successful translational tissue engineering of the IVD.

Future work in developing this platform should consider incorporating hydrolytically or enzymatically cleavable crosslinks, in order to make the scaffold more permissive for matrix elaboration. As mentioned earlier, gels were formed at room temperature in rigid molds, neither of which truly recapitulate *in situ* gelation. Prior work has shown that redox-initiated gelation of methacrylated cellulosic hydrogels *in situ* resulted in gels with E_Y half that of gels made within custom molds (Varma et al. 2018). The softer gels are likely due to inefficient crosslinking with exposure to oxygen. While our previous investigation showed that this formulation is able to form stable hydrogels within the void space of the IVD post-nucleotomy, softer gels may also be better able to support MSC differentiation, matrix elaboration, and nutrient transport. Additionally, the current work was performed under static culture conditions. As the native disc is constantly mechanically loaded, dynamic culture will be necessary to ascertain the construct's performance in supporting differentiation and survival of MSCs under more physiologically relevant conditions. Mechanical loading can stimulate differentiation of embedded cells and drive convective transport of TGF-β3 and elaborated matrix, all of which can potentially increase the success of this tissue engineering platform (Safshekan et al. 2012; Shah and Chahine 2018; Tsai et al. 2014; Huang et al. 2010; Li et al. 2010; Thorpe et al. 2010; Mauck et al. 2003).

4.5 Conclusion

This study examined the ability of artificially sulfonated MC scaffolds to support hMSC differentiation toward an NP-like phenotype as a potential injectable NP repair strategy. TGF-β3 was successfully sequestered within sulfonated hydrogels and the combined effects of enhanced growth factor bioavailability and stimulation due to presumed sulfonate interactions were able to

maintain cell viability and promote the elaboration of NP-specific matrix components, namely sulfated GAGs and type II collagen. All the MC-based scaffolds maintained stable mechanical and swelling behavior over time that were within the range of compressive and swelling properties of the native NP. Matrix elaboration was limited to pericellular regions and did not distribute evenly throughout the construct, nor did gross levels of ECM components approach the quantities found in the NP, which was likely due to the limited ability to diffuse through the construct. The stability of the sMC hydrogels demonstrates its strong potential as a candidate for acellular NP replacement therapies; however, the limited matrix elaboration and low cell survival suggest further optimization is necessary to make the platform amenable to cell differentiation and biological repair. Future studies will investigate the efficacy of this platform for MSC-driven NP repair when combined with degradable linkages.

4.6 Acknowledgements

The II-II6B3 monoclonal antibody developed by TF Linsenmayer was obtained from the Developmental Studies Hybridoma Bank under the auspices of the NICHD and maintained by the University of Iowa, Department of Biological Sciences, Iowa City, IA. This work was supported in part by a grant from the National Science Foundation (IIP 1701120 to S.B.N.) and NIH/NIAMS grant R01 AR057397 (to J.C.I). The authors wish to thank Damien Laudier of CCNY and MSSM for assistance with histology, Dr. Sihong Wong and Dr. Mitchell Schaffler for the use of microscopy equipment, David Alpert, Sabrina Shafi, Jing Shi, and Lucy Cai of CCNY for technical assistance and Tyler Distefano of MSSM for valuable scientific discussions.

Chapter 5: Conclusions, Limitations, and Future Directions

5.1 Overview

The global objective of this thesis was to develop an injectable, MC-based hydrogel system as a functional NP replacement for both cell-based and acellular therapies for early IVDD. Previous studies have shown successful NP-like differentiation of encapsulated hMSCs within CMC hydrogels but were unsuccessful in forming gels directly in the disc, and it was found that the thermogelling capacity of MC combined with redox-initiated covalent crosslinking was necessary for retaining the injectable NP replacement within the disc. Thus, the focus of this work was to optimize a tissue engineering platform for the NP, centered on MC and taking cues from the successes of the previous CMC-based tissue engineering studies while preserving the thermogelation of MC that was necessary for clinical translation.

Although there is anecdotal evidence that the thermogelling behavior is preserved in methacrylated MC, the effect of methacrylate modification and percent modification on the thermoresponsive behavior of MC had not been investigated. As methacrylate groups are hydrophobic, it was hypothesized that methacrylates would enhance the thermogelation of MC. Thus, rheometric analysis of the influence of temperature and time was explored for various methacrylation percentages (Chapter 2). The addition of methacrylate groups was shown to lower the thermogelation onset temperature and increase the thermoresponsiveness of MC hydrogels. It was also seen that there was a threshold of methacrylate concentration above which redox-initiated crosslinking efficiency was limited at physiologic temperatures, thus informing the most desirable degree of methacrylation for future studies.

MC hydrogels have a much lower swelling capacity than CMC hydrogels. The swelling capacity of CMC is afforded by the negatively charged carboxyl groups on the polysaccharide background that increase hydration and subsequently make CMC more susceptible to hydrolytic

degradation of ester bonds within methacrylate crosslinks. Sulfonates were incorporated onto MC during redox polymerization in order to fabricate a "GAG-mimetic" sulfonated MC (sMC) hydrogel (Chapter 3). Using factorial design, sulfonated MC hydrogels were investigated for material properties and injectability. Sulfonate incorporation did not have any effect on the swelling ratio of MC hydrogels, which was tunable by modifying macromer concentration. *Ex vivo* bovine motion segment models for injection and retention showed that a minimum of 3% MC crosslinked with 10 mM APS and TEMED each was necessary to form hydrogels *in situ*. As another challenge to translation of tissue-engineered NP replacements has been delivery of TGF-β3 within the hydrogel system, the ability of the GAG-mimetic sMC to sequester encapsulated TGF-β3 was investigated as well. Sulfonate concentration allowed for sequestration of TGF-β3 in a tunable fashion proportional to the concentration of sulfonates.

Using the results of the factorial study in Chapter 3, 5 mM sulfonate concentration with 3% MC macromer concentration was selected for encapsulation of hMSCs. Sulfonation and TGF-β3 delivery for hMSC-laden MC scaffolds was investigated over 6 weeks. The constructs showed moderate matrix deposition, with clear superiority in the groups that were both sulfonated and received TGF-β3 stimulation, regardless of delivery route, although cell viability decreased over time in all groups except those with both sulfonates and TGF-β3, indicating a potentially synergistic effect on survival and differentiation. The hydrogels exhibited no change in mechanical or swelling properties over time, indicating that MC remained resistant to hydrolytic degradation. The results suggested that scaffold sulfonation and encapsulated TGF-β3 delivery hold promise for cellulose-based hydrogels for NP tissue engineering, and elucidated areas for further optimization. The major findings and limitations of these studies, as well as recommendations for future work, are presented in this chapter.

5.2 Rheological Analysis of the Effect of Methacrylation on the Thermoresponsive Gelation of Methylcellulose in Aqueous Solutions (Chapter 2)

Methylcellulose is a unique cellulose derivative that is water soluble and exhibits reverse thermogelation behavior, forming a physically crosslinked hydrogel at increasing temperatures. The modification of hydroxyls on cellulose with methoxy groups interrupt the strong interchain hydrogen bonds that render cellulose insoluble in water. Somewhat paradoxically, this solubility is afforded by methoxy groups which are hydrophobic themselves. Thus, the thermoresponsive behavior is mediated by the aggregation of hydrophobic groups at increasing temperatures. Previous studies in our lab have explored the effect of macromer concentration, molecular weight, and methacrylation percentage on hydrogel mechanics in unconfined compression, as well as swelling behavior. Additionally, the gelation kinetics of redox-polymerized gels were only investigated at room temperature, and so the effect of the thermoresponsive nature of MC on redox-initiated gelation was not explored. Methacrylate groups are hydrophobic; thus, it was hypothesized that methacrylation of MC would enhance the thermal response and lower the gelation temperature of MC.

Rheology was chosen as the primary means for measuring the thermal response of MC as it was directly relatable to the physical behavior of the gel and has implications for its handling and injectability. A preliminary challenge lay in the fact that the definition of thermogelation temperature varies widely in the literature, and so it is difficult to compare studies without first comparing the definition used in each study. As such, MC with varying methacrylation percentages was tested over a temperature ramp of 4°C to 80°C, and the onset of thermogelation was determined using three different methods based off of the literature. While the trend of decreasing thermogelation onset temperature with increasing methacrylation percent was mostly preserved

across all methods, the meaningfulness of the physical behavior depended how the definition is applied. For example, when the traditional Winter-Chambon definition of a gel, *G'>G"* is taken as indication of thermogelation, it can be seen that methacrylated MC frequently gels at temperatures well under physiologic temperature, but that this crossover point does not correspond to the sharp increase in *G'* associated with the ordering of MC chains in response to increased temperatures. Rather, it likely has to do with the passive aggregation of hydrophobic moieties at a higher concentration. Similarly, taking the derivative of the log of *G'* as the point of sharpest increase in *G'* to be the point of thermogelation onset (when it is more accurately the midpoint of the thermogelation process) selects for a higher temperature above 37°C for all groups, and may cause researchers to artificially and inaccurately conclude that a particular material does not achieve thermoresponsiveness at physiologic temperatures.

The influence of methacrylation on thermogelation was then investigated under the formation of purely physically crosslinked gels at 37°C. As the temperature ramp data indicated, increasing methacrylation percentage resulted in stiffer gels at 37°C, and that the contributions of salts in PBS nearly doubled the stiffness at higher methacrylation percentages, while it had little effect with the low and unmethacrylated groups. Interestingly, strain stiffening behavior was observed at 37° in MC of higher methacrylation precents. This was attributed to the gradual ordering of MC chains at 37°C, along with a steady rate of increasing strain that strengthened the interchain bonds rather than slowly breaking them. This had direct implications on the injectability of the gels, so cyclic strain tests were employed to see how quickly the gels responded to rapid changes in strain. Even at high methacrylation percentages the gels were immediately able to respond to high strain, and that the recovery at low strain was gradual, a classic behavior of thixotropic materials.

The combined effects of methacrylation percentage and redox-initiated polymerization on the gelation kinetics at room temperature versus physiologic temperature were then examined. Gelation was observed to begin much more rapidly at 37°C than at 20°C, although it is likely that this can at least partially be attributed to the effect of temperature on the reaction chemistry; the observed "toe" region in the gelation profile at 20°C did not decrease significantly with increasing methacrylation, indicating that the process of free-radical formation and crosslinking was independently influenced by temperature and not the interaction of MC chains. The predefined completion of the redox-initiated reaction was reached at approximately the same time for all methacrylation percentages, which was predictably faster at 37°C than at 20°C. At this completion point, gels formed at 37°C were significantly stiffer than those formed at 20°C, but gels continued to stiffen slightly, and it was observed that if the reaction was allowed to continue, the maximum stiffness was reached by 20 minutes and was no longer significantly different between temperatures. The rapidity of the reaction at physiologic temperature is important for injectability and retention. In addition to decreasing the amount of time unconsumed free radicals would persist *in situ,* faster gelation could potentially prevent extravasation from the injection site.

Interestingly, there was not an additive effect of the dual crosslinking mechanism on final stiffness, but rather the dual crosslinking played more of a role in kinetics of network formation. What was surprising to observe was the difference in stiffness measured between high methacrylation MC at differing temperatures. Specifically, the highest methacrylated MC (9.54%) formed significantly stiffer gels at 20°C than at 37°C, the opposite effect of what was observed at lower methacrylation percentages (5.84%, 2.44%). Furthermore, rather than reaching equivalence at the end of the reaction time, the *G'* of mMC_9 continued to diverge, with the stiffness at 20°C more than double that at 37°C. This seems to indicate that unused free radicals persist and that at

37°C the network formation of mMC_9 may have been strong enough to resist chain movement and mixing to allow for completion of chemical crosslinking. Such network formation may also have contributed to microphase separations, which pushed free radical-containing water from the vicinity of hydrophobic methacrylate groups, diminishing the reaction efficiency. These observations have implications for the usage of methacrylated MC at room temperature versus physiologic temperature. If high methacrylation percentage MC macromers form stiffer gels at room temperature rather than physiologic temperature, it brings into question the comparison of data acquired with room temperature formed gels compared with their behavior *in situ*. Because this divergence was not observed in methacrylation percentages of ~6% and lower, only macromer methacrylated below that threshold was used for future studies so as not to introduce confounding factors. Overall, the results of this study show that methacrylation influences the thermoresponsiveness of MC, which is proportional to the modification percentage of the macromer and should inform future decisions in designing MC-based hydrogel systems.

5.3 Injectable Sulfonated Methylcellulose Hydrogels with Tunable Growth Factor Sequestration as Potential Nucleus Pulposus Replacements (Chapter 3)

Extensive investigation of methacrylated CMC has shown that it is a promising candidate material for NP tissue engineering applications. In particular, the negatively charged carboxyl groups on the polysaccharide backbone allow CMC to behave as a sort of GAG-mimetic material, with a high swelling capacity. Being a non-animal derived natural polysaccharide, it is not susceptible to hydrolytic degradation, which is a concern for implantation within the degenerate IVD space characterized by increased catabolic enzyme activity. The hydration of CMC also exposes the ester linkage within methacrylate crosslinks to hydrolytic degradation, which renders the scaffold permissive to matrix elaboration by encapsulated cells. As recent studies showed,

despite the adoption of a redox-initiated polymerization system which is amenable to injectable applications, CMC did not gel rapidly enough within the disc space to be retained *in situ*. Earlier preliminary studies with NP cells encapsulated in MC hydrogels showed less encouraging results than those generated with CMC gels. Thus, modification methods for MC hydrogel system were sought that would retain the thermogelling characteristic that allowed for *in situ* gelation and retention in the IVD, while incorporating similar features as CMC that would make it more supportive of cell differentiation. In addition, TGF-β3 was directly loaded into CMC hydrogels previously in order to examine the ability of negatively charged carboxyls to deliver cell-instructive factors within the scaffold together with cells in a fully contained tissue engineering construct. Despite the negative charge of the carboxyl groups, CMC was not able to electrostatically sequester encapsulated TGF-β3. Incorporation of heparin into the CMC system also did not improve biological performance of cells encapsulated with growth factor, which was attributed to over-sequestration of TGF-β3, although this was not definitively proven. As such, development of a GAG-mimetic using MC as the base polymer was pursued, in order retained thermogelation behavior but increased swelling capacity and sequestered growth factors as a result of the incorporation of charged sulfonates at varying concentrations. coupled negatively charged sulfonates to the MC polymer was network using sulfonated methacrylate monomers during redox polymerization. Interestingly, no effect of the addition of sulfonates on any of the material properties of the scaffolds was observed. Thermogelation behavior was preserved, attributed to the fact that sulfonates were not covalently attached to the MC backbone until redox polymerization. It is likely that directly attaching negatively charged groups to the MC backbone would counteract the hydrophobic effects of the methoxy groups and reduced the thermogelation capacity of the polymer. As thermogelation was measured on uncrosslinked polymer, 2SEM was in solution,

rather than attached to the polymer, so hydrophobic aggregation continued as normal and was not affected. Interestingly, the incorporation of sulfonates had no effect on the swelling behavior of the hydrogels, further supporting the assumption that the sulfonates did not change the network formation of MC. Injection into *ex vivo* bovine motion segments showed that a minimum macromer concentration of 3% was necessary for gelation and retention when using 10 mM redox initiator concentration (higher initiator concentrations were not attempted, as were used in the prior *in situ* study using CMC-MC with 20 mM initiators (Varma et al. 2018). 3% MC hydrogels were further characterized for long-term stability, cytocompatibility, and growth factor sequestration. Similar to the swelling results, it was found that sulfonation had no effect on the stability of MC gels, which showed no evidence of hydrolytic breakdown over 8 weeks. Also, all sulfonate monomer concentrations were cytocompatible. Growth factor retention studies showed successful sequestration of TGF-β3 that correlated with the concentration of sulfonates. The combination of 3% MC with 5 mM 2SEM for future hMSC encapsulation studies was chosen, as there was no significant difference between 5 mM and 10 mM 2SEM concentration. Although the hydrogels did not show evidence of increased swelling or hydrolysis despite the addition of negatively charged sulfonates, the ability to sequester growth factor, which was not achieved in the CMC system, was a promising step in the development of a clinically translatable, injectable NP tissue-engineered system.

5.4 TGF-β3 Sequestering, Sulfonated Methylcellulose Hydrogels Support Nucleus Pulposus-Like Matrix Elaboration by Encapsulated Human MSCs (Chapter 4)

The sulfated GAGs of the NP play a critical role in NP mechanics and hydration, as well as cell homeostasis. Negatively charged sulfates attract and sequester growth factors within the ECM, extending their half-life and making them more locally available to cells. Disorders of sulfation

cause profound defunction in musculoskeletal development, resulting in debilitating and sometimes fatal chondrodysplasias. As such, a sGAG mimetic sMC hydrogels as potential cell-instructive scaffolds was investigated. Having previously shown the injectability and ability to sequester growth factors in the prior chapters, the sMC material holds promise as a potentially translational tissue engineering platform. Here, hMSCs from a pooled batch of donors were encapsulated and investigated the effects of sulfonation and growth factor delivery over the course of 6 weeks *in vitro*. Similar to previous results, the hydrogels still exhibited a burst release of unbound growth factor, but the sulfonated hydrogels retained the majority of the loaded growth factor for the course of the study, while unsulfonated hydrogels released the entire payload in under 2 weeks. Cell viability decreased in most groups, which was not unexpected based on earlier preliminary studies of NPCs in photocrosslinked MC. There was no statistical change in cellularity in gels that were both sulfonated and received growth factor, indicating that the two variables combined may have provided a synergistic protective effect on cells. Still, gross images showed that cells were more sparsely distributed even within those gels. Though it is not immediately clear what drove cell death, particularly as there was no spatial pattern indicative of limited nutrient distribution or diffusion, it is hypothesized that the resistance of the MC scaffold to degradation limited the cells ability to proliferate and elaborate matrix, which can also influence cell survival. Sulfonated gels with TGF-β3 stimulation exhibited greater production of matrix components Col II and sGAGs, although the absolute values of the ECM components were extremely small and did not begin to approach native levels. There was no net change in swelling and mechanical properties across any of the groups over the course of the study. While this is in keeping with previous data showing the long-term stability of MC hydrogels and their resistance to hydrolysis, it was interesting to note that the matrix produced was not enough to have an effect on the material

behavior of the scaffolds, likely due to the scaffolds' resistance to degradation, which limited the permissiveness of the hydrogel to hMSC matrix deposition. Taken together, the results demonstrate that scaffold sulfonation and TGF-β3 sequestration show promise for future NP tissue engineering studies, but that the stability of MC may not be amenable to cell survival or matrix elaboration. It is possible that sMC + TGF-β3 can be used as a potential acellular NP replacement that delivers growth factor to local cells, or that this scaffold system can be made more permissive to cell differentiation by incorporating degradable crosslinking sites.

5.5 Limitations and Future Directions

This thesis has advanced the development of an injectable, MC-based hydrogel for cellular and acellular NP replacement and repair. However, there are several limitations to be noted and considerations to be made in determining future development of these biomaterials for clinical translation.

The first study presented here focused on the rheological behavior of methacrylated MC as a thermoresponsive polymer. Rheological analysis was used to determine thermogelation rather than other methods, including differential scanning calorimetry (DSC) and turbidimetry, because rheology gives the most clinically relevant data in terms of material behavior. The conclusions with regards to the contribution of hydrophobic methacrylates to the hydrophobic aggregation of MC was based on knowledge of the thermogelation mechanism of MC from the literature and interpretation of the experimental results. Further analysis of the mechanism and structure of aggregating MC could be determined with cryogenic transmission electron microscopy (cryo-TEM) and small-angle neutron scattering (Lott et al. 2013), however, it is not immediately clear whether this would provide any clinical relevance, and the investigation may be purely academic. Still, MC has been shown to exhibit unique behaviors related to the interaction of hydrophobic

groups even when chemically crosslinked. As such, a deeper understanding of network formation at 37°C and its impact on parameters such as gelation kinetics and mesh size may have important implications on solute transport and hydration within the construct. Scanning electron microscopy (SEM) of chemically crosslinked gels would also potentially provide more insight into the gel structural network at a scale relevant to cell encapsulation. Even observation of MC thermogelation via optical microscopy can sometimes provide information about the clustering of MC at increasing temperatures, although the resolution would be low (Wu et al. 2021). Thermogelation of MC has been extensively characterized with respect to macromer concentration and molecular weight previously, so they were not further characterized here. The results observed here are expected to scale with different molecular weight distributions and macromer concentrations. With increasing macromer concentration, the differences between methods for determining thermogelation onset temperature disappear, as higher concentrations of macromer respond to temperature with greater magnitude, and so the distinctions in this study may not be relevant. However, for low macromer concentrations, which are more desirable for cell-based studies, the distinction is still important. Finally, the difference in *G'* of high methacrylation % MC between 20°C and 37°C, which was not observed at lower methacrylation percentages, presents a number of questions. Firstly, methacrylation between 5.84% and 9.54% was not titrated in order to find the point at which this diversion in behavior begins, so an accurate threshold could not be identified beyond stating that 5.84% methacrylated MC did not exhibit such behavior. Elucidating the mechanism of this diversion is important as it does have implications on the biological performance and clinical translation of MC-based materials. All our previous studies investigating gelation kinetics and material properties of methacrylated MC were performed at room temperature; the assumption was that the chemical crosslinks would dominate the behavior

and that the hydrophobic interactions of MC would not factor in. This is clearly not the case in terms of the gelation behavior, and it raises the question of whether compressive mechanics and swelling behavior are significantly different between room temperature and physiologic temperature. If they are significantly different, this may impact the assumptions made from all tests of MC-based materials at room temperature, and future studies should all be performed under careful temperature control.

The second study attempted to modify MC such that it would behave more like CMC hydrogels, which are well suited for NP matrix elaboration, while retaining the thermogeling capacity of MC. Sulfonates were incorporated during the redox gelation reaction; this made characterization of the sulfonates difficult, as the size of the hydrogels was not amenable to ζ-potential analysis. Using the same gelation procedure, it may be possible to generate microparticles, or thin hydrogel films which may more easily undergo ζ-potential measurement to ascertain the charge of these gels. Preliminary ATR-FTIR analysis was not able to identify sulfonate peaks on the spectra of these gels, despite the fact that the intensity of DMMB staining correlated with the amount of 2SEM incorporated, indicating the presence of sulfonates in the hydrogel. Further optimization of the chemistry of the material will be necessary for validating the system. The finding that the inclusion of sulfonates had no effect on swelling behavior was surprising, but further points to the fact that the network formed by chemically crosslinked MC was unperturbed by the introduction of negatively charged groups. The negatively charged sulfonates *did* have an effect on protein adsorption and TGF-β3 sequestration, showing that they influence the electrochemical behavior of molecules in their vicinity. It is possible that the hydrophobic portions of MC resist the influx of water, which seems paradoxical for hydrogels in general, but also may be problematic for cell encapsulation. It is not immediately obvious whether

this can be overcome without risking losing the thermogelation capacity of MC. Direct sulfation of MC was not attempted, as has been performed previously with cellulose and other non-sulfated polysaccharides (Portocarrero Huang et al. 2018; Zeng, Groth, and Zhang 2019; Freeman, Kedem, and Cohen 2008; Purcell et al. 2014). It was hypothesized that the addition of a negatively charged group to the backbone of MC would inhibit its thermogelation. It may be worth attempting, however. Hydroxypropylmethylcellulose (HPMC) and hydroxyethylcellulose (HEMC) are derivatives of methylcellulose that contain both hydrophobic and hydrophilic moieties, and can form thermoresponsive hydrogels, albeit less strong than MC. The observed thermogelation behavior is proportional to the balance between hydrophobic methoxy groups and hydrophilic groups. This may give insight into the functionality a partially sulfated MC via direct modification, which may result in diminished, but not lost, thermogelation of MC. Still, it should be noted that the hydrophilicity of hydroxypropyl and hydroxyethyl are much less than that of sulfates and sulfonates, and so direct sulfation of MC still carries the risk of obliterating the thermogelling capacity of MC.

Gross quantification of protein was performed when examining the adhesion of serum proteins on sMC gels. Further investigation could involve selectively exposing sMC to proteins of various charges to determine the mechanism of protein adsorption. Mass spectrometry of adsorbed serum proteins may also give insight into the types and features of serum proteins that adsorb onto the material, which would enable better understanding of potential cell adhesion and immune responses to sMC, particularly for applications outside of the IVD that are more vulnerable to immune reactions. Additionally, if sMC is to be used as an acellular growth factor depot in the intradiscal space, titrating the sequestration to promote some, but not total release of sequestered

TGF-β3 may be necessary to provide controlled release of the growth factor to local cells within the IVD.

Bioactivity of TGF-β3 was not directly measured in this study. As the ELISA used only detects active TGF-β3, a cell-based bioactivity assay. Furthermore, the remaining TGF-β3 within the gels was not able to be extracted in order to quantify the total actual loaded within gels, and so calculations of percent release were based on the amount of theoretical load, assuming 100% loading efficiency. Placing TGF-β3 in the TEMED barrel of the dual-barrel syringe system protected it from the oxidizing effects of APS, but upon mixture during gel formation, it is possible some growth factor was denatured, and so break down of the gels and quantification of encapsulated TGF-β3 would give a more accurate understanding of both encapsulation and sequestration efficiency. While the results from chapter 4 appear to indicate that the encapsulated TGF-β3 is in fact bioactive (based on responsiveness of encapsulated hMSCs with encapsulated TGF-β3, as compared to exogenous delivery), a mink lung epithelial cell growth inhibition study to quantify the activity of released and encapsulated TGF-β3 could provide a more complete understanding of the effect of the encapsulation process on the growth factor.

In the final study, hMSCs were encapsulated within the sMC hydrogel system optimized in Chapter 3. The first and most obvious limitation is the lack of degradation of the MC-based gels. Numerous studies have shown that matrix elaboration within hydrogels is limited when the hydrogels do not degrade, and so the main modification to the system should be the incorporation of degradable crosslinks. Given the hydrophobicity of MC, introducing hydrolytically cleavable crosslinks like those that contain lactic acid may not actually influence the degradation of the gels. Incorporation of MMP-sensitive crosslinks may allow the cells to break down the matrix as necessary, or MMPs could be incorporated into the cell culture media to simulate the catabolic

environment of the degenerate NP. This study was also conducted in neutral pH media. While previous studies have shown that acidic culture conditions that attempt to replicate the degenerate NP are not amenable to MSC differentiation (Wuertz, Godburn, and Iatridis 2009; Li et al. 2012), the fact is that the construct would be exposed to an acidic environment in the clinical scenario. Acidic medium may be better able to hydrolytically cleave the ester bonds within the methacrylate crosslinks. A short study investigating the effect of an acidic environment on hydrogel stability and encapsulated MSC survival would be able to give more insight into *in vivo* performance.

Gene expression was not investigated in this study; instead, matrix elaboration was used as a more functional evaluation of hMSC differentiation, as mRNA expression does not always translate to actual protein production. Additionally, there is still no consensus on gene markers for the NP-phenotype, and so the chondrogenic markers COL II, ACAN and Sox9 would give an indication of chondrogenic differentiation but not necessarily distinguish between NP and AC phenotypes.

Further analysis for apoptosis, such as the TUNEL assay or cleaved caspase-3 staining, was not performed. Production of matrix components was indicative of active metabolism; as such it was assumed that the cells were not necrotic, and that instead cell death was occurring via a controlled mechanism. Still, the presence of lysed and potentially hypertrophic cells on the H&E-stained sections raises the question of mechanism of cell death, and so further analysis should be pursued. Cells that die via apoptosis and are not able to be consumed by macrophages (as is the case in *in vitro* cell culture, proceed on to secondary necrosis, and so visual inspection is not sufficient to ascertain the mode of cell death. Moreover, staining for the hypertrophic marker, type X collagen, would determine whether the remaining cells were undergoing hypertrophy.

The cell-laden sMC study was conducted under static culture, while it is known that the native tissue environment experiences cyclic loading. A dynamic culture system might contribute to convective transport of TGF-β3 and water throughout the hydrogel, which could promote cell survival and nutrient transport. As it stands, the mechanical testing system used in this study utilizes unconfined compression; while there are data on NP tissue in unconfined compression for comparison, it is not directly relevant to the *in vivo* condition, and confined compression would not only be more relevant to the *in situ* behavior of any NP replacement, but can give information about the constructs permeability, which is relevant to transport of nutrients and encapsulated growth factor into and out of the gel. In general, a more physiologically relevant loading regime must be incorporated into the analysis of any NP replacement.

General limitations to this approach must also be addressed before clinical translation can be achieved. Reduced nutrient transfer within the degenerate IVD puts any cell-based therapeutic at a disadvantage; the introduction of a tissue-engineered construct with higher cell count than the adult disc might further stress the system by increasing nutritional demands on the already compromised tissue. Also, the constructs studied here are of a much smaller scale than the size of the human disc. Scaling up would not only require enormous amounts of cells and growth factor but would alter the transport of nutrients. Even within studies on successful NP-like differentiation in CMC, limited nutrient diffusion into some gels was observed as limiting the differentiation and matrix elaboration of cells within the center of the constructs. As mentioned above, dynamic culture might alleviate some of the diffusional issues presented with scale up, and so it is critical that the relevant *in vitro* models and testing be done to ensure that even preclinical *in vivo* studies are conducted with the best possible chance of success, having eliminated as many unknowns as possible before committing valuable resources.

The cells used in this study were acquired from a commercially available supplier and pooled from 3 donors. The usage of pooled donors is meant to eliminate the need for repeated studies in which donor cell quality is a variable added on top of variables that come naturally between studies. Pooled donor studies have shown that they can eliminate confounding donor variability without any negative impact on viability, proliferation, and differentiation, and have immunomodulatory effects equivalent to those of individual donors (Widholz et al. 2019; Hejretová et al. 2020). Pooled donor studies have frequently been used in NP tissue engineering (Frith et al. 2014; Potier and Ito 2014; Wang et al. 2016; Thorpe et al. 2010). Still, the donors used in this study were all young and healthy (in their 20s), and a study using donors from a more representative population may give better insight into the actual clinical performance of the construct.

The mechanics and swelling behavior of the sMC gels both with and without encapsulated cells matched those of the native NP. Additionally, injectability of the material was validated by performing *ex vivo* injections into a bovine motion segment nucleotomy model. The motion segment was not subjected to further mechanical testing, however. Further motion segment testing should be performed to measure the restoration of disc height, compression and torsional mechanics, and resistance to extrusion/reherniation and failure before this material is tested in preclinical *in vivo* models.

Finally, as mentioned earlier, direct sulfation of MC, or the use of HPMC or HEMC may alleviate some of the MC-specific issues of this culture platform while maintaining thermogelation and injectability but would require a full repeat of the studies performed here to determine the rheological behavior of the pre-gelled polymers, as well as a complete materials characterization of acellular HPMC or HEMC hydrogels before moving forward with any cell-based studies.

5.6 Final Conclusions

Collectively, this thesis has contributed to the characterization and development of an MC-based hydrogel system with potential as both an acellular and cell-laden NP replacement for IVD repair and regeneration. MC is a fascinating biopolymer with unique behaviors that require further investigation in order to anticipate the behavior of an MC-based system within a clinical setting. The dual-crosslinking mechanism of thermogelation and methacrylate-mediated free-radical polymerization results in a robust hydrogel with many potential applications outside of the disc and should be explored. Sulfonation of the MC hydrogel generated an effective growth factor sequestration depot that retained its mechanical and structural integrity over time. Although the sMC hydrogel supported NP-like matrix elaboration by encapsulated hMSCs, cell survival was not optimized, and matrix elaboration was limited by the lack of available void space for diffusion of freshly synthesized matrix components. Future work should focus on incorporation of degradable moieties within the sMC hydrogel to enhance cell survival and differentiation. Additionally, as sMC gels *in situ* and can achieve relevant NP-like mechanical properties, *ex vivo* motion segment testing should be the next step in validating the material's acellular performance before moving forward. Despite the study limitations, we were able to produce a stable hydrogel material that is injectable and retained *in situ,* that exhibits mechanical and material properties relevant to the healthy human NP and sequesters encapsulated TGF-β3. This scaffold supported the deposition of relevant NP matrix components by encapsulated MSCs *in vitro,* and although gross matrix production was limited, it is an important first step in further developing an MC-based platform for injectable NP tissue engineering therapeutics. In summary, this thesis has advanced the development of injectable NP biomaterials and has laid the groundwork for future

development of MC-based hydrogels for IVD repair and may be translated into beneficial uses in numerous other medical applications in soft tissue replacement.

Appendix: Detailed Protocols

Methacrylated Methylcellulose Macromer Synthesis

Materials

Large Beaker (flat bottom)
Stir bar
Methacrylic anhydride (Aldrich, 27, 668-5, 760-93-0, MW = 154.17, density = 1.035g/mL)
1N NaOH
1N HCl
Spectra/por membrane, MW cut-off 6-8kDa, flat width 110mm

Day 1

1. Dissolve 1.5g methyl cellulose (MC) in sterile H2O to a volume of 150mL. (adjust as necessary for desired volume)
2. Heat ~100mL of sterile water to 80°C on a hot plate.
3. Cool ~200mL of sterile water to 4°C in an ice-water bath.
4. Measure 1.5g of methyl cellulose. (for low/med mix, measure out equal amounts of low viscosity and med viscosity MC and mix)
5. Check the temperature of the heated and cooled sterile water before continuing.
6. Pipet 50mL (1/3 of the total final volume) of 80°C sterile water into a new beaker containing a magnetic stir bar. Place the beaker on the heated stir plate.
7. Slowly add MC as the hot water is stirring. As the clumps begin to dissolve, add more MC. Continue this process until all of the MC is added.
8. Place the MC solution on an UNHEATED stir plate.
9. Add 50mL of 4°C sterile water to the MC solution and allow the solution to continue stirring. The solution should become less cloudy with the addition of cold sterile water.
10. Add an additional 50mL of 4°C sterile water to the MC solution making up a total volume of 150mL.
11. Allow the MC solution to stir at 4C overnight or over weekend before using in macromere reaction

Day 4

1. Standardize the pH meter. Make sure the hole at the top of the electrode is in the open position prior to standardizing in the 4.0, 7.0, & 10.0 buffers.
2. Place ~100mL of 1% MC in a 250mL round bottom flask containing a football stir bar. The entire flask should be on ice for the entire reaction.
3. Calculate the amount of methacrylic anhydride (MA)
4. Grams x (1/335 g/mol) x (percent modification) x (amount excess) x (154.17 g/mol of MA) x (1/1.035 g/mL)
5. Example: (1.0)(1/(335g/mol))(0.1)(20)(154.17g/mol)(1/(1.035g/mL))
6. In the hood, on ice, adjust pH to 8 with NaOH.
7. Note the initial pH of the solution.
8. Add 1/3 the calculated amount of MA all at once (note the lot # of MA used).
9. Every 15 minutes readjust the pH to 8.5 for an hour (this is equivalent to 4 adjustments in 1 hour).
10. Note the pH after adding NaOH and at the end of each 15 minute interval.

11. After adjusting the pH to 8.5 for the 4th time, add the second 1/3 of the calculated amount of MA all at once.
12. Every 15 minutes readjust the pH to 8.5 for an hour (this is equivalent to 4 adjustments in 1 hour)
13. Note the pH after adding NaOH and at the end of each 15 minute interval.
14. After the 4th time, place the reaction in cold room overnight at 4°C (in ice, on stir-plate).

Day 5

1. In the morning note the reaction pH.
2. Standardize the pH meter. Make sure the hole at the top of the electrode is in the open position prior to standardizing in the 4.0, 7.0, & 10.0 buffers.
3. Readjust the pH to 8.5.
4. Add the last 1/3 of the calculated amount of MA all at once (make sure you are using the same batch of MA from Day 1).
5. Every 15 minutes readjust the pH to 8.5 for 45 minutes (for a total of 3 adjustments).
6. Note the pH after adding NaOH and at the end of each 15 minute interval.
7. Begin setting up for dialysis:
8. Cut a piece of dialysis membrane.
9. Place the membrane in sterile water to soften.
10. Fifteen minutes after the third adjustment, the pH should be close to 7.0. If not, readjust the pH to between 7-7.5 until it is stable.
11. Note the pH at which the reaction stabilizes.

Day 6-8

1. Dialyze the solution against sterile water for a total of 5-6 water changes (~8hrs between each water change) and 2 membrane changes (1 each day).

Day 9

2. Check to make sure all of the MA is dialyzed out by the 5th/6th water change. If it is, continue to the next step. If it is not, dialyze for longer.
3. Filter dialyzed solution through a 40µm filter into a 200mL beaker. Make sure the resulting solution does not smell of MA. If it does, distribute the filtered sample into 50mL conical of equal volumes and place on the centrifuge for ~5 minutes at ½ the centrifuge speed.
4. Remove the supernatant avoiding the pelleted MA and pipet it into a NEW 200mL beaker.
5. Distribute this solution into 50mL conical (~25mL per conical).
6. Freeze all tubes at -80°C at an angle to prevent cracking of the plastic conical when the sample expands with freezing.

Day 10-12

1. Lyophilize sample for 2-3 days or until the sample looks completely dry.
2. Store at -20ºC.

Methylcellulose Acid Hydrolysis

Materials

50mL Round bottom flask
Small football stir bar
1N NaOH
1N HCl

Protocol

1. Warm oil bath to 80°C. Make sure electronic temperature probe and analogue thermometer are both in the oil and read the correct temperature.
2. While oil bath is heating, place 20mg (0.02g) of polymer and 20mL of DI H_2O in 50mL round bottom flask.
3. Place round bottom flask with cork base on stir plate and stir at room temperature for ~5 minutes, making sure all the polymer gets wetted.
4. Polymer should be mostly dissolved. Place on ice and stir 15-20 minutes to complete dissolving.
5. Once dissolved, move polymer back to room temperature. Allow solution to warm up to room temperature (17-20°C).
6. Calibrate pH meter.
7. Use pH probe to check temperature of solution. Record initial pH and temperature. If up to 17-20°C, begin to pH down to 2 using 1N HCl (~150µL total, add 100µL at once, then finish in 10-25µL increments to pH 2).
8. Let sit at room temperature ~5 minutes to ensure pH is steady at 2. Record final pH and temperature.
9. Cover with rubber stopper top and use wire to tighten around rubber stopper. Use ring stand to hold round bottom flask and lower into oil bath (at 80°C) for 2 hours and 20 minutes (the 20 minutes are to allow solution temperature to heat up, can see MC drop out of solution and solution become cloudy). Stir at 200rpm. Make sure the liquid line in round bottom flask is below that of bath oil level (so that the total polymer solution is submerged).
10. After 2 hr 20 minutes in oil bath, move straight to ice for ~10 minutes to dissolve polymer back into solution and come to room temperature.
11. TURN OFF OIL BATH.
12. Once solution goes from cloudy back to clear, move back to room temperature. Wait for solution temperature to move up to 17-20°C, the pH to 7 using 1N NaOH. (Use small increments of NaOH, as you get closer to pH 7, jumps in pH will happen more dramatically and you may overshoot. Use HCl to bring pH back down if needed).
13. Once stable at pH 7, transfer solution to 50mL conical tube and place at -80°C to freeze overnight.
14. About 4 days before scheduled NMR session, place frozen sample on lyophilizer for 2-3 days and then immediately dissolve in 1 mL D_2O once off the lyophilizer for NMR analysis. Do not take sample off the lyophilizer if you can't run NMR immediately – need to have ALL water removed from sample in order to minimize water peak in NMR spectrum.

^{1}H-NMR Analysis

Sample Preparation

Day 1:

1. The day before scheduled NMR session, remove modified, hydrolyzed, lyophilized sample off lyophilizer.
2. Use a metal probe to quickly compress polymer into a ball at the bottom of the 50mL conical tube.
3. Use a micropipette to transfer 1 mL of D_2O into the conical tube; make sure that the entire polymer is wetted. Try to minimize exposure to air to reduce the water peak in NMR graph.
4. Parafilm the conical tube. Place the tube in a beaker of ice then place into the 4oC fridge to dissolve the polymer overnight.

Day 2:

1. Using a 200µL-micropipette, transfer 700µL of dissolved, hydrolyzed sample solution into a NMR tube (200 + 200 + 200 + 100). If the solution gets stuck, put on the tube cap and carefully shake/flick the tube.

Varian 500 Protocol

Login: Nicoll
Password: sbn428

Sample preparation & shimming:

1. Start menu -> Lock On -> click "Eject"
2. Remove placement tube and insert sample tube -> click "Insert"
3. Lock On (lock magnetic field)
4. Click "Find z0" to automate
   a. Z0 ~20
   b. Lock level ~40-50
   c. Power ~27 (should be <40)
   d. Gain ~38 (should be <40, usually = power + 10)
   e. Phase ~112
5. Shim menu
   a. Can click "gradient shim" to automate shimming z1-z4
   b. Or manually adjust z1 & z2 to maximize lock level (~50-60; indicative of homogeneity of sample)

Spectra acquisition:

1. Settings
   a. Spectral width: -2 to 14
   b. # of scan (nt=): 92 or 128
   c. Relaxation (dl=): 5 sec
   d. Pulse angle: 45 degrees
2. Check autogain box
3. Type in command: bs = 8
4. Click "acquire" or type command "go" to start experiment (usually take ~10 minutes to complete)

Spectra integration:

1. Type “wft” to show spectra
2. Use mouse scroll to adjust height of the spectra
3. Type “aph” for autophasing
4. Type “lb=0.2” for line broadening to reduce noise
5. Use right-hand side tool box to phase
   a. Click “phase mode” icon -> click left area of spectra, hold left click to drag and even out baseline
   b. Adjust spectra so that the baseline is even/horizontal
6. After phase completion, click “redraw” icon
7. Integrate peaks
   a. Process tab -> Integration tab
   b. Partial mode
   c. “Clear integral”
   d. Integration level -> scroll up/down over region so that the green line at the left side of the spectra is as flat as possible
   e. Command “dc” for digital correction
   f. “redraw” after operation
   g. Click “scissors” icon to cut peaks
   h. Click “red vertical line(s)” icon and place a single red vertical line on methyl peak (~2.0ppm)
   i. Integration -> “set integral area” -> single peak -> integral value = 1.00 -> click “set int value”
   j. Click “show integral values”
   k. Command “wp = 7p” and “sp = -0.2p”

Save & Email/Print:

1. Save file as .fid file
2. Plot -> autplot preview -> okay: will produce a pdf file of the spectra with integral values and text descriptions
3. Can email or print the pdf file

Additional notes:

- To load old settings: “file” -> “open” -> pick an old file to open -> now the settings for the old file should be loaded (check?)
- “wp=7p” and “sp=-0.2p” after setting integral values, not sure what it means?
- Lp = 0 (<100); rp = 0 (<100) to check shimming?

Rheometry

Instrument: AR2000ex
Geometry: Cone & Plate
Cone angle 1:59:28
Cone diameter 20 mm
Truncation 53 µm

Protocol settings optimized for methacrylated methylcellulose by Gittel Gold. May need adjustments based on different materials

SET UP MACHINE

1. About an hour before working, make sure water tower (behind rheometer) is turned on and set to 3˚C so that peltier plate will cool properly**.**
2. **MAKE SURE AIR IS ON.** Red knob should be parallel to open air valve. Machine will not work otherwise. Gauge should read ~30 psi
3. Take black cap off spindle and white cover off of base
4. Turn on power from surge protector, then power switch on back of rheometer
5. Raise upper platform if necessary to attach Peltier plate (bottom plate)
    a. Magnet snaps Peltier plate into place
    b. Attach smart swap and flow & return tubes (push hard to snap in)
6. Open software: ***AR Instrument Control***
7. Options → instrument → inertia → Calibrate
    a. After calibration, attach geometry from bottom. Tighten from top spindle. Stop at first bit of resistance
8. Geometry → open → 20 mm 2˚ steel cone
    a. "Invalidate any zero point" → Yes
    b. "Map instrument now" → Yes → Perform Mapping
9. Instrument → oscillatory mapping
    a. Constant amplitude
    b. Frequency: 0.1000 to 100.00
    c. % strain: 1.00
    d. # points: 15
    e. Click *perform new mapping*
10. Click *zero gap*
    a. Use arrows to bring platform down to ~5mm above base, taking care not to hit the base
    b. Continue
    c. When finished, *back of distance* → *Yes* (may need to change to 15000)

SET UP EXPERIMENTAL PROCEDURE:

11. Change file name/experiment name. Make sure destination of file is in the correct folder.
12. Oscillation procedure: *set up as necessary for your experiment*
    a. **Conditioning step** (if necessary)
        i. Good if starting with specific temperature, may not be good if you're under time constraint (i.e. with redox initiators)
    b. Example Frequency Sweep:

i. Frequency: 0.1 – 10 Hz
ii. Mode: log
iii. Points per decade: 20
iv. Temp: whatever temp desired
v. % strain: 1.000

c. Example Temperature Ramp (good for measuring thermogelation, without redox initiators):

i. Temperature: 4 to 40 ˚C
ii. Ramp rate: 1˚C/min
iii. Delay time: 15 sec
iv. % strain: 1.000
v. Frequency: 1 Hz

d. Example Time Sweep (good for gelation with initiators):

i. Delay 00:00:00
ii. Duration: minimum 30 min
iii. Temp: 37 ˚C
iv. % strain: 1.000
v. Frequency (single): 1 Hz

e. Example Strain Sweep:

i. Delay 00:00:00
ii. Duration: 20 min
iii. Temp: 4˚C or 37˚C
iv. % strain range : 0.001 to max desired (100 to 500%)
v. Frequency (single): 1 Hz

f. Example Cyclic Strain Recovery:

i. Time sweep
   1. Duration: 2 min
   2. Temp: 37˚C
   3. % strain range : 0.001%
   4. Frequency (single): 1 Hz
ii. Time sweep
   1. Duration: 2 min
   2. Temp: 37˚C
   3. % strain range: 500%
   4. Frequency (single): 1 Hz
iii. Repeat for as many cycles as desired
iv. Plot against global time

g. Post experiment step usually not necessary (can help to return temp to starting temp if doing a ramp)

13. Double click everything on main page to zero (0→set→go)
14. Fill top chamber of geometry with dH_2O for moisture
15. For analysis **without** initiators (not time sensitive):
    a. Place ~200 µl in center of bottom plate, using pipet top to spread it a little. Avoid bubbles
    b. **START** (machine will come down to proper height based on input geometry)
    c. During conditioning step, check for overflow.

d. Cover geometry with cover chamber, taking care to keep it centered and not bump the geometry.

16. For analysis **with** initiators (time sensitive):
    a. Lower geometry to ~2000 (close to peltier but allowing enough space for injecting sample)
    b. Have a timer nearby to record lag-time
    c. Click START. Machine will ask if you want to bring geometry down. Don't click yes until polymer has been dispensed.
    d. Using dual barrel syringe and mixing tip, inject a small amount of polymer onto a kimwipe to avoid bubbles, then inject 150-200 ul of polymer on to center of peltier.
        i. Immediately click yes to bring geometry down and start the procedure. Do not spread polymer out.
        ii. Start timer to record lag time. Stop when first data point is taken.
    e. Cover geometry with cover chamber, taking care to keep it centered and not bump the geometry.
17. When sample is finished, remove cover, clean bottom Peltier plate and upper geometry, first with dry kim-wipe, then with ethanol and kim-wipe. If necessary, reset temperature before adding next sample.

DATA COLLECTION

18. Open software: ***TA Data Analysis***
19. File → Open → select file
20. View → Table
21. Copy table data into excel spreadsheet
22. Switch between experimental steps using bar at the top. Make sure to copy table data from all experimental steps
23. You can access the procedure and notes from the experiment in this program as well. (Not able to edit)
24. Save excel spreadsheet(s) on desktop and send to yourself/copy to flashdrive.

CLOSE EVERYTHING IN BACKWARDS ORDER THAT YOU SET UP:

25. Close software
26. Remove water from geometry well
27. Raise platform and gently remove geometry
28. Detach smart swap and flow & return tubes
29. Push release button on machine to remove Peltier plate. Store in box in drawer
30. Turn off power from back of rheometer.
31. Turn off water tower.

Differential Scanning Calorimetry

Instrument: TA Instruments DSC Q200

may want to do in conjunction with TGA to account for mass loss

1. **Turn on nitrogen gas**
    a. Delivery pressure should be 15 PSI
2. May need to turn on using on/off switch on back of machine
3. Open TA Instruments explorer
4. Control → lid → open
5. Prepare reference dish
    a. For samples in solution, use same solvent as reference
    b. Use cover for liquid sample and reference
6. Weigh sample
    a. For liquid samples, use deep dish with lid
    b. Weigh dish and lid first, then add material
    c. 9-13 mg (do not exceed 13 mg)
    d. Close lid (poke hole in lid with needle if concerned about pressure build up)
    e. Don't touch anything else after weighing (don't want to add anything to weight of sample)
7. Place sample on top of thermocouple.
    a. Make sure to remove any left over ash/debris
    b. Far thermocouple is for reference
    c. Close thermocouple is for sample
8. Control → lid → close
9. Summary (sample info)
    a. Mode: standard
    b. Test: custom
    c. Pan: Tzero Aluminum
    d. Sample size (- pan)
10. Data file: Network → TA-PC → TA → Data → Your folder
11. Procedure: editor
    a. *don't use "initial temp"
    b. Remember to Apply changes
12. Green button to start
13. Don't open lid until temperature comes back down to at least 40C (there's no active cooling system)
14. Sample purge flow ~ 30 Ml/MIN
    a. May change if using a coolant?
15. **Shutting Down**
    a. Close Nitrogen gas – close main valve first
    b. When pressure on both gauges is 0, close second valve
16. TA universal data analysis
    a. Right click – label point
    b. Integrate peak, select endpoints
        i. Right click: accept limits

Hydrogel Mechanical Testing

Unconfined Compression using Multi-Ramp SRL

Preparation

1. Let frozen gel sample rehydrate in PBS for overnight at 4°C before testing.
2. Turn on SENSOTEC 250 gram load cell 1 hour before testing to warm up.

I. Setup

1. Change multimeter wiring so that voltmeter is reading load cell.
    a. Multimeter should be in –V setting.
    b. Clip alligator clips to read load cell (far left black/red wires on board).
2. Calibrate load cell.
    a. Adjust by using screwdriver to turn "zero" until display on load cell zero setting read 000.0 (no + or – signs). The display on the multimeter should read <0.002V.
    b. Press and hold "calibration" button, meanwhile use screwdriver to adjust "span" in order to obtain values taped on load meter. Both the multimeter and the load cell should read appropriate values. (If too jumpy, pop off front face of Sensotec load cell read-out. Unscrew face plate, adjust screw 2nd from bottom, between span and zero; this is the fine adjust for zero. The screw above span is the fine adjust for span. Be careful, these are very sensitive to small movements.)
3. Switch alligator clips so that the multimeter reads from LVDT wires (on right on DAQ board).
4. Clean platform and chamber with ethanol. Tape on the chamber so that it is suspended around the load cell but not touching. The load meter should read 19-20g.
5. Clean the indenter with ethanol. Screw on the indenter tight but be careful not the push up on load cell.
6. Clean the glass base plate with ethanol. Place the plate at the center of the platform.
7. Lower the indenter so that it is approximately 5mm above the base plate. Adjust the stage so that the multimeter reads -3 to -5V.
    a. Note that the multimeter voltage should be between -5 and 5V during the entire testing process to stay within the linear range.
    b. To raise or lower the top stage, use the 340-RC knob. Be sure that the inner rod does not touch QB condenser.
    c. Glass plates should be entirely parallel when touching, if not adjust front center hold with Allen wrench.
8. Turn on stepper motor. Connect stepper motor to the testing device via rainbow wires.
9. Check Labview document folder to ensure that previous crp.dat and srl.dat files have been deleted.
10. Open National Instrument software. Open VI "creep_with_daq(cont pulse)_250g_Initial_AIC". Adjust load window axes so that load meter values are within display window. Press "run". Once the load jumps, stop the run, disconnect rainbow wires, and raise the indenter.
11. Open crp.dat file [time/load/displacement/voltage]. Scatterplot load vs. time. Determine, highlight, and record a base voltage, then save the excel file.

II. Sample Placement

12. Image gel sample in order to obtain area
13. Wet glass base plate with a few drops of PBS. Load gel onto plate using a metal spatula; center gel. Add more PBS to submerge gel. Place plate with gel onto the platform
14. Lower indenter until indenter barely touches the gel. Bring down and seal chamber
15. Slowly add PBS along the wall of the chamber, make sure the gel does not slip out. Add PBS until chamber is ¾ full.
16. Slowly raise indenter such that it hovers right above the gel.

III. Initial Creep – Sample Height

17. Delete crp.dat file from previous base voltage step.
18. Connect rainbow wire.
19. Open initial creep VI "creep_with_daq(cont pulse)_250g_Initial_AIC".
20. Adjust load window axes accordingly. Make sure ramp velocity is 10μm/s. Run program.
21. Watch load read out to determine when the indenter hits the gel sample; there should be a sharp increase in load. Once the indenter has touched the sample, stop the program. Disconnect the rainbow wire and raise the indenter slightly.
22. Open crp.dat file. Scatterplot time (x) vs. load (y). Paste table. Determine, find, and highlight contact point. Copy/paste contact point information into table. Enter base voltage and LVDT constant. Record initial thickness and initial tare load. Save excel file

	time	load	disp	voltage
Contact point:	47.662	-18.509	412.763	0.419
Base voltage (V):	-3.768			
Desired Tare Load (g):	1	(set to 1)		
change in voltage:	4.187	(contact point voltage - base voltage)		
LVDT #1 (um/V):	558.21	(a constant value, calculated prior by calibrating LVDT)		
thickness (um):	2337.225	(change in voltage * LVDT)		
Initial Tare Load:	-17.509	(contact point load + desired tare load)		

IV. Creep Test

23. Delete crp.dat file from previous initial creep step.
24. Open creep vi "creep_w_daq(cont pulse)_250g".
25. Change load limit to calculated initial tare load. The input ramp velocity should be 10μm/s. Run the program. Start timer when load reaches initial tare load then let the program run for 45min.
26. After 45min, stop the program. Open crp.dat file. Scatterplot time (x) vs. load (y). Paste table. Determine, find, and highlight final test point and the point 10min/600sec before that final point (choose points in the middle for representative points). Copy/paste information for those two points into table. (note that <10μm thickness change over 10min is Alice's equilibrium criteria.) Enter base voltage and LVDT constant. Record post-creep thickness. Save excel file.

	time	load	disp	voltage	
Final Point:	2755.528	-17.395	392.662	0.112	
10min prior Point:	2156.614	-17.41	390.447	0.116	
Base voltage (V):	-3.768		displacement(um)		
Desired Tare Load (g):	1		2.215		< 10um displacement
change in voltage:	3.88				
LVDT #1 (um/V):	558.21				
thickness (um):	2165.855				

V. Stress-Relaxation Test

27. Delete any old crp.dat or srl.dat files.
28. Open stress-relaxation vi "Desktop SRL (multi_ramp)_250g".
29. Enter post-creep thickness. Set ramp velocity to 10μm/sec. Set strain to 0.05. Set #ramps to 3. Set relaxation time to 2000sec. And set stop time to 6500sec. Then run the program.
30. When test is complete, open srl.date file. Scatterplot time (x) vs. load (y). Then save the excel file. Delete the srl.dat file. Close National Instrument software.

VI. Sample Removal and Clean-Up

31. Raise indenter all the way.
32. Remove PBS using a plastic transfer pipette.
33. Carefully remove the plastic chamber. Carefully unscrew the indenter. Clean the platform, indenter, and glass base plate with ethanol. Clean all remaining surfaces.
34. Place tested gel in original Petri dish, parafilm, and store at -20°C freezer.
35. Turn off step motor/power strip.

Bovine Tail Motion Segment Injury and Repair

Materials:

- Cleaned, thawed motion segment (soak in PBS and leave in 4°C the night before; leave in 37°C room for 1 hr prior to experiment)
- Dissolved polymer solution in double-barrel syringes
- Initiator stock; trypan blue;
- #4 scalpel and #20 or #22 blade for cleaning motion segment
- #3 scalpel and #15 blade for creating injury
- Rongeur, curette, and forceps

Procedure:

1. Work on blue pads
2. Add initiators, trypan blue to polymer solution and mix with glass stir rod for visualization
3. Leave polymer solution mixture in 37°C for 30 min
4. Measure disc diameter and height
5. Use #20/22 blade to clean segment
6. Use #15 blade to make X annular tear (up to the length of sharpened part)
7. Use curette to dislodge NP tissue
8. Use rongeur to remove 0.15-0.2g of NP (Might need to repeat curette & rongeur action a few times)
9. Once injury is complete, inject polymer solution
10. Leave motion segment in 37°C for 30 min for gel to form (wrap motion segment in PBS soaked Kim-wipe to avoid tissue dehydration)

Live/Dead Staining of Hydrogels

Materials:

-1 mM Calcein AM (dissolved in DMSO)
-2 mM Ethidium homodimer (dissolved in DMSO)
-Sterile PBS
-24-well plate

Protocol:

1. Warm PBS in water bath.
2. Remove calcein AM & ethidium homodimer from the -20ºC freezer and thaw to room temperature by placing in a drawer (both are light sensitive and must be protected from light while thawing). Once thawed, vortex to ensure homogenous mixture.
3. In the tissue culture hood with the lights turned off, measure out 3.2 mL of PBS and place in a 15 mL conical wrapped in foil. (this is for 2 gels)
4. Add 2.4 µL of 1 mM calcein AM to the PBS
5. Add 1.2 µL of 2 mM ethidium homodimer to complete the Live/Dead solution. You can scale up the mixture accordingly for the # of samples you have, just keep everything in the same proportions.
6. Return calcein AM and ethidium homodimer stock solutions to -20ºC.
7. Vortex Live/Dead solution and return to tissue culture hood.
8. Remove gels from incubator and transfer them into a new 24-well plate.
9. Wash samples twice with 1.5mL PBS.
10. Transfer samples into new wells. Add 1.5 mL of Live/Dead solution to each well containing a gel.
11. Wrap the 24-well plate in foil and place allow the gels to incubate for 45 minutes at room temperature, protected from light.
12. Turn on fluorescence lamp for imaging at least 20 minutes prior to end of incubation period. The fluorescence lamp requires at least 20 minutes of warm-up time prior to use and must be on for at least one hour total, so make note of the time you turn the lamp on.
13. After 45 minute incubation, in the TC hood, rinse each gel twice with 1.5 mL PBS.
14. Take microscope images of each sample while leaving the other samples in 1.5mL PBS covered.

Imaging:

1. Focus condensor at 10X. Using Phase 1 filter, take a phase picture of gel. Change light source from all to eyepiece to all to camera (this is especially important for fluorescence pictures).
2. Using FITC filter, take live images (cells should be green).
3. Using TRITC filter, take dead images (cells should be red).

Pepsin Digest

Digest to break down cell culture gels prior to PicoGreen Assay and ELISAs. Needs to be done 2 days prior to these assays.

Prior to digestion:

1. Collect gels in preweighed 1.5 ml microcentrifuge tubes. Blot excess liquid prior to saving gels.
2. Immediately record wet weight and then freeze at -80°C
3. Lyophilize gels for ~3 days until completely dry.
4. Remove gels from lyophilizer, record dry weight. Store at -80°C until digestion protocol.
5. Calculate swelling ratio for each gel.

Materials and Solutions to Prepare:

Pestle (one for each gel, to prevent cross contamination)

0.05N Acetic Acid:

0.05N CH_3COOH in sterile water, pH 2.8-3.0 with formic acid.

Add 1.437mL of 17.4M acetic acid stock to 498.56mL of sterile water. Adjust pH to 2.8 with formic acid (starts ~3.0)

Pepsin (4560 units/mL AA):

13.22mg/mL solution in 0.05N Acetic Acid (for pepsin at activity of 345 units/mg solid). Alter mg/mL concentration (13.22) for different lot or activity of pepsin to keep units/mL consistent.

10X TBS #2:

1.0M Tris, 1.5M NaCl

For 100mL: 12.114g Tris, 8.766g NaCl

Dissolve in 70mL sterile water. pH down to 8.0 (starts ~10.5). Fill to 100mL. Readjust pH to 8.0 [Start with 12N HCl ~400µL increments.]

Digest:

1. Pulverize dry gel using 0.5mL pestle. Add 425µL 0.05N Acetic Acid per tube. Pulverize more.
2. Add 100µL pepsin solution. Vortex to mix.
3. Rotate samples at 4°C for 48hours.
4. Stop pepsin digestion reaction.
    a. Add 100µL of 10X TBS#2 (1:1 ratio with how much pepsin was added) and vortex sample. Sample pH should be ~8.0 (pH must be >5 to neutralize pepsin).
5. Aliquot 20 µL of each sample into new tubes and add 5 µL 5% Triton-X and store at -20°C for PicoGreen Assay.
6. Use remaining sample for Collagen ELISAs and DMMB assay.

Collagen ELISA

ELISA Protocol for both Type I and Type II Collagen in parallel

2 days before ELISA, start Pepsin Digest: (See Pepsin Digest Protocol for reagents and instructions) Pulverize and digest gels with pepsin, rotating at 4°C for 48 hours.

Associated Spreadsheets:
ELISA-setup

Supplies:
ELISA plates: Nunc Maxisorp 96-well plates (Fisher Item # 12-565-136)
25X Wash Buffer: R&D Systems Item # WA126
TMB Substrate Kit: Vector Labs Item # SK-4400
Streptavidin HRP: R&D Systems Item # DY998
Human Collagen (type I and type II) Standards:
Collagen Type I: Chondrex CN: 1005
Collagen Type II: Chondrex CN: 2015
Primary antibody (Col I: Sigma; Col II: DSHB)
Secondary antibodies (Vector Labs Item # BA-1400)

Buffers & Solutions:
Store all buffers and solutions at 4°C
Complete ELISA with all standards/samples held at 4°C
Do not use ultrapure water for any of the below solutions. It may contain inhibitors of the peroxidase reactions.

Coating Buffer:
1.59g Na_2CO_3 Sodium Carbonate
2.94g $NaHCO_3$ Sodium Bicarbonate
0.2g NaN_3 Sodium Azide
Dissolve in 850mL DI water and adjust pH to 9.6 (starts ~ 9.7). Fill to 1L and readjust.

Washing Solution (PBS-T):
5% (v/v) Tween 20 in PBS
Make from 25X stock solution in 4°C fridge. Dilute in DI H_2O.

Stopping Solution:
1N sulfuric acid
Add 13.3mL of sulfuric acid to 487mL of distilled water.

10X TBS:
1.0M Tris, 2M NaCL, 50mM $CaCl_2$
To 250mL of deionized water, add:
30.285g of Tris (MW: 121.14)
29.22g of NaCl (MW: 58.44)
1.8378g of $CaCl_2$ (MW: 147.02)

Adjust pH to 8.0 (starts ~10.7)

10X TBS #2:

1.0M Tris, 1.5M NaCl

For 100mL:

12.114g Tris

8.766g NaCl

Dissolve in 70mL sterile water. pH down to 8.0 (starts ~10.5). Fill to 100mL. Readjust pH to 8.0 [Start with 12N HCl ~400µL increments.]

Blocking Solution: (make fresh)

2% BSA Fraction V and 0.1% NaN_3 in non-sterile PBS

Dissolve 2g of BSA in 100ml PBS. Add 0.1g of NaN_3 to the solution and stir.

AA/Pepsin/TBS#2:

To dilute Coll II Standards when using DSHB 1° Ab – from digestion solution ratios:

425µL 0.05N Acetic Acid

100µL Pepsin

100µL 10X TBS#2

Scale up for total volume needed.

DAY 1:

1. Prepare plate layout and calculate amount needed for standards and solutions using Excel spreadsheet. Col I and Col II ELISAs run on separate plates – Primary antibodies are different, but all other steps are the same.
2. Label all tubes
   14 standards + 3 stock tubes for each type Col
   1 for each sample and standard (50/50 dilution in coating buffer)
3. Prepare all standards on ice. Dissolve collagen I standard in 0.05N acetic acid and collagen II standard in AA/Pepsin/TBS#2 solution to make 0.1mg/mL stock solutions. Make serial dilutions in 0.05N AA or AA/Pepsin/TBS#2 for standards.
   a. Collagen I (stock concentration = 0.5mg/mL)
      i. For 0.1mg/mL solution – 2:10 dilution of Col I standard (at 0.5mg/mL) in 0.05N acetic acid
      ii. For 10µg/mL solution – 1:10 dilution of 0.1mg/mL solution in 0.05N acetic acid
      iii. For 1µg/mL solution – 1:10 dilution of 10µg/mL solution in 0.05N acetic acid
   b. Collagen II (stock concentration = 0.5mg/mL)
      i. Prepare same way as collagen I standards except that the diluent is AA/Pepsin/TBS#2 instead of acetic acid.
4. Stop pepsin digestion reaction.
   a. Add 100µL of 10X TBS#2 (1:1 ratio with how much pepsin was added) and vortex sample. Sample pH should be ~8.0 (pH must be >5 to neutralize pepsin).
5. Vortex standards and samples, and then prepare 50/50 dilutions of each with coating buffer in 1.5mL microcentrifuge tubes (Take solutions from top of tube).
6. Add 100µL per well of CB/standards and CB/samples to Nunc maxisorp plates.

7. Parafilm plates and incubate overnight at 4°C.
8. Set aside samples for other Biochemistry (at least 20 µL needed for PicoGreen and 20 µL for DMMB)

DAY 2:

1. Wash plate 4 times in PBS-T (one quick wash and three 5 minute washes).
2. Add 100µL of blocking solution per well and incubate at room temperature for 1-2 hours. (1hr).
3. Remove Blocking Solution but DO NOT WASH.
4. Prepare 1° immediately before use. Add 100µL of primary antibody to each well (0.5µg/mL of antibody per well).
    a. 1:10,000 Collagen I (Sigma) primary antibody diluted in blocking solution
    b. 1:100 Collagen II (DSHB) primary antibody diluted in blocking solution
5. Parafilm plates and incubate overnight at 4°C.

DAY 3:

1. Wash 4 times in PBS-T (one quick wash and three 5-minute washes).
    a. Make 2° Ab solution - 50 µL of 2° Ab in 10mL of blocking solution (Collagen 2°: biotinylated anti-mouse IgG/anti-rabbit IgG H+L)
2. Add 100µL of secondary to each well and incubate for 30 minutes.
3. Wash 4 times in PBS-T (one quick wash and three 5 minute washes).
4. Add 100µL of Streptavidin HRP to each well and incubate for 30 minutes.
    a. 1:200 dilution in PBS
5. Wash 4 times in PBS-T (one quick wash and three 5 minute washes).
6. Make TMB Substrate Solution (immediately before use)
    a. Add 2 drops of Buffer Stock Solution to 5mL of dH_2O and mix well
    b. Add 3 drops of TMB Substrate Solution and mix well
    c. Add 2 drops of Hydrogen Peroxide and mix well
7. Add 100µL of TMB Substrate Solution and allow blue color to develop at room temperature for 10-30 minutes. (4 min. for Col I, Col II, and CSPG)
8. Add 50µL of Stopping Solution and read plate at 450nm absorbance. Wells should turn from blue to yellow with the addition of Stopping Solution. (TMB absorption may be read without use of Stopping Solution (650nm), but stopping the reaction increases the absorbance of the reaction product two- to four-fold.)

REFERENCES: Chondrex, Inc. (www.chondrex.com) Human Type I Collagen Detection Kit (Catalog #6008) digestion protocol

PicoGreen Assay

Hydrogel constructs must go through pepsin digest before assaying (See pepsin digest protocol). Before performing PicoGreen assay, make sure that samples have gone through two freeze/thaw cycles.

Associated spreadsheets:
PicoGreen-Setup: Solution Additive, PicoGreen Solution and Plate Setup
PicoGreen-Analysis

Supplies:
96 well plates
PicoGreen reagent

Reagents:
Pepsin digested samples (see Pepsin Digest Protocol
5% Triton-X (from Triton-X 100 in Acetic Acid)
Pepsin Solution Additive
425 µL 0.05N Acetic Acid
100 µLPepsin
100 µL 10X TBS
156.25 µL 5% Triton-X (for a 1% solution)
DNA standard
1X TE (Tris-EDTA Buffer)
10X TBS
1.0M Tris, 2M NaCL, 50mM $CaCl_2$
To 250mL of deionized water, add:
30.285g of Tris (MW: 121.14)
29.22g of NaCl (MW: 58.44)
1.8378g of $CaCl_2$ (MW: 147.02)
Adjust pH to 8.0 (starts ~10.7)

METHODS:

1. Calculate volumes for 1X TE, DNA Standards, and PicoGreen solution. (solutions and plate set up excel sheet)

DNA standards:
1mL for absorbance + ~120µL for standards (x 3 to run in triplicates x number of plates)

1X PicoGreen (diluted from 200X stock from Molecular Probes, diluted in 1X TE):
Volume for standards (~100µL per standard x 5 standards x 3 to run in triplicate x number of plates) +
Volume for samples (~100µL per sample x 3 to run in triplicate x total number of samples)

1X TE (diluted from 20X TE in sterile H_2O – dilute TE immediately before use):
Volume for standards (~100µL per standard x 5 standards x 3 to run in triplicate x number of plates) +

Volume for samples (~100µL per sample x 3 to run in triplicate x total number of samples) + 1mL for DNA absorbance +
Volume to dilute DNA standard into 2µg/mL +
Volume to dilute 200X PicoGreen stock to 1X

2. Turn on plate reader; set up for DNA absorbance reading. Thaw PicoGreen samples and Solution Additive on ice.

3. Prepare samples (usually done immediately after Pepsin digest): 20µL sample + 5µL 5% Triton-X for 1% solution, then go through 2 freeze/thaw cycles to lyse cells.

4. Dilute 20X TE in sterile H_2O to obtain an appropriate amount of 1X TE.

5. Dilute DNA stock in 1X TE to obtain an appropriate amount of DNA with concentration approximately equal to 2µg/mL.

$$Volume_{DNA-Stock}[\mu L] = \frac{2\left[\frac{\mu g}{mL}\right] * Volume_{\text{diluted-DNA-standard-needed}}[\mu L]}{concentration_{DNA-Stock}\left[\frac{\mu g}{mL}\right]}$$

6. Read DNA absorbance at 260nm using cuvettes.
   - Protocol name: Biocell PicoGreen Std
   - Include blank: add 1mL 1X TE to Biocell cuvette #1
   - Include 2µg/mL DNA sample: add 1mL DNA standard to Biocell cuvette #2
   - Note: reading/opening of Biocell cuvette are on opposite sides. Make sure that there are no air bubbles, especially on the reading side.
   - Read plate and save plate reading.
   - Calculate actual DNA concentration (µg/mL):

$$DNA_{concentration}\left[\frac{\mu g}{mL}\right] = \frac{DNAstandard - blank\ 1X\ TE}{0.02}$$

   - From Molecular Probes PicoGreen product sheet, $absorbance_{260}$ of 0.04 corresponds to 2µg/mL double-stranded DNA solution, which is where 0.02 in the equation above comes from.

7. Read blank black plate with clear bottom.
   - Protocol name: PicoGreen Assay (ex/em: 485/528)
   - Plate reader may ask you to wait 3 minutes for fluorescence to warm up before reading plate, in this case, place the plate on an orange plastic base (to protect clear bottom film) and leave in a drawer to incubate.
   - Read plate and save reading.

8. Prepare standards in triplicates.
   - In general, add solutions directly into wells along the sides in order to avoid puncturing the bottom of the wells. Run each standard in triplicate.
   - Add appropriate amount of 1X TE according to the chart below.

- Add appropriate amount of DNA according to the chart below.
- Add appropriate amount of Solution Additive according to the chart below.
- Note: do not add PicoGreen until samples have been plated as well since PicoGreen solution is light-sensitive.

Standard	Vol. of DNA Stock (~2µg/mL) (µl)	Vol. 1X TE (µL)	Sample Solution Additive (pepsin/acetic acid) (µl)	Vol. 1X PicoGreen (µL)	Final DNA Concentration
1	100	0	1	100	1 µg/mL
2	10	89	1	100	100 ng/mL
3	1	98	1	100	10 ng/mL
4	0.1	98.9	1	100	1 ng/mL
5	0	99	1	100	0 (Blank)

9. Add samples; run each sample in triplicate.
   - Vortex and spin down (~1min) samples before adding to plate.
   - Using a multi-channel pipette, add 99µL of 1X TE to all the wells that will contain samples.
   - Add 1µL sample to each appropriate well; take sample from the top of the microcentrifuge tube).

10. Add 1X PicoGreen to all wells.
    - Dilute 200X PicoGreen stock in 1X TE to obtain an appropriate amount of 1X PicoGreen solution.
    - Using a multi-channel pipette, add 100µL of 1X PicoGreen to all wells containing either standards or samples. Mix by pipetting up and down but make sure to not introduce any air bubbles! Also make sure to switch to new tips when appropriate.
    - Incubate plate in a drawer for ~3min while setting up the plate reader.
    - Protocol: PicoGreen Assay.
    - Read plate (excitation/emission: 485/528) and save reading.

11. Clean up and analyze
    - Note that PicoGreen has its own waste bottle!

DMMB Assay

DMMB binds to sulfated GAGs

Preparation:

1. Have prepared DMMB Dye (see next page).
2. Have prepared Chondroitin Sulfate C stock (1µg/µL, 0.25µg/µL, 0.1µg/µL, 0.01µg/µL).

Assay:

1. Turn on plate reader approximately 20min before beginning the assay.
2. Read blank plate.
   - Place a new 96-well plate into the plate reader.
   - Open DMMB protocol. Read absorbance at **525nm** and **595nm**.
3. For standards, add appropriate volumes of both stock solution and DI H_2O per well in triplicate.
   - Make sure to vortex stock solution in order to obtain homogeneous aliquots. See next page for further notes.
4. For each sample, vortex sample, then add 5µL of sample per well in triplicate.
   - Samples may have to be diluted depending on absorbance values relative to standards.
5. Set up plate reader for reading.
   - DMMB protocol should be already open.
   - Add a new plate for actual sample readings.
6. In a dark room, pour DMMB dye into multichannel pipette reservoir immediately prior to use, as it is light sensitive.
7. Using a multichannel pipette, add 200µL of DMMB dye to each well for both standards and samples. Mix by pipetting up and down but be careful to not introduce bubbles.
8. Read samples at 525 and 595nm. Subtract 595 from 525 and extrapolate values.

Standards	µg GAG	Stock Solution	Amt of stock (µL)	Amt of DI H_2O (µL)
1	0	N/A	0	5
2	0.05	0.01 µg/µL	5	0
3	0.1	0.1 µg/µL	1	4
4	0.2	0.1 µg/µL	2	3
5	0.5	0.1 µg/µL	5	0
6	0.75	0.25 µg/µL	3	2
7	1	0.25 µg/µL	4	1
8	1.25	0.25 µg/µL	5	0
9	2	1 µg/µL	2	3

Associated spreadsheets:

1. DMMB analysis (include plate setup)

Preparing DMMB Dye:
(light sensitive)

Materials:
8mg DMMB (1,9 dimethylmethylene blue)
2.5mL 100% ethanol
1g sodium formate
1mL formic acid

Procedures:
1. Weigh out DMMB. Place DMMB into a 15mL conical tube, covered in aluminum foil.
2. Add 2.5mL of 100% ethanol and vortex thoroughly to get DMMB into solution.
3. In a 600mL beaker with a stir bar and covered in aluminum foil, add 350mL DI H_2O. Add 1g sodium formate and 1mL formic acid. Pour in DMMB/ethanol solution.
4. Use a 1mL pipette and 10mL DI H_2O (to bring to a total of 500mL DI H_2O) to rinse out DMMB conical as dye gets stuck along walls and cap of conical.
5. pH DMMB dye down to 1.5 (original dye pH ~3-3.5) using formic acid.
    - Adjusting pH may take 20-80mL of formic acid.
6. Add appropriate amount of DI H_2O to obtain a final volume of 500mL of DMMB dye.
7. Read absorbance at 525 nm and 595nm. Subtract 595 from 525.
    - pH 1.5 and subtracting absorbances eliminates errors from non-GAG specific artifacts (carboxyls, DNA…) without sacrificing sensitivity, particularly for tissue engineered samples
    - Reference: Zheng and Levenston, "Fact versus artifact: Avoiding erroneous estimates of sulfated glycosaminoglycan content using the dimethylmethylene blue colorimetric assay for tissue-engineered constructs," *European Cells and Materials* (2015)

Standard Curve:
The stock solutions should be prepared ahead of time from Chondroitin Sulfate C (Sigma C-4384) and stored at -20°C until use. The stock solutions can be refrozen and used again. Dissolve the stock in a solvent applicable to your samples, or be sure to include a blank on your plate with the solution your samples are in.
Note: Vortex stock solutions well and frequently so that you are taking aliquots from a homogenous mixture. Also wear gloves as it is easy to contaminate the samples/standards with GAGs, which may be on your hands.

Hematoxylin and Eosin (H&E) Staining (Paraffin Embedded Slides)

Materials

- CitriSolv ® - Fisher Scientific, cat. # 22-143-975
- Absolute Ethanol - Fisher Scientific, cat. # A406P-4
- Hematoxylin Gill no. 2 – Sigma, cat. # GHS-2-32
- Eosin Y Alcoholic – Sigma, cat. # HT110-1-32
- Cytoseal-60 – Richard and Allan Scientific cat. # 8310-4
- Coverglass – Corning - Thickness-1 22X50mm cat. # 2975-225

Acid Alcohol (for H&E):

Combine	95% Ethanol	495mL
	Concentrated HCl	5mL

Scott's Buffer:

Combine	Sodium Bicarbonate	2.0g
	Magnesium Sulfate	20.0g
	Distilled Water	1Liter

Staining Procedure:

1. CitriSolv ® — 3 min
2. 100% EtOH — 1 min
   Repeat steps 1-2 if necessary
3. 95% EtOH — 1 min
4. 70% EtOH — 1 min
5. 50% EtOH — 1 min
6. Distilled H_2O — 1 min
7. Hematoxylin Solution (Gill no.2) — 10 min
8. Tap H_2O — 3 min
9. Acid Alcohol (for H & E) — 20 sec
10. Tap H_2O — 3 min
11. Scott's Buffer — 20 sec – 1 min
    (this is the bluing step for the nuclear stain, longer incubation leads to more intense bluing and thus contrast between nuclei and other structures)
12. Tap H_2O — 3 min
13. Eosin Y Solution Alcoholic — 1 min
14. 95% EtOH — 1 min
15. 95% EtOH — 1 min
16. 100% EtOH — 1 min
17. CitriSolv ® — 1 min
18. Mount and coverslip with Cytoseal-60. Seal with nail polish the next day.

Alcian Blue Staining (Paraffin Embedded Slides)

Materials

- CitriSolv ® - Fisher Scientific, cat. # 22-143-975
- Absolute Ethanol - Fisher Scientific, cat. # A406P-4
- Alcian Blue 8GX – Sigma, cat. # A-9186
- Glacial Acetic Acid – Fisher Scientific, cat. # A38-212
- Cytoseal-60 – Richard and Allan Scientific cat. # 8310-4
- Coverglass – Corning, cat. # 2975-225

3% Acetic Acid (500mL):

Combine	Glacial Acetic Acid	15mL
	Distilled Water	485mL

Acid Alcohol (for Alcian Blue):

Combine	70% Ethanol	495mL
	Concentrated HCl	5mL

pH to 1.0 with concentrated HCl

1% Alcian Blue Dye (500mL):

1. Dissolve 5.0 g of Alcian blue 8GX in 450 mL of 0.1N HCl by stirring for at least six hours at room temperature.
2. Adjust pH to 1.0 and fill volume to 500mL.
3. Filter dye with büchner funnel and filter paper. This process takes approximately 10-20min.

Staining Procedure:

1.	CitriSolv ®	3 min
2.	100% EtOH	1 min
	Repeat steps 1-2 if necessary	
3.	95% EtOH	1 min
4.	70% EtOH	1 min
5.	50% EtOH	1 min
6.	Distilled H_2O	1 min
7.	3% Acetic Acid	3 min
8.	1% Alcian Blue (pH 1.0)	15 min
9.	Acid Alcohol (for Alcian Blue)	3 min
10.	Acid Alcohol (for Alcian Blue)	3 min
11.	95% EtOH	1 min
12.	100% EtOH	1 min
13.	CitriSolv ®	1 min

14. Mount and coverslip with Cytoseal-60. Seal with nail polish the next day.

Collagen ImmunoHistoChemistry

Materials:

- Water resistant Pen - Silver Permanent Marker – PILOT – Staples (on shelf)
- Hyaluronidase Type IV-S – Sigma Cat# H-4272 (stored at -20ºC)
- Hydrogen Peroxide – Fisher Scientific Cat# H325-100 (stored at 4ºC)
- Methanol – Fisher Scientific Cat# A412-1 (stored at room temp, in 5th floor chemical hood)
- 10% Horse Serum – (stored at -20ºC)
- IgG from Mouse – Sigma Cat# I8765 (stored at -20ºC)
- Type I Collagen antibody – Sigma Cat# C-2456. (stored at -20ºC)
- Type II Collagen antibody – Developmental Studies Hybridoma Bank Antibody #II-II6B3-S (stored at 4ºC)
- Type VI Collagen antibody – Developmental Studies Hybridoma Bank Antibody 5C6-s (stored at 4ºC)
- Type X Collagen antibody – Developmental Studies Hybridoma Bank Antibody X-AC9-s (stored at 4ºC)
- Biotinylated secondary antibody anti-mouse anti-rabbit IgG (H+L) – VECTOR Laboratories BA-1400 (stored at 4ºC)
- VECTASTAIN Universal Elite ABC Kit – VECTOR Laboratories Cat# PK-6200 (stored at 4ºC)
- DAB Peroxidase Substrate Kit – VECTOR Laboratories Cat# SK-4100 (stored at 4ºC)
- CLEAR-MOUNT with TRIS Buffer – Electron Microscopy Sciences Cat# 17985-12 (stored at 4ºC)
- FITC-conjugated secondary antibodies
- Invitrogen™ Fluoromount-G™ Mounting Medium

Day 1:

1. IHC can be performed on 4-6 slides at a time. For paraffin-embedded samples: De-paraffinize and rehydrate.
    a. CitriSolv® 3min
    b. 100% EtOH 1min
    Repeat steps a-b if necessary
    c. 95% EtOH 1min
    d. 70% EtOH 1min
    e. 50% EtOH 1min
    f. Distilled H_2O 1min
2. For 4 slides, thaw ~2mL of 0.5mg/mL hyaluronidase (in PBS, aliquots stored at -20ºC). Turn on oven and set temperature to 37ºC.
3. Use a water-resistant pen to mark around samples. Make sure edges and corners are touching and boxes are complete. Each slide should have 1 non-immune control and 3 experimental samples.

4. Incubate all samples in ~300µL of 0.5mg/mL hyaluronidase for **30 min** at 37°C. Use oven in the backroom; add a few drops of H_2O in the glass PetriDish. (Hyaluronidase step is necessary to expose collagen antigens)
5. Rinse 2X with PBS. Use gel-loading 200µL pipette tips for aspirating liquids.
6. Incubate samples in 0.5N acetic acid for **2 hours** at 4°C. (Be gentle with fridge doors; leave a note.)
7. Rinse 2X with PBS.
   (Step 8 ONLY for DAB Protocol; Skip to step 11 if doing Fluorescence)
8. Incubate samples in 3% H_2O_2 (hydrogen peroxide) in methanol for **10 min** at room temp (25°C). To prepare, perform 1:10 dilution from stock solution of 30% H_2O_2. (prepare ~2mL for 4 slides)
   Note: H_2O_2 has low surface tension. Also cover samples during incubation so H_2O_2 does not evaporate too quickly
9. Take out 10% horse serum to thaw. Keep on ice.
10. Rinse 2X with PBS.
11. Apply ~300µL of 10% horse serum to cover samples and incubate for **20 min** at room temp (25°C).
12. Remove horse serum (blocking solution) but **do not rinse**.
13. For non-immune controls apply ~300µL of 10% horse serum with **1µg/mL** IgG-from-mouse to cover sample and incubate overnight at 4°C. (prepare ~2mL for 4 slides)
14. For experimental samples, apply ~300µL of primary antibody (diluted in 10% horse serum in PBS) to cover sample and incubate overnight at 4°C.
    a. Primary antibody dilution should have a final concentration of **1µg/mL**.
    b. Prepare ~2mL for 4 slides.

Day 2 (DAB):

1. Thaw 10% horse serum. Keep on ice.
2. Rinse 2X with PBS. Aspirate non-immune controls first, then change tip for actual samples, as to eliminate chances of cross-staining.
3. Apply ~300µL of biotinylated secondary antibody (biotinylated horse anti-mouse/anti-rabbit IgG (H&L)) to cover samples and incubate for **30 min** at room temp.
   a. Biotinylated horse ∝-mouse/∝-rabbit IgG secondary antibody dilution: **1:50** in 10% horse serum.
   b. Prepare ~2mL for 4 slides.
4. **While incubating**: Make VECTASTAIN ABC Reagent: 1 drop Reagent A and 1 drop of Reagent B in 2.5mL **PBS**, vortex and **allow to stand for 30 min** prior to use.
5. Rinse 2X with PBS. Use different tips for non-immune controls and actual samples in order to eliminate chances of cross-staining.
6. Apply ~300µL of VECTASTAIN ABC Reagent to cover samples and incubate for **30 min** at room temp.
7. At the end of 30 min, turn on oven and set temperature to 45ºC.
8. Rinse 2X with PBS. Use different tips for non-immune controls and actual samples in order to eliminate chances of cross-staining.
9. Apply ~300µL of DAB substrate solution to cover samples for **5 min exactly**. Immediately remove DAB and rinse with tap water 3X. Leave tap water on slide after 3rd rinse.

a. DAB: In 2.5mL **DI H_2O**, add 1 drop of Buffer Stock Solution and vortex. Then add 2 drops of DAB Stock Solution and vortex. Then add 1 drop of Hydrogen Peroxide Solution and vortex.
b. Add DAB to 2 slides at a time, spaced 2 min apart in order to avoid hecticity.

10. If counterstain desired: use hematoxylin to visualize nuclei:
    - Apply hematoxylin stain directly to slides for 5 min (submerging slides in slide box runs the risk of samples sliding off slide)
    - Rinse 2x with tap H_2O
    - Acid alcohol (for H&E) for 20 seconds
    - Rinse 2x with tap H_2O
    - Scotts buffer for ~20 seconds
    - Rinse 2x with tap H_2O
11. Aspirate tap water. Use Kim-wipes to remove excess water. Cover samples using Clear-mount, use 200µL pipette tip to spread mounting medium evenly, then place slide in oven at 45˚C for at least **30min.**
12. All DAB containing solutions must be treated with DAB Neutralizing solution. Dispose of all DAB containing solutions and pipette tips in the appropriate waste containers.
13. Remove slides from oven, leave at room temp (in plastic box) overnight to ensure that mounting medium is solidified before putting slides back into histology boxes.

Day 2 (Immunofluorescence):

1. Thaw 10% horse serum. Keep on ice.
2. Rinse 2X with PBS. Aspirate non-immune controls first, then change tip for actual samples, as to eliminate chances of cross-staining.
3. Apply 100 µl of **FITC-conjugated secondary antibody** (diluted 1:200 in 10% goat serum in PBS) to cover cells and incubate for 30-60 (**30**) min. **Protect slides from light from here on.**
4. Rinse cells three times with PBS, 2 min. per rinse.
5. If using DAPI for nuclear stain. Apply DAPI diluted at 1:15,000 in PBS for 10 minutes at room temperature.
6. Rinse once with distilled water, 2 min.
7. Mount using fluorescence protecting mounting medium (Invitrogen™ Fluoromount-G™ Mounting Medium). Let dry (in the dark) and then store at 4°C.

References

Adams, M. A., D. S. McNally, and P. Dolan. 1996. "'Stress' Distributions inside Intervertebral Discs." *The Journal of Bone and Joint Surgery* 78 (6): 965–72. https://doi.org/10.1302/0301-620x78b6.1287.

Adams, Michael A. MA, and PJ Peter J. Roughley. 2006. "What Is Intervertebral Disc Degeneration, and What Causes It?" *Spine* 31 (18): 2151–61. https://doi.org/10.1097/01.brs.0000231761.73859.2c.

Adams, Michael A., Manos Stefanakis, and Patricia Dolan. 2010. "Healing of a Painful Intervertebral Disc Should Not Be Confused with Reversing Disc Degeneration: Implications for Physical Therapies for Discogenic Back Pain." *Clinical Biomechanics* 25 (10): 961–71. https://doi.org/10.1016/j.clinbiomech.2010.07.016.

Aguiar, D J, S L Johnson, and T R Oegema. 1999. "Notochordal Cells Interact with Nucleus Pulposus Cells: Regulation of Proteoglycan Synthesis." *Experimental Cell Research* 246: 129–37. https://doi.org/10.1006/excr.1998.4287.

Ahrens, Michael, Anthony Tsantrizos, Peter Donkersloot, Frederic Martens, Philippe Lauweryns, Jean Charles Le Huec, Slawomir Moszko, et al. 2009. "Nucleus Replacement with the DASCOR Disc Arthroplasty Device: Interim Two-Year Efficacy and Safety Results from Two Prospective, Non-Randomized Multicenter European Studies." *Spine* 34 (13): 1376–84. https://doi.org/10.1097/BRS.0b013e3181a3967f.

Alinejad, Yasaman, Atma Adoungotchodo, Michael P. Grant, Laura M. Epure, John Antoniou, Fackson Mwale, and Sophie Lerouge. 2019. "Injectable Chitosan Hydrogels with Enhanced Mechanical Properties for Nucleus Pulposus Regeneration." *Tissue Engineering - Part A* 25 (5–6): 303–13. https://doi.org/10.1089/ten.tea.2018.0170.

Almdal, K., J. Dyre, S. Hvidt, and O. Kramer. 1993. "Towards a Phenomenological Definition of

the Term 'Gel.'" *Polymer Gels and Networks* 1 (1): 5–17. https://doi.org/10.1016/0966-7822(93)90020-I.

Almeida, Nalinda, Leela Rakesh, and Jin Zhao. 2018. "The Effect of Kappa Carrageenan and Salt on Thermoreversible Gelation of Methylcellulose." *Polymer Bulletin* 75 (9): 4227–43. https://doi.org/10.1007/s00289-017-2256-z.

Ambrossi, Giannina L.Garcés, Matthew J. McGirt, Daniel M. Sciubba, Timothy F. Witham, Jean Paul Wolinsky, Ziya L. Gokaslan, and Donlin M. Long. 2009. "Recurrent Lumbar Disc Herniation after Single-Level Lumbar Discectomy: Incidence and Health Care Cost Analysis." *Neurosurgery* 65 (3): 574–78. https://doi.org/10.1227/01.NEU.0000350224.36213.F9.

Amirdelfan, Kasra, Hyun Bae, Tory McJunkin, Michael DePalma, Kee Kim, William J. Beckworth, Gary Ghiselli, et al. 2021. "Allogeneic Mesenchymal Precursor Cells Treatment for Chronic Low Back Pain Associated with Degenerative Disc Disease: A Prospective Randomized, Placebo-Controlled 36-Month Study of Safety and Efficacy." *Spine Journal* 21 (2): 212–30. https://doi.org/10.1016/j.spinee.2020.10.004.

Amsden, Brian. 1998. "Solute Diffusion within Hydrogels. Mechanisms and Models." *Macromolecules* 31 (23): 8382–95. https://doi.org/10.1021/ma980765f.

Anseth, Kristi S., Christopher N. Bowman, and Lisa Brannon-Peppas. 1996. "Mechanical Properties of Hydrogels and Their Experimental Determination." *Biomaterials* 17 (17): 1647–57. https://doi.org/10.1016/0142-9612(96)87644-7.

Ansteinsson, V., H. B. Kopperud, E. Morisbak, and J. T. Samuelsen. 2013. "Cell Toxicity of Methacrylate Monomers-The Role of Glutathione Adduct Formation." *Journal of Biomedical Materials Research - Part A* 101 (12): 3504–10.

https://doi.org/10.1002/jbm.a.34652.

Antoniou, John, Thomas Steffen, Fred Nelson, Neil Winterbottom, Anthony P Hollander, Robin a Poole, and Max Aebi. 1996. "The Human Lumbar Intervertebral Disc" 98 (4): 996–1003.

Arora, Aditya, Aman Mahajan, and Dhirendra S. Katti. 2017. "TGF-B1 Presenting Enzymatically Cross-Linked Injectable Hydrogels for Improved Chondrogenesis." *Colloids and Surfaces B: Biointerfaces* 159: 838–48. https://doi.org/10.1016/j.colsurfb.2017.08.035.

Arslan, Elif, Mustafa O. Guler, and Ayse B. Tekinay. 2016. "Glycosaminoglycan-Mimetic Signals Direct the Osteo/Chondrogenic Differentiation of Mesenchymal Stem Cells in a Three-Dimensional Peptide Nanofiber Extracellular Matrix Mimetic Environment." *Biomacromolecules* 17 (4): 1280–91. https://doi.org/10.1021/acs.biomac.5b01637.

Arvidson, S. A., J. R. Lott, J. W. McAllister, J. Zhang, F. S. Bates, T. P. Lodge, R. L. Sammler, Y. Li, and Meinolf Brackhagen. 2013. "Interplay of Phase Separation and Thermoreversible Gelation in Aqueous Methylcellulose Solutions." *Macromolecules* 46 (1): 300–309. https://doi.org/10.1021/ma3019359.

Bai, Deng Yan, Long Liang, Bing Bing Zhang, Tao Zhu, Hai Jun Zhang, Zhi Guo Yuan, and Yan Fei Chen. 2019. "Total Disc Replacement versus Fusion for Lumbar Degenerative Diseases - a Meta-Analysis of Randomized Controlled Trials." *Medicine* 98 (29): e16460. https://doi.org/10.1097/MD.0000000000016460.

Bain, Mrinal Kanti, Biplab Bhowmick, Dipanwita Maity, Dibyendu Mondal, Md Masud Rahaman Mollick, Dipak Rana, and Dipankar Chattopadhyay. 2012. "Synergistic Effect of Salt Mixture on the Gelation Temperature and Morphology of Methylcellulose Hydrogel." *International Journal of Biological Macromolecules* 51 (5): 831–36. https://doi.org/10.1016/j.ijbiomac.2012.07.028.

Barbosa, Isabelle, Stéphanie Garcia, Véronique Barbier-Chassefière, Jean Pierre Caruelle, Isabelle Martelly, and Dulce Papy-García. 2003. "Improved and Simple Micro Assay for Sulfated Glycosaminoglycans Quantification in Biological Extracts and Its Use in Skin and Muscle Tissue Studies." *Glycobiology* 13 (9): 647–53. https://doi.org/10.1093/glycob/cwg082.

Barry, F, R E Boynton, B Liu, and J M Murphy. 2001. "Chondrogenic Differentiation of Mesenchymal Stem Cells from Bone Marrow: Differentiation-Dependent Gene Expression of Matrix Components." *Experimental Cell Research* 268 (2): 189–200. https://doi.org/10.1006/excr.2001.5278.

Belair, David G., Ngoc Nhi Le, and William L. Murphy. 2014. "Design of Growth Factor Sequestering Biomaterials." *Chemical Communications* 50 (99): 15651–68. https://doi.org/10.1039/c4cc04317k.

Benoit, Danielle S W, and Kristi S Anseth. 2005. "Heparin Functionalized PEG Gels That Modulate Protein Adsorption for HMSC Adhesion and Differentiation." *Acta Biomaterialia* 1 (4): 461–70. https://doi.org/10.1016/j.actbio.2005.03.002.

Bhat, A. H., Imran Khan, Mohd Amil Usmani, Reddicherla Umapathi, and Salma M.Z. Al-Kindy. 2019. "Cellulose an Ageless Renewable Green Nanomaterial for Medical Applications: An Overview of Ionic Liquids in Extraction, Separation and Dissolution of Cellulose." *International Journal of Biological Macromolecules* 129: 750–77. https://doi.org/10.1016/j.ijbiomac.2018.12.190.

Bian, Liming, Murat Guvendiren, Robert L Mauck, and Jason A Burdick. 2013. "Hydrogels That Mimic Developmentally Relevant Matrix and N-Cadherin Interactions Enhance MSC Chondrogenesis." *Proceedings of the National Academy of Sciences of the United States of*

America 110 (25): 10117–22. https://doi.org/10.1073/pnas.1214100110.

Bian, Liming, Chieh Hou, Elena Tous, Reena Rai, Robert L. Mauck, and Jason A. Burdick. 2013. "The Influence of Hyaluronic Acid Hydrogel Crosslinking Density and Macromolecular Diffusivity on Human MSC Chondrogenesis and Hypertrophy." *Biomaterials* 34 (2): 413–21. https://doi.org/10.1016/j.biomaterials.2012.09.052.

Bian, Liming, David Y. Zhai, Elena Tous, Reena Rai, Robert L. Mauck, and Jason A. Burdick. 2011. "Enhanced MSC Chondrogenesis Following Delivery of TGF-B3 from Alginate Microspheres within Hyaluronic Acid Hydrogels in Vitro and in Vivo." *Biomaterials* 32 (27): 6425–34. https://doi.org/10.1016/j.biomaterials.2011.05.033.

Blanco, Juan F, Ignacio F Graciani, Fermin M Sanchez-Guijo, Sandra Muntión, Pilar Hernandez-Campo, Carlos Santamaria, Soraya Carrancio, et al. 2010. "Isolation and Characterization of Mesenchymal Stromal Cells from Human Degenerated Nucleus Pulposus: Comparison with Bone Marrow Mesenchymal Stromal Cells from the Same Subjects." *Spine* 35 (26): 2259–65. https://doi.org/10.1097/BRS.0b013e3181cb8828.

Bone and Joint Initiative USA. 2015. *The Burden of Musculosketal Diseases in the United States: Prevalence, Societal and Economic Cost*.

Borges, A C, P. E. Bourban, D P Pioletti, and J A.E. Månson. 2010. "Curing Kinetics and Mechanical Properties of a Composite Hydrogel for the Replacement of the Nucleus Pulposus." *Composites Science and Technology* 70 (13): 1847–53. https://doi.org/10.1016/j.compscitech.2010.07.018.

Borges, Ana C., Christian Eyholzer, Fabien Duc, Pierre-etienne Etienne Bourban, Philippe Tingaut, Tanja Zimmermann, Dominique P. Pioletti, and Jan-anders E Månson. 2011. "Nanofibrillated Cellulose Composite Hydrogel for the Replacement of the Nucleus

Pulposus." *Acta Biomaterialia* 7 (9): 3412–21. https://doi.org/10.1016/j.actbio.2011.05.029.

Bouma, Gerrit J., Martin Barth, Darko Ledic, and Milorad Vilendecic. 2013. "The High-Risk Discectomy Patient: Prevention of Reherniation in Patients with Large Anular Defects Using an Anular Closure Device." *European Spine Journal* 22 (5): 1030–36. https://doi.org/10.1007/s00586-013-2656-1.

Bowles, Robby D, Harry H Gebhard, Roger Härtl, and Lawrence J Bonassar. 2011. "Tissue-Engineered Intervertebral Discs Produce New Matrix, Maintain Disc Height, and Restore Biomechanical Function to the Rodent Spine." *Proceedings of the National Academy of Sciences of the United States of America* 108 (32): 13106–11. https://doi.org/10.1073/pnas.1107094108.

Bowles, Robert D., and Lori A. Setton. 2017. "Biomaterials for Intervertebral Disc Regeneration and Repair." *Biomaterials* 129: 54–67. https://doi.org/10.1016/j.biomaterials.2017.03.013.

Boyd, Lawrence M, and Andrew J Carter. 2006. "Injectable Biomaterials and Vertebral Endplate Treatment for Repair and Regeneration of the Intervertebral Disc." In *European Spine Journal*, 15:S414–21. https://doi.org/10.1007/s00586-006-0172-2.

Brazel, Christopher S., and Nikolaos A. Peppas. 2000. "Modeling of Drug Release from Swellable Polymers." *European Journal of Pharmaceutics and Biopharmaceutics* 49 (1): 47–58. https://doi.org/10.1016/S0939-6411(99)00058-2.

Bridgen, Devin T., Bailey V. Fearing, Liufang Jing, Johannah Sanchez-Adams, Megan C. Cohan, Farshid Guilak, Jun Chen, and Lori A. Setton. 2017. "Regulation of Human Nucleus Pulposus Cells by Peptide-Coupled Substrates." *Acta Biomaterialia* 55: 100–108. https://doi.org/10.1016/j.actbio.2017.04.019.

Bron, Johannes Leendert, Marco N. Helder, Hans Jorg Meisel, Barend J. Van Royen, and

Theodoor H. Smit. 2009. “Repair, Regenerative and Supportive Therapies of the Annulus Fibrosus: Achievements and Challenges.” *European Spine Journal* 18 (3): 301–13. https://doi.org/10.1007/s00586-008-0856-x.

Brophy, Carl M, and Daniel J Hoh. 2018. “Posterior Instrumented Fusion” 29 (August): 1–5. https://doi.org/10.3171/2018.1.SPINE17867.130.

Bruehlmann, Sabina B, Jerome B Rattner, John R Matyas, and Neil a Duncan. 2002. “Regional Variations in the Cellular Matrix of the Annulus Fibrosus of the Intervertebral Disc.” *Journal of Anatomy* 201 (2): 159–71. http://www.pubmedcentral.nih.gov/articlerender.fcgi?artid=1570900&tool=pmcentrez&rendertype=abstract.

Bryant, Stephanie J., and Kristi S. Anseth. 2002. “Hydrogel Properties Influence ECM Production by Chondrocytes Photoencapsulated in Poly(Ethylene Glycol) Hydrogels.” *Journal of Biomedical Materials Research* 59 (1): 63–72. https://doi.org/10.1002/jbm.1217.

Bryant, Stephanie J., and Kristi S. Anseth. 2003. “Controlling the Spatial Distribution of ECM Components in Degradable PEG Hydrogels for Tissue Engineering Cartilage.” *Journal of Biomedical Materials Research - Part A* 64 (1): 70–79. https://doi.org/10.1002/jbm.a.10319.

Buchtová, N., A. D’Orlando, P. Judeinstein, O. Chauvet, P. Weiss, and J. Le Bideau. 2018. “Water Dynamics in Silanized Hydroxypropyl Methylcellulose Based Hydrogels Designed for Tissue Engineering.” *Carbohydrate Polymers* 202 (July): 404–8. https://doi.org/10.1016/j.carbpol.2018.08.143.

Buckwalter, J.A., V C Mow, S D Boden, D R Eyre, and M Weidenbaum. 2000. “Intervertebral Disc Structure, Composition, and Mechanical Function.” In *Orthopaedic Basic Science*,

edited by J.A. Buckwalter, T.A. Einhorn, and S.R. Simon, 2nd ed., 547–56. Rosemont, IL.

Burdick, Jason A., Cindy Chung, Xinqiao Jia, Mark A. Randolph, and Robert Langer. 2005. "Controlled Degradation and Mechanical Behavior of Photopolymerized Hyaluronic Acid Networks." *Biomacromolecules* 6 (1): 386–91. https://doi.org/10.1021/bm049508a.

Burdick, Jason A., Robert L. Mauck, and Sharon Gerecht. 2016. "To Serve and Protect: Hydrogels to Improve Stem Cell-Based Therapies." *Cell Stem Cell* 18 (1): 13–15. https://doi.org/10.1016/j.stem.2015.12.004.

Buxton, Amanda N., Junmin Zhu, Roger Marchant, Jennifer L. West, Jung U. Yoo, and Brian Johnstone. 2007. "Design and Characterization of Poly(Ethylene Glycol) Photopolymerizable Semi-Interpenetrating Networks for Chondrogenesis of Human Mesenchymal Stem Cells." *Tissue Engineering* 13 (10): 2549–60. https://doi.org/10.1089/ten.2007.0075.

Caicco, Matthew J., Tasneem Zahir, Andrea J. Mothe, Brian G. Ballios, Anthony J. Kihm, Charles H. Tator, and Molly S. Shoichet. 2013. "Characterization of Hyaluronan-Methylcellulose Hydrogels for Cell Delivery to the Injured Spinal Cord." *Journal of Biomedical Materials Research - Part A* 101 A (5): 1472–77. https://doi.org/10.1002/jbm.a.34454.

Calderon, Laura, Estelle Collin, Diego Velasco-Bayon, Mary Murphy, Damien O'Halloran, and Abhay Pandit. 2010. "Type II Collagen-Hyaluronan Hydrogel - A Step Towards A Scaffold For Intervertebral Disc Tissue Engineering." *European Cells and Materials* 20: 134–48. https://doi.org/10.22203/eCM.v020a12.

Canal, Tiziana, and Nikolaos A. Peppas. 1989. "Correlation between Mesh Size and Equilibrium Degree of Swelling of Polymeric Networks." *Journal of Biomedical Materials Research* 23

(10): 1183–93. https://doi.org/10.1002/jbm.820231007.

Cao, L, F Guilak, and LA Setton. 2011. “Three-Dimensional Finite Element Modeling of Pericellular Matrix and Cell Mechanics in the Nucleus Pulposus of the Intervertebral Disk Based on in Situ Morphology.” *Biomechanics Model Mechanobiol.* 10 (1): 1–10. https://doi.org/10.1007/s10237-010-0214-x.Three-dimensional.

Cao, Li, Farshid Guilak, and Lori a Setton. 2007. “Three-Dimensional Morphology of the Pericellular Matrix of Intervertebral Disc Cells in the Rat.” *Journal of Anatomy* 211 (4): 444–52. https://doi.org/10.1111/j.1469-7580.2007.00784.x.

Cao, Li, Farshid Guilak, and Lori A Setton. 2009. “Pericellular Matrix Mechanics in the Anulus Fibrosus Predicted by a Three-Dimensional Finite Element Model and In Situ Morphology.” *Cellular and Molecular Bioengineering* 2 (3): 306–19. https://doi.org/10.1007/s12195-009-0081-7.

Cappello, Rodolfo, Joseph L E Bird, Dirk Pfeiffer, Michael T Bayliss, and Jayesh Dudhia. 2006. “Notochordal Cell Produce and Assemble Extracellular Matrix in a Distinct Manner, Which May Be Responsible for the Maintenance of Healthy Nucleus Pulposus.” *Spine* 31 (8): 873–82; discussion 883. https://doi.org/10.1097/01.brs.0000209302.00820.fd.

Censi, Roberta, Piera Di Martino, Tina Vermonden, and Wim E. Hennink. 2012. “Hydrogels for Protein Delivery in Tissue Engineering.” *Journal of Controlled Release* 161 (2): 680–92. https://doi.org/10.1016/j.jconrel.2012.03.002.

Ceylan, Ayşegül, İbrahim Aşik, G. Enver Özgencil, and Burak Erken. 2019. “Clinical Results of Intradiscal Hydrogel Administration (GelStix) in Lumbar Degenerative Disc Disease.” *Turkish Journal of Medical Sciences* 49 (6): 1634–39. https://doi.org/10.3906/sag-1901-1.

Chang, Jiang, and C. Anthony Poole. 1996. “Sequestration of Type VI Collagen in the

Pericellular Microenvironment of Adult Chrondrocytes Cultured in Agarose." *Osteoarthritis and Cartilage / OARS, Osteoarthritis Research Society* 4: 275–85.

Chen, Daniel T.N., Qi Wen, Paul A. Janmey, John C. Crocker, and Arjun G. Yodh. 2010. "Rheology of Soft Materials." *Annual Review of Condensed Matter Physics* 1: 301–22. https://doi.org/10.1146/annurev-conmatphys-070909-104120.

Chen, J., W. Yan, and L. a. Setton. 2005. "Molecular Phenotypes of Notochordal Cells Purified from Nucleus Pulposus." *European Cells and Materials* 10: 16. https://doi.org/10.1007/s00586-006-0088-x.

Chen, Jun, Wei Yan, and Lori a. Setton. 2004. "Static Compression Induces Zonal-Specific Changes in Gene Expression for Extracellular Matrix and Cytoskeletal Proteins in Intervertebral Disc Cells in Vitro." *Matrix Biology* 22: 573–83. https://doi.org/10.1016/j.matbio.2003.11.008.

Chen, Minna H., Leo L. Wang, Jennifer J. Chung, Young Hun Kim, Pavan Atluri, and Jason A. Burdick. 2017. "Methods to Assess Shear-Thinning Hydrogels for Application As Injectable Biomaterials." *ACS Biomaterials Science and Engineering* 3 (12): 3146–60. https://doi.org/10.1021/acsbiomaterials.7b00734.

Chen, S, S Liu, K Ma, L Zhao, H Lin, and Z Shao. 2019. "TGF-β Signaling in Intervertebral Disc Health and Disease." *Osteoarthritis and Cartilage*. https://doi.org/10.1016/j.joca.2019.05.005.

Chen, Song, Peiliang Fu, Haishan Wu, and Ming Pei. 2017. "Meniscus, Articular Cartilage and Nucleus Pulposus: A Comparative Review of Cartilage-like Tissues in Anatomy, Development and Function." *Cell and Tissue Research* 370 (1): 53–70. https://doi.org/10.1007/s00441-017-2613-0.

Chen, Yong Mei, Rie Ogawa, Akira Kakugo, Yoshihito Osada, and Jian Ping Gong. 2009. "Dynamic Cell Behavior on Synthetic Hydrogels with Different Charge Densities." *Soft Matter* 5 (9): 1804–11. https://doi.org/10.1039/b818586g.

Chen, Yu Chun, Wen Yu Su, Shu Hua Yang, Amit Gefen, and Feng Huei Lin. 2013. "In Situ Forming Hydrogels Composed of Oxidized High Molecular Weight Hyaluronic Acid and Gelatin for Nucleus Pulposus Regeneration." *Acta Biomaterialia* 9 (2): 5181–93. https://doi.org/10.1016/j.actbio.2012.09.039.

Cheng, Yung-Hsin, Yu-Chun Chen, Shu-Hua Yang, Kai-Chiang Yang, Shinn-Chih Wu, Wen-Yu Su, Winston Teng-Kuei Cheng, and Feng-Huei Lin. 2010. "Thermosensitive Chitosan – Gelatin – Glycerol Phosphate Hydrogels as a Cell Carrier for Nucleus Pulposus." *TISSUE ENGINEERING: Part A* 16 (2): 695–703.

Cho, Young Rae, Sun Joo Lee, Hong Bae Jeon, Zee Yong Park, Jang Soo Chun, and Yung Joon Yoo. 2004. "Under-Sulfation by PAPS Synthetase Inhibition Modulates the Expression of ECM Molecules during Chondrogenesis." *Biochemical and Biophysical Research Communications* 323 (3): 769–75. https://doi.org/10.1016/j.bbrc.2004.08.173.

Choi, Kyung-Suk, and Brian D Harfe. 2011. "Hedgehog Signaling Is Required for Formation of the Notochord Sheath and Patterning of Nuclei Pulposi within the Intervertebral Discs." *Proceedings of the National Academy of Sciences of the United States of America* 108 (23): 9484–89. https://doi.org/10.1073/pnas.1007566108.

Choi, Kyung Suk, Martin J. Cohn, and Brian D. Harfe. 2008. "Identification of Nucleus Pulposus Precursor Cells and Notochordal Remnants in the Mouse: Implications for Disk Degeneration and Chordoma Formation." *Developmental Dynamics* 237 (November): 3953–58. https://doi.org/10.1002/dvdy.21805.

Choi, Un Yong, Hari Prasad Joshi, Samantha Payne, Kyoung Tae Kim, Jae Won Kyung, Hyemin Choi, Michael J. Cooke, et al. 2020. "An Injectable Hyaluronan–Methylcellulose (HAMC) Hydrogel Combined with Wharton's Jelly-Derived Mesenchymal Stromal Cells (WJ-MSCs) Promotes Degenerative Disc Repair." *International Journal of Molecular Sciences* 21 (19): 1–20. https://doi.org/10.3390/ijms21197391.

Choi, Youngjoo, Min Hee Park, and Kangwon Lee. 2019. "Tissue Engineering Strategies for Intervertebral Disc Treatment Using Functional Polymers." *Polymers*. https://doi.org/10.3390/polym11050872.

Chon, Brian H., Esther J. Lee, Liufang Jing, Lori A. Setton, and Jun Chen. 2013. "Human Umbilical Cord Mesenchymal Stromal Cells Exhibit Immature Nucleus Pulposus Cell Phenotype in a Laminin-Rich Pseudo-Three-Dimensional Culture System." *Stem Cell Research and Therapy* 4 (5): 1. https://doi.org/10.1186/scrt331.

Chou, Alice I, and Steven B Nicoll. 2009. "Characterization of Photocrosslinked Alginate Hydrogels for Nucleus Pulposus Cell Encapsulation." *Journal of Biomedical Materials Research - Part A* 91 (1): 187–94. https://doi.org/10.1002/jbm.a.32191.

Chung, Cindy, Michael Beecham, Robert L. Mauck, and Jason A. Burdick. 2009. "The Influence of Degradation Characteristics of Hyaluronic Acid Hydrogels on in Vitro Neocartilage Formation by Mesenchymal Stem Cells." *Biomaterials* 30 (26): 4287–96. https://doi.org/10.1016/j.biomaterials.2009.04.040.

Cleland, Robert L. 1970. "Ionic Polysaccharides. IV. Free-rotation Dimensions for Disaccharide Polymers. Comparison with Experiment for Hyaluronic Acid." *Biopolymers* 9 (7): 811–24. https://doi.org/10.1002/bip.1970.360090707.

Cloyd, Jordan M., Neil R. Malhotra, Lihui Weng, Weiliam Chen, Robert L. Mauck, and Dawn

M. Elliott. 2007. “Material Properties in Unconfined Compression of Human Nucleus Pulposus, Injectable Hyaluronic Acid-Based Hydrogels and Tissue Engineering Scaffolds.” *European Spine Journal* 16: 1892–98. https://doi.org/10.1007/s00586-007-0443-6.

Cortes, Mauricio, Alexis T Baria, and Nancy B Schwartz. 2009. “Sulfation of Chondroitin Sulfate Proteoglycans Is Necessary for Proper Indian Hedgehog Signaling in the Developing Growth Plate.” *Development* 136 (10): 1697–1706. https://doi.org/10.1242/dev.030742.

Courtenay, James C., Ram I. Sharma, and Janet L. Scott. 2018. “Recent Advances in Modified Cellulose for Tissue Culture Applications.” *Molecules* 23 (3). https://doi.org/10.3390/molecules23030654.

Cox, Megan K, Brittany L Appelboom, Ga I Ban, and Rosa Serra. 2014. “Erg Cooperates with TGF-β to Control Mesenchymal Differentiation.” *Experimental Cell Research* 8 (2): 410–18. https://doi.org/10.1016/j.yexcr.2014.08.015.

D’Este, Matteo, David Eglin, and Mauro Alini. 2018. “Lessons to Be Learned and Future Directions for Intervertebral Disc Biomaterials.” *Acta Biomaterialia* 78: 13–22. https://doi.org/10.1016/j.actbio.2018.08.004.

Dahia, Chitra Lekha, Eric J Mahoney, Atiq A Durrani, and Christopher Wylie. 2009a. “Intercellular Signaling Pathways Active during Intervertebral Disc Growth, Differentiation, and Aging.” *Spine* 34 (5): 456–62. https://doi.org/10.1097/BRS.0b013e3181913e98.

Dahia, Chitra Lekha, Eric J Mahoney, Atiq A Durrani, and Christopher Wylie.2009b. “Postnatal Growth, Differentiation, and Aging of the Mouse Intervertebral Disc.” *Spine* 34 (5): 447–55. https://doi.org/10.1097/BRS.0b013e3181990c64.

Dai, Lei, Ting Cheng, Chao Duan, Wei Zhao, Weipeng Zhang, Xuejun Zou, Joseph Aspler, and Yonghao Ni. 2019. "3D Printing Using Plant-Derived Cellulose and Its Derivatives: A Review." *Carbohydrate Polymers* 203 (September 2018): 71–86. https://doi.org/10.1016/j.carbpol.2018.09.027.

Desbrières, J., M. Hirrien, and S. B. Ross-Murphy. 2000. "Thermogelation of Methylcellulose: Rheological Considerations." *Polymer* 41 (7): 2451–61. https://doi.org/10.1016/S0032-3861(99)00413-9.

Desmoulin, Geoffrey Thor, Vikram Pradhan, and Theodore Edgar Milner. 2020. "Mechanical Aspects of Intervertebral Disc Injury and Implications on Biomechanics." *Spine* 45 (8): E457–64. https://doi.org/10.1097/BRS.0000000000003291.

Dieleman, Joseph L., Jackie Cao, Abby Chapin, Carina Chen, Zhiyin Li, Angela Liu, Cody Horst, et al. 2020. "US Health Care Spending by Payer and Health Condition, 1996-2016." *JAMA - Journal of the American Medical Association* 323 (9): 863–84. https://doi.org/10.1001/jama.2020.0734.

DiMicco, M. a., J. D. Kisiday, H. Gong, and a. J. Grodzinsky. 2007. "Structure of Pericellular Matrix around Agarose-Embedded Chondrocytes." *Osteoarthritis and Cartilage* 15: 1207–16. https://doi.org/10.1016/j.joca.2007.03.023.

Ding, Fan, Zhiwei Jia, Zhigang Zhao, Lin Xie, Xinfeng Gao, Dezhang Ma, and Ming Liu. 2017. "Total Disc Replacement versus Fusion for Lumbar Degenerative Disc Disease: A Systematic Review of Overlapping Meta-Analyses." *European Spine Journal* 26 (3): 806–15. https://doi.org/10.1007/s00586-016-4714-y.

Discher, Dennis E, Paul Janmey, and Yu-Li Wang. 2005. "Tissue Cells Feel and Respond to the Stiffness of Their Substrate." *Science (New York, N.Y.)* 310 (5751): 1139–43.

https://doi.org/10.1126/science.1116995.

Distefano, Tyler J, Jennifer O Shmukler, George Danias, and James C Iatridis. 2020. “The Functional Role of Interface Tissue Engineering in Annulus Fibrosus Repair: Bridging Mechanisms of Hydrogel Integration with Regenerative Outcomes.” *ACS Biomaterials Science and Engineering*. https://doi.org/10.1021/acsbiomaterials.0c01320.

Doench, Ingo, Maria E.W. Torres-Ramos, Alexandra Montembault, Paula Nunes de Oliveira, Celia Halimi, Eric Viguier, Laurent Heux, Robin Siadous, Rossana M.S.M. Thiré, and Anayancy Osorio-Madrazo. 2018. “Injectable and Gellable Chitosan Formulations Filled with Cellulose Nanofibers for Intervertebral Disc Tissue Engineering.” *Polymers* 10 (11). https://doi.org/10.3390/polym10111202.

Elliott, Dawn M., Chandra S. Yerramalli, Jesse C. Beckstein, John I. Boxberger, Wade Johannessen, and Edward J. Vresilovic. 2008. “The Effect of Relative Needle Diameter in Puncture and Sham Injection Animal Models of Degeneration.” *Spine* 33 (6): 588–96. https://doi.org/10.1097/BRS.0b013e318166e0a2.

Erickson, I. E., A. H. Huang, S. Sengupta, S. Kestle, J. A. Burdick, and R. L. Mauck. 2009. “Macromer Density Influences Mesenchymal Stem Cell Chondrogenesis and Maturation in Photocrosslinked Hyaluronic Acid Hydrogels.” *Osteoarthritis and Cartilage* 17 (12): 1639–48. https://doi.org/10.1016/j.joca.2009.07.003.

Erk, Kendra A., Kevin J. Henderson, and Kenneth R. Shull. 2010. “Strain Stiffening in Synthetic and Biopolymer Networks.” *Biomacromolecules* 11 (5): 1358–63. https://doi.org/10.1021/bm100136y.

Errington, R J, K Puustjarvi, I R White, S Roberts, and J P Urban. 1998. “Characterisation of Cytoplasm-Filled Processes in Cells of the Intervertebral Disc.” *Journal of Anatomy* 192 (

Pt 3 (April): 369–78. http://www.pubmedcentral.nih.gov/articlerender.fcgi?artid=1467781&tool=pmcentrez&rendertype=abstract.

Eyholzer, Christian, A. Borges De Couraça, F. Duc, P. E. Bourban, P. Tingaut, T. Zimmermann, J. A.E. Månson, and K. Oksman. 2011. "Biocomposite Hydrogels with Carboxymethylated, Nanofibrillated Cellulose Powder for Replacement of the Nucleus Pulposus." *Biomacromolecules* 12 (5): 1419–27. https://doi.org/10.1021/bm101131b.

Falcone, Samuel J., and Richard A. Berg. 2008. "Crosslinked Hyaluronic Acid Dermal Fillers: A Comparison of Rheological Properties." *Journal of Biomedical Materials Research - Part A* 87 (1): 264–71. https://doi.org/10.1002/jbm.a.31675.

Falcone, Samuel J., and Richard A. Berg. 2009. "Temporary Polysaccharide Dermal Fillers: A Model for Persistence Based on Physical Properties." *Dermatologic Surgery* 35 (8): 1238–43. https://doi.org/10.1111/j.1524-4725.2009.01218.x.

Fearing, Bailey V., Paula A. Hernandez, Lori A. Setton, and Nadeen O. Chahine. 2018. "Mechanotransduction and Cell Biomechanics of the Intervertebral Disc." *JOR Spine* 1 (3): e1026. https://doi.org/10.1002/jsp2.1026.

Feng, Ganjun, Li Li, Ying Hong, Hao Liu, Yueming Song, Fuxing Pei, Peter X Ma, Quan Gong, and Melanie J Gupte. 2014. "Hypoxia Promotes Nucleus Pulposus Phenotype in 3D Scaffolds in Vitro and in Vivo." *Journal of Neurosurgery. Spine* 21 (2): 303–9. https://doi.org/10.3171/2014.4.SPINE13870.

Feng, Qian, Sien Lin, Kunyu Zhang, Chaoqun Dong, Tianyi Wu, Heqin Huang, Xiaohui Yan, Li Zhang, Gang Li, and Liming Bian. 2017. "Sulfated Hyaluronic Acid Hydrogels with Retarded Degradation and Enhanced Growth Factor Retention Promote HMSC

Chondrogenesis and Articular Cartilage Integrity with Reduced Hypertrophy." *Acta Biomaterialia* 53: 329–42. https://doi.org/10.1016/j.actbio.2017.02.015.

Ferry, John D. 1980. *Viscoelastic Properties of Polymers*. *Viscoelastic Properties of Polymers*. John Wiley & Sons, Incorporated. https://doi.org/10.1149/1.2428174.

Flory, Paul J., and John Rehner. 1943a. "Statistical Mechanics of Cross-Linked Polymer Networks I. Rubberlike Elasticity." *The Journal of Chemical Physics* 11 (11): 512–20. https://doi.org/10.1063/1.1723791.

Flory, Paul J., and John Rehner.1943b. "Statistical Mechanics of Cross-Linked Polymer Networks II. Swelling." *The Journal of Chemical Physics* 11 (11): 521–26. https://doi.org/10.1063/1.1723792.

Fox, S. Carter, Bin Li, Daiqiang Xu, and Kevin J. Edgar. 2011. "Regioselective Esterification and Etherification of Cellulose: A Review." *Biomacromolecules* 12 (6): 1956–72. https://doi.org/10.1021/bm200260d.

Francisco, AT, RJ Mancino, RD Bowles, Jonathan M. Brunger, David M. Tainter, Yi-Te Chen, William J Richardson, Farshid Guilak, and Lori A. Setton. 2013. "Injectable Laminin-Functionalized Hydrogel for Nucleus Pulposus Regeneration." *Biomaterials* 34 (30): 7381–88. https://doi.org/10.1016/j.biomaterials.2013.06.038.Injectable.

Francisco, Aubrey T, Priscilla Y. Hwang, Claire G Jeong, Liufang Jing, Jun Chen, Lori A. Setton, Jun Chen, and Lori A. Setton. 2014. "Photocrosslinkable Laminin-Functionalized Polyethylene Glycol Hydrogel for Intervertebral Disc Regeneration." *Acta Biomaterialia* 27 (3): 417–28. https://doi.org/10.1016/j.actbio.2013.11.013.

Fraylich, Michael R., Ruixue Liu, Stephen M. Richardson, Pauline Baird, Judith Hoyland, Anthony J. Freemont, Cameron Alexander, Kevin Shakesheff, Francesco Cellesi, and Brian

R. Saunders. 2010. “Thermally-Triggered Gelation of PLGA Dispersions: Towards an Injectable Colloidal Cell Delivery System.” *Journal of Colloid and Interface Science* 344 (1): 61–69. https://doi.org/10.1016/j.jcis.2009.12.030.

Freeman, Inbar, Alon Kedem, and Smadar Cohen. 2008. “The Effect of Sulfation of Alginate Hydrogels on the Specific Binding and Controlled Release of Heparin-Binding Proteins.” *Biomaterials* 29 (22): 3260–68. https://doi.org/10.1016/j.biomaterials.2008.04.025.

Frith, Jessica E., Andrew R. Cameron, Donna J. Menzies, Peter Ghosh, Darryl L. Whitehead, Stan Gronthos, Andrew C.W. Zannettino, and Justin J. Cooper-White. 2013. “An Injectable Hydrogel Incorporating Mesenchymal Precursor Cells and Pentosan Polysulphate for Intervertebral Disc Regeneration.” *Biomaterials* 34 (37): 9430–40. https://doi.org/10.1016/j.biomaterials.2013.08.072.

Frith, Jessica E., Donna J. Menzies, Andrew R. Cameron, P. Ghosh, Darryl L. Whitehead, S. Gronthos, Andrew C.W. Zannettino, and Justin J. Cooper-White. 2014. “Effects of Bound versus Soluble Pentosan Polysulphate in PEG/HA-Based Hydrogels Tailored for Intervertebral Disc Regeneration.” *Biomaterials* 35 (4): 1150–62. https://doi.org/10.1016/j.biomaterials.2013.10.056.

Gaharwar, Akhilesh K, Nicholas a Peppas, and Ali Khademhosseini. 2014. “Nanocomposite Hydrogels for Biomedical Applications.” *Biotechnology and Bioengineering* 111 (3): 441–53. https://doi.org/10.1002/bit.25160.

Galbusera, Fabio, Marc Van Rijsbergen, Keita Ito, Jacques M. Huyghe, Marco Brayda-Bruno, and Hans Joachim Wilke. 2014. “Ageing and Degenerative Changes of the Intervertebral Disc and Their Impact on Spinal Flexibility.” *European Spine Journal* 23: 324–32. https://doi.org/10.1007/s00586-014-3203-4.

Gilchrist, CL, and Jun Chen. 2007. “Functional Integrin Subunits Regulating Cell–Matrix Interactions in the Intervertebral Disc.” *Journal of* ..., no. June: 829–40. https://doi.org/10.1002/jor.

Goins, Maurice L., David W. Wimberley, Philip S. Yuan, Laurence N. Fitzhenry, and Alexander R. Vaccaro. 2005. “Nucleus Pulposus Replacement: An Emerging Technology.” *Spine Journal* 5 (6 SUPPL.): S317–24. https://doi.org/10.1016/j.spinee.2005.02.021.

Gold, Gittel T. 2017. “Development of an Injectable, Cellulose-Based Hydrogel System for Soft Tissue Reconstruction.” The City College of New York.

Gold, Gittel T., Devika M. Varma, David Harbottle, Michelle S. Gupta, Simone S. Stalling, Peter J. Taub, and Steven B. Nicoll. 2014. “Injectable Redox-Polymerized Methylcellulose Hydrogels as Potential Soft Tissue Filler Materials.” *Journal of Biomedical Materials Research - Part A* 102 (12): 4536–44. https://doi.org/10.1002/jbm.a.35132.

Gold, Gittel T., Devika M. Varma, Peter J. Taub, and Steven B. Nicoll. 2015. “Development of Crosslinked Methylcellulose Hydrogels for Soft Tissue Augmentation Using an Ammonium Persulfate-Ascorbic Acid Redox System.” *Carbohydrate Polymers* 134: 497–507. https://doi.org/10.1016/j.carbpol.2015.07.101.

Gorgieva, Selestina, and Janja Trček. 2019. “Bacterial Cellulose: Production, Modification and Perspectives in Biomedical Applications.” *Nanomaterials* 9 (10): 1–20. https://doi.org/10.3390/nano9101352.

Gou, Shanmiao, Shawn C Oxentenko, Jason S Eldrige, Lizu Xiao, Mathew J Pingree, Zhen Wang, Carmen Perez-Terzic, and Wenchun Qu. 2014. “Stem Cell Therapy for Intervertebral Disk Regeneration.” *American Journal of Physical Medicine & Rehabilitation / Association of Academic Physiatrists* 93 (11 Suppl 3): S122-31.

https://doi.org/10.1097/PHM.0000000000000152.

Guan, Xiaofei, Meltem Avci-Adali, Emine Alarçin, Hao Cheng, Sara Saheb Kashaf, Yuxiao Li, Aditya Chawla, Hae Lin Jang, and Ali Khademhosseini. 2017. "Development of Hydrogels for Regenerative Engineering." *Biotechnology Journal* 12 (5): 1–20. https://doi.org/10.1002/biot.201600394.

Guehring, Thorsten, Andreas Nerlich, Markus Kroeber, Wiltrud Richter, and Georg W Omlor. 2010. "Sensitivity of Notochordal Disc Cells to Mechanical Loading: An Experimental Animal Study." *European Spine Journal : Official Publication of the European Spine Society, the European Spinal Deformity Society, and the European Section of the Cervical Spine Research Society* 19 (1): 113–21. https://doi.org/10.1007/s00586-009-1217-0.

Guehring, Thorsten, Geoff Wilde, Matthew Sumner, Thijs Grünhagen, Graeme B. Karney, Uday K. Tirlapur, and Jill P G Urban. 2009. "Notochordal Intervertebral Disc Cells: Sensitivity to Nutrient Deprivation." *Arthritis and Rheumatism* 60 (4): 1026–34. https://doi.org/10.1002/art.24407.

Gullbrand, Sarah E., Beth G. Ashinsky, Edward D. Bonnevie, Dong Hwa Kim, Julie B. Engiles, Lachlan J. Smith, Dawn M. Elliott, Thomas P. Schaer, Harvey E. Smith, and Robert L. Mauck. 2018. "Long-Term Mechanical Function and Integration of an Implanted Tissue-Engineered Intervertebral Disc." *Science Translational Medicine* 10 (468): 1–11. https://doi.org/10.1126/SCITRANSLMED.AAU0670.

Gupta, Dimpy, Charles H. Tator, and Molly S. Shoichet. 2006. "Fast-Gelling Injectable Blend of Hyaluronan and Methylcellulose for Intrathecal, Localized Delivery to the Injured Spinal Cord." *Biomaterials* 27 (11): 2370–79. https://doi.org/10.1016/j.biomaterials.2005.11.015.

Gupta, Michelle S, Elana S Cooper, and Steven B Nicoll. 2011. "Transforming Growth Factor-

Beta 3 Stimulates Cartilage Matrix Elaboration by Human Marrow-Derived Stromal Cells Encapsulated in Photocrosslinked Carboxymethylcellulose Hydrogels: Potential for Nucleus Pulposus Replacement." *Tissue Engineering - Part A* 17 (23–24): 2903–10. https://doi.org/10.1089/ten.tea.2011.0152.

Gupta, Michelle S, and Steven B Nicoll. 2014. "Functional Nucleus Pulposus-like Matrix Assembly by Human Mesenchymal Stromal Cells Is Directed by Macromer Concentration in Photocrosslinked Carboxymethylcellulose Hydrogels." *Cell and Tissue Research* 358 (2): 527–39. https://doi.org/10.1007/s00441-014-1962-1.

Gupta, Michelle S, and Steven B Nicoll. 2015. "Duration of TGF-B3 Exposure Impacts the Chondrogenic Maturation of Human MSCs in Photocrosslinked Carboxymethylcellulose Hydrogels." *Annals of Biomedical Engineering* 43 (5): 1145–57. https://doi.org/10.1007/s10439-014-1179-1.

Haberstroh, K, a Enz, M L Zenclussen, a a Hegewald, K Neumann, a Abbushi, C Thomé, M Sittinger, M Endres, and C Kaps. 2009. "Human Intervertebral Disc-Derived Cells Are Recruited by Human Serum and Form Nucleus Pulposus-like Tissue upon Stimulation with TGF-Beta3 or Hyaluronan in Vitro." *Tissue & Cell* 41 (6): 414–20. https://doi.org/10.1016/j.tice.2009.05.006.

Hachim, Daniel, Thomas E. Whittaker, Hyemin Kim, and Molly M. Stevens. 2019. "Glycosaminoglycan-Based Biomaterials for Growth Factor and Cytokine Delivery: Making the Right Choices." *Journal of Controlled Release* 313 (October): 131–47. https://doi.org/10.1016/j.jconrel.2019.10.018.

Haghpanah, Jennifer S, Raymond Tu, Sandra Da Silva, Deng Yan, Silvana Mueller, Christoph Weder, E Johan Foster, Iulia Sacui, Jeffery W. Gilman, and Jin Kim Montclare. 2013.

"Bionanocomposites: Differential Effects of Cellulose Nanocrystals on Protein Diblock Copolymers." *Biomacromolecules* 14 (12): 4360–67. https://doi.org/10.1021/bm401304w.

Halloran, Damien O., Sibylle Grad, Martin Stoddart, Peter Dockery, Mauro Alini, and Abhay S. Pandit. 2008. "An Injectable Cross-Linked Scaffold for Nucleus Pulposus Regeneration." *Biomaterials* 29 (4): 438–47. https://doi.org/10.1016/j.biomaterials.2007.10.009.

Handa, T, H Ishihara, H Ohshima, R Osada, H Tsuji, and K Obata. 1997. "Effects of Hydrostatic Pressure on Matrix Synthesis and Matrix Metalloproteinase Production in the Human Lumbar Intervertebral Disc." *Spine*.

Haque, Anwarul, and Edwin R. Morris. 1993. "Thermogelation of Methylcellulose. Part I: Molecular Structures and Processes." *Carbohydrate Polymers* 22 (3): 161–73. https://doi.org/10.1016/0144-8617(93)90137-S.

Hartvig, Rune A., Marco Van De Weert, Jesper Østergaard, Lene Jorgensen, and Henrik Jensen. 2011. "Protein Adsorption at Charged Surfaces: The Role of Electrostatic Interactions and Interfacial Charge Regulation." *Langmuir* 27 (6): 2634–43. https://doi.org/10.1021/la104720n.

Hartvigsen, Jan, Mark J. Hancock, Alice Kongsted, Quinette Louw, Manuela L. Ferreira, Stéphane Genevay, Damian Hoy, et al. 2018. "What Low Back Pain Is and Why We Need to Pay Attention." *The Lancet* 391 (10137): 2356–67. https://doi.org/10.1016/S0140-6736(18)30480-X.

Hayes, AJ, M Benjamin, and JR Ralphs. 2001. "Extracellular Matrix in Development of the Intervertebral Disc." *Matrix Biology*, 107–21. http://www.sciencedirect.com/science/article/pii/S0945053X01001251.

Hejretová, L., M. Čedíková, M. Dolejšová, T. Vlas, P. Jindra, D. Lysák, and M. Holubová. 2020.

"Comparison of the Immunomodulatory Effect of Single MSC Batches versus Pooled MSC Products." *Cell and Tissue Banking* 21 (1): 119–29. https://doi.org/10.1007/s10561-019-09805-3.

Henriksson, Helena, Maria Thornemo, Camilla Karlsson, Olle Hägg, Katarina Junevik, Anders Lindahl, and Helena Brisby. 2009. "Identification of Cell Proliferation Zones, Progenitor Cells and a Potential Stem Cell Niche in the Intervertebral Disc Region: A Study in Four Species." *Spine* 34 (21): 2278–87. https://doi.org/10.1097/BRS.0b013e3181a95ad2.

Henry, Nina, Johann Clouet, Jean Le Bideau, Catherine Le Visage, Jérôme Guicheux, Jean Le, and Catherine Le. 2018. "Innovative Strategies for Intervertebral Disc Regenerative Medicine : From Cell Therapies to Multiscale Delivery Systems." *Biotechnology Advances* 36 (December 2017): 281–94. https://doi.org/10.1016/j.biotechadv.2017.11.009.

Henry, Nina, Johann Clouet, Audrey Fragale, Louise Griveau, Joëlle Véziers, Pierre Weiss, Jean Le Bideau, et al. 2017. "Pullulan Microbeads / Si-HPMC Hydrogel Injectable System for the Sustained Delivery of GDF-5 and TGF- β 1 : New Insight into Intervertebral Disc Regenerative Medicine." *Drug Delivery* 0 (0): 999–1010. https://doi.org/10.1080/10717544.2017.1340362.

Hettiaratchi, Marian H., Tobias Miller, Johnna S. Temenoff, Robert E. Guldberg, and Todd C. McDevitt. 2014. "Heparin Microparticle Effects on Presentation and Bioactivity of Bone Morphogenetic Protein-2." *Biomaterials* 35 (25): 7228–38. https://doi.org/10.1016/j.biomaterials.2014.05.011.

Hettiaratchi, Marian H., and Molly S. Shoichet. 2019. "Modulated Protein Delivery to Engineer Tissue Repair." *Tissue Engineering - Part A* 25 (13–14): 925–30. https://doi.org/10.1089/ten.tea.2019.0066.

Hintze, V., A. Miron, S. Moeller, M. Schnabelrauch, H. P. Wiesmann, H. Worch, and D. Scharnweber. 2012. “Sulfated Hyaluronan and Chondroitin Sulfate Derivatives Interact Differently with Human Transforming Growth Factor-B1 (TGF-B1).” *Acta Biomaterialia* 8 (6): 2144–52. https://doi.org/10.1016/j.actbio.2012.03.021.

Hofmeister, Franz. 1888. “Zur Lehre von Der Wirkung Der Salze.” *Archiv Für Experimentelle Pathologie Und Pharmakologie* 24 (4): 247–60. https://doi.org/10.1007/BF01918191.

Holland, Theresa A, Yasuhiko Tabata, and Antonios G Mikos. 2003. “In Vitro Release of Transforming Growth Factor-B1 from Gelatin Microparticles Encapsulated in Biodegradable, Injectable Oligo(Poly(Ethylene Glycol) Fumarate) Hydrogels.” *Journal of Controlled Release* 91 (3): 299–313. https://doi.org/10.1016/S0168-3659(03)00258-X.

Hom, Warren W., Melanie Tschopp, Huizi A. Lin, Philip Nasser, Damien M. Laudier, Andrew C. Hecht, Steven B. Nicoll, and James C. Iatridis. 2019. “Composite Biomaterial Repair Strategy to Restore Biomechanical Function and Reduce Herniation Risk in an Ex Vivo Large Animal Model of Intervertebral Disc Herniation with Varying Injury Severity.” *PLoS ONE* 14 (5): 1–20. https://doi.org/10.1371/journal.pone.0217357.

Horner, HA, and J Urban. 2001. “2001 Volvo Award Winner in Basic Science Studies: Effect of Nutrient Supply on the Viability of Cells from the Nucleus Pulposus of the Intervertebral Disc.” *Spine* 26 (23): 2543–49. http://www.ncbi.nlm.nih.gov/pubmed/11725234.

Hoven, Voravee P., Varawut Tangpasuthadol, Yaowamand Angkitpaiboon, Napanporn Vallapa, and Suda Kiatkamjornwong. 2007. “Surface-Charged Chitosan: Preparation and Protein Adsorption.” *Carbohydrate Polymers* 68 (1): 44–53. https://doi.org/10.1016/j.carbpol.2006.07.008.

Hoy, Damian, Lyn March, Peter Brooks, Fiona Blyth, Anthony Woolf, Christopher Bain, Gail

Williams, et al. 2014. “The Global Burden of Low Back Pain: Estimates from the Global Burden of Disease 2010 Study.” *Annals of the Rheumatic Diseases* 73 (6): 968–74. https://doi.org/10.1136/annrheumdis-2013-204428.

Hsieh, Adam H, and Julianne D Twomey. 2010. “Cellular Mechanobiology of the Intervertebral Disc: New Directions and Approaches.” *Journal of Biomechanics* 43 (1): 137–45. https://doi.org/10.1016/j.jbiomech.2009.09.019.

Huang, Alice H., Megan J. Farrell, Minwook Kim, and Robert L. Mauck. 2010. “Long-Term Dynamic Loading Improves the Mechanical Properties of Chondrogenic Mesenchymal Stem Cell-Laden Hydrogels.” *European Cells and Materials* 19 (215): 72–85. https://doi.org/vol019a08 [pii].

Huang, Alice H., Ashley Stein, Rocky S. Tuan, and Robert L. Mauck. 2009. “Transient Exposure to Transforming Growth Factor Beta 3 Improves the Mechanical Properties of Mesenchymal Stem Cell-Laden Cartilage Constructs in a Density-Dependent Manner.” *Tissue Engineering - Part A* 15 (11): 3461–72. https://doi.org/10.1089/ten.tea.2009.0198.

Huang, G. Portocarrero, A. Molina, N. Tran, G. Collins, and Treena Livingston Arinzeh. 2018. “Investigating Cellulose Derived Glycosaminoglycan Mimetic Scaffolds for Cartilage Tissue Engineering Applications.” *Journal of Tissue Engineering and Regenerative Medicine* 12 (1): e592–603. https://doi.org/10.1002/term.2331.

Huang, Gloria Portocarrero, Roseline Menezes, Richard Vincent, Willis Hammond, Louis Rizio, George Collins, Treena Livingston Arinzeh, et al. 2017. “Gelatin Scaffolds Containing Partially Sulfated Cellulose Promote Mesenchymal Stem Cell Chondrogenesis.” *Tissue Engineering Part A* 00 (00): ten.TEA.2016.0461. https://doi.org/10.1089/ten.TEA.2016.0461.

Huang, Yong-Can Can, Jill P.G. Urban, and Keith D.K. Luk. 2014. "Intervertebral Disc Regeneration: Do Nutrients Lead the Way?" *Nature Reviews Rheumatology*. Nature Publishing Group. https://doi.org/10.1038/nrrheum.2014.91.

Huang, Yong Can, Yong Hu, Zhen Li, and Keith D.K. Luk. 2018. "Biomaterials for Intervertebral Disc Regeneration: Current Status and Looming Challenges." *Journal of Tissue Engineering and Regenerative Medicine* 12 (11): 2188–2202. https://doi.org/10.1002/term.2750.

Hudson, Katherine D, Marjan Alimi, Peter Grunert, Roger Härtl, and Lawrence J Bonassar. 2013. "Recent Advances in Biological Therapies for Disc Degeneration: Tissue Engineering of the Annulus Fibrosus, Nucleus Pulposus and Whole Intervertebral Discs." *Current Opinion in Biotechnology* 24 (5): 872–79. https://doi.org/10.1016/j.copbio.2013.04.012.

Humzah, M D, and R W Soames. 1988. "Human Lntervertebral Disc: Structure and Function" 356: 337–56.

Hunter, Christopher J., John R. Matyas, and Neil a. Duncan. 2004. "Cytomorphology of Notochordal and Chondrocytic Cells from the Nucleus Pulposus: A Species Comparison." *Journal of Anatomy* 205: 357–62. https://doi.org/10.1111/j.0021-8782.2004.00352.x.

Hunter, Christopher J, John R Matyas, and Neil a Duncan. 2003. "The Three-Dimensional Architecture of the Notochordal Nucleus Pulposus: Novel Observations on Cell Structures in the Canine Intervertebral Disc." *Journal of Anatomy* 202 (Pt 3): 279–91. http://www.pubmedcentral.nih.gov/articlerender.fcgi?artid=1571084&tool=pmcentrez&rendertype=abstract.

Hwang, Priscilla Y., Liufang Jing, Keith W. Michael, William J. Richardson, Jun Chen, and Lori a. Setton. 2014. "N-Cadherin-Mediated Signaling Regulates Cell Phenotype for Nucleus

Pulposus Cells of the Intervertebral Disc." *Cellular and Molecular Bioengineering* 8 (1): 51–62. https://doi.org/10.1007/s12195-014-0373-4.

Hwang, Priscilla Y, Jun Chen, Liufang Jing, Brenton D Hoffman, Lori a Setton, Jun Chen, Liufang Jing, and Brenton D Hoffman. 2014. "The Role of Extracellular Matrix Elasticity and Composition in Regulating the Nucleus Pulposus Cell Phenotype in the Intervertebral Disc: A Narrative Review." *Journal of Biomechanical Engineering* 136 (February): 021010. https://doi.org/10.1115/1.4026360.

Hynninen, Ville, Sami Hietala, Jason R. McKee, Lasse Murtomäki, Orlando J Rojas, Olli Ikkala, and Nonappa. 2018. "Inverse Thermoreversible Mechanical Stiffening and Birefringence in a Methylcellulose/Cellulose Nanocrystal Hydrogel." *Biomacromolecules* 19 (7): 2795–2804. https://doi.org/10.1021/acs.biomac.8b00392.

Iatridis, James C., Lori a. Setton, Mark Weidenbaum, and Van C. Mow. 1997. "The Viscoelastic Behavior of the Non-Degenerate Human Lumbar Nucleus Pulposus in Shear." *Journal of Biomechanics* 30 (97): 1005–13. https://doi.org/10.1016/S0021-9290(97)00069-9.

Iatridis, James C., Mark Weidenbaum, Lori A. Setton, and C. Van Mow. 1996. "Is the Nucleus Pulposus a Solid or a Fluid? Mechanical Behaviors of the Nucleus Pulposus of the Human Intervertebral Disc." In *Spine*, 21:1174–84. https://doi.org/10.1097/00007632-199605150-00009.

Iatridis, James C, Steven B Nicoll, Arthur J Michalek, Benjamin A Walter, and Michelle S Gupta. 2013. "Role of Biomechanics in Intervertebral Disc Degeneration and Regenerative Therapies: What Needs Repairing in the Disc and What Are Promising Biomaterials for Its Repair?" *Spine Journal* 13 (3): 243–62. https://doi.org/10.1016/j.spinee.2012.12.002.

Illien-Jünger, Svenja, Girish Pattappa, Marianna Peroglio, Lorin M. Benneker, Martin J.

Stoddart, Daisuke Sakai, Joji Mochida, Sibylle Grad, and Mauro Alini. 2012. "Homing of Mesenchymal Stem Cells in Induced Degenerative Intervertebral Discs in a Whole Organ Culture System." *Spine* 37 (22): 1865–73. https://doi.org/10.1097/BRS.0b013e3182544a8a.

Illien-Jünger, Svenja, Dillon D. Sedaghatpour, Damien M. Laudier, Andrew C. Hecht, Sheeraz A. Qureshi, and James C. Iatridis. 2016. "Development of a Bovine Decellularized Extracellular Matrix-Biomaterial for Nucleus Pulposus Regeneration." *Journal of Orthopaedic Research* 34 (5): 876–88. https://doi.org/10.1002/jor.23088.

Jeon, Oju, Kamal H Bouhadir, Joseph M Mansour, and Eben Alsberg. 2009. "Photocrosslinked Alginate Hydrogels with Tunable Biodegradation Rates and Mechanical Properties." *Biomaterials* 30 (14): 2724–34. https://doi.org/10.1016/j.biomaterials.2009.01.034.

Jeon, Oju, Caitlin Powell, Loran D. Solorio, Melissa D. Krebs, and Eben Alsberg. 2011. "Affinity-Based Growth Factor Delivery Using Biodegradable, Photocrosslinked Heparin-Alginate Hydrogels." *Journal of Controlled Release* 154 (3): 258–66. https://doi.org/10.1016/j.jconrel.2011.06.027.

Jeong, Byeongmoon, Li Qiong Wang, and Anna Gutowska. 2001. "Biodegradable Thermoreversible Gelling PLGA-g-PEG Copolymers." *Chemical Communications* 1 (16): 1516–17. https://doi.org/10.1039/b102819g.

Jha, Amit K., Anurag Mathur, Felicia L. Svedlund, Jianqin Ye, Yerem Yeghiazarians, and Kevin E. Healy. 2015. "Molecular Weight and Concentration of Heparin in Hyaluronic Acid-Based Matrices Modulates Growth Factor Retention Kinetics and Stem Cell Fate." *Journal of Controlled Release* 209: 308–16. https://doi.org/10.1016/j.jconrel.2015.04.034.

Jha, Amit K., Kevin M. Tharp, Jianqin Ye, Jorge L. Santiago-Ortiz, Wesley M. Jackson, Andreas Stahl, David V. Schaffer, Yerem Yeghiazarians, and Kevin E. Healy. 2015. "Enhanced

Survival and Engraftment of Transplanted Stem Cells Using Growth Factor Sequestering Hydrogels." *Biomaterials* 47: 1–12. https://doi.org/10.1016/j.biomaterials.2014.12.043.

Ji, Sun Park, Gyun Woo Dae, Na Yang Han, Kun Na, and Keun Hong Park. 2009. "Transforming Growth Factor B-3 Bound with Sulfate Polysaccharide in Synthetic Extracellular Matrix Enhanced the Biological Activities for Neocartilage Formation in Vivo." *Journal of Biomedical Materials Research - Part A* 91 (2): 408–15. https://doi.org/10.1002/jbm.a.32271.

Johannessen, Wade, and Dawn M Elliott. 2005. "Effects of Degeneration on the Biphasic Material Properties of Human Nucleus Pulposus in Confined Compression." *Spine* 30 (24): E724–29. https://doi.org/10.1097/01.brs.0000192236.92867.15.

Johnson, W E B, and S Roberts. 2003. "Human Intervertebral Disc Cell Morphology and Cytoskeletal Composition: A Preliminary Study of Regional Variations in Health and Disease." *Journal of Anatomy* 203 (6): 605–12. http://www.pubmedcentral.nih.gov/articlerender.fcgi?artid=1571197&tool=pmcentrez&rendertype=abstract.

Johnstone, Brian, Mauro Alini, Magali Cucchiarini, George R Dodge, David Eglin, Farshid Guilak, Henning Madry, et al. 2013. "Tissue Engineering for Articular Cartilage Repair--the State of the Art." *European Cells & Materials* 25: 248–67. https://doi.org/vol025a18 [pii].

Joshi, Sunil C. 2011. "Sol-Gel Behavior of Hydroxypropyl Methylcellulose (HPMC) in Ionic Media Including Drug Release." *Materials* 4 (10): 1861–1905. https://doi.org/10.3390/ma4101861.

Jung, Hyeong Seop, Hee Cheol Kim, and Won Ho Park. 2019. "Robust Methylcellulose Hydrogels Reinforced with Chitin Nanocrystals." *Carbohydrate Polymers* 213 (March):

311–19. https://doi.org/10.1016/j.carbpol.2019.03.009.

Kabir, S M Fijul, Partha P. Sikdar, B. Haque, M. A. Rahman Bhuiyan, A. Ali, and M. N. Islam. 2018. "Cellulose-Based Hydrogel Materials: Chemistry, Properties and Their Prospective Applications." *Progress in Biomaterials* 7 (3): 153–74. https://doi.org/10.1007/s40204-018-0095-0.

Kamide, Kenji. 1977. "Molecular Characterization of Cellulose and Its Derivatives." *Sen'i Gakkaishi* 33 (3): P101–10. https://doi.org/10.2115/fiber.33.3_P101.

Karami, Peyman, Azadeh Khoushabi, Andreas Schmocker, Martin Broome, Christophe Moser, Pierre-etienne Bourban, and Dominique P Pioletti. 2018. "Composite Double-Network Hydrogels To Improve Adhesion on Biological Surfaces." https://doi.org/10.1021/acsami.8b10735.

Khan, Aysha N., Hayley E. Jacobsen, Jansher Khan, Christopher G. Filippi, Mitchell Levine, Ronald A. Lehman, K. Daniel Riew, Lawrence G. Lenke, and Nadeen O. Chahine. 2017. "Inflammatory Biomarkers of Low Back Pain and Disc Degeneration: A Review." *Annals of the New York Academy of Sciences* 1410 (1): 68–84. https://doi.org/10.1111/nyas.13551.

Khoushabi, A., A. Schmocker, D. P. Pioletti, C. Moser, C. Schizas, J. A. Månson, and P. E. Bourban. 2015. "Photo-Polymerization, Swelling and Mechanical Properties of Cellulose Fibre Reinforced Poly(Ethylene Glycol) Hydrogels." *Composites Science and Technology* 119: 93–99. https://doi.org/10.1016/j.compscitech.2015.10.002.

Kim, Eun Ji, Ji Suk Choi, Jun Sung Kim, Young Chan Choi, and Yong Woo Cho. 2016. "Injectable and Thermosensitive Soluble Extracellular Matrix and Methylcellulose Hydrogels for Stem Cell Delivery in Skin Wounds." *Biomacromolecules* 17 (1): 4–11. https://doi.org/10.1021/acs.biomac.5b01566.

Kim, Ki-Won, Tae-Hong Lim, Jesse G Kim, Soon-Taek Jeong, Koichi Masuda, and Howard S An. 2003. "The Origin of Chondrocytes in the Nucleus Pulposus and Histologic Findings Associated with the Transition of a Notochordal Nucleus Pulposus to a Fibrocartilaginous Nucleus Pulposus in Intact Rabbit Intervertebral Discs." *Spine* 28 (10): 982–90. https://doi.org/10.1097/01.BRS.0000061986.03886.4F.

Kim, Ki Won, Kee Yong Ha, Jun Seok Lee, Suk Woo Nam, Young Kyun Woo, Tae Hong Lim, and Howard S. An. 2009. "Notochordal Cells Stimulate Migration of Cartilage End Plate Chondrocytes of the Intervertebral Disc in in Vitro Cell Migration Assays." *Spine Journal* 9 (4): 323–29. https://doi.org/10.1016/j.spinee.2008.05.003.

Kim, Kyoung-Tae, Seung-Won Park, and Young-Baeg Kim. 2009. "Disc Height and Segmental Motion as Risk Factors for Recurrent Lumbar Disc Herniation." *Spine* 34 (24): 2674–78. https://doi.org/10.1097/BRS.0b013e3181b4aaac.

Kim, Minwook, Isaac E. Erickson, Marwa Choudhury, Nancy Pleshko, and Robert L. Mauck. 2012. "Transient Exposure to TGF-B3 Improves the Functional Chondrogenesis of MSC-Laden Hyaluronic Acid Hydrogels." *Journal of the Mechanical Behavior of Biomedical Materials* 11: 92–101. https://doi.org/10.1016/j.jmbbm.2012.03.006.

Klemm, Dieter, Brigitte Heublein, Hans Peter Fink, and Andreas Bohn. 2005. "Cellulose: Fascinating Biopolymer and Sustainable Raw Material." *Angewandte Chemie - International Edition* 44 (22): 3358–93. https://doi.org/10.1002/anie.200460587.

Klouda, Leda, and Antonios G. Mikos. 2008. "Thermoresponsive Hydrogels in Biomedical Applications." *European Journal of Pharmaceutics and Biopharmaceutics* 68 (1): 34–45. https://doi.org/10.1016/j.ejpb.2007.02.025.

Klüppel, Michael, Thomas N Wight, Christina Chan, Aleksander Hinek, and Jeffrey L Wrana.

2005. “Maintenance of Chondroitin Sulfation Balance by Chondroitin-4-Sulfotransferase 1 Is Required for Chondrocyte Development and Growth Factor Signaling during Cartilage Morphogenesis.” *Development (Cambridge, England)* 132 (17): 3989–4003. https://doi.org/10.1242/dev.01948.

Knarr, Matthias, and Roland Bayer. 2014. “The Shear Dependence of the Methylcellulose Gelation Phenomena in Aqueous Solution and in Ceramic Paste Dedicated to Dr. Walter Bayer on the Occasion of His 90th Birthday on January 4, 2014.” *Carbohydrate Polymers* 111: 80–88. https://doi.org/10.1016/j.carbpol.2014.04.078.

Korecki, Casey L., John J. Costi, and James C. Iatridis. 2008. “Needle Puncture Injury Affects Intervertebral Disc Mechanics and Biology in an Organ Culture Model.” *Spine* 33 (3): 235–41. https://doi.org/10.1097/BRS.0b013e3181624504.

Korecki, Casey L, Juan M Taboas, Rocky S Tuan, and James C Iatridis. 2010. “Notochordal Cell Conditioned Medium Stimulates Mesenchymal Stem Cell Differentiation toward a Young Nucleus Pulposus Phenotype.” *Stem Cell Research & Therapy* 1 (2): 18. https://doi.org/10.1186/scrt18.

Kregar Velikonja, Nevenka, Jill Urban, Mirjam Fröhlich, Cornelia Neidlinger-Wilke, Dimitris Kletsas, Urska Potocar, Sarah Turner, and Sally Roberts. 2014. “Cell Sources for Nucleus Pulposus Regeneration.” *European Spine Journal : Official Publication of the European Spine Society, the European Spinal Deformity Society, and the European Section of the Cervical Spine Research Society* 23 Suppl 3 (June): S364-74. https://doi.org/10.1007/s00586-013-3106-9.

Kretlow, James D., Leda Klouda, and Antonios G. Mikos. 2007. “Injectable Matrices and Scaffolds for Drug Delivery in Tissue Engineering.” *Advanced Drug Delivery Reviews* 59

(4–5): 263–73. https://doi.org/10.1016/j.addr.2007.03.013.

Kumar, Deepak, Irini Gerges, Margherita Tamplenizza, Cristina Lenardi, Nicholas R. Forsyth, and Yang Liu. 2014. "Three-Dimensional Hypoxic Culture of Human Mesenchymal Stem Cells Encapsulated in a Photocurable, Biodegradable Polymer Hydrogel: A Potential Injectable Cellular Product for Nucleus Pulposus Regeneration." *Acta Biomaterialia* 10 (8): 3463–74. https://doi.org/10.1016/j.actbio.2014.04.027.

Kumar, Deepak, Alex Lyness, Irini Gerges, Christina Lenardi, Nicholas R. Forsyth, and Yang Liu. 2016. "Stem Cell Delivery with Polymer Hydrogel for Treatment of Intervertebral Disc Degeneration: From 3D Culture to Design of the Delivery Device for Minimally Invasive Therapy." *Cell Transplantation* 25 (12): 2213–20. https://doi.org/10.3727/096368916X692618.

Kwon, Hyuck Joon. 2012. "Chondrogenesis on Sulfonate-Coated Hydrogels Is Regulated by Their Mechanical Properties." *Journal of the Mechanical Behavior of Biomedical Materials* 17: 337–46. https://doi.org/10.1016/j.jmbbm.2012.10.006.

Kwon, Hyuck Joon, Kazunori Yasuda, Yoshihiro Ohmiya, Ken ichi Honma, Yong Mei Chen, and Jian Ping Gong. 2010. "In Vitro Differentiation of Chondrogenic ATDC5 Cells Is Enhanced by Culturing on Synthetic Hydrogels with Various Charge Densities." *Acta Biomaterialia* 6 (2): 494–501. https://doi.org/10.1016/j.actbio.2009.07.033.

Leach, Jennie Baier, Kathryn A. Bivens, Charles W. Patrick, and Christine E. Schmidt. 2003. "Photocrosslinked Hyaluronic Acid Hydrogels: Natural, Biodegradable Tissue Engineering Scaffolds." *Biotechnology and Bioengineering* 82 (5): 578–89. https://doi.org/10.1002/bit.10605.

Leckie, Ashley E., Margarete K. Akens, Kimberly A. Woodhouse, Albert J.M. Yee, and Cari M.

Whyne. 2012. “Evaluation of Thiol-Modified Hyaluronan and Elastin-like Polypeptide Composite Augmentation in Early-Stage Disc Degeneration: Comparing 2 Minimally Invasive Techniques.” *Spine* 37 (20). https://doi.org/10.1097/BRS.0b013e318266ecea.

Lee, Cynthia R., Daisuke Sakai, Tomoko Nakai, Kanae Toyama, Joji Mochida, Mauro Alini, and Sibylle Grad. 2007. “A Phenotypic Comparison of Intervertebral Disc and Articular Cartilage Cells in the Rat.” *European Spine Journal* 16: 2174–85. https://doi.org/10.1007/s00586-007-0475-y.

Lee, Kangwon, Eduardo A. Silva, and David J. Mooney. 2011. “Growth Factor Delivery-Based Tissue Engineering: General Approaches and a Review of Recent Developments.” *Journal of the Royal Society Interface*. https://doi.org/10.1098/rsif.2010.0223.

Lee, Sang Cheon, Yong Woo Cho, and Kinam Park. 2005. “Control of Thermogelation Properties of Hydrophobically-Modified Methylcellulose.” *Journal of Bioactive and Compatible Polymers* 20 (1): 5–13. https://doi.org/10.1177/0883911505049652.

Lei, J, L T McLane, J E Curtis, and J S Temenoff. 2014. “Characterization of a Multilayer Heparin Coating for Biomolecule Presentation to Human Mesenchymal Stem Cell Spheroids.” *Biomaterials Science* 2 (5): 666–73. https://doi.org/10.1039/C3BM60271K.

Lei, Jennifer, Elda Trevino, and Johnna Temenoff. 2016. “Cell Number and Chondrogenesis in Human MSC Aggregates Is Affected by the Sulfation Level of Heparin Used as a Cell Coating.” *Journal of Biomedical Materials Research Part A* 104 (7): n/a-n/a. https://doi.org/10.1002/jbm.a.35713.

Lewis, Gladius. 2012. “Nucleus Pulposus Replacement and Regeneration/Repair Technologies: Present Status and Future Prospects.” *Journal of Biomedical Materials Research - Part B Applied Biomaterials* 100 B (6): 1702–20. https://doi.org/10.1002/jbm.b.32712.

Lewis, K. M., D. Spazierer, M. D. Urban, L. Lin, H. Redl, and A. Goppelt. 2013. "Comparison of Regenerated and Non-Regenerated Oxidized Cellulose Hemostatic Agents." *European Surgery - Acta Chirurgica Austriaca* 45 (4): 213–20. https://doi.org/10.1007/s10353-013-0222-z.

Li, Hao, Chengzhen Liang, Yiqing Tao, Xiaopeng Zhou, Fangcai Li, Gang Chen, and Qi xin Chen. 2012. "Acidic PH Conditions Mimicking Degenerative Intervertebral Discs Impair the Survival and Biological Behavior of Human Adipose-Derived Mesenchymal Stem Cells." *Experimental Biology and Medicine* 237 (7): 845–52. https://doi.org/10.1258/ebm.2012.012009.

Li, Jianjun, Qun Zhao, Enbo Wang, Chuanhui Zhang, Guangbin Wang, and Quan Yuan. 2012. "Dynamic Compression of Rabbit Adipose-Derived Stem Cells Transfected with Insulin-like Growth Factor 1 in Chitosan/Gelatin Scaffolds Induces Chondrogenesis and Matrix Biosynthesis." *Journal of Cellular Physiology* 227 (July): 2003–12. https://doi.org/10.1002/jcp.22927.

Li, L., H. Shan, C. Y. Yue, Y. C. Lam, K. C. Tam, and X. Hu. 2002. "Thermally Induced Association and Dissociation of Methylcellulose in Aqueous Solutions." *Langmuir* 18 (20): 7291–98. https://doi.org/10.1021/la020029b.

Li, Lin. 2002. "Thermal Gelation of Methylcellulose in Water: Scaling and Thermoreversibility." *Macromolecules* 35 (15): 5990–98. https://doi.org/10.1021/ma0201781.

Li, Ning, Meihua Yu, Liandong Deng, Jun Yang, and Anjie Dong. 2012. "Thermosensitive Hydrogel of Hydrophobically-Modified Methylcellulose for Intravaginal Drug Delivery." *Journal of Materials Science: Materials in Medicine* 23 (8): 1913–19. https://doi.org/10.1007/s10856-012-4664-9.

Li, Xiaowei, Brian Cho, Russell Martin, Michelle Seu, Chi Zhang, Zhengbing Zhou, Ji Suk Choi, et al. 2019. "Nanofiber-Hydrogel Composite–Mediated Angiogenesis for Soft Tissue Reconstruction." *Science Translational Medicine* 11 (490): 1–12. https://doi.org/10.1126/scitranslmed.aau6210.

Li, Zhen, Laszlo Kupcsik, Shan Jing Yao, Mauro Alini, and Martin J. Stoddart. 2010. "Mechanical Load Modulates Chondrogenesis of Human Mesenchymal Stem Cells through the TGF-β Pathway." *Journal of Cellular and Molecular Medicine* 14 (6): 1338–46. https://doi.org/10.1111/j.1582-4934.2009.00780.x.

Li, Zhen, Gernot Lang, Lindsay S. Karfeld-Sulzer, Kerstin T. Mader, R. Geoff Richards, Franz E. Weber, Chris Sammon, et al. 2017. "Heterodimeric BMP-2/7 for Nucleus Pulposus Regeneration—In Vitro and Ex Vivo Studies." *Journal of Orthopaedic Research* 35 (1): 51–60. https://doi.org/10.1002/jor.23351.

Liang, Jue, Bedia Begüm Karakoçak, Jessica J. Struckhoff, and Nathan Ravi. 2016. "Synthesis and Characterization of Injectable Sulfonate-Containing Hydrogels." *Biomacromolecules* 17 (12): 4064–74. https://doi.org/10.1021/acs.biomac.6b01368.

Liang, Yingkai, and Kristi L. Kiick. 2014. "Heparin-Functionalized Polymeric Biomaterials in Tissue Engineering and Drug Delivery Applications." *Acta Biomaterialia* 10 (4): 1588–1600. https://doi.org/10.1016/j.actbio.2013.07.031.

Likhitpanichkul, M., M. Dreischarf, S. Illien-Junger, B. A. Walter, T. Nukaga, R. G. Long, D. Sakai, A. C. Hecht, and James C. Iatridis. 2014. "Fibrin-Genipin Adhesive Hydrogel for Annulus Fibrosus Repair: Performance Evaluation with Large Animal Organ Culture, in Situ Biomechanics, and in Vivo Degradation Tests." *European Cells and Materials* 28: 25–38. https://doi.org/10.1530/ERC-14-0411.Persistent.

Lim, Jeremy J., and Johnna S. Temenoff. 2013. “The Effect of Desulfation of Chondroitin Sulfate on Interactions with Positively Charged Growth Factors and Upregulation of Cartilaginous Markers in Encapsulated MSCs.” https://doi.org/10.1016/j.biomaterials.2013.03.037.

Lin, Chien Chi, and Andrew T. Metters. 2006. “Hydrogels in Controlled Release Formulations: Network Design and Mathematical Modeling.” *Advanced Drug Delivery Reviews* 58 (12–13): 1379–1408. https://doi.org/10.1016/j.addr.2006.09.004.

Lin, Hua, Cuilan Yin, Anchun Mo, and Guang Hong. 2021. “Applications of Hydrogel with Special Physical Properties in Bone and Cartilage Regeneration.” *Materials* 14 (1): 1–20. https://doi.org/10.3390/ma14010235.

Lin, Huizi a., Michelle S. Gupta, Devika M. Varma, M. Lane Gilchrist, and Steven B. Nicoll. 2016. “Lower Crosslinking Density Enhances Functional Nucleus Pulposus-like Matrix Elaboration by Human Mesenchymal Stem Cells in Carboxymethylcellulose Hydrogels.” *Journal of Biomedical Materials Research - Part A* 104 (1): 165–77. https://doi.org/10.1002/jbm.a.35552.

Lin, Huizi Anna, Devika M. Varma, Warren W. Hom, Michelle A. Cruz, Philip R. Nasser, Robert G. Phelps, James C. Iatridis, and Steven B. Nicoll. 2019. “Injectable Cellulose-Based Hydrogels as Nucleus Pulposus Replacements: Assessment of in Vitro Structural Stability, Ex Vivo Herniation Risk, and in Vivo Biocompatibility.” *Journal of the Mechanical Behavior of Biomedical Materials* 96 (March): 204–13. https://doi.org/10.1016/j.jmbbm.2019.04.021.

Lin, Jiun-Hao, Hsun-Yun Chang, Wei-Lun Kao, Kang-Yi Lin, Hua-Yang Liao, Yun-Wen You, Yu-Ting Kuo, et al. 2014. “Effect of Surface Potential on Extracellular Matrix Protein

Adsorption." *Langmuir* 30 (34): 10328–35. https://doi.org/10.1021/la5020362.

Liu, Gen-Zhe, Hirokazu Ishihara, Ryusuke Osada, Tomoatsu Kimura, and Haruo Tsuji. 2001. "Nitric Oxide Mediates the Change of Proteoglycan Synthesis in the Human Lumbar Intervertebral Disc in Response to Hydrostatic Pressure." Spine. 2001. http://journals.lww.com/spinejournal/Abstract/2001/01150/Nitric_Oxide_Mediates_the_Change_of_Proteoglycan.5.aspx.

Liu, Yongxing, Susan Fu, Mohamed N. Rahaman, Jeremy J. Mao, and B. Sonny Bal. 2014. "Native Nucleus Pulposus Tissue Matrix Promotes Notochordal Differentiation of Human Induced Pluripotent Stem Cells with Potential for Treating Intervertebral Disc Degeneration." *Journal of Biomedical Materials Research. Part A*, June, 8–11. https://doi.org/10.1002/jbm.a.35243.

Loebel, Claudia, Christopher B. Rodell, Minna H. Chen, and Jason A. Burdick. 2017. "Shear-Thinning and Self-Healing Hydrogels as Injectable Therapeutics and for 3D-Printing." *Nature Protocols* 12 (8): 1521–41. https://doi.org/10.1038/nprot.2017.053.

Loibl, Markus, Karin Wuertz-Kozak, Gianluca Vadala, Siegmund Lang, Jeremy Fairbank, and Jill P. Urban. 2019. "Controversies in Regenerative Medicine: Should Intervertebral Disc Degeneration Be Treated with Mesenchymal Stem Cells?" *Jor Spine* 2 (1): e1043. https://doi.org/10.1002/jsp2.1043.

Long, Rose G., Olivia M. Torre, Warren W. Hom, Dylan J. Assael, and James C. Iatridis. 2016. "Design Requirements for Annulus Fibrosus Repair: Review of Forces, Displacements and Material Properties of the Intervertebral Disc and a Summary of Candidate Hydrogels for Repair." *Journal of Biomechanical Engineering* 138 (c): 1–14. https://doi.org/10.1115/1.4032353.

Lott, Joseph R., John W. McAllister, Sara A. Arvidson, Frank S. Bates, and Timothy P. Lodge. 2013. “Fibrillar Structure of Methylcellulose Hydrogels.” *Biomacromolecules* 14 (8): 2484–88. https://doi.org/10.1021/bm400694r.

Lotz, J C, a H Hsieh, a L Walsh, E I Palmer, and J R Chin. 2002. “Mechanobiology of the Intervertebral Disc.” *Biochemical Society Transactions* 30: 853–58. https://doi.org/10.1042/BST0300853.

Lv, Fengjuan, Victor Y L Leung, Shishu Huang, Yongcan Huang, Yi Sun, and Kenneth M C Cheung. 2014. “In Search of Nucleus Pulposus-Specific Molecular Markers.” *Rheumatology (Oxford, England)* 53 (4): 600–610. https://doi.org/10.1093/rheumatology/ket303.

Mackay, Alastair M., Stephen C. Beck, J. Mary Murphy, Frank P. Barry, Clinton O. Chichester, and Mark F. Pittenger. 1998. “Chondrogenic Differentiation of Cultured Human Mesenchymal Stem Cells from Marrow.” *Tissue Engineering* 4 (4): 415–28. https://doi.org/10.1089/ten.1998.4.415.

Madry, Henning, Ana Rey-Rico, Jagadeesh K. Venkatesan, Brian Johnstone, and Magali Cucchiarini. 2014. “Transforming Growth Factor Beta-Releasing Scaffolds for Cartilage Tissue Engineering.” *Tissue Engineering - Part B: Reviews* 20 (2): 106–25. https://doi.org/10.1089/ten.teb.2013.0271.

Maidhof, Robert, D Olivier Alipui, Asfi Rafiuddin, Mitchell Levine, Daniel a Grande, and Nadeen O Chahine. 2012. “Emerging Trends in Biological Therapy for Intervertebral Disc Degeneration.” *Discovery Medicine* 14 (79): 401–11. http://www.ncbi.nlm.nih.gov/pubmed/23272692.

Maitre, Christine Lyn Le, Jennie Frain, Jane Millward-Sadler, Andrew P Fotheringham, Anthony

John Freemont, and Judith Alison Hoyland. 2009. “Altered Integrin Mechanotransduction in Human Nucleus Pulposus Cells Derived from Degenerated Discs.” *Arthritis and Rheumatism* 60 (2): 460–69. https://doi.org/10.1002/art.24248.

Malhotra, Neil R., Woojin M. Han, Jesse Beckstein, Jordan Cloyd, Weiliam Chen, and Dawn M Elliott. 2012. “An Injectable Nucleus Pulposus Implant Restores Compressive Range of Motion in the Ovine Disc.” *Spine* 37 (18): E1099-105. https://doi.org/10.1097/BRS.0b013e31825cdfb7.

Malvern Instruments. 2016. “A Basic Introduction to Rheology.” *Whitepaper*. https://cdn.technologynetworks.com/TN/Resources/PDF/WP160620BasicIntroRheology.pdf.

Mann, Brenda K, Rachael H Schmedlen, and Jennifer L West. 2001. “Tethered-TGF-β Increases Extracellular Matrix Production of Vascular Smooth Muscle Cells.” *Biomaterials* 22 (5): 439–44. https://doi.org/10.1016/S0142-9612(00)00196-4.

Markstedt, Kajsa, Athanasios Mantas, Ivan Tournier, H??ctor Mart??nez ??vila, Daniel H??gg, and Paul Gatenholm. 2015. “3D Bioprinting Human Chondrocytes with Nanocellulose-Alginate Bioink for Cartilage Tissue Engineering Applications.” *Biomacromolecules* 16 (5): 1489–96. https://doi.org/10.1021/acs.biomac.5b00188.

Marquardt, Laura M., and Sarah C. Heilshorn. 2016. “Design of Injectable Materials to Improve Stem Cell Transplantation.” *Current Stem Cell Reports* 2 (3): 207–20. https://doi.org/10.1007/s40778-016-0058-0.

Marsano, E., E. Bianchi, S. Gagliardi, and F. Ghioni. 2000. “Hydroxypropyl-Cellulose Derivatives: Phase Behaviour of Hydroxypropylcellulose Methacrylate.” *Polymer* 41 (2): 533–38. https://doi.org/10.1016/S0032-3861(99)00218-9.

Marsano, E., S. Gagliardi, F. Ghioni, and E. Bianchi. 2000. “Behaviour of Gels Based on (Hydroxypropyl) Cellulose Methacrylate.” *Polymer* 41 (21): 7691–98. https://doi.org/10.1016/S0032-3861(00)00142-7.

Martin, John T., Sarah E. Gullbrand, Bhavana Mohanraj, Beth G. Ashinsky, Dong Hwa Kim, Kensuke Ikuta, Dawn M. Elliott, Lachlan J. Smith, Robert L. Mauck, and Harvey E. Smith. 2017. “* Optimization of Preculture Conditions to Maximize the In Vivo Performance of Cell-Seeded Engineered Intervertebral Discs.” *Tissue Engineering. Part A* 23 (17–18): 923–34. https://doi.org/10.1089/ten.tea.2016.0491.

Martino, Alberto Di, Alexander R. Vaccaro, Joon Yung Lee, Vincenzo Denaro, and Moe R. Lim. 2005. “Nucleus Pulposus Replacement: Basic Science and Indications for Clinical Use.” *Spine* 30 (16 SUPPL.): 16–22. https://doi.org/10.1097/01.brs.0000174530.88585.32.

Mason, Mariah N., Andrew T. Metters, Christopher N. Bowman, and Kristi S. Anseth. 2001. “Predicting Controlled-Release Behavior of Degradable PLA-b-PEG-b-PLA Hydrogels.” *Macromolecules* 34 (13): 4630–35. https://doi.org/10.1021/ma010025y.

Mathew, Ansuja Pulickal, Saji Uthaman, Ki Hyun Cho, Chong Su Cho, and In Kyu Park. 2018. “Injectable Hydrogels for Delivering Biotherapeutic Molecules.” *International Journal of Biological Macromolecules* 110: 17–29. https://doi.org/10.1016/j.ijbiomac.2017.11.113.

Mauck, Robert L., Steven B. Nicoll, Sara L. Seyhan, Gerard A. Ateshian, and Clark T. Hung. 2003. “Synergistic Action of Growth Factors and Dynamic Loading for Articular Cartilage Tissue Engineering.” *Tissue Engineering* 9 (4): 597–611. https://doi.org/10.1089/107632703768247304.

McCall, Joshua D., Chien Chi Lin, and Kristi S. Anseth. 2011. “Affinity Peptides Protect Transforming Growth Factor Beta during Encapsulation in Poly(Ethylene Glycol)

Hydrogels." *Biomacromolecules* 12 (4): 1051–57. https://doi.org/10.1021/bm101379v.

McCall, Joshua D., Jacob E. Luoma, and Kristi S. Anseth. 2012. "Covalently Tethered Transforming Growth Factor Beta in PEG Hydrogels Promotes Chondrogenic Differentiation of Encapsulated Human Mesenchymal Stem Cells." *Drug Delivery and Translational Research* 2 (5): 305–12. https://doi.org/10.1007/s13346-012-0090-2.

McCann, M. R., O. J. Tamplin, J. Rossant, and C. a. Seguin. 2012. "Tracing Notochord-Derived Cells Using a Noto-Cre Mouse: Implications for Intervertebral Disc Development." *Disease Models & Mechanisms* 5: 73–82. https://doi.org/10.1242/dmm.008128.

McKee, Jason R., Sami Hietala, Jani Seitsonen, Janne Laine, Eero Kontturi, and Olli Ikkala. 2014. "Thermoresponsive Nanocellulose Hydrogels with Tunable Mechanical Properties." *ACS Macro Letters* 3 (3): 266–70. https://doi.org/10.1021/mz400596g.

Merceron, Christophe, Sophie Portron, Caroline Vignes-Colombeix, Emilie Rederstorff, Martial Masson, Julie Lesoeur, Sophie Sourice, et al. 2012. "Pharmacological Modulation of Human Mesenchymal Stem Cell Chondrogenesis by a Chemically Oversulfated Polysaccharide of Marine Origin: Potential Application to Cartilage Regenerative Medicine." *Stem Cells* 30 (3): 471–80. https://doi.org/10.1002/stem.1686.

Mertz, Edward L., Marcella Facchini, Anna T. Pham, Benedetta Gualeni, Fabio De Leonardis, Antonio Rossi, and Antonella Forlino. 2012. "Matrix Disruptions, Growth, and Degradation of Cartilage with Impaired Sulfation." *Journal of Biological Chemistry* 287 (26): 22030–42. https://doi.org/10.1074/jbc.M110.116467.

Mihardja, Shirley S., Jose A. Gonzales, Dongwei Gao, Richard E. Sievers, Qizhi Fang, Carol A. Stillson, Jiashing Yu, Michelle Peng, and Randall J. Lee. 2013. "The Effect of a Peptide-Modified Thermo-Reversible Methylcellulose on Wound Healing and LV Function in a

Chronic Myocardial Infarction Rodent Model." *Biomaterials* 34 (35): 8869–77. https://doi.org/10.1016/j.biomaterials.2013.07.028.

Minogue, Ben M, Stephen M Richardson, Leo a H Zeef, Anthony J Freemont, and Judith a Hoyland. 2010. "Characterization of the Human Nucleus Pulposus Cell Phenotype and Evaluation of Novel Marker Gene Expression to Define Adult Stem Cell Differentiation." *Arthritis and Rheumatism* 62 (12): 3695–3705. https://doi.org/10.1002/art.27710.

Molinos, Maria, Catarina R. Almeida, Joana Caldeira, Carla Cunha, Raquel M. Gonçalves, and Mário A. Barbosa. 2015. "Inflammation in Intervertebral Disc Degeneration and Regeneration." *Journal of the Royal Society Interface* 12 (104). https://doi.org/10.1098/rsif.2014.1191.

Molladavoodi, Sara, John McMorran, and Diane Gregory. 2020. "Mechanobiology of Annulus Fibrosus and Nucleus Pulposus Cells in Intervertebral Discs." *Cell and Tissue Research* 379 (3): 429–44. https://doi.org/10.1007/s00441-019-03136-1.

Morozova, Svetlana, McKenzie L. Coughlin, Julia T. Early, S. Piril Ertem, Theresa M. Reineke, Frank S. Bates, and Timothy P. Lodge. 2019. "Properties of Chemically Cross-Linked Methylcellulose Gels." *Macromolecules*. https://doi.org/10.1021/acs.macromol.9b01401.

Moss, Isaac L., Lyle Gordon, Kimberly A. Woodhouse, Cari M. Whyne, and Albert J.M. Yee. 2011. "A Novel Thiol-Modified Hyaluronan and Elastin-like Polypetide Composite Material for Tissue Engineering of the Nucleus Pulposus of the Intervertebral Disc." *Spine* 36 (13): 1022–29. https://doi.org/10.1097/BRS.0b013e3181e7b705.

Motte, Stéphanie, and Laura J. Kaufman. 2013. "Strain Stiffening in Collagen i Networks." *Biopolymers* 99 (1): 35–46. https://doi.org/10.1002/bip.22133.

Moysidou, Chrysanthi Maria, Chiara Barberio, and Róisín Meabh Owens. 2021. "Advances in

Engineering Human Tissue Models." *Frontiers in Bioengineering and Biotechnology* 8 (January). https://doi.org/10.3389/fbioe.2020.620962.

Muir, Victoria G., and Jason A. Burdick. 2021. "Chemically Modified Biopolymers for the Formation of Biomedical Hydrogels." *Chemical Reviews*. https://doi.org/10.1021/acs.chemrev.0c00923.

Mwale, F., P. Roughley, J. Antoniou, M. Alini, a. Hollander, T. Kirsch, and I. Stokes. 2004. "Distinction between the Extracellular Matrix of the Nucleus Pulposus and Hyaline Cartilage: A Requisite for Tissue Engineering of Intervertebral Disc." *European Cells and Materials* 8: 58–64.

Nasatto, Pauline L., Frédéric Pignon, Joana L.M. Silveira, Maria Eugênia R. Duarte, Miguel D. Noseda, and Marguerite Rinaudo. 2015. "Methylcellulose, a Cellulose Derivative with Original Physical Properties and Extended Applications." *Polymers* 7 (5): 777–803. https://doi.org/10.3390/polym7050777.

Natarajan, Raghu N., and Gunnar B.J. Andersson. 2017. "Lumbar Disc Degeneration Is an Equally Important Risk Factor as Lumbar Fusion for Causing Adjacent Segment Disc Disease." *Journal of Orthopaedic Research* 35 (1): 123–30. https://doi.org/10.1002/jor.23283.

Navaro, Yosi, Nadav Bleich-Kimelman, Lena Hazanov, Iris Mironi-Harpaz, Yonatan Shachaf, Shai Garty, Yoav Smith, et al. 2015. "Matrix Stiffness Determines the Fate of Nucleus Pulposus–Derived Stem Cells." *Biomaterials* 49: 68–76. https://doi.org/10.1016/j.biomaterials.2015.01.021.

Neidlinger-Wilke, Cornelia, Fabio Galbusera, Harris Pratsinis, Eleni Mavrogonatou, Antje Mietsch, Dimitris Kletsas, and Hans-Joachim Wilke. 2013. "Mechanical Loading of the

Intervertebral Disc: From the Macroscopic to the Cellular Level." *European Spine Journal : Official Publication of the European Spine Society, the European Spinal Deformity Society, and the European Section of the Cervical Spine Research Society*, June. https://doi.org/10.1007/s00586-013-2855-9.

Neidlinger-Wilke, Cornelia, Karin Würtz, Astrid Liedert, Carla Schmidt, Wolfgang Börm, Anita Ignatius, Hans-Joachim Wilke, and Lutz Claes. 2005. "A Three-Dimensional Collagen Matrix as a Suitable Culture System for the Comparison of Cyclic Strain and Hydrostatic Pressure Effects on Intervertebral Disc Cells." *Journal of Neurosurgery. Spine* 2: 457–65. https://doi.org/10.3171/spi.2005.2.4.0457.

Nerlich, Andreas G. A.G. G, Erwin D. E.D. D Schleicher, and Norbert Boos. 1997. "Immunohistologic Markers for Age-Related Changes of Human Lumbar Intervertebral Discs." *Spine-Hagerstown* 22 (24): 2781–2795. https://doi.org/10.1097/00007632-199712150-00001.

Nerurkar, Nandan L., Dawn M. Elliott, and Robert L. Mauck. 2011. "Mechanical Design Criteria for Intervertebral Disc." *J Biomech.* 43 (6): 1017–30. https://doi.org/10.1016/j.jbiomech.2009.12.001.MECHANICAL.

Nettles, Dana L, William J Richardson, and Lori a Setton. 2004. "Integrin Expression in Cells of the Intervertebral Disc." *Journal of Anatomy* 204 (6): 515–20. https://doi.org/10.1111/j.0021-8782.2004.00306.x.

Nguyen, Christelle, Isabelle Boutron, Gabriel Baron, Katherine Sanchez, Clémence Palazzo, Raphaël Benchimol, Guillaume Paris, et al. 2017. "Intradiscal Glucocorticoid Injection for Patients with Chronic Low Back Pain Associated with Active Discopathy: A Randomized Trial." *Annals of Internal Medicine* 166 (8): 547–56. https://doi.org/10.7326/M16-1700.

Ni, Bin Bin, Bo Li, Yue Hua Yang, Jiang Wei Chen, Ke Chen, Sheng Dan Jiang, and Lei Sheng Jiang. 2014. "The Effect of Transforming Growth Factor B1 on the Crosstalk between Autophagy and Apoptosis in the Annulus Fibrosus Cells under Serum Deprivation." *Cytokine* 70 (2): 87–96. https://doi.org/10.1016/j.cyto.2014.07.249.

Nie, Ting, Aaron Baldwin, Nori Yamaguchi, and Kristi L. Kiick. 2007. "Production of Heparin-Functionalized Hydrogels for the Development of Responsive and Controlled Growth Factor Delivery Systems." *Journal of Controlled Release* 122 (3): 287–96. https://doi.org/10.1016/j.jconrel.2007.04.019.

Nunley, Pierce D., Ajay Jawahar, David A. Cavanaugh, Charles R. Gordon, Eubulus J. Kerr, and Phillip Andrew Utter. 2013. "Symptomatic Adjacent Segment Disease after Cervical Total Disc Replacement: Re-Examining the Clinical and Radiological Evidence with Established Criteria." *Spine Journal* 13 (1): 5–12. https://doi.org/10.1016/j.spinee.2012.11.032.

O'Halloran, Damien M, and Abhay S Pandit. 2007. "Tissue-Engineering Approach to Regenerating the Intervertebral Disc." *Tissue Engineering* 13 (8): 1927–54. https://doi.org/10.1089/ten.2005.0608.

Ogushi, Yuko, Shinji Sakai, and Koei Kawakami. 2007. "Synthesis of Enzymatically-Gellable Carboxymethylcellulose for Biomedical Applications." *Journal of Bioscience and Bioengineering* 104 (1): 30–33. https://doi.org/10.1263/jbb.104.30.

Oğuz, öznur Demir, and Duygu Ege. 2018. "Rheological and Mechanical Properties of Thermoresponsive Methylcellulose/Calcium Phosphate-Based Injectable Bone Substitutes." *Materials* 11 (4). https://doi.org/10.3390/ma11040604.

Ohnishi, Takashi, Emanuel J. Novais, and Makarand V. Risbud. 2020. "Alterations in ECM Signature Underscore Multiple Sub-Phenotypes of Intervertebral Disc Degeneration."

Matrix Biology Plus 6–7: 100036. https://doi.org/10.1016/j.mbplus.2020.100036.

Ohshima, H., J. P G Urban, and D. H. Bergel. 1995. "Effect of Static Load on Matrix Synthesis Rates in the Intervertebral Disc Measured in Vitro by a New Perfusion Technique." *Journal of Orthopaedic Research* 13 (25): 22–29. https://doi.org/10.1002/jor.1100130106.

Ohtori, Seiji, Masayuki Miyagi, and Gen Inoue. 2018. "Sensory Nerve Ingrowth, Cytokines, and Instability of Discogenic Low Back Pain: A Review." *Spine Surgery and Related Research* 2 (1): 11–17. https://doi.org/10.22603/ssrr.2017-0046.

Paganini, Chiara, Chiara Gramegna Tota, Andrea Superti-Furga, and Antonio Rossi. 2020. "Skeletal Dysplasias Caused by Sulfation Defects." *International Journal of Molecular Sciences* 21 (8): 1–17. https://doi.org/10.3390/ijms21082710.

Pakulska, Malgosia M., Katarina Vulic, Roger Y. Tam, and Molly S. Shoichet. 2015. "Hybrid Crosslinked Methylcellulose Hydrogel: A Predictable and Tunable Platform for Local Drug Delivery." *Advanced Materials* 27 (34): 5002–8. https://doi.org/10.1002/adma.201502767.

Panebianco, C. J., J. H. Meyers, J. Gansau, W. W. Hom, and J. C. Iatridis. 2020. "Balancing Biological and Biomechanical Performance in Intervertebral Disc Repair: A Systematic Review of Injectable Cell Delivery Biomaterials." *European Cells & Materials* 40: 239–58. https://doi.org/10.22203/eCM.v040a15.

Park, Ji Sun, Dae Gyun Woo, Han Na Yang, Hye Jin Lim, Hyung Min Chung, and Keun Hong Park. 2008. "Heparin-Bound Transforming Growth Factor-B3 Enhances Neocartilage Formation by Rabbit Mesenchymal Stem Cells." *Transplantation* 85 (4): 589–96. https://doi.org/10.1097/TP.0b013e3181639b3a.

Park, Ji Sun, Han Na Yang, Dae Gyun Woo, Su Yeon Jeon, and Keun-Hong Park. 2012. "SOX9 Gene plus Heparinized TGF-β 3 Coated Dexamethasone Loaded PLGA Microspheres for

Inducement of Chondrogenesis of HMSCs." *Biomaterials* 33 (29): 7151–63. https://doi.org/10.1016/j.biomaterials.2012.06.023.

Pastewka, V. 1974. "And Carbohydrate of Nucleic Acids , Conjugated Proteins and Containing Carbohydrate-."

Pattappa, Girish, Zhen Li, Marianna Peroglio, Nadine Wismer, Mauro Alini, and Sibylle Grad. 2012. "Diversity of Intervertebral Disc Cells: Phenotype and Function." *Journal of Anatomy* 221 (6): 480–96. https://doi.org/10.1111/j.1469-7580.2012.01521.x.

Payne, Christina, Eimear B. Dolan, Janice O'Sullivan, Sally Ann Cryan, and Helena M. Kelly. 2017. "A Methylcellulose and Collagen Based Temperature Responsive Hydrogel Promotes Encapsulated Stem Cell Viability and Proliferation in Vitro." *Drug Delivery and Translational Research* 7 (1): 132–46. https://doi.org/10.1007/s13346-016-0347-2.

Pelletier, Matthew H., Charles S. Cohen, Paul Ducheyne, and William R. Walsh. 2016. "Restoring Segmental Biomechanics through Nucleus Augmentation." *Clinical Spine Surgery* 29 (10): 461–67. https://doi.org/10.1097/BSD.0b013e3182aa6841.

Peng, Bao Gan. 2013. "Pathophysiology, Diagnosis, and Treatment of Discogenic Low Back Pain." *World Journal of Orthopedics* 4 (2): 42–52. https://doi.org/10.5312/wjo.v4.i2.42.

Peppas, Nicholas A., J. Zach Hilt, Ali Khademhosseini, and Robert Langer. 2006. "Hydrogels in Biology and Medicine: From Molecular Principles to Bionanotechnology." *Advanced Materials* 18 (11): 1345–60. https://doi.org/10.1002/adma.200501612.

Pereira, Diana R, Joana Silva-correia, Joaquim M Oliveira, Rui L Reis, Abhay Pandit, and Manus J Biggs. 2018. "Nanocellulose Reinforced Gellan-Gum Hydrogels as Potential Biological Substitutes for Annulus Fibrosus Tissue Regeneration." *Nanomedicine: Nanotechnology, Biology, and Medicine* 14 (3): 897–908.

https://doi.org/10.1016/j.nano.2017.11.011.

Potier, Esther, and Keita Ito. 2014. “Can Notochordal Cells Promote Bone Marrow Stromal Cell Potential for Nucleus Pulposus Enrichment? A Simplified in Vitro System.” *Tissue Engineering. Part A* 00 (00): 1–11. https://doi.org/10.1089/ten.TEA.2013.0703.

Purcell, Brendan P., Iris L. Kim, Vanessa Chuo, Theodore Guenin, Shauna M. Dorsey, and Jason A. Burdick. 2014. “Incorporation of Sulfated Hyaluronic Acid Macromers into Degradable Hydrogel Scaffolds for Sustained Molecule Delivery.” *Biomater. Sci.* 2 (5): 693–702. https://doi.org/10.1039/C3BM60227C.

Qiao, Congde, Guangxin Chen, Jianlong Zhang, and Jinshui Yao. 2016. “Structure and Rheological Properties of Cellulose Nanocrystals Suspension.” *Food Hydrocolloids* 55: 19–25. https://doi.org/10.1016/j.foodhyd.2015.11.005.

Raj, Prithvi PP. 2008. “Intervertebral Disc: Anatomy-Physiology-Pathophysiology-Treatment.” *Pain Practice* 8 (1): 18–44. http://onlinelibrary.wiley.com/doi/10.1111/j.1533-2500.2007.00171.x/full.

Rajwade, J. M., K. M. Paknikar, and J. V. Kumbhar. 2015. “Applications of Bacterial Cellulose and Its Composites in Biomedicine.” *Applied Microbiology and Biotechnology* 99 (6): 2491–2511. https://doi.org/10.1007/s00253-015-6426-3.

Raucci, Maria Grazia, Ugo D’Amora, Alfredo Ronca, and Luigi Ambrosio. 2020. “Injectable Functional Biomaterials for Minimally Invasive Surgery.” *Advanced Healthcare Materials* 9 (13): 1–20. https://doi.org/10.1002/adhm.202000349.

Re’em, Tali, Yael Kaminer-Israeli, Emil Ruvinov, and Smadar Cohen. 2012. “Chondrogenesis of HMSC in Affinity-Bound TGF-Beta Scaffolds.” *Biomaterials* 33 (3): 751–61. https://doi.org/10.1016/j.biomaterials.2011.10.007.

Reeves, Robert, Andreia Ribeiro, Leonard Lombardo, Richard Boyer, and Jennie B Leach. 2010. "Synthesis and Characterization of Carboxymethylcellulose-Methacrylate Hydrogel Cell Scaffolds." *Polymers* 2 (3): 252–64. https://doi.org/10.3390/polym2030252.

Rehmann, Matthew S., Kelsi M. Skeens, Prathamesh M. Kharkar, Eden M. Ford, Emanual Maverakis, Kelvin H. Lee, and April M. Kloxin. 2017. "Tuning and Predicting Mesh Size and Protein Release from Step Growth Hydrogels." *Biomacromolecules* 18 (10): 3131–42. https://doi.org/10.1021/acs.biomac.7b00781.

Ren, Kaixuan, Haitao Cui, Qinghua Xu, Chaoliang He, Gao Li, and Xuesi Chen. 2016. "Injectable Polypeptide Hydrogels with Tunable Microenvironment for 3D Spreading and Chondrogenic Differentiation of Bone-Marrow-Derived Mesenchymal Stem Cells." *Biomacromolecules* 17 (12): 3862–71. https://doi.org/10.1021/acs.biomac.6b00884.

Reza, Anna T., Simone S. Stalling, and Steven B. Nicoll. 2006. "Development of Photocrosslinked Methylcellulose Hydrogels for Encapsulation of Nucleus Pulposus Cells." In *54th Annual Meeting of the Orthopaedic Research*, 1490.

Reza, Anna T, and Steven B Nicoll. 2010a. "Characterization of Novel Photocrosslinked Carboxymethylcellulose Hydrogels for Encapsulation of Nucleus Pulposus Cells." *Acta Biomaterialia* 6 (1): 179–86. https://doi.org/10.1016/j.actbio.2009.06.004.

Reza, Anna T, and Steven B Nicoll. 2010b. "Serum-Free, Chemically Defined Medium with TGF-Beta(3) Enhances Functional Properties of Nucleus Pulposus Cell-Laden Carboxymethylcellulose Hydrogel Constructs." *Biotechnology and Bioengineering* 105 (2): 384–95. https://doi.org/10.1002/bit.22545.

Risbud, Makarand V., Zachary R. Schoepflin, Fackson Mwale, Rita A. Kandel, Sibylle Grad, James C. Iatridis, Daisuke Sakai, and Judith A. Hoyland. 2015. "Defining the Phenotype of

Young Healthy Nucleus Pulposus Cells: Recommendations of the Spine Research Interest Group at the 2014 Annual ORS Meeting." *Journal of Orthopaedic Research* 33 (3): 283–93. https://doi.org/10.1002/jor.22789.

Risbud, Makarand V, Todd J Albert, Asha Guttapalli, Edward J Vresilovic, Alan S Hillibrand, Alexander R Vaccaro, and Irving M Shapiro. 2004. "Differentiation of Mesenchymal Stem Cells towards a Nucleus Pulposus-like Phenotype in Vitro: Implications for Cell-Based Transplantation Therapy." *Spine* 29 (23): 2627–32. http://www.ncbi.nlm.nih.gov/pubmed/15564911.

Risbud, Makarand V, and Irving M Shapiro. 2011. "Notochordal Cells in the Adult Intervertebral Disc: New Perspective on an Old Question." *Critical Reviews in Eukaryotic Gene Expression* 21 (1): 29–41. http://www.dl.begellhouse.com/journals/6dbf508d3b17c437,11cd40597f36b79e,053f1ce5027f805a.html.

Ritger, Philip L., and Nikolaos A. Peppas. 1987a. "A Simple Equation for Description of Solute Release I. Fickian and Non-Fickian Release from Non-Swellable Devices in the Form of Slabs, Spheres, Cylinders or Discs." *Journal of Controlled Release* 5 (1): 23–36. https://doi.org/10.1016/0168-3659(87)90034-4.

Ritger, Philip L., and Nikolaos A. Peppas. 1987b. "A Simple Equation for Description of Solute Release II. Fickian and Anomalous Release from Swellable Devices." *Journal of Controlled Release* 5 (1): 37–42. https://doi.org/10.1016/0168-3659(87)90035-6.

Roberts, S., J. Menage, and J. P. Urban. 1989. "Biochemical and Structural Properties of the Cartilage End-Plate and Its Relation to the Intervertebral Disc." *Spine* 14 (2): 166–74. https://doi.org/10.1097/00007632-198902000-00005.

Rodrigues-Pinto, Ricardo, Stephen M Richardson, and Judith a Hoyland. 2014. "An Understanding of Intervertebral Disc Development, Maturation and Cell Phenotype Provides Clues to Direct Cell-Based Tissue Regeneration Therapies for Disc Degeneration." *European Spine Journal : Official Publication of the European Spine Society, the European Spinal Deformity Society, and the European Section of the Cervical Spine Research Society*, April. https://doi.org/10.1007/s00586-014-3305-z.

Rohowsky, Juta, Katja Heise, Steffen Fischer, and Kay Hettrich. 2016. "Synthesis and Characterization of Novel Cellulose Ether Sulfates." *Carbohydrate Polymers* 142: 56–62. https://doi.org/10.1016/j.carbpol.2015.12.060.

Rother, Sandra, Vanessa D. Galiazzo, David Kilian, Karen M. Fiebig, Jana Becher, Stephanie Moeller, Ute Hempel, et al. 2017. "Hyaluronan/Collagen Hydrogels with Sulfated Hyaluronan for Improved Repair of Vascularized Tissue Tune the Binding of Proteins and Promote Endothelial Cell Growth." *Macromolecular Bioscience* 17 (11): 1–13. https://doi.org/10.1002/mabi.201700154.

Roughley, Peter, Caroline Hoemann, Eric DesRosiers, Fackson Mwale, John Antoniou, and Mauro Alini. 2006. "The Potential of Chitosan-Based Gels Containing Intervertebral Disc Cells for Nucleus Pulposus Supplementation." *Biomaterials* 27 (3): 388–96. https://doi.org/10.1016/j.biomaterials.2005.06.037.

Roughley, Peter J. 2004. "Biology of Intervertebral Disc Aging and Degeneration: Involvement of the Extracellular Matrix." *Spine* 29 (23): 2691–99. https://doi.org/10.1097/01.brs.0000146101.53784.b1.

Safshekan, Farzaneh, Mohammad Tafazzoli-Shadpour, Mohammad Ali Shokrgozar, Nooshin Haghighipour, Reza Mahdian, and Alireza Hemmati. 2012. "Intermittent Hydrostatic

Pressure Enhances Growth Factor-Induced Chondroinduction of Human Adipose-Derived Mesenchymal Stem Cells." *Artificial Organs* 36 (12): 1065–71. https://doi.org/10.1111/j.1525-1594.2012.01507.x.

Sahoo, Sujata, Cindy Chung, Sudhir Khetan, and Jason A. Burdick. 2008. "Hydrolytically Degradable Hyaluronic Acid Hydrogels with Controlled Temporal Structures." *Biomacromolecules* 9 (4): 1088–92. https://doi.org/10.1021/bm800051m.

Sakai, Daisuke, and Gunnar B J Andersson. 2015. "Stem Cell Therapy for Intervertebral Disc Regeneration: Obstacles and Solutions." *Nature Reviews. Rheumatology* 11 (4): 243–56. https://doi.org/10.1038/nrrheum.2015.13.

Sakai, Daisuke, and Sibylle Grad. 2015. "Advancing the Cellular and Molecular Therapy for Intervertebral Disc Disease." *Advanced Drug Delivery Reviews* 84 (June): 159–71. https://doi.org/10.1016/j.addr.2014.06.009.

Sarkar, N. 1979. "Thermal Gelation Properties of Methyl and Hydroxypropyl Methylcellulose." *Journal of Applied Polymer Science* 24 (4): 1073–87. https://doi.org/10.1002/app.1979.070240420.

Schmocker, Andreas, Azadeh Khoushabi, Daniela A. Frauchiger, Benjamin Gantenbein, Constantin Schizas, Christophe Moser, Pierre-Etienne Etienne Bourban, and Dominique P. Pioletti. 2016. "A Photopolymerized Composite Hydrogel and Surgical Implanting Tool for a Nucleus Pulposus Replacement." *Biomaterials* 88: 110–19. https://doi.org/10.1016/j.biomaterials.2016.02.015.

Schneider, Margaret C., Stanley Chu, Mark A. Randolph, and Stephanie J. Bryant. 2019. "An in Vitro and in Vivo Comparison of Cartilage Growth in Chondrocyte-Laden Matrix Metalloproteinase-Sensitive Poly(Ethylene Glycol) Hydrogels with Localized Transforming

Growth Factor B3." *Acta Biomaterialia* 93: 97–110. https://doi.org/10.1016/j.actbio.2019.03.046.

Schoenfeld, Andrew J., and Bradley K. Weiner. 2011. "Treatment of Lumbar Disc Herniation: Evidence-Based Practice." *American Journal of Clinical Hypnosis* 53 (4): 209–14. https://doi.org/10.2147/ijgm.s12270.

Serhan, Hassan A., Andrew P. Dooris, Matthew L. Parsons, Paul J. Ares, and Stefan M. Gabriel. 2006. "In Vitro Wear Assessment of the Charité Artificial Disc According to ASTM Recommendations." *Spine* 31 (17): 1900–1910. https://doi.org/10.1097/01.brs.0000228716.60863.ab.

Setton, Lori a, and Jun Chen. 2006. "Mechanobiology of the Intervertebral Disc and Relevance to Disc Degeneration." *The Journal of Bone and Joint Surgery. American Volume* 88 Suppl 2 (April): 52–57. https://doi.org/10.2106/JBJS.F.00001.

Shah, Bhranti S., and Nadeen O. Chahine. 2018. "Dynamic Hydrostatic Pressure Regulates Nucleus Pulposus Phenotypic Expression and Metabolism in a Cell Density-Dependent Manner." *Journal of Biomechanical Engineering* 140 (2): 1–10. https://doi.org/10.1115/1.4038758.

Shepard, Nicholas, and Woojin Cho. 2019. "Recurrent Lumbar Disc Herniation: A Review." *Global Spine Journal* 9 (2): 202–9. https://doi.org/10.1177/2192568217745063.

Shih, Wan Y., Wei Heng Shih, and Ilhan A. Aksay. 1999. "Elastic and Yield Behavior of Strongly Flocculated Colloids." *Journal of the American Ceramic Society* 82 (3): 616–24. https://doi.org/10.1111/j.1151-2916.1999.tb01809.x.

Shim, Eun Kyung, Jung Seok Lee, Dong Eun Kim, Seul Ki Kim, Byung Joo Jung, Eun Young Choi, and Chang Sung Kim. 2016. "Autogenous Mesenchymal Stem Cells from the

Vertebral Body Enhance Intervertebral Disc Regeneration via Paracrine Interaction: An in Vitro Pilot Study." *Cell Transplantation* 25 (10): 1819–32. https://doi.org/10.3727/096368916X691420.

Shin, Hyeongho, Bradley D. Olsen, and Ali Khademhosseini. 2012. "The Mechanical Properties and Cytotoxicity of Cell-Laden Double-Network Hydrogels Based on Photocrosslinkable Gelatin and Gellan Gum Biomacromolecules." *Biomaterials* 33 (11): 3143–52. https://doi.org/10.1016/j.biomaterials.2011.12.050.

Shin, Ji Youn, Yong Ho Yeo, Jae Eun Jeong, Su A. Park, and Won Ho Park. 2020. "Dual-Crosslinked Methylcellulose Hydrogels for 3D Bioprinting Applications." *Carbohydrate Polymers* 238 (March): 116192. https://doi.org/10.1016/j.carbpol.2020.116192.

Showalter, Brent L, Dawn M Elliott, Weiliam Chen, and Neil R Malhotra. 2015. "Evaluation of an In Situ Gelable and Injectable Hydrogel Treatment to Preserve Human Disc Mechanical Function Undergoing Physiologic Cyclic Loading Followed by Hydrated Recovery." *Journal of Biomechanical Engineering* 137 (8): 081008. https://doi.org/10.1115/1.4030530.

Silva, Amanda K.Andriola, Cyrille Richard, Michel Bessodes, Daniel Scherman, and Otto Wilhelm Merten. 2009. "Growth Factor Delivery Approaches in Hydrogels." *Biomacromolecules*. https://doi.org/10.1021/bm801103c.

Silva, Manuel T. 2010. "Secondary Necrosis: The Natural Outcome of the Complete Apoptotic Program." *FEBS Letters* 584 (22): 4491–99. https://doi.org/10.1016/j.febslet.2010.10.046.

Singh, Saarang, Ankur A. Patel, and Jaspal R. Singh. 2021. "Intervertebral Disc Degeneration: The Role and Evidence for Non–Stem-Cell-Based Regenerative Therapies." *International Journal of Spine Surgery* 15 (s1): 54–67. https://doi.org/10.14444/8055.

Sivakamasundari, V, and Thomas Lufkin. 2012. "Bridging the Gap: Understanding Embryonic

Intervertebral Disc Development." *Cell & Developmental Biology* 1 (2): 1–15. http://www.ncbi.nlm.nih.gov/pmc/articles/PMC3481539/.

Sivan, S. S., S. Roberts, J. P G Urban, J. Menage, J. Bramhill, D. Campbell, V. J. Franklin, et al. 2014. "Injectable Hydrogels with High Fixed Charge Density and Swelling Pressure for Nucleus Pulposus Repair: Biomimetic Glycosaminoglycan Analogues." *Acta Biomaterialia* 10 (3): 1124–33. https://doi.org/10.1016/j.actbio.2013.11.010.

Sivan, Sarit Sara, Ellen Wachtel, and Peter Roughley. 2014. "Structure, Function, Aging and Turnover of Aggrecan in the Intervertebral Disc." *Biochimica et Biophysica Acta* 1840 (10): 3181–89. https://doi.org/10.1016/j.bbagen.2014.07.013.

Sivashanmugam, A, R. Arun Kumar, M. Vishnu Priya, Shantikumar V Nair, and R Jayakumar. 2015. "An Overview of Injectable Polymeric Hydrogels for Tissue Engineering." *European Polymer Journal* 72: 543–65. https://doi.org/10.1016/j.eurpolymj.2015.05.014.

Smith, Lachlan J., Deborah J. Gorth, Brent L. Showalter, Joseph A. Chiaro, Elizabeth E. Beattie, Dawn M. Elliott, Robert L. Mauck, Weiliam Chen, and Neil R. Malhotra. 2014. "In Vitro Characterization of a Stem-Cell-Seeded Triple-Interpenetrating- Network Hydrogel for Functional Regeneration of the Nucleus Pulposus." *Tissue Engineering - Part A* 20 (13–14): 1841–49. https://doi.org/10.1089/ten.tea.2013.0516.

Smith, Lachlan J., Nandan L. Nerurkar, Kyung Suk Choi, Brian D. Harfe, and Dawn M. Elliott. 2011. "Degeneration and Regeneration of the Intervertebral Disc: Lessons from Development." *DMM Disease Models and Mechanisms* 4 (1): 31–41. https://doi.org/10.1242/dmm.006403.

Soares Da Costa, Diana, Rui L. Reis, and Iva Pashkuleva. 2017. "Sulfation of Glycosaminoglycans and Its Implications in Human Health and Disorders." *Annual Review*

of Biomedical Engineering 19: 1–26. https://doi.org/10.1146/annurev-bioeng-071516-044610.

Soltz, M. A., and G. A. Ateshian. 2000. "A Conewise Linear Elasticity Mixture Model for the Analysis of Tension-Compression Nonlinearity in Articular Cartilage." *Journal of Biomechanical Engineering* 122 (6): 576–86. https://doi.org/10.1115/1.1324669.

Stabenfeldt, Sarah E., Andres J. Garcia, and Michelle C. LaPlaca. 2006. "Thermoreversible Laminin-Functionalized Hydrogel for Neural Tissue Engineering." *Journal of Biomedial Materials Research Part A*. https://doi.org/10.1002/jbm.a.30638.

Stalling, Simone S, Sunday O Akintoye, and Steven B Nicoll. 2009. "Development of Photocrosslinked Methylcellulose Hydrogels for Soft Tissue Reconstruction." *Acta Biomaterialia* 5 (6): 1911–18. https://doi.org/10.1016/j.actbio.2009.02.020.

Steck, Eric, Helge Bertram, Rainer Abel, Bohua Chen, Anja Winter, and Wiltrud Richter. 2005. "Induction of Intervertebral Disc-like Cells from Adult Mesenchymal Stem Cells." *Stem Cells* 23: 403–11. https://doi.org/10.1634/stemcells.2004-0107.

Stergar, Janja, Lidija Gradisnik, Tomaz Velnar, and Uros Maver. 2019. "Intervertebral Disc Tissue Engineering: A Brief Review." *Bosnian Journal of Basic Medical Sciences* 19 (2): 130–37. https://doi.org/10.17305/bjbms.2019.3778.

Stevanic, Jasna S., Elina Mabasa Bergström, Paul Gatenholm, Lars Berglund, and Lennart Salmén. 2012. "Arabinoxylan/Nanofibrillated Cellulose Composite Films." *Journal of Materials Science* 47 (18): 6724–32. https://doi.org/10.1007/s10853-012-6615-8.

Strehl, Raimund, Karl Schumacher, Uwe De Vries, and Will W. Minuth. 2002. "Proliferating Cells versus Differentiated Cells in Tissue Engineering." *Tissue Engineering* 8 (1): 37–42. https://doi.org/10.1089/107632702753503036.

Sukarto, Abby, Claire Yu, Lauren E Flynn, and Brian G Amsden. 2012. "Co-Delivery of Adipose-Derived Stem Cells and Growth Factor-Loaded Microspheres in RGD-Grafted N-Methacrylate Glycol Chitosan Gels for Focal Chondral Repair." *Biomacromolecules* 13 (8): 2490–2502. https://doi.org/10.1021/bm300733n.

Tae, Giyoong, Marta Scatena, Patrick S Stayton, and Allan S Hoffman. 2006. "PEG-Cross-Linked Heparin Is an Affinity Hydrogel for Sustained Release of Vascular Endothelial Growth Factor." *Journal of Biomaterials Science. Polymer Edition* 17 (1–2): 187–97. http://www.ncbi.nlm.nih.gov/pubmed/16411608.

Tamrakar, Mamata, Priti Kharel, Adrian Traeger, Chris Maher, Mary O'Keeffe, and Giovanni Ferreira. 2021. "Completeness and Quality of Low Back Pain Prevalence Data in the Global Burden of Disease Study 2017." *BMJ Global Health* 6 (5): e005847. https://doi.org/10.1136/bmjgh-2021-005847.

Tang, Ruhang, Liufang Jing, Vincent P. Willard, Chia Lung Wu, Farshid Guilak, Jun Chen, and Lori A. Setton. 2018. "Differentiation of Human Induced Pluripotent Stem Cells into Nucleus Pulposus-like Cells." *Stem Cell Research and Therapy* 9 (1). https://doi.org/10.1186/s13287-018-0797-1.

Tate, Matthew C., Deborah A. Shear, Stuart W. Hoffman, Donald G. Stein, and Michelle C. LaPlaca. 2001. "Biocompatibility of Methylcellulose-Based Constructs Designed for Intracerebral Gelation Following Experimental Traumatic Brain Injury." *Biomaterials* 22 (10): 1113–23. https://doi.org/10.1016/S0142-9612(00)00348-3.

Tellier, Liane E., Tobias Miller, Todd C. McDevitt, and Johnna S. Temenoff. 2015. "Hydrolysis and Sulfation Pattern Effects on Release of Bioactive Bone Morphogenetic Protein-2 from Heparin-Based Microparticles."

Temenoff, Johnna S., Heungsoo Shin, Daniel E. Conway, Paul S. Engel, and Antonios G. Mikos. 2003. “In Vitro Cytotoxicity of Redox Radical Initiators for Cross-Linking of Oligo(Poly(Ethylene Glycol) Fumarate) Macromers.” *Biomacromolecules* 4 (6): 1605–13. https://doi.org/10.1021/bm030056w.

Tendulkar, Gauri, Tao Chen, Sabrina Ehnert, Hans Peter Kaps, and Andreas K. Nüssler. 2019. “Intervertebral Disc Nucleus Repair: Hype or Hope?” *International Journal of Molecular Sciences* 20 (15). https://doi.org/10.3390/ijms20153622.

Thirumala, Sreedhar, Jeffrey Gimble, and Ram Devireddy. 2013. “Methylcellulose Based Thermally Reversible Hydrogel System for Tissue Engineering Applications.” *Cells* 2 (3): 460–75. https://doi.org/10.3390/cells2030460.

Thomas, Jonathan D., Garland Fussell, Sumona Sarkar, Anthony M. Lowman, and Michele Marcolongo. 2010. “Synthesis and Recovery Characteristics of Branched and Grafted PNIPAAm-PEG Hydrogels for the Development of an Injectable Load-Bearing Nucleus Pulposus Replacement.” *Acta Biomaterialia* 6 (4): 1319–28. https://doi.org/10.1016/j.actbio.2009.10.024.

Thomé, Claudius, Peter Douglas Klassen, Gerrit Joan Bouma, Adisa Kuršumović, Javier Fandino, Martin Barth, Mark Arts, et al. 2018. “Annular Closure in Lumbar Microdiscectomy for Prevention of Reherniation: A Randomized Clinical Trial.” *Spine Journal* 18 (12): 2278–87. https://doi.org/10.1016/j.spinee.2018.05.003.

Thorpe, A. A., G. Dougill, L. Vickers, N. D. Reeves, C. Sammon, G. Cooper, and C. L. Le Maitre. 2017. “Thermally Triggered Hydrogel Injection into Bovine Intervertebral Disc Tissue Explants Induces Differentiation of Mesenchymal Stem Cells and Restores Mechanical Function.” *Acta Biomaterialia* 54: 212–26.

https://doi.org/10.1016/j.actbio.2017.03.010.

Thorpe, Abbey A, Abbie L A Binch, Laura B Creemers, Christopher Sammon, and Christine L Le Maitre. 2015. "Nucleus Pulposus Phenotypic Markers to Determine Stem Cell Differentiation : Fact or Fiction ?" *Oncotarget* 7 (3): 2189–2200. https://doi.org/10.18632/oncotarget.6782.

Thorpe, Stephen D., Conor T. Buckley, Tatiana Vinardell, Fergal J. O'Brien, Veronica a. Campbell, and Daniel J. Kelly. 2010. "The Response of Bone Marrow-Derived Mesenchymal Stem Cells to Dynamic Compression Following Tgf-B3 Induced Chondrogenic Differentiation." *Annals of Biomedical Engineering* 38 (9): 2896–2909. https://doi.org/10.1007/s10439-010-0059-6.

Tsai, Tsung-Lin Lin, Brenton C. Nelson, Paul a. Anderson, Thomas a. Zdeblick, and Wan-Ju Ju Li. 2014. "Intervertebral Disc and Stem Cells Cocultured in Biomimetic Extracellular Matrix Stimulated by Cyclic Compression in Perfusion Bioreactor." *Spine Journal* 14 (9): 2127–40. https://doi.org/10.1016/j.spinee.2013.11.062.

Tsaryk, Roman, Antonio Gloria, Teresa Russo, Laura Anspach, Roberto De Santis, Shahram Ghanaati, Ronald E. Unger, Luigi Ambrosio, and C. James Kirkpatrick. 2015. "Collagen-Low Molecular Weight Hyaluronic Acid Semi-Interpenetrating Network Loaded with Gelatin Microspheres for Cell and Growth Factor Delivery for Nucleus Pulposus Regeneration." *Acta Biomaterialia* 20: 10–21. https://doi.org/10.1016/j.actbio.2015.03.041.

Tsaryk, Roman, Joana Silva-Correia, Joaquim Miguel Oliveira, Ronald E. Unger, Constantin Landes, Christoph Brochhausen, Shahram Ghanaati, Rui L. Reis, and C. James Kirkpatrick. 2014. "Biological Performance of Cell-Encapsulated Methacrylated Gellan Gum-Based Hydrogels for Nucleus Pulposus Regeneration." *Journal of Tissue Engineering and*

Regenerative Medicine 11 (3): 637–48. https://doi.org/10.1002/term.1959.

Urban, Jill P G, Stanton Smith, and Jeremy C T Fairbank. 2004. "Nutrition of the Intervertebral Disc." *Spine* 29 (23): 2700–2709. https://doi.org/10.1097/01.brs.0000146499.97948.52.

Urban, JPG, S Roberts, and JR Ralphs. 2000. "The Nucleus of the Intervertebral Disc from Development to Degeneration." *American Zoologist* 61: 53–61. http://icb.oxfordjournals.org/content/40/1/53.short.

Urits, Ivan, Alexander Capuco, Medha Sharma, Alan D. Kaye, Omar Viswanath, Elyse M. Cornett, and Vwaire Orhurhu. 2019. "Stem Cell Therapies for Treatment of Discogenic Low Back Pain: A Comprehensive Review." *Current Pain and Headache Reports* 23 (9). https://doi.org/10.1007/s11916-019-0804-y.

Urits, Ivan, Omar Viswanath, Annemarie C. Galasso, Emily R. Sottosani, Keenan M. Mahan, Christopher M. Aiudi, Alan D. Kaye, and Vwaire J. Orhurhu. 2019. "Platelet-Rich Plasma for the Treatment of Low Back Pain: A Comprehensive Review." *Current Pain and Headache Reports* 23 (7). https://doi.org/10.1007/s11916-019-0797-6.

Varma, D. M., H. A. Lin, R. G. Long, G. T. Gold, A. C. Hecht, J. C. Iatridis, and Steven B. Nicoll. 2018. "Thermoresponsive, Redox-Polymerized Cellulosic Hydrogels Undergo in Situ Gelation and Restore Intervertebral Disc Biomechanics Post Discectomy." *European Cells and Materials* 35: 300–317. https://doi.org/10.22203/eCM.v035a21.

Varma, Devika M., Gittel T. Gold, Peter J. Taub, and Steven B. Nicoll. 2014. "Injectable Carboxymethylcellulose Hydrogels for Soft Tissue Filler Applications." *Acta Biomaterialia* 10 (12): 4996–5004. https://doi.org/10.1016/j.actbio.2014.08.013.

Varma, Devika M, Michelle S DiNicolas, and Steven B Nicoll. 2018. "Injectable, Redox-Polymerized Carboxymethylcellulose Hydrogels Promote Nucleus Pulposus-like

Extracellular Matrix Elaboration by Human MSCs in a Cell Density-Dependent Manner." *Journal of Biomaterials Applications* 33 (4): 576–89. https://doi.org/10.1177/0885328218805216.

Vassilaki, Maria, and Eric L. Hurwitz. 2014. "Insights in Public Health: Perspectives on Pain in the Low Back and Neck: Global Burden, Epidemiology, and Management." *Hawai'i Journal of Medicine & Public Health : A Journal of Asia Pacific Medicine & Public Health* 73 (4): 122–26.

Vergroesen, P. P.A., I. Kingma, K. S. Emanuel, R. J.W. Hoogendoorn, T. J. Welting, B. J. van Royen, J. H. van Dieën, and T. H. Smit. 2015. "Mechanics and Biology in Intervertebral Disc Degeneration: A Vicious Circle." *Osteoarthritis and Cartilage* 23 (7): 1057–70. https://doi.org/10.1016/j.joca.2015.03.028.

Vernengo, J., G. W. Fussell, N. G. Smith, and A. M. Lowman. 2008. "Evaluation of Novel Injectable Hydrogels for Nucleus Pulposus Replacement." *Journal of Biomedical Materials Research - Part B Applied Biomaterials* 84 (1): 64–69. https://doi.org/10.1002/jbm.b.30844.

Vo, Tuoi T.N., and Martin G. Meere. 2013. "Minimizing the Passive Release of Heparin-Binding Growth Factors from an Affinity-Based Delivery System." *Mathematical Medicine and Biology* 30 (4): 357–82. https://doi.org/10.1093/imammb/dqs027.

Vulic, Katarina, Malgosia M. Pakulska, Rohit Sonthalia, Arun Ramachandran, and Molly S. Shoichet. 2015. "Mathematical Model Accurately Predicts Protein Release from an Affinity-Based Delivery System." *Journal of Controlled Release : Official Journal of the Controlled Release Society* 197: 69–77. https://doi.org/10.1016/j.jconrel.2014.10.032.

Waghmare, Neha Ashok, Aditya Arora, Arijit Bhattacharjee, and Dhirendra S. Katti. 2018. "Sulfated Polysaccharide Mediated TGF-B1 Presentation in Pre-Formed Injectable

Scaffolds for Cartilage Tissue Engineering." *Carbohydrate Polymers* 193 (November 2017): 62–72. https://doi.org/10.1016/j.carbpol.2018.03.091.

Walter, BA, D Purmessur, A Moon, J Occiogrosso, DM Laudier, AC Hecht, and JC Iatridis. 2016. "Reduced Tissue Osmolarity Increases TRPV4 Expresseion and Pro-Inflammatory Cytokines in Intervertebral Disc Cells." *European Cells and Materials* 32: 123–36. http://www.ecmjournal.org/journal/papers/vol032/pdf/v032a08.pdf.

Walter, Benjamin A., Morakot Likhitpanichkul, Svenja Illien-Junger, Peter J. Roughley, Andrew C. Hecht, and James C. Iatridis. 2015. "TNFα Transport Induced by Dynamic Loading Alters Biomechanics of Intact Intervertebral Discs." *PLoS ONE* 10 (3): 1–16. https://doi.org/10.1371/journal.pone.0118358.

Wang, Feng, Li ping Nan, Shi feng Zhou, Yang Liu, Ze yu Wang, Jing cheng Wang, Xin min Feng, and Liang Zhang. 2019. "Injectable Hydrogel Combined with Nucleus Pulposus-Derived Mesenchymal Stem Cells for the Treatment of Degenerative Intervertebral Disc in Rats." *Stem Cells International* 2019. https://doi.org/10.1155/2019/8496025.

Wang, Hai, Yue Zhou, Tong Wei Chu, Chang Qing Li, Jian Wang, Zheng Feng Zhang, and Bo Huang. 2016. "Distinguishing Characteristics of Stem Cells Derived from Different Anatomical Regions of Human Degenerated Intervertebral Discs." *European Spine Journal*, 2016. https://doi.org/10.1007/s00586-016-4522-4.

Wang, Nick X., and Horst A. Von Recum. 2011. "Affinity-Based Drug Delivery." *Macromolecular Bioscience*. https://doi.org/10.1002/mabi.201000206.

Wang, Qiqiang, and Lin Li. 2005. "Effects of Molecular Weight on Thermoreversible Gelation and Gel Elasticity of Methylcellulose in Aqueous Solution." *Carbohydrate Polymers* 62 (3): 232–38. https://doi.org/10.1016/j.carbpol.2005.07.030.

Wang, Zhao Mei, Lin Li, Bi Sheng Zheng, Nodirali Normakhamatov, and Si Yuan Guo. 2007. "Preparation and Anticoagulation Activity of Sodium Cellulose Sulfate." *International Journal of Biological Macromolecules* 41 (4): 376–82. https://doi.org/10.1016/j.ijbiomac.2007.05.007.

Wang, Zhenming, Zhefeng Wang, William Weijia Lu, Wanxin Zhen, Dazhi Yang, and Songlin Peng. 2017. "Novel Biomaterial Strategies for Controlled Growth Factor Delivery for Biomedical Applications." *NPG Asia Materials* 9 (10): e435-17. https://doi.org/10.1038/am.2017.171.

Weber, Kathryn T., Timothy D. Jacobsen, Robert Maidhof, Justin Virojanapa, Chris Overby, Ona Bloom, Shaheda Quraishi, Mitchell Levine, and Nadeen O. Chahine. 2015. "Developments in Intervertebral Disc Disease Research: Pathophysiology, Mechanobiology, and Therapeutics." *Current Reviews in Musculoskeletal Medicine*, no. Ivd: 18–31. https://doi.org/10.1007/s12178-014-9253-8.

Widholz, Benedikt, Stefanos Tsitlakidis, Bruno Reible, Arash Moghaddam, and Fabian Westhauser. 2019. "Pooling of Patient-Derived Mesenchymal Stromal Cells Reduces Inter-Individual Confounder-Associated Variation without Negative Impact on Cell Viability, Proliferation and Osteogenic Differentiation." *Cells* 8 (6): 633. https://doi.org/10.3390/cells8060633.

Wilke, H-J, P Neef, M Caimi, T Hoogland, and L E Claes. 1999. "New in Vivo Measurements of Pressures in the Intervertebral Disc in Daily Life." *Spine* 24 (8): 755–62. https://doi.org/10.1097/00007632-199904150-00005.

Wilke, Hans Joachim, Lena Ressel, Frank Heuer, Nicolas Graf, and Stefan Rath. 2013. "Can Prevention of a Reherniation Be Investigated? Establishment of a Herniation Model and

Experiments with an Anular Closure Device." *Spine* 38 (10): 587–93. https://doi.org/10.1097/BRS.0b013e31828ca4bc.

Wilusz, Rebecca E, Johannah Sanchez-Adams, and Farshid Guilak. 2014. "The Structure and Function of the Pericellular Matrix of Articular Cartilage." *Matrix Biology* 39: 25–32. https://doi.org/10.1016/j.matbio.2014.08.009.

Winter, H. Henning, and Francois Chambon. 1986. "Analysis of Linear Viscoelasticity of a Crosslinking Polymer at the Gel Point." *Journal of Rheology* 30 (2): 367–82. https://doi.org/10.1122/1.549853.

Wu, Dianguo, Jinliang Cheng, Xin Su, and Yujun Feng. 2021. "Hydrophilic Modification of Methylcellulose to Obtain Thermoviscosifying Polymers without Macro-Phase Separation." *Carbohydrate Polymers* 260 (February): 117792. https://doi.org/10.1016/j.carbpol.2021.117792.

Wu, Pang Hung, Hyeun Sung Kim, and Il Tae Jang. 2020. "Intervertebral Disc Diseases Part 2: A Review of the Current Diagnostic and Treatment Strategies for Intervertebral Disc Disease." *International Journal of Molecular Sciences* 21 (6). https://doi.org/10.3390/ijms21062135.

Wuertz, Karin, Karolyn Godburn, and James C. Iatridis. 2009. "MSC Response to PH Levels Found in Degenerating Intervertebral Discs." *Biochemical and Biophysical Research Communications* 379 (4): 824–29. https://doi.org/10.1016/j.bbrc.2008.12.145.

Xie, Jingjing, Bo Li, Bing Yao, Pingchao Zhang, Lixin Wang, Hua Lu, and Xuan Song. 2020. "Transforming Growth Factor-B1-Regulated Fas/FasL Pathway Activation Suppresses Nucleus Pulposus Cell Apoptosis in an Inflammatory Environment." *Bioscience Reports* 40 (2): 1–8. https://doi.org/10.1042/BSR20191726.

Xu, Yirong, and Lin Li. 2005. “Thermoreversible and Salt-Sensitive Turbidity of Methylcellulose in Aqueous Solution.” *Polymer* 46 (18): 7410–17. https://doi.org/10.1016/j.polymer.2005.05.128.

Xu, Yirong, Lin Li, Peijie Zheng, Yee Cheong Lam, and Xiao Hu. 2004. “Controllable Gelation of Methylcellulose by a Salt Mixture.” *Langmuir* 20 (15): 6134–38. https://doi.org/10.1021/la049907r.

Xu, Yirong, C. Wang, K. C. Tam, and L. Li. 2004. “Salt-Assisted and Salt-Suppressed Sol-Gel Transitions of Methylcellulose in Water.” *Langmuir* 20 (3): 646–52. https://doi.org/10.1021/la0356295.

Yan, Hong Ji, Tommaso Casalini, Gry Hulsart-Billström, Shujiang Wang, Oommen P. Oommen, Matteo Salvalaglio, Sune Larsson, Jöns Hilborn, and Oommen P. Varghese. 2018. “Synthetic Design of Growth Factor Sequestering Extracellular Matrix Mimetic Hydrogel for Promoting in Vivo Bone Formation.” *Biomaterials* 161: 190–202. https://doi.org/10.1016/j.biomaterials.2018.01.041.

Yang, Fan, Victor YL VYL Leung, KDK Keight DK Luk, Danny Chan, and Kenneth MC Cheung. 2009. “Injury-Induced Sequential Transformation of Notochordal Nucleus Pulposus to Chondrogenic and Fibrocartilaginous Phenotype in the Mouse.” *The Journal of ...* 220 (January): 113–21. https://doi.org/10.1002/path.

Yang, Junchuan, Le Wang, Wei Zhang, Zhen Sun, Ying Li, Mingzhu Yang, Di Zeng, et al. 2018. “Reverse Reconstruction and Bioprinting of Bacterial Cellulose-Based Functional Total Intervertebral Disc for Therapeutic Implantation.” *Small* 14 (7): 1–9. https://doi.org/10.1002/smll.201702582.

Yang, Sai Wei, Noshir A Langrana, and Casey K Lee. 1986. “Biomechanics of Lumbosacral

Spinal Fusion in Combined Compression-Torsion Loads." *Spine*. https://doi.org/10.1007/s00586-008-0739-1.

Yang, Xinlin, and Xudong Li. 2009. "Nucleus Pulposus Tissue Engineering: A Brief Review." *European Spine Journal : Official Publication of the European Spine Society, the European Spinal Deformity Society, and the European Section of the Cervical Spine Research Society* 18 (11): 1564–72. https://doi.org/10.1007/s00586-009-1092-8.

Yaylaci, Seher Ustun, Merve Sen, Ozlem Bulut, Elif Arslan, Mustafa O Guler, and Ayse B Tekinay. 2016. "Chondrogenic Differentiation of Mesenchymal Stem Cells on Glycosaminoglycan-Mimetic Peptide Nanofibers." *ACS Biomaterials Science & Engineering* 2 (5): 871–78. https://doi.org/10.1021/acsbiomaterials.6b00099.

Yeo, Yong Ho, and Won Ho Park. 2021. "Dual-Crosslinked, Self-Healing and Thermo-Responsive Methylcellulose/Chitosan Oligomer Copolymer Hydrogels." *Carbohydrate Polymers* 258 (November 2020): 117705. https://doi.org/10.1016/j.carbpol.2021.117705.

Zeng, Kui, Thomas Groth, and Kai Zhang. 2019. "Recent Advances in Artificially Sulfated Polysaccharides for Applications in Cell Growth and Differentiation, Drug Delivery, and Tissue Engineering." *ChemBioChem* 20 (6): 737–46. https://doi.org/10.1002/cbic.201800569.

Zhang, Chenghao, Sarah E. Gullbrand, Thomas P. Schaer, Sophie Boorman, Dawn M. Elliott, Weiliam Chen, George R. Dodge, Robert L. Mauck, Neil R. Malhotra, and Lachlan J. Smith. 2021. "Combined Hydrogel and Mesenchymal Stem Cell Therapy for Moderate-Severity Disc Degeneration in Goats." *Tissue Engineering - Part A* 27 (1–2): 117–28. https://doi.org/10.1089/ten.tea.2020.0103.

Zhang, Qilei, Dongqiang Lin, and Shanjing Yao. 2015. "Review on Biomedical and

Bioengineering Applications of Cellulose Sulfate." *Carbohydrate Polymers* 132: 311–22. https://doi.org/10.1016/j.carbpol.2015.06.041.

Zhang, Shuang, Danyang Huang, Hai Lin, Yun Xiao, and Xingdong Zhang. 2020. "Cellulose Nanocrystal Reinforced Collagen-Based Nanocomposite Hydrogel with Self-Healing and Stress-Relaxation Properties for Cell Delivery." *Biomacromolecules* 21 (6): 2400–2408. https://doi.org/10.1021/acs.biomac.0c00345.

Zhao, Chang Qing, Li Min Wang, Lei Sheng Jiang, and Li Yang Dai. 2007. "The Cell Biology of Intervertebral Disc Aging and Degeneration." *Ageing Research Reviews* 6: 247–61. https://doi.org/10.1016/j.arr.2007.08.001.

Zhao, Lei, Laxmaiah Manchikanti, Alan David Kaye, and Alaa Abd-Elsayed. 2019. "Treatment of Discogenic Low Back Pain: Current Treatment Strategies and Future Options—a Literature Review." *Current Pain and Headache Reports* 23 (11). https://doi.org/10.1007/s11916-019-0821-x.

Zheng, C. H., and M. E. Levenston. 2015. "Fact versus Artifact: Avoiding Erroneous Estimates of Sulfated Glycosaminoglycan Content Using the Dimethylmethylene Blue Colorimetric Assay for Tissue-Engineered Constructs." *European Cells and Materials* 29: 224–36. https://doi.org/10.22203/eCM.v029a17.

Zheng, Peijie, Lin Li, Xiao Hu, and Xiongyan Zhao. 2004. "Sol-Gel Transition of Methylcellulose in Phosphate Buffer Saline Solutions." *Journal of Polymer Science, Part B: Polymer Physics* 42 (10): 1849–60. https://doi.org/10.1002/polb.20070.

Zhu, J. 2010. "Bioactive Modification of Poly (Ethylene Glycol) Hydrogels for Tissue Engineering." *Biomaterials* 31 (17): 4639–56. https://doi.org/10.1016/j.biomaterials.2010.02.044.Bioactive.

Zhu, Jian, Kaishun Xia, Wei Yu, Yitian Wang, Jianming Hua, Bing Liu, Zhe Gong, et al. 2019. "Sustained Release of GDF5 from a Designed Coacervate Attenuates Disc Degeneration in a Rat Model." *Acta Biomaterialia* 86: 300–311. https://doi.org/10.1016/j.actbio.2019.01.028.

Zhu, Junmin, and Roger E Marchant. 2011. "Design Properties of Hydrogel Tissue-Engineering Scaffolds." *Expert Review of Medical Devices* 8 (5): 607–26. https://doi.org/10.1586/erd.11.27.

Zuidema, Jonathan M., Christopher J. Rivet, Ryan J. Gilbert, and Faith A. Morrison. 2014. "A Protocol for Rheological Characterization of Hydrogels for Tissue Engineering Strategies." *Journal of Biomedical Materials Research - Part B Applied Biomaterials* 102 (5): 1063–73. https://doi.org/10.1002/jbm.b.33088.

رَبَّنَا تَقَبَّلْ مِنَّآ ۖ إِنَّكَ أَنتَ ٱلسَّمِيعُ ٱلْعَلِيمُ

Rabbana taqabbal minna inaka Antas Samee'ul Aleem

Our Lord, accept [this] from us. Indeed, You are the Hearing, the Knowing.